



HAL
open science

Characterization and contribution of colloidal fraction in the mobility and bioavailability of sedimentary phosphorus

Ngoc Diep Nguyen

► **To cite this version:**

Ngoc Diep Nguyen. Characterization and contribution of colloidal fraction in the mobility and bioavailability of sedimentary phosphorus. Earth Sciences. Université de Limoges, 2020. English. NNT : 2020LIMO0078 . tel-04844563

HAL Id: tel-04844563

<https://theses.hal.science/tel-04844563v1>

Submitted on 18 Dec 2024

HAL is a multi-disciplinary open access archive for the deposit and dissemination of scientific research documents, whether they are published or not. The documents may come from teaching and research institutions in France or abroad, or from public or private research centers.

L'archive ouverte pluridisciplinaire **HAL**, est destinée au dépôt et à la diffusion de documents scientifiques de niveau recherche, publiés ou non, émanant des établissements d'enseignement et de recherche français ou étrangers, des laboratoires publics ou privés.

**Université de Limoges
ED 614 - Chimie , Environnement, Géosciences, Agrosociences (CEGA)
GEIST PEIRENE EA 7500**

Thèse pour obtenir le grade de
Docteur de l'Université de Limoges
Eau, Sol et Environnement

Présentée et soutenue par

Ngoc Diep NGUYEN

Le 17 décembre 2020

**Characterization and contribution of colloidal fraction in the
mobility and bioavailability of sedimentary phosphorus**

**Caractérisation et contribution de la fraction colloïdale dans la
mobilité et la (bio)disponibilité du phosphore sédimentaire**

Thèse dirigée par Pr. Véronique Deluchat ; Dr. Malgorzata Grybos ; Dr. Marion Rabiet

JURY :

Rapporteurs

M. Gérard GRUAU, Directeur de recherche, UMR CNRS 6118, Université de Rennes 1

M. Erwin KLUMPP, Professeur, Institute of Bio and Geosciences, Forschungszentrum Jülich

Examineurs

M. Pierre ANSCHUTZ, Professeur, UMR CNRS 5805 EPOC, Université de Bordeaux

M. Gilles GUIBAUD, Professeur, PEIRENE-Eau EA 7500, Université de Limoges

Mme Delphine LATOUR, Maître de conférences HDR LMGE - UMR CNRS 6023, Université de
Clermont-Ferrand

Invités

M. Tim KESTENS, Ingénieur Environnement, EDF



Droits d'auteurs

Cette création est mise à disposition selon le Contrat :

« **Attribution-Pas d'Utilisation Commerciale-Pas de modification 3.0 France** »

disponible en ligne : <http://creativecommons.org/licenses/by-nc-nd/3.0/fr/>



Acknowledgement

I am pleased to express my gratitude to the people who have been continuously given me guidance and supports throughout my three years of study.

First of all, I would like to express my warmest and sincere gratitude to my three thesis directors, Prof. Véronique Deluchat, Dr. Malgorzata Grybos and Dr. Marion Rabiet for their guidance, encouragement and patience that pursued me to have this unique and very enriching experience.

Thank you to the members of the Jury: Prof. Gérard Gruau, Prof. Erwin Klumpp, Prof. Pierre Anschutz, Mrs. Delphine Latour and Mr. Tim Kestens for accepting to judge my work and for the interest and insightful comments you have shown in it.

Thank you to the PEIRENE laboratory, and more particularly to GRESE team who welcomed and supported me during these three years. I would like to thank the director of GRESE laboratory, Prof. Michel Baudu, for giving me the opportunity to work in the lab. Thank you to Patrice, Karine, Francois, Isabelle, Sophie, Mathias, Sylvain, Robin, Geneviève, Hélène, Virginie, Cédric. You have all participated in this 3-years fruitful research journey through your constructive advice, your analytical and technical experience and sharing supports that you have brought to me.

Thank you to the master trainees, Floriane and Hind for the help you had given me and for the support you had always expressed.

Thank you to my family and to my friends, Anne-lise, Noël, Marilia, Thibault, Claire, Maya, ... who have repeatedly expressed curiosity towards my work and continuously encouragement.

I would like to thank all of you for my lovely and unforgettable experience in Limoges. I wish all the best to you and your families.



Table of contents

Droits d’auteurs	2
Table of contents	4
Table of figures	6
Table of tables	10
Table of equations	12
General introduction.....	13
Part I. General background.....	16
I.1. Why do we study phosphorus mobility?.....	16
I.1.1. Phosphorus as a key role in limiting eutrophication	16
I.1.2. Sources of phosphorus in natural freshwater	17
I.1.3. Phosphorus cycle.....	20
I.1.4. Physico-chemical factors controlling phosphorus mobility at the water/sediment interface.....	23
Conclusion.....	26
I.2. Temporary storage of phosphorus in dam reservoir.....	26
I.2.1. Phosphorus entrapment in dam reservoir	26
I.2.2. Reservoir functioning and its impacts on within-system and downstream river	27
I.2.3. Dam reservoir management and impacts on within-system.....	29
I.2.4. Internal loads of phosphorus in reservoir.....	31
Conclusion.....	31
I.3. Why do we focus on colloidal fraction?	32
I.3.1. Colloids	32
I.3.2. Evidences on release of colloidal phosphorus at sediment-water interface	41
I.3.3. Is colloidal phosphorus bioavailable to organisms?.....	42
Conclusion.....	43
I.4. Current states of natural colloid extraction, separation, fractionation and characterization	44
I.4.1. Colloid extraction.....	44
I.4.2. Colloid separation	45
I.4.3. Colloid characterization	47
Conclusion.....	48
I.5. Global conclusion for literature review.....	63
Part II. Materials and methods.....	65
II.1. Studying area and sampling method.....	65
II.1.1. Characteristics of Champsanglard reservoir	65
II.1.2. Sampling methods	66
II.2. Laboratory experimentation.....	68
II.2.1. Isolation of colloids from sediment matrix.....	68
II.2.3. Incubation of sediment in anoxic/oxic alternation for investigation of colloidal P dynamic at sediment-water interface	71
II.3. Analytical methods	74
II.3.1. Particulate phase	74
II.3.2. Dissolved phase	78
Part III. Results and discussions.....	81

III.1. Impact of methods of sediment preconditionning, extraction and separation methods of colloids for sediment matrix	81
III.1.1. Introduction	81
III.1.2. How do colloid separation and sediment storage methods affect water-mobilizable colloids and phosphorus? An insight into dam reservoir sediment	83
III.1.3. Comparison of three methods of colloid extraction for characterization of mobilizable colloids from Champsanglard sediment.	104
III.1.4. Conclusion.....	117
III.2. Impacts of reservoir management on the size partitioning and mobilization of phosphorus from sediment.....	118
III.2.1. Introduction	118
III.2.2. Spatial distribution of water-mobilizable colloids from dam sediment and the risk of water-level fluctuation on phosphorus release	119
III.2.3. Conclusion.....	143
III.3. Effects of redox oscillation on the release of dissolved and colloidal phosphorus	144
III.3.1. Introduction	144
III.3.2. How does anoxia promote mobilization of P-bearing colloids from dam reservoir sediment?.....	145
III.3.3. Limitation of freeze drying pretreatment on quantification of colloid suspension.....	166
III.3.4. Conclusion.....	170
Part IV : General discussion and conclusion	171
IV.1. How sediment storage mode and colloid extraction/separation protocol influence on the quantity and quality of colloids recovered from sediment matrix?	171
IV.2. What is the potential of reservoir sediment to release colloids and colloidal P?	173
IV.3. The releasing risk of water-mobilizable P from reservoir sediment to water column	179
IV.4. Environmental aspects and impacts/practices	182
Bibliographic references.....	184
Appendix	218
Hybrid silica gel as a new tool for testing the bioavailability of colloidal P for phytoplankton uptake.	218
I. Introduction.....	218
II. Biotest for algal uptake of colloidal P	219
II.1 Preparation of colloidal suspension for embedding in silica gel	219
II.2. Hybrid silica gel (HSG)	220
II.3. Microorganismes, culture medium and incubation.....	220
III. Growth evolution of <i>Chlorella vulgaris</i> and <i>Microcystis aeruginosa</i> in response to colloidal P	223
IV. Algal uptake rate of phosphorus.....	225
V. Conclusion and perspective	226

Table of figures

Figure 1. The eutrophication progress of a water system with increase nutrient loads (P and N) (Glibert, 2017).....	16
Figure 2. Phosphorus trends in European rivers and lakes from 1992 to 2017. Data series were determined as average annual mean concentration of phosphate in 799 rivers and total phosphorus in 284 lakes (Waterbase-Water Quality, provided by European Environment Agency, https://www.eea.europa.eu/data-and-maps/indicators/nutrients-in-freshwater/nutrients-in-freshwater-assessment-published-9).....	19
Figure 3. Water pollution level (WPL) per river basin due to anthropogenic P loads (catchment runoff from agricultural, industrial and domestic sectors) to freshwater from 2002 to 2010 (Mekonnen and Hoekstra, 2018). WPL was estimated by grey water footprint (m^3/yr) dividing catchment runoff (m^3/yr).	19
Figure 4. Phosphorus cycle from terrestrial to aquatic environment with impacts of anthropogenic activities (simplified and adapted from (Worsfold et al., 2016)).....	20
Figure 5. The sequence of sedimentary diagenesis reactions (Froelich et al., 1979; Stumm and Morgan, 1995; Tromp et al., 1995; Aller, 2014).	23
Figure 6. Phosphate speciation in natural environments (Azam et al., 2019).	24
Figure 7. The bioturbation enhancing nutrient transport from sediment to overlying water during sediment resuspension induced by flow perturbation (Xie et al., 2018).	25
Figure 8. The vertical and horizontal zonation of a stereotypical deep reservoir with summer thermocline ending at 4°C at the bottom sediment (Ruhl et al., 2014).	27
Figure 9. Strategies for sediment management in dam reservoir (International Hydropower Association 2019).....	30
Figure 10. Simplified internal P cycle in reservoir adapted from (Cavalcante et al., 2018a).....	31
Figure 11. The interaction between two colloids described by DLVO theory with the total potential energy (V_T), repulsive energy due to electric double layer (V_R) and attractive energy due to Van der Waals (V_A). (1) corresponds to long Debye length at low electrolyte concentration. (2) corresponds to short Debye length at high electrolyte concentration. (Hamad-Schifferli, 2014).....	33
Figure 12. Electric double layer of colloidal particle (Park and Seo, 2011)	34
Figure 13. The distribution of different types of P-carrying colloids as function of pH and size in soil (Chen and Arai, 2020).	41
Figure 14. The surfaces of tortuous path membranes (1) 1.2 μm cellulose nitrate filter, (2) 1.0 μm glass fiber filter and polymer track-etched membrane (3) 1.0 μm polycarbonate filter. A: before filtration. B: after filtration of 10 mL soil suspension (S/L of 1/10). Images are taken from the work of Zirkler et al. (2012).	46
Figure 15. Schema for the mobility of water-mobilizable P (sized below 1 μm) in reservoir bottom sediment.	63
Figure 16. Watershed for Creuse river and location of the Age complex and champsanglard reservoir.	65
Figure 17. Geological map of Age complex watershed.	66

Figure 18. Localization of sampling sites in Champsanglard reservoir	67
Figure 19. Diagram for the examination of various sediment storage modes, colloids extraction and separation protocols.....	68
Figure 20. Schema for sediment incubation under oscillation between anoxic (closed system) and oxic (opened system) conditions	72
Figure 21. Size separation of water-mobilizable fraction (smaller than 1 μm) using successive filtrations	73
Figure 22. Colloid extraction and separation protocols applied on wet sediment.....	88
Figure 23. Variation in dry mass of the colloidal fraction sized 0.2 - 1 μm by means of different colloid separation protocols. The error bar depicted 1 SD.....	91
Figure 24. Effect of colloid separation protocols on the size distribution of the water-mobilizable fraction smaller than 1 μm , except for protocol "e", which presents the 0.2 - 1 μm fraction size. The error bar depicted 1 SD.	92
Figure 25. Impacts of colloid separation methods on the elemental composition, expressed per dry mass of sediment for: a) large colloidal fraction (0.2 - 1 μm), and b) fraction below 0.2 μm ; versus c) the concentration per dry mass of large colloids (0.2 - 1 μm). The error bar depicted 1 SD.	93
Figure 26. Distribution of water-mobilizable phosphorus extracted from wet sediment using five separation protocols. Large colloidal P sized from 0.2 – 1 μm . Small colloidal P sized smaller than 0.2 μm . Dissolved P represented dissolved inorganic phosphate in fraction smaller than 0.2 μm . The error bar depicted 1 SD.	95
Figure 27. Effect of the rewetting of previously air-, oven-, and freeze-dried sediments on the dry mass of colloids sized 0.2 - 1 μm . The employed colloid separation protocol was high-speed centrifugation combined with filtration (i.e. protocol “d”, Fig. 1). The error bar depicted 1 SD.....	97
Figure 28. Effect of the rewetting of previously air-, oven-, and freeze-dried sediments on the size distribution of the water-mobilizable fraction smaller than 1 μm . The employed colloid separation protocol was high-speed centrifugation combined with filtration (i.e. protocol “d”, Fig. 1). The error bar depicted 1 SD.	98
Figure 29. Impacts of the rewetting of previously air-, oven-, and freeze-dried sediments on the elemental composition, expressed per dry mass of sediment of: a) large colloidal fraction (0.2 - 1 μm), and b) fraction below 0.2 μm ; versus c) the concentration per dry mass of large colloids (0.2 - 1 μm). Extraction using the high-speed centrifugation protocol combined with filtration (i.e. protocol “d”, Fig. 1). The error bar depicted 1 SD.	98
Figure 30. Distribution of water-mobilizable phosphorus extracted from wet and rewetted previously air-, oven-, and freeze-dried sediments using the high-speed centrifugation protocol combined with filtration (i.e. protocol “d”, Fig. 1). Large colloidal P sized from 0.2 – 1 μm . Small colloidal P sized smaller than 0.2 μm . Dissolved P represented dissolved inorganic phosphate in fraction smaller than 0.2 μm . The error bar depicted 1 SD.....	101
Figure 31. Effect of colloid separation protocols on size distribution of fraction smaller than 0.2 μm : protocols “a” through “d” were separated by filtration, whereby protocol “e” was separated by centrifugation. <i>The error bar depicted 1 SD.</i>	103
Figure 32. Variation in dry mass of colloidal fraction sized 0.2 – 1 μm recovered from three modes of extraction.....	108

Figure 33. Effect of extraction protocols on the size distribution of water-mobilizable colloids: (A) size fractionation and (B) cumulative distribution.	109
Figure 34. Scanning electronic microscopic images of extracted colloids from Champsanglard sediments.	111
Figure 35. Impacts of extraction protocols on elemental masses of P, OC, Fe, Al, Ca, Mn and Mg in (a) large colloids sized 0.2 – 1 μm and (b) fraction smaller than 0.2 μm	112
Figure 36. Distribution of water-mobilizable phosphorus extracted from wet sediment using three colloid extraction protocols.	113
Figure 37. Distributions of (a) phosphorus (P) and (b) organic carbon (OC) in three size classes of water-mobilizable fraction smaller than 1 μm	114
Figure 38. Impacts of extraction protocols on elemental composition of recovered large colloids sized 0.2 – 1 μm , expressed by dry mass of colloids.	115
Figure 39. Sampling sites along Champsanglard dam reservoir (permanently submerged bottom sediments) and in two zones of water-level fluctuation (WFZ-1 and WFZ-2 areas; non-permanently submerged sediments) (<i>source : Geoportail, EPTB Vienne 2018</i>).	123
Figure 40. Sediment characteristics deposited along the reservoir (sites 1-9) and in WFZ-1 (8A, 8B, 8C) and WFZ-2 (9B) areas: (A) grain size distribution, (B) quantity of OM, Al, Fe, Ca, Mn, Mg and (C) amount of total phosphorus content and pH. WFZ - water-level fluctuation zone, OM – organic matter.	126
Figure 41. Size distribution of water-mobilizable colloids (< 1 μm): (A) along reservoir, (B) in WFZ-1 area and (C) in WFZ-2 area. WFZ stands for water-level fluctuation zone.	130
Figure 42. Spatial variability of large colloids (0.2 – 1 μm): (A) along reservoir, (B) in WFZ-1 area and (C) in WFZ-2 area. WFZ stands for water-level fluctuation zone.	130
Figure 43. Chemical composition (OC, Fe, Al, Ca, Mg, Mn) of large colloids presented in % of dry sediment, mg/g _{DW-Sediment} (A1-A3) and in % of dry large colloids, mg/g _{DW-Colloids} (B1-B3). WFZ stands for water-level fluctuation zone.	132
Figure 44. Distribution of water-mobilizable P: (A) along reservoir, (B) in WFZ-1 area and (C) in WFZ-2 area. WFZ stands for water-level fluctuation zone.	132
Figure 45. Size separation of water-mobilizable fraction (smaller than 1 μm) using successive filtrations.	149
Figure 46. Evolution of redox potential, pH, alkalinity throughout the incubation.	153
Figure 47. Evolution of water-mobilizable P release throughout the incubation.	154
Figure 48. Evolution of N-NH ₄ ⁺ and N-NO ₃ ⁺ concentration throughout the incubation.	155
Figure 49. Evolution of OC, Fe, Ca, Mg and Mn in water-mobilizable fraction during anoxic and oxic conditions.	157
Figure 50. Evolution of Fe ²⁺ in fraction below 10 kDa along the incubation.	158
Figure 51. The concentrations of total dissolved salts (TDS) and calculated colloidal concentration in freeze-dried fraction sample (< 1 μm). Data obtained from the incubation of fresh sediment under redox oscillation (see section II.2.3). Method of colloid quantification was freeze-drying of fraction below 1 μm	168

Figure 52. The concentration of colloidal fractions (10 kDa – 1 µm) estimated by sum of analyzed elements (P, OC*, Fe, Al, Ca, Mn, Mg) in fresh water-mobilizable fraction (below 1 µm) without freeze-drying. Data obtained from the incubation of fresh sediment under redox oscillation (see section II.2.3). *Colloidal concentration of OC was accounted for fraction 0.2 – 1 µm due to contamination from ultrafiltration material for fraction 10 kDa – 0.2 µm.....	168
Figure 53. Effect of water evaporation at 30°C (a) and freeze-drying (b) on structure of water-mobilizable fraction (including colloids and dissolved species).	169
Figure 54. Framework for selecting a method for of colloid extraction from a sediment matrix.	173
Figure 55. Variability in mass (mg/g _{DW-sediment}) and chemical composition of large colloids (mg/g _{DW-colloid}), and partitioning of water-mobilizable P between riverine and lacustrine regions of Champsanglard reservoir.....	175
Figure 56. Variabilities in mass (mg/g _{DW-sediment}) and chemical composition of large colloids (mg/g _{DW-colloid}), and partitioning of water-mobilizable P under downstream influence of tributaries.....	176
Figure 57. Variabilities in mass (mg/g _{DW-sediment}) and chemical composition (mg/g _{DW-colloid}) of large colloids, and partitioning of water-mobilizable P across two transects of water-level fluctuation zones (WFZ-1 and WFZ-2).....	177
Figure 58. Testing conditions for algal and cyanobacterial growth responding to colloidal P (test 3), in comparison with nutrient-rich medium (test 1) and nutrient-free medium (test 2). MA is annotated for <i>Microcystis aeruginosa</i> . CV is annotated for <i>Chlorella vulgaris</i>	222
Figure 59. Comparison of green algal growth curve (<i>Chlorella vulgaris</i>) and cyanobacteria (<i>Microcystis aeruginosa</i>) in different conditions: Test 1: M-Z8 culture medium, Test 2: P-free M-Z8 culture medium, Test 3: P-free M-Z8 containing HSG ; Test 4: M-Z8 culture medium containing HSG.	223
Figure 60. Photography of <i>M. aeruginosa</i> (left) and <i>C. vulgaris</i> (right) in different test mediums on day 9.	225
Figure 61. Comparison of residual dissolved inorganic phosphate (DIP) in culture medium of (A) <i>Chlorella vulgaris</i> and (B) <i>Microcystis aeruginosa</i> in different growing conditions: Test 1: M-Z8 culture medium, Test 2: P-free M-Z8 culture medium, Test 3: P-free M-Z8 containing HSG.....	226

Table of tables

Table 1. Characteristic of various trophic status in water (adapted from (Smith et al., 1999; Yang et al., 2008)).	17
Table 2. Sources of P in natural freshwater (adapted from (Azam et al., 2019)).	17
Table 3. Particle and colloidal properties of a mole of water versus spherical particle size. The specific area is applicable for spherical particles of specific gravity of 1.0, for other materials, divide this number by the specific gravity of the solid material for the given particle radius (Bajpai, 2018; Biermann, 1996).	35
Table 4. The classification and some common examples of colloids in natural environment (Kretzschmar et al., 1999).	36
Table 5. The classification of colloids based on size ranges.	44
Table 6. Colloid separation using filtration, centrifugation, and the combination.	49
Table 7. Colloid fractionation using field-flow fractionation.	55
Table 8. Colloid fractionation using cross-flow ultrafiltration (CFF).	59
Table 9. Application of other separation methods.	61
Table 10. Composition of synthetic water simulating the major elemental composition of bottom water in Champsanglard reservoir.	72
Table 11. List of analysis for each fraction during one sampling day for redox oscillation experiment.	74
Table 12. Characteristics of sediment collected in the Champsanglard dam reservoir.	87
Table 13. Determination of colloidal and dissolved P through size fractionation of PWM.	107
Table 14. The percentage of analysis detecting the presence of a given element in recovered sedimentary colloids. Chemical composition of colloids was determined by SEM-EDS analysis based on the number of total independent analysis of 22 for colloids recovered by agitation, 12 by sonication at pH_{sed} and 47 by sonication at pH_9 .	115
Table 15. The variation in solution chemistry before and after extraction by three different modes: agitation, sonication at pH_{sed} and sonication at pH_9 .	116
Table 16. Chemical composition of sediment along reservoir and at two zones of water-level fluctuation (WFZ-1 and WFZ-2).	127
Table 17. Chemical composition of the fraction below $0.2 \mu m$ (in mg per g dry sediment) along reservoir and at two zones of water-level fluctuation (WFZ-1 and WFZ-2).	128
Table 18. Chemical composition of large colloids (fraction $0.2 - 1 \mu m$) in mg/g dry sediment along reservoir and at two zones of water-level fluctuation (WFZ-1 and WFZ-2).	129
Table 19. Chemical composition of large colloids ($0.2 - 1 \mu m$) expressed in mg per g dry colloids along reservoir and at two zones of water-level fluctuation (WFZ-1 and WFZ-2).	131
Table 20. Elemental colloid-sediment ratio (R) corresponding to the amount of an element in a large colloidal fraction (expressed in mg/g of dry weight colloids, Table 19) to the amount of a given element in the sediment (mg/g of dry weight sediment, Table 16).	138

Table 21. Correlation coefficient (R^2) between elemental concentrations in sediment and various sediment size fractions.	142
Table 22. Correlation coefficient (R^2) between element concentrations in large colloids (0.2 – 1 μm) for lacustrine regions (accounted for sites 1, 2, 4, 5 and excluded impacts of tributary entrance at site 3).....	143
Table 23. The chemical analysis of different size class subfractions of water-mobilizable extract.	151
Table 24. Sediment characteristics.....	152
Table 25. Comparison in water-mobilizable P, small/nano and large colloidal P release from sediment under various conditions (mechanical resuspension and changing redox condition) between riverine and lacustrine areas and between bank and bottom deposition. Releasing condition of resuspension refers to agitation of sediment under laboratory condition (orbital agitation at 200 rpm, results showed in Part III.2). Releasing condition under oxic phase refers to gentle agitation under the first oxic phase of redox changing experiment (results showed in Part III.3.2). Releasing condition under anoxic phase refers to gentle agitation under the anoxic phase of redox changing experiment (results showed in Part III.3.2).....	180
Table 26. Comparison of the content of large colloidal OC, Fe, Al and Ca released from sediments under various conditions (mechanical resuspension and changing redox condition) between riverine and lacustrine regions and between bank and bottom deposition. Releasing condition of resuspension refers to sediment agitation under laboratory condition (results showed in Part III.2). Releasing condition under oxic phase refers to gentle agitation under the first oxic phase of redox changing experiment (results showed in Part III.3.2). Releasing condition under anoxic phase refers to gentle agitation under the anoxic phase of redox changing experiment (results showed in Part III.3.2).....	181
Table 27. Composition of M-Z8 medium.....	221
Table 28. Sampling planification and the analysis for each sampling day during biotest for colloidal P bioavailability in two species <i>Microcystis aeruginosa</i> and <i>Chlorella vulgaris</i>	223
Table 29. Growth rate of <i>C. vulgaris</i> and <i>M. aeruginosa</i> in different test mediums.....	225

Table of equations

Equation 1. Formula to determine particle diameter after gravitational sedimentation.	69
Equation 2. Formula to determine centrifugation speed and time.	70
Equation 3. Formula to determine angular velocity of centrifuge.	70
Equation 4. Formula to convert revolution per minute (rpm) to relative centrifugal force (g).	70
Equation 5. Calculation of sediment Siccity.	74
Equation 6. Formula to determine bulk density.	75
Equation 7. Formula to determine porosity.	75
Equation 8. Formula to determine particle density.	75
Equation 9. Formula to estimate organic matter content (in %) from loss on ignition.	76
Equation 10. Determination of colloid concentration in extracted solution (in mg/L).	76
Equation 11. Determination of colloid concentration in dry weight of sediment (in mg/g _{DW-Sed}).	76
Equation 12. Determination of total sedimentary phosphorus.	77
Equation 13. Measurement of dissolved inorganic phosphorus according to method of Murphy and Riley, (1962).	77
Equation 14. Dilution factor used in measurement of total phosphorus.	77
Equation 15. Determination of sediment dry mass to calculate total sedimentary phosphorus.	78
Equation 16. Formula to correct redox potential according to standard hydrogen electrode.	79
Equation 17. Estimation of colloidal concentration (CC ₁) by subtraction of concentration of water-mobilizable fraction (C _{WM}) to total dissolved salts (TDS). C _{WM} was determined after freeze-drying water-mobilizable fraction.	167
Equation 18. Estimation of colloidal concentration (CC ₂) as the sum of colloidal concentrations (ΣCC _i) of analyzed elements “i” varying among P, OC, Fe, Al, Ca, Mn, Mg) in fraction 10 kDa – 1μm.	167

General introduction

Phosphorus (P), an essential nutrient for primary production, is considered as one of the key limiting factors together with nitrogen (N) in controlling freshwater eutrophication (Conley et al., 2009). Eutrophication (consisting in excessive nutrient enrichment of water) may cause a wide range of negative effects in aquatic ecosystems (degradation of water quality, loss of biodiversity, algal and cyanobacteria bloom, limitation of recreational uses...).

Despite important efforts in controlling anthropogenic input of P to natural freshwater systems (the controlled use of P fertilizer, phosphate ban in detergents, wastewater treatment improved for P removal) that allowed a marked decrease in average phosphate concentration in European rivers, the freshwater eutrophication was not attenuated and is still considered as a priority issue in particular in lake and reservoirs systems.

One of the reasons put forward to explain this delay in the recovery of reservoir water quality is the presence of an internal P stock in sedimentary compartment, which can be mobilized in water and contributes to maintain or trigger eutrophication.

Indeed, it is well-known that P has strong affinity to solid phases, such as soil, sediment or suspended particulate and colloidal matters. Consequently, transporting in rivers flow, P can accumulate in low-energy water systems, such as lake and reservoir sediments (Maavara et al., 2015). Thousands of large artificial dams have been built to response to the raising demand for renewable energy sources since the past few decades. In spite of numerous benefits, such as flood control, water supply, electricity production, these engineering structures interrupt the continuity of water flow and sediment transport, thus alter fluvial morphology. The changing flow regime of water by dam construction is associated to change in material flows. It is estimated that global large dam reservoirs can trap 30 % of river sediment and could cause about 17 % of global river P flux to be sequestered by 2030s (Vörösmarty et al., 2003; Maavara et al., 2015).

In sediment, phosphorus is associated (via sorption, (co)precipitation or occlusion) to organic and inorganic phase (clay mineral, Fe, Al, Mn oxy(hydr)oxides, carbonates, calcium, etc.). The P trapped in reservoir sediment could return to overlying water in various forms, mainly in dissolved (for example phosphates) and/or suspended forms. The release of phosphates is a function of complex mechanisms (dissolution/precipitation, desorption/adsorption, organic matter mineralization) depending on physico-chemical parameters such as oxygen level, temperature, pH, hydrological conditions, bioturbation, etc. In addition, P can also be reloaded to the water column in dissolved, colloidal and particulate form when sediment is resuspended.

Up to date, studies of P mobility at the sediment/water interface have focused mainly on dissolved P, which is the most bioavailable form of P for plankton uptake (Kowalczywska-Madura et al., 2018). However, this view neglects an important, very highly mobile and potential bioavailable colloids; and thus, limits the understanding of sedimentary P mobility in reservoirs.

The mobilization of sedimentary colloidal P in reservoir context have never been illustrated elsewhere, whereas a plethora of studies in soil system showed that colloids are effective carrier of P.

Colloids are omnipresence in natural environment. They are heterogenous in size and composition (organic, mineral, organo-mineral), and generally have surface charges allowing association with various nutrients and contaminants, including P (Stumm, 1993; Doucet et al., 2007; Van Riemsdijk et

al., 2007). The carrying of P by colloids is well established in soil surface runoff and leachate, forest stream water or wetlands (Heathwaite et al., 2005; Zang et al., 2013; Bol et al., 2016; Gu, 2017).

The presence of colloidal P is often observed in the water of rivers, lakes and reservoirs. For instance, the delivery of colloidal P in runoff water from agriculture land to river sediment had been pointed out by He et al., (2019). Upon sediment resuspension or change in water chemistry, this colloidal P could be liberated back to water column, probably at comparative level with dissolved P. Moreover, freshly colloids can be directly produced in water, *e.g.* by degradation of particulate organic matter and its association with dissolved cations or in the area at the boundary of the anoxic/oxic through the formation of secondary minerals (precipitation of iron and/or manganese). The colloids could also be generated in the sediments, *e.g.* the formation of colloidal FeS (Noël et al., 2020).

Therefore, according to little knowledge on the potential of sediment to release colloidal P, as well as on their favorable release in reservoir context, the aim of this thesis is to evaluate the potential of reservoir sediments to release water-mobilizable colloids, and to characterize them (quantity and composition). A special attention is paid to their involvement in P mobility. In this context, the objectives which are attempted to be achieved in this thesis are following:

1. What is the impact of river damming on the level and distribution of colloids and associated P in sediment throughout the length and the width of reservoir?
2. What is the key parameter involved in the variability of colloids and associated P in reservoir sediment?
3. What is the preferential condition for the release of colloidal P from sediment to water-column?
4. What is the potential of colloidal P to be available for phytoplankton uptake?

To answer these questions, the experimental part of this work was conducted with sediments collected in Champsanglard dam reservoir (Creuse, France). This reservoir was chosen because it has been previously demonstrated to contain P-rich sediment and exhibit temporal anoxic surface sediment that involved in high P release (dissolved and colloidal form sized below 0.45 μm) at sediment-water interface (Rapin, 2018).

The present PhD thesis is divided into four parts.

The first part provides a bibliographic overview about the topic, including the biogeochemical cycle of P, the impacts of dam reservoir in trapping riverine P, the role of colloids as P bearing phase. Finally, the state-of-art for colloid recovery and characterization in natural environment is presented.

The second part presents the studied site, experimental conditions, equipment and analysis methods used to produce this work.

The third part addresses to answer the objective questions in form of three subordinations:

- (1) Evaluating proper method to recover colloids, considering sediment storage, colloids extraction and separation protocols.
- (2) Exploring the spatial distribution (longitudinal and lateral) of colloids and associated P along the reservoir. To access to the key parameters controlling the distribution and mobility of sedimentary colloids, the following were considered: channel characteristics, sediment grain size and chemical composition, and the amount and quality of colloidal and dissolved fraction.

(3) Investigating the effect of changing redox condition on the mobility of colloidal P. The chemistry of solution (Eh, alkalinity) and elemental composition of colloidal and dissolved fractions were considered to identify the key parameters controlling colloids and associated P mobility.

Each subordination is presented in form of publication article.

The fourth part devotes to a general discussion and conclusion encompassing the main outcomes of this thesis. A framework to choose the best colloid recovery method will be proposed. The conditions of reservoir sediment that would induce the highest colloids and associated P release will be discussed and some implications for dam management will be proposed.

An appendix includes the development of hybrid silica gel materials doped with natural P-colloids as a novel technique for the assessment of colloids bioavailability.

Part I. General background

I.1. Why do we study phosphorus mobility?

I.1.1. Phosphorus as a key role in limiting eutrophication

Eutrophication is a raising global environmental crisis on water quality impairment in the past few decades and causes negative and harmful impacts on many marine and freshwater areas worldwide (Smith, 2003; Ferreira et al., 2011; Glibert, 2017; Le Moal et al., 2019).

The term eutrophication was initially used to describe the natural aging process of aquatic system independently to human activities (Anderson et al., 2002). Recently, due to the dramatically increasing nutrients runoff from anthropogenic activities, the term eutrophication eventually becomes an appellation for the human-induced accelerated nutrient addition in lakes, rivers, reservoirs, estuaries and coastal marine water and results in the rapid and massive proliferation of aquatic plants, microalgae and cyanobacteria (Cordell and White, 2011; Chislock et al., 2013). Diffuse nitrogen (N) and phosphorus (P) release are the two major drivers of eutrophication in many freshwater and marine water body (Le Moal et al., 2019). These two nutrients are vital to biological processes in aquatic ecosystems; however, their immoderate input lays stress on the whole ecosystems by a series of adverse effects: increasing algal biomass, development of pervasive macrophytes, water deoxygenation, alteration of the food web structure and production of toxins from cyanobacteria. Eutrophication induces thus water quality alteration and biodiversity decrease (Fig. 1).

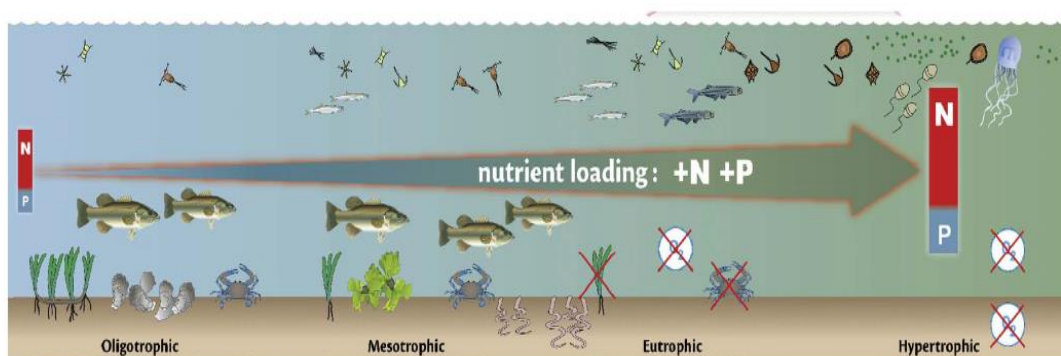


Figure 1. The eutrophication progress of a water system with increase nutrient loads (P and N) (Glibert, 2017).

Both N and P have been considered as limiting nutrients for algal proliferation, thus the reduction input of the dual nutrients is essential and judicious to control eutrophication in aquatic ecosystems (Correll, 1998; Conley et al., 2009; Schindler et al., 2016). Table 1 presents the various trophic status in water, considering N and P concentrations. However, P receives greater awareness than N in freshwater systems. In many lakes, the presence of P even at very low concentration (few micrograms per liter) showed ability to support bloom. A phosphate concentration of 10 $\mu\text{g/L}$ is already enough to support development of plankton and concentrations from 30 to 100 $\mu\text{g/L}$ or higher will be likely to promote blooms (Smith, 2003). The common indicator for eutrophication is phytoplanktonic blooms (Ferreira et al., 2011). Some cyanobacteria can fix nitrogen from the atmosphere thanks to heterocyst (Grover et al., 2020; Wang et al., 2018). The N_2 -fixing capability of cyanobacteria helps them to overcome N deficiency and maintain growth independently of N input. Therefore, P is considered as eutrophication limiting factor in continental waters, as demonstrated by (Smith and Schindler, 2009).

Table 1. Characteristic of various trophic status in water (adapted from (Smith et al., 1999; Yang et al., 2008)).

Eutrophic status	Total P (µg/L)	Total N (µg/L)	Total nutrient status index	Chlorophyll-a (µg/L)	Secchi depth (m)
Oligotrophic	5 – 10	250 – 600	0 – 30	< 3.5	> 4
Mesotrophic	10 – 30	601 – 1100	31 – 60	3.5 – 9	2 – 4
Eutrophic	31 – 100	1101 – 2000	61 – 100	9 – 25	1 – 2
Hypereutrophic	> 100	> 2000	> 100	> 25	< 1

I.1.2. Sources of phosphorus in natural freshwater

Phosphorus is the twelfth most abundant element in the lithosphere (Reynolds and Davies, 2001) and the sixth major elements in human body (Salm et al., 2015). P is found on the surface of the Earth in combination with metals, halogens, sulphur, nitrogen, and oxygen. P compounds are not volatile, except the trace volcanic emissions of phosphines and atmospheric transportation of P is mainly with plant pollen, water droplets, dusts, and particulates (Correll, 1998; Glindemann et al., 2004). However, the atmospheric flux rates (0.1-0.4 kg P/ha/yr) are minor in comparison to surface water flux (3.4-10.1 Mt P/yr) (Glenn et al., 2000; Decina et al., 2018; Berthold et al., 2019; Alewell et al., 2020). P in water can derive from natural sources such as plant and animal residues, natural runoff and erosion of rocks and soils, but also from anthropogenic sources such as chemical phosphorus manufacture, agricultural activities (1.7-20 kg P/ha/yr), urban runoff and sewage (2.34 kg P/ha/yr), industrial uses of phosphorus-based chemicals (Alewell et al., 2020; Gs et al., 2017) (Table 2).

Table 2. Sources of P in natural freshwater (adapted from (Azam et al., 2019))

Natural sources	Anthropogenic sources		
	Agricultural	Domestic	Industrial
Surface runoff	Livestock production	Urban runoff	Chemical manufacture
River inflow	Fertilizers	Solid waste disposal	Metal treatment
Fauna and flora decomposition	Managed forests	Detergents	Water treatment
Atmospheric deposition			Phosphorus mining

I.1.2.1. Natural sources

P is a naturally occurring element in minerals, soils and living organisms. In geochemical viewpoint, there are four main sources of P as followed (Ruttenberg, 2019; Schröder et al., 2011):

- (1) tectonic uplift and exposure of phosphorus-bearing rocks to the forces of weathering,

- (2) physical erosion and chemical weathering of rocks producing soils and providing dissolved and particulate P to rivers,
- (3) riverine transport of P to flood plains, lakes, and oceans,
- (4) sedimentation of P associated with organic and mineral matter and burial in sediments.

Generally, P occurs in rocks as igneous apatite deposits such as apatite $\text{Ca}_{10}(\text{PO}_4)_4(\text{F}, \text{Cl}, \text{OH})_2$, lazulite $(\text{Mg}, \text{Fe})\text{Al}_2(\text{PO}_4)_2(\text{OH})_2$, strengite $\text{FePO}_4 \cdot 2\text{H}_2\text{O}$, vauxite $\text{FeAl}_2(\text{PO}_4)_2(\text{OH})_2 \cdot 6\text{H}_2\text{O}$, vivianite $\text{Fe}_3(\text{PO}_4)_2 \cdot 8\text{H}_2\text{O}$, and variscite $\text{AlPO}_4 \cdot 2\text{H}_2\text{O}$ (Azam et al., 2019). The natural reservoirs of phosphorus-bearing rock are estimated to be 37 trillion tons and distributed unevenly around the Earth's surface with major stocks in Morocco, United States and South Africa (FAO, 2004). Weathering of those rocks, especially the apatite, results in the dissolution of the more soluble components surrounding phosphate deposits (Filippelli, 2008). Other natural sources of P in receiving water comprise organic matter (OM) such as plant residues, wild animal, and bird wastes, leaching and water erosion from watersheds. The decomposition of those OM liberates organic and inorganic P to receiving water. Those natural sources of P are considered as non-point sources because they diffuse P generally with surface runoff (Edwards and Withers, 2007; Filippelli, 2008).

I.1.2.2. Anthropogenic sources

Most anthropogenic usage of P is supplied from P mining industry. Phosphate rock mining provides 19 million tons per year (Mt/yr) of P for fertilizer production and other part used in industry (Schröder et al., 2011). The environmental pollution related to P in aquatic environment has increased since several decades. P has been used widely in many sectors such as food processing, agriculture, industry, and it is found in fertilizers, animal manure, detergents, anti-lime scaling in cooling systems or boiler water systems.

The main sources of intensive anthropogenic load of P are extensive practice of fertilizers in agriculture, deforestation, soil erosion, domestic and industrial discharges (Filippelli, 2008; Southam et al., 2008). Over the past 50 years, the mining of phosphate rock has transferred about half million tons of P to the hydrosphere (Cordell and White, 2011). Approximately 90 % of total mined P is used in agricultural practices and 9 % in industrial application (Schröder et al., 2011). The increase of domestic and industrial wastes together with non-point discharges from overfertilized agricultural practices, deforestation, and leaching from urban waste disposal have enhanced the P transfer from terrestrial to aquatic systems (Ruttenberg, 2003). It has been estimated that up to 25 % of annually applied P was served for growing crop, the other 75 % became retained in the soil or lost to water (Bomans et al., 2005).

With the practice of phosphorus legislation in agriculture, the improvement of urban wastewater treatment and the polyphosphate ban in detergents, positive effects have been achieved in European water quality (Fig. 2), the number of water bodies has been impacted by nutrient pollution decrease to 28 % (European Environment Agency, 2018). The anthropogenic input of P to environmental water are now dominantly originated from non-point sources such as runoff from agricultural land (20 % of mined P), managed forest and urban runoff; meanwhile about only 6 % of total P losses coming from point sources (Rittmann et al., 2011; Macintosh et al., 2018). The discharge of P to environment causes severe pollution in many river catchments around the world (Fig. 3). Most of P in diffuse runoff is associated to particles and, thus, settle down in wetlands, rivers, reservoirs, and lakes (Macintosh et al., 2018).

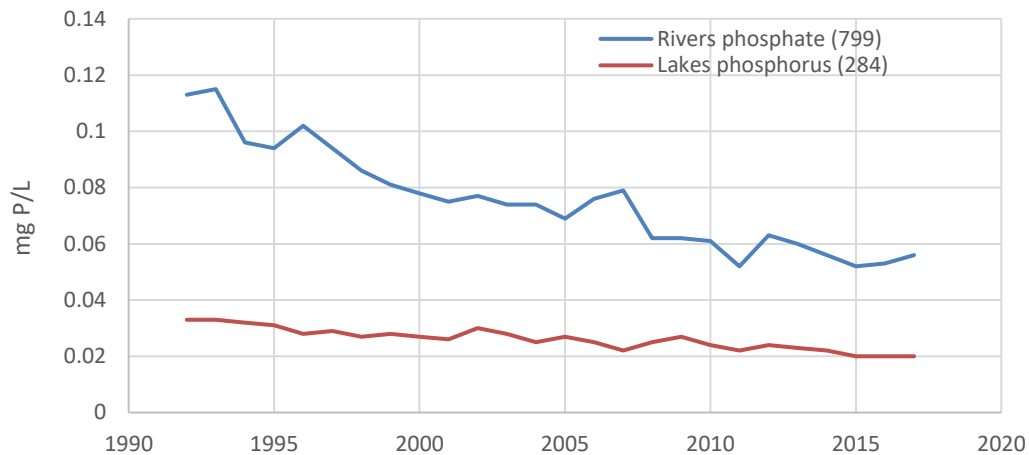


Figure 2. Phosphorus trends in European rivers and lakes from 1992 to 2017. Data series were determined as average annual mean concentration of phosphate in 799 rivers and total phosphorus in 284 lakes (Waterbase-Water Quality, provided by European Environment Agency, <https://www.eea.europa.eu/data-and-maps/indicators/nutrients-in-freshwater/nutrients-in-freshwater-assessment-published-9>)

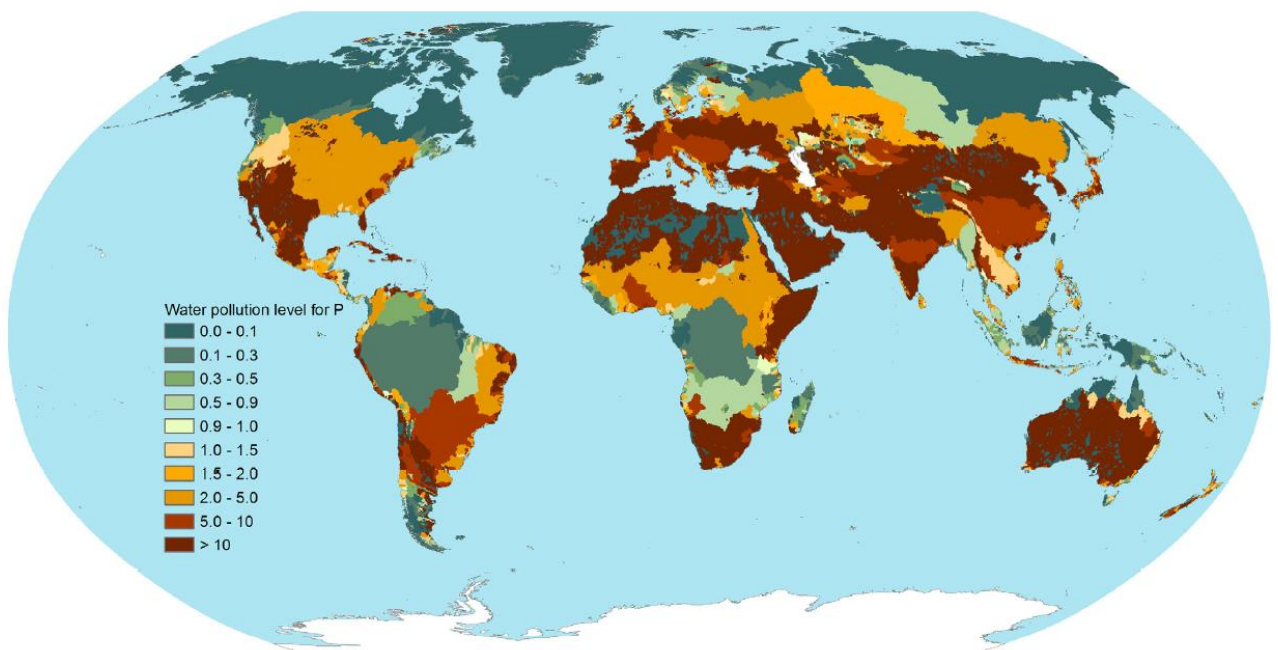


Figure 3. Water pollution level (WPL) per river basin due to anthropogenic P loads (catchment runoff from agricultural, industrial and domestic sectors) to freshwater from 2002 to 2010 (Mekonnen and Hoekstra, 2018). WPL was estimated by grey water footprint (m^3/yr) dividing catchment runoff (m^3/yr).

Figure 4 presents a simplified P cycle in environment. Input of phosphorus in aquatic environment has been accelerated by anthropogenic activities since the transfer of dissolved P from soil to receiving waters has been doubled from the pre-industrial time of approximately 2-3 Mt/yr up to nowadays input of 4-6 Mt/yr (Filippelli, 2008).

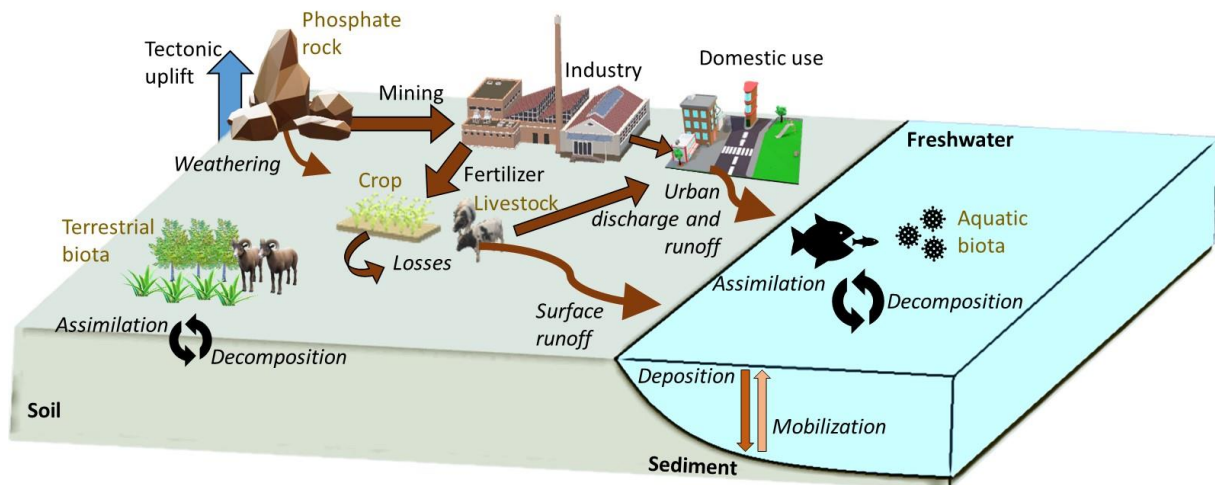


Figure 4. Phosphorus cycle from terrestrial to aquatic environment with impacts of anthropogenic activities (simplified and adapted from Worsfold et al., (2016)).

In reservoir, P is mainly derived from external loads (upstream transport, surface runoff, anthropogenic emissions) and internal loads of P (from sediments) (Wen et al., 2020). The decline of total P concentration in lakes and reservoirs occurs gradually and at lower intensity compared to riverine phosphate concentration decrease, because the P stored in bottom sediment can be released to water column and maintain high P level in reservoir despite the effort in P input control (European Environment Agency, 2018). Therefore, more efforts are needed in controlling the dynamics of P sources in relevant to ecological context to target the environmental remedial actions.

Within the Water Framework Directive of the European environmental policies (2000/60/EC), phosphorus is defined as one of the most critical parameters to achieve good quality objectives in water bodies and was put into the European sustainable phosphorus platform (ESPP). The further perspectives of this platform are set to reduce phosphorus emissions from municipal wastewater and agricultural losses, action plans to reduce phosphorus levels in rivers and lakes taking into account all sources (urban wastewater, small sewage discharge, non-point sources and phosphorus stocks in sediments), nutrient recovery and recycling. The ESPP brings together a range of both industry sectors and stakeholders regarding sustainable phosphorus management, for the core objectives are reducing phosphorus losses to the environment (in order to limit eutrophication) and developing phosphorus recycling (considering P resource depletion).

I.1.3. Phosphorus cycle

Terrestrial systems of phosphorus are the principal reservoir of P with three major pools: bedrock (10,000 – 38,000 Mt P in mineable rock), soil (96,000 – 200,000 Mt P), and terrestrial biota (2600 - 3000 Mt P) (Ruttenberg, 2003; Worsfold et al., 2016).

Phosphorus is weathered from sedimentary rock to soil solution by the dissolution of phosphorus-bearing minerals such as apatite ($\text{Ca}_{10}(\text{PO}_4)_6(\text{OH},\text{F},\text{Cl})_2$), the most abundant primary P-mineral family in crustal rocks. Weathering reactions are driven by exposure of minerals to naturally occurring acids in rainwater or derived from microbial activities, organic matter degradation and in the vicinity of plant roots (Filippelli, 2008). Solubilized phosphorus (phosphates) during weathering is available for uptake

by terrestrial plants which are then consumed by animals. P is returned to the soil and soil water by the decay of litterfall, animal excretion and death (Likens and Loucks, 1978). The erosion of soil material and the leaching of P through surface and subsurface runoff transfer P from soil to river in particulate, colloidal and dissolved forms. Within aquatic environment, particulate P deposits to bottom sediment while the dissolved labile P can be used and accumulated by aquatic biota (Worsfold et al., 2016). The sedimentation of phosphorus-containing compounds from the dead bodies or wastes of aquatic organisms will latter settle down. Through several geochemical processes, phosphorus retained in sediment can then mobilized to upper water layer and again be available for aquatic organisms.

During chemical weathering of sedimentary rock, phosphorus, as well as other rock-derived plant nutrients such as potassium or calcium, are leached to the environment in both available and unavailable forms (Ruttenberg, 2014). In all biological active fractions and in important minerals, P principally corresponds to the ions of orthophosphoric acid, which are soluble in water as orthophosphate anions PO_4^{3-} , HPO_4^{2-} , H_2PO_4^- with varying proportions according to pH.



Phosphates have high binding affinity for many metals. Orthophosphates of alkaline earth and transition elements such as iron (Fe), aluminum (Al), manganese (Mn) and calcium (Ca) are highly insoluble except under acidic leaching, and they represent the dominant geochemical forms of the global phosphate residues (Reynolds and Davies, 2001). Those secondary P minerals have different dissolution rates depending on the size of the minerals and the soil pH (Shen et al., 2011). The higher soil pH favors the solubility of Fe and Al phosphates meanwhile decreases the solubility of Ca phosphate (Hinsinger, 2001).

The sorption of phosphate on Fe and Al oxy(hydr)oxides are in great concern in terrestrial systems since these processes can limit the availability of P (Guzman et al., 1994). In the whole manuscript, oxy(hydr)oxides referred to both oxides, hydroxides and oxy(hydr)oxides. The bioavailability of orthophosphates is strongly driven by the ion exchange for hydroxyls on the surface of metal oxides that they are immobilized on. They also co-precipitate within or be included in the molecular matrices of metal oxy(hydr)oxides (Reynolds and Davies, 2001). The association of Fe and Al with organic matter (OM) are one important sink of phosphate, while phosphate bonding to clay lattices is a less efficient scavenger than oxy(hydr)oxides (Ruttenberg, 2014). The P sorption varies relatively with mineralogy and morphology of oxy(hydr)oxides, for instance, goethite is more efficient support than hematite. The poor crystalline Fe/Al oxy(hydr)oxides have higher reactive surface area and further higher sorption capacity than crystalline Fe-Al oxy(hydr)oxides (de Mesquita Filho and Torrent, 1993; Duiker et al., 2003).

The adsorption-desorption and precipitation-dissolution reactions of phosphates highly influence bioavailability of P in soils. In acidic soils, P is mainly associated to Fe/Al oxy(hydr)oxides (Parfitt, 1989) while in neutral to calcareous soil, P is dominantly under precipitated forms with Ca (Arai and Sparks, 2007). The redox-sensitive Fe and Mn oxy(hydr)oxides can undergo reductive dissolution when the redox potential is under +200 mV/ESH and induce P release back to the soil solution (Reynolds and Davies, 2001). In contrary, increase in redox potential leads to the oxidation of ferrous iron in ferric iron

that can precipitate as ferric oxy(hydr)oxides (eg. $\text{Fe}(\text{OH})_3$) and scavenging dissolved phosphates, resulting in the immobilization of phosphate and reduced availability for biological uptake. Furthermore, the degradation of organic matter is a great source of dissolved inorganic and organic phosphorus (Blackwell et al., 2009). P can also be desorbed by the competition with organic acids for sorption site and the alteration of bonding energy of sorbed P (Fink et al., 2016; Lindegren and Persson, 2009). Chemical interaction between organic matter and phosphates is another important process in soil solution. Humic substances can strongly form surface complexes with metals, especially Al(III) and Fe(III), by carboxylic and phenolic groups (Tipping, 2002). Orthophosphate ions are not bound directly to humic molecules but bound to Al or Fe at the surface of humic substance in similar mechanism to Fe/Al oxy(hydr)oxides. Phosphate anions compete with OH^- or H_2O via ligand exchange (Lindegren and Persson, 2009). Humic-Metal (Al or Fe) support have high P sorption capacities and are sometimes dominant P species in soil solution. At pH below 5, the stability of these humic-metal complexes decreases leading to the release of Al and Fe along with P, and thus contribute to P availability (Gerke, 2010; Urrutia et al., 2014).

Phosphorus enters receiving water via several pathways, primarily from water-born, in a mixture of dissolved, colloidal and particulate loads. About 90 % of P input is associated with particulate matter since P has high affinity to solid. Dissolved phosphorus in rivers is in both inorganic and organic forms. From 20 to 40 % of phosphorus in suspended particulars are organic; particulate inorganic P is shared mainly between ferric oxy(hydr)oxides and apatite (Cosmidis et al., 2014; Ruttenger and Berner, 1993). Aluminum oxy(hydr)oxides and clays may also be significant carriers of phosphorus (Shen et al., 2011).

Once P has been transported to receiving water, the soluble phosphorus can either stay in solution, or be scavenged by Fe/Mn/Al oxyhydroxide colloids and particulates, or be assimilated directly by bacteria, algae and plants. Particulate P may settle to bottom sediments where the microbial communities consume these organic constituents and release P back to water column as free orthophosphates (Correll, 1998). In low retentive aquatic basin, P can be flushed to downstream without chemical modification or biotic uptake and become biomass supportive in downstream river and ocean. In lakes and reservoirs that have longer retention time, P can be consumed by microorganisms, but also acts as suspended particulate loads and settle at the bottom sediment (Reynolds and Davies, 2001). All the algal cells and bacterial excreta are considered as a part of autochthonous sedimentary flux (Reynolds and Davies, 2001). In general, excluding influences from hydraulic residence time and bathymetry, sediments are likely a substantial destination and trap for P loads in water bodies (Maavara et al., 2015).

At bottom sediment, deposited P is subjected to several complex diagenesis processes, which are driven by the sequence of redox reactions and the organic matter mineralization via microbial activities. One third of organic matters can be decomposed by oxidation within one day and another second one third requires weeks to months to be degraded, meanwhile the last third portion constituted of mainly cellulose and skeletal that are considered as recalcitrant (Reynolds and Davies, 2001). At the surface layer of sediment, the mineralization of freshly deposited biogenic P can release phosphate. A portion of phosphate mobilized at this stage transfers to interstitial pore water, which latterly moves to overlying water via diffusion or advection, whereas the other portion is susceptible to chemical interactions with other sediment constituents. Phosphates are rapidly sorbed onto the surface of metal oxy(hydr)oxides or of clay minerals, forming the “readily bioavailable” or “conditionally available” fraction. Ferric oxy(hydr)oxides present a high affinity to phosphate; thus, a high capability of P immobilization and at some extents, the ferric-bound P is stated as the largest pool of P in most of freshwater lake sediments (Reynolds and Davies, 2001). Calcium carbonate and apatite are also efficient support in trapping free phosphates by coprecipitation. The CaCO_3 sedimentation contributes little to P transformation but

importantly in the permanent burial of P (Hupfer et al., 1995). The degradation of organic matter occurs through a vertical sequence of oxido-reduction reactions (Reynolds and Davies, 2001). The depletion of oxygen underneath the sediment-water interface allows a suit of reduction of nitrate, manganese (IV), iron (III), sulfates and finally organic carbon (Fig. 5) (Froelich et al., 1979; Postma and Jakobsen, 1996; Anschutz et al., 2007).

Process	Reaction	$\dagger \Delta G^\circ$
(1) <i>Aerobic respiration</i>	$(\text{CH}_2\text{O})_x(\text{NH}_3)_y(\text{H}_3\text{PO}_4)_z + (x+2y)\text{O}_2 \rightarrow x\text{CO}_2 + (x+y)\text{H}_2\text{O} + y\text{HNO}_3 + z\text{H}_3\text{PO}_4$	-475
(2) <i>Nitrate reduction</i>	$5(\text{CH}_2\text{O})_x(\text{NH}_3)_y(\text{H}_3\text{PO}_4)_z + 4x\text{NO}_3^- \rightarrow x\text{CO}_2 + 3x\text{H}_2\text{O} + 4x\text{HCO}_3^- + 2x\text{N}_2 + 5y\text{NH}_3 + 5z\text{H}_3\text{PO}_4$	-448
(3) <i>Manganese reduction</i>	$(\text{CH}_2\text{O})_x(\text{NH}_3)_y(\text{H}_3\text{PO}_4)_z + 2x\text{MnO}_2 + 3x\text{CO}_2 + x\text{H}_2\text{O} \rightarrow 2x\text{Mn}^{++} + 4x\text{HCO}_3^- + y\text{NH}_3 + z\text{H}_3\text{PO}_4$	-349
(4) <i>Iron reduction</i>	$(\text{CH}_2\text{O})_x(\text{NH}_3)_y(\text{H}_3\text{PO}_4)_z + 4x\text{Fe}(\text{OH})_3 + 3x\text{CO}_2 + x\text{H}_2\text{O} \rightarrow 4x\text{Fe}^{++} + 8x\text{HCO}_3^- + 3x\text{H}_2\text{O} + y\text{NH}_3 + z\text{H}_3\text{PO}_4$	-114
(5) <i>Sulfate reduction</i>	$2(\text{CH}_2\text{O})_x(\text{NH}_3)_y(\text{H}_3\text{PO}_4)_z + x\text{SO}_4^{--} \rightarrow x\text{H}_2\text{S} + 2x\text{HCO}_3^- + 2y\text{NH}_3 + 2z\text{H}_3\text{PO}_4$	-77
(6) <i>Methane production</i>	$(\text{CH}_2\text{O})_x(\text{NH}_3)_y(\text{H}_3\text{PO}_4)_z \rightarrow x\text{CH}_4 + x\text{CO}_2 + 2y\text{NH}_3 + 2z\text{H}_3\text{PO}_4$	-58

Figure 5. The sequence of sedimentary diagenesis reactions (Froelich et al., 1979; Stumm and Morgan, 1995; Tromp et al., 1995; Aller, 2014).

I.1.4. Physico-chemical factors controlling phosphorus mobility at the water/sediment interface

I.1.4.1. Redox condition

The presence of oxygen at sediment surface accelerates the decomposition of OM by aerobic heterotroph organisms, oxygen being the first-order electron acceptor during metabolism of microorganisms. Mineralized P will remain in sediment water and increase P concentration in pore water. Redox states of Fe and Mn depend strongly to oxygen level by both chemical reductive dissolution and by microbial metabolism (Orihel et al., 2017). Under anoxic condition, microorganisms use alternative electron acceptors such as nitrate, iron, manganese, and sulfate instead of oxygen. Thereby, iron and manganese oxy(hydr)oxides are subjected to dissimilatory reduction by anaerobic bacteria and release previously adsorbed or occluded P to solution. Besides, the microbial sulfate reduction at low redox conditions limits the mobility of metals by the formation of metal sulfides precipitates (FeS and FeS₂) (Borch et al., 2010). Moreover, if conditions permit, the Fe(II) released in reducing condition can precipitate with phosphate to form vivianite (Fe₃(PO₄)₂·8H₂O) and contribute greatly to P retention during early diagenesis (Rothe et al., 2016).

I.1.4.2. pH

The pH controls the phosphate speciation and also the precipitation and dissolution of many secondary minerals such as apatite, calcite, siderite. P is commonly present as HPO₄²⁻ in alkaline environment and as H₂PO₄⁻ at pH lower than 7 (Fig. 6) (Azam et al., 2019). For pH between 7 and 8.5, P can co-precipitate with Ca to form hydroxyapatite and this complex dissolve when the pH decreases to lower than 5 (Hinsinger, 2001). In contrary, the increase of pH to be neutral or slightly alkaline below 8.5 increase the solubility of Fe and Al phosphates (Reitzel et al., 2013; Willard, 1979) and limit the P retention onto sediment.

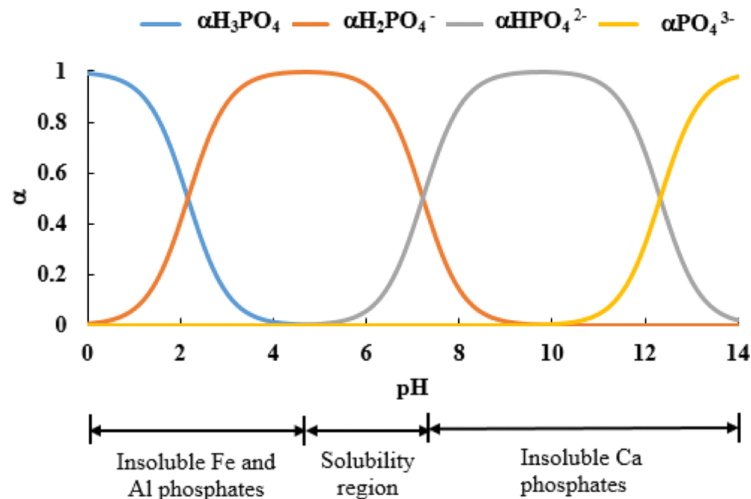


Figure 6. Phosphate speciation in natural environments (Azam et al., 2019).

I.1.4.3. Microbial activities

The microbial community attributes important role during the degradation of OM. Microorganisms can exudate extracellular enzymes, electron shuttles and chelating agents into pore water to increase the bioavailability of P (Różyło and Bohacz, 2020). The structure of these exudates depends on their purpose. The extracellular hydrolytic enzymes act on both particulate and aqueous organic P species to produce free orthophosphates, which are the only form of P accessible to biota. The microorganisms can alter the amount of P in surrounding environment by accumulation within the cells. The polyphosphate content in aerobic microbes can count for 10 % of TP of surface sediment (Hupfer et al., 2007). The limit in P availability puts stress on the microbes and stimulates a system that transforms orthophosphate into insoluble polyphosphate to store inside the cell (Hupfer et al., 2007). The P accumulating bacteria therefore contribute potentially to a portion of the P fluxes between the sediment and the overlying water.

Benthic biota induces physical perturbation of sediment, called bioturbation. The mechanism of bioturbation includes bioirrigation which transport solutes, bioconveying which transport particulate and sediment mixing (Fig. 7) (Andersson et al., 1988; Meysman et al., 2006). The disturbing of surface sediment, that are rich in P, mobilizes P to water column. The movement of invertebrate constructs burrow tubes and enhance the transport of solute from pore water to water column (Chaffin and Kane, 2010; Gautreau et al., 2020). The burrow construction also introduces oxygen, it results in the precipitation of Fe and Mn oxy(hydr)oxides at burrow wall and limits the P mobilization (Lewandowski and Hupfer, 2005).

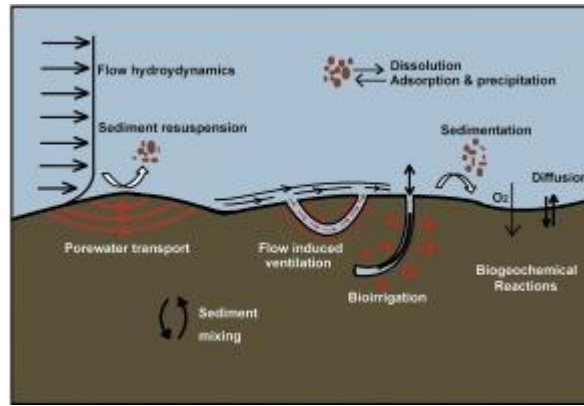


Figure 7. The bioturbation enhancing nutrient transport from sediment to overlying water during sediment resuspension induced by flow perturbation (Xie et al., 2018).

I.1.4.4. Temperature

Temperature has been shown to stimulate primary production in water surface and induce higher biomass density to bottom sediment (Søndergaard et al., 2003). The higher temperature also improves microbial activities in mineralization of organic matter, especially of organic P, and consequently enhance mobilization of dissolved P (Gudasz et al., 2010). Furthermore, the seasonal temperature variation resulted in the seasonal stratification in lakes. In summer, warm weather results in higher primary production at surface water. The deposition of dead organisms provides a new carbon supply to biomass present in the sediment. The decomposition of these organic matters and thermal stabilization of water column, which is caused by the difference in water density of warm surface and colder bottom, induces anoxic condition at the sediment-water interface at hypolimnion zone.

I.1.4.5. Drying and rewetting cycles

The drying and rewetting (DRW) cycles alter water content in soils and sediments; they are caused either by seasonal fluctuation in water level of rivers, lakes, reservoirs or on purposes such as power production or flood monitoring. The P bound to soils and sediments that undergo drying and rewetting cycles can be significantly impacted by the physical, chemical and biological exchange with aqueous environment (Zhang et al., 2012). The main mechanisms contributing to P dynamics during drying/rewetting of sediment are the change in bacteria community and change in water chemistry at sediment-water interface. The alternate DRW of soils and sediment are shown to enhance the release of TP upon rewetting (Schönbrunner et al., 2012) by stimulating the mineralization rates and iron oxyhydroxide dissolution. During desiccation, the oxidation of metal sulfides resulting in acidification leads to higher consumption of alkalinity, dissolution of calcite, cation exchange reactions and subsequently the weathering of Al and Fe oxy(hydr)oxides. However, the prolonged drying periods show acceleration in mineral aging, results in the higher crystallinity of ferric oxy(hydr)oxides and in the decrease of reactive binding site for P (Schönbrunner et al., 2012). The desiccation of sediments also acts on microbial community. The loss of obligate anaerobic bacteria, who die or shift to resting stage during drying (Blackwell et al., 2009), limits the reduction of ferric oxy(hydr)oxides and sulfate, thereby, P remains sorbed to ferric minerals. Overall, repeated drying and rewetting are likely promoting P release upon rewetting.

Conclusion

Due to its high affinity to solid phases, P is often found in association to soil and sediment particles. The largest pool of P in global cycles are terrestrial soil and aquatic benthic sediment. The amount of soluble P compounds present in watershed is relatively minor compared to the fraction associated to soil materials, such as iron oxy(hydr)oxides (Cavaliere and Homann, 2012) and to carbonate species (Toner and Catling, 2020). Soil erosion due to forest clear-cutting and widespread cultivation has increased riverine suspended matter concentrations, and thus increased the riverine particulate-P flux. Dams, in contrast, decrease sediment loads in rivers and therefore diminish the phosphorus flux to the oceans. According to a model calculation of Maavara et al., (2015), the dam building reduces greatly the downstream transfer of P to coastal marine environments by 12 % from 1970 to 2000 and could extent to 17 % by 2030 due to the construction of about 3700 new dams globally. The P retention in reservoirs can significantly constraint the delivery of P to downstream areas, influencing regional nutrient patterns, trophic conditions, and food web dynamics (Friedl and Wüest, 2002). Nevertheless, P accumulation in dam reservoir can become a source since dam reservoirs often possess large lake-like features that can induce anoxic condition at the bottom zone via transformation of biogeochemical properties occurring in lentic water bodies (Habets et al., 2018). This internal P load is estimated to be approximately 24 % of annual external TP load (North et al., 2015) and triggers long-term in reservoir water. All these effects of river damming represent critical anthropogenic perturbation of the continental P cycle, consequently, requiring the better evaluation of river damming on riverine P fluxes and any transformation of P within reservoir to fully determine the associated environmental impacts.

I.2. Temporary storage of phosphorus in dam reservoir

I.2.1. Phosphorus entrapment in dam reservoir

The intensive river impoundment constructions over the past few decades have significantly affected the hydrologic and hydraulic characteristics of river-ocean continuum. It is estimated that more than 50 % of the world's streams and rivers flow through one or more dams before reaching the oceans (Van Cappellen and Maavara, 2016). Large reservoirs decrease the global sea level by approximately 30 mm (Chao et al., 2008) and capture 30 % of total annual runoff (Postel et al., 1996). Water storage in large reservoirs retains nutrients through biological consumption, physical sedimentation, and results in the interruption of nutrient transport to downstream of the dam. The nutrient retention within dam reservoir has shown impacts on nutrient delivery from inland to ocean areas and also on the water and sediment quality of reservoir themselves (Wang et al., 2019). The sedimentation of mineral particles and organic debris carries P to the bed sediment. The sediment acts as a sink and also a potential source of P depending on the biogeochemical condition of overlying water as well as the speciation of sedimentary P (Rapin et al., 2019; Wang et al., 2009).

With raising in economic development and high demand on non-fossil fuel-based energy resources, about 3700 hydropower dams are under construction or planned to be implemented in near future (Zarfl et al., 2014). Therefore, the global river TP retention by river damming will notably increase compared to the last century. It has been estimated that the retention fluxes of TP by dams in the years 1970 and 2000 were 22 and 42 Gmol/year, in correspondence to global riverine fluxes of P increase from 312 to 349 Gmol/year from 1970 to 2000 (Maavara et al., 2015). Thereby, global TP retained by dam construction had increased from approximately 7 % to 12 % for 30 years. The higher sequestered pool of P in reservoir were due to the building of 2500 new dams (65 % have residence time of more than 6 months) (Maavara et al., 2015).

In Europe and South America, it is interestingly that the TP load input from river to coastal areas declined significantly in impounded rivers compared to no-dam rivers, despite the watershed received higher anthropogenic TP loads (Maavara et al., 2015). This effect could imply firmly the implicit retention of P in reservoir sediments. As P is an important element to control aquatic primary production, the effect of riverine damming on P transport should be well identified in order to better understand the associated impacts on interconnected environment.

I.2.2. Reservoir functioning and its impacts on within-system and downstream river

Reservoirs are often characterized by specific features against rivers and lakes, including the control of outlet, origin and geographical placement in river network (Hayes et al., 2017). Reservoirs are usually divided into three zones: river (lotic), transitional and lacustrine (lentic) (Fig. 8).

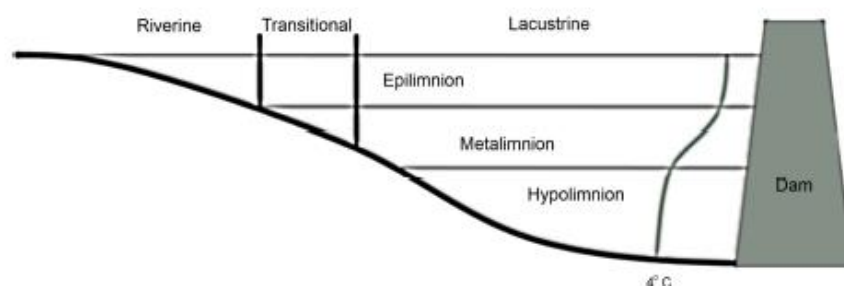


Figure 8. The vertical and horizontal zonation of a stereotypical deep reservoir with summer thermocline ending at 4°C at the bottom sediment (Ruhl et al., 2014).

According to Jørgensen et al., (2005), the inflow riverine region is characterized by narrow channel cross-section, shallow water level depth and rapid water flow, which reaches maximal velocity near the center and surface. At transitional region, the river flow becomes slower and less turbid before entering the more stagnant lacustrine water. The lacustrine zone possesses some characteristics similar to lake such as more balanced and stagnant water, but also contains deeper zones, superior surface area, larger drainage basin, strongly vertical stratification and higher shoreline development (Galizia Tundisi, 2018). In many reservoirs, the variation in water level is higher than in natural lakes as the combined effect of natural inflow variability and operational purposes. The highest fluctuation often takes place in the regions subjected to high periodically varied inflow (Jørgensen et al., 2005).

Dam reservoirs have brought various social and economic benefits, but their construction impacts all river system they fragment (Galizia Tundisi, 2018; Hoeinghaus, 2018).

Dam reservoirs disrupt the continuity of river flow, lead to the deposition of bedload (gravel, cobbles and sand) and a portion of washload (suspended materials that carry mainly silt and clay) within the upstream reservoir and the release of sediment-starved water flow to downstream, causing channel incision downstream and the coarsening of downstream bed sediment due to the lack of upstream compensation for the loss of fine sediment (Csiki and Rhoads, 2014; East et al., 2018; Guo et al., 2020; Kondolf et al., 2014). The changes in flow and sediment regimes are often received more announced attention for their negative impacts on downstream system of the dam. However, their influences on upstream system are also significant because the variability in sediment pulses of river channel can alter geomorphological properties of upstream flow. The sedimentation along riverbanks can narrow down the cross-section of river before it reaches the reservoir, meanwhile the accumulation of sediment materials modifies the bottom terrain of reservoir (Csiki and Rhoads, 2014; Liro, 2016). The river flow

generally slows down in the reservoir upstream during the period of high-water level and stimulates sediment deposition in the channel and on the floodplain (Liro, 2014). Fine-grained sediment is crucial for the structure of some riverine forms (vertically accreted floodplains and estuarine mud flats), it can act as a turbidity source and play important role in transportation of nutrients and contaminants (Kondolf et al., 2014). The reservoirs with long residence time can trap the suspended load; the percentage of suspended sediment to be trapped within a reservoir increases with residence time (Kondolf et al., 2014). According to Vörösmarty et al., (2003), it is estimated that a 1-day residence time can result in a substantial percentage (more than 80 %) of inflowing suspended sediment to be trapped by the large dams, with 55 % of coarse sediment and 30 % of colloidal and dispersed fine sediment (silt and clay). The sequestration of sediment is mainly occurring during rainy season when the suspended load is high (Xu and Milliman, 2009; Yang et al., 2014). The allocation of suspended sediment depends greatly on the material properties and flow velocity, in which the abundance of fine particles is always found predominantly in the reservoir front area and coarsening laterally with increasing elevation (Fonseca et al., 2010; Guo et al., 2020; Tang et al., 2018a). The sediment trapped in the reservoir upstream area is comprised of mainly finer material (fine and medium silt with 50 % is clay minerals), whereas the sediment in the immediately downstream of the dam contain coarser texture, mainly fine and medium sand (Guo et al., 2020; Rapin et al., 2020).

The siltation in reservoir terrain reduces the water storage capacity and particularly threatens the reservoir water quality. An example in Missouri River showed an average bed rise of 7 cm/year which contributes to an average of 3 m increase of bed rise to the pre-dam period, that forced a town to be reinstallation in higher altitude due to increased flooding (Coker et al., 2009). The global reservoir storage can be half filled by 2100 and the consequently impaired functions of the dam demand cautious actions to achieve sustainability in water supply and sediment management to replenish ecological loss of coastal land (Kondolf et al., 2014).

The decantation of (in)organic matter and nutrients/contaminants sorbed to and transported by fine sediment in reservoir, due to the decreased flow velocity, can improve the downstream water quality, but in contrary, could act as a long-term source of pollution, particularly for phosphorus (Jan et al., 2013; Zarfl and Lucía, 2018).

The dammed rivers have been taken into account as one of the hot spots for methane emissions and the large dam reservoirs are estimated to increase the global methane emission from freshwater bodies by up to 7 % (Maeck et al., 2013). Since the methane release has higher potential to increase global warming than carbon dioxide release (Cole et al., 2007), the deposited sediment in dammed reservoir promoting anaerobic degradation of organic matter will increase the global climatic impacts further than aerobic degradation. Another major parameter to assess aquatic environment is the limiting nutrient P. Various researches have established the massive retention of P in dam reservoirs (Jossette et al., 1999; Teodoru and Wehrli, 2005; Lopez et al., 2009; Kunz et al., 2011; Maavara et al., 2015; Van Cappellen and Maavara, 2016; Tang et al., 2018a) and its cohesively anoxic release from deposited sediment to surface water can cause severe effect to water quality, especially the eutrophication (Nürnberg, 2009; Welch and Cooke, 2005).

Furthermore, the alterations in the amount and composition of sediment, water quality, temperature and food availability upon dam construction lead to significant negative impacts on the ecology of aquatic ecosystems, increase the fish mortality (*ie.*, *Corieus guichenoti*) and decrease the reproduction success (Wu et al., 2019). The major effects encompass the increase abundance and proliferation of phytoplankton (Li et al., 2013), especially cyanobacteria such as *Microcystis aeruginosa*; decline of

zooplankton such as rotifers (Dickerson et al., 2010); blocking migration pathways and consequently decrease abundance and biodiversity of fish and aquatic mammals (Hoeinghaus, 2018); loss of natural habitats and animal-plant symbiosis (Emer et al., 2013).

I.2.3. Dam reservoir management and impacts on within-system

I.2.3.1. Flow management

Many reservoirs lead to alteration in hydrology due to flow management in response to multi-purposes by water storage and discharge. Depending on the purpose, the level of water in reservoir changes daily, weekly, monthly or seasonally throughout the year (Kaczmarek and Kindler, 1982). At some critical periods of the year, the inflow supply is insufficient to the outlet discharge of the reservoir in comparison to hydrological drought condition and can subsequently result in the lower level of water at all points of reservoir, particularly in the riverine section. During that period, the sediment at the bank of reservoir are potentially exposed to the air and eventually to drying partially or thoroughly. During the filling by upstream river water, the water level raise and inundate once more the dried sediment. This phenomenon occurs regularly and alternately at the bank of reservoir and is different than the natural fluctuation of water level in most lakes and rivers (Zhang et al., 2012). The alternating inundation and desiccation of sediments have shown complexity in physical, chemical and biological transformation processes between interstitial and overlying water. Gu et al., (2018) notified the release of both reactive and unreactive dissolved phosphorus in fraction lower than 0.45 μm , which can comprise the presence of colloidal P, following the rewetting of dried soils. Gu et al., (2018) also suggested an important amount of colloidal/nanoparticulate P mobilized during rewetting and this fraction is constituted by Fe/Al oxy(hydr)oxides and organic matter. The release of colloidal P caused by dry/wet cycles can become potential source of P for aquatic organism and support eutrophication. In addition, some reservoirs experienced the water emptying event can lead to the drying of sediment and probably induce impacts on nutrients exchange along water column during following reflooding events. The exposure of sediment during water drawdown enhances the contact of oxygen to previously inundated sediment. In particular, previously reduced species (for example, Fe and Mn) are oxidized, thus immobilizing phosphate via sorption and/or (co)precipitation and lowering the dissolved P concentration in restored flow. However, on the other side, the larger amount of particulate P would be mobilized under resuspension (Ahearn and Dahlgren, 2005; Cavaliere and Homann, 2012).

Other options for water quality management includes hypolimnetic oxygenation system (HO), sub-dam or bypass channel for preventing nutrient or sediment from coming into reservoir, advanced hydrological forecasts and climate prediction to be more flexible in flow management/mimic natural flow. The HO system is a technique used to inject air or oxygenated water to the bottom layer and thus maintain the well-oxygenated condition of many seasonally stratified reservoirs (Munger et al., 2016). The use of HO system has advantages in increase DO level to more than 8 mg/L (Munger et al., 2016), increase P sequestration by limiting redox-dependent P release (Munger et al., 2016; Niemistö et al., 2019; Preece et al., 2019), decrease NH_4^+ concentration by stimulating activities and population of nitrifying bacteria (Beutel, 2006). In contrary, in some cases, the HO system shows disadvantages by increasing hypolimnetic temperature and turbulence, consequently, enhances nutrient recycling from sediment to water column and reallocates settling materials, resulted in the higher primary production and organic matter deposition to bottom layer (Niemistö et al., 2019).

I.2.3.2. Sediment management

In reservoir, sediments accumulation induces a reduction of their capacity to store water, causing degradation in dam infrastructure and safety problems (Kondolf et al., 2014; Wang et al., 2018). In order to restore reservoir capacity, various management activities have been applied (Fig. 9) and are composing of four major approaches: (1) to reduce sediment entrainment via bank/slope protection and reforestation; (2) to minimize sediment trapping, for example, via venting turbid flow during high sediment load season and the implementing sediment by-pass channels; (3) to remove trapped sediment in reservoirs by dry/wet excavation or suction dredging; (4) to develop adaptive structural and functional strategies (International Hydropower Association, 2019; Kondolf et al., 2014; Morris, 2020).

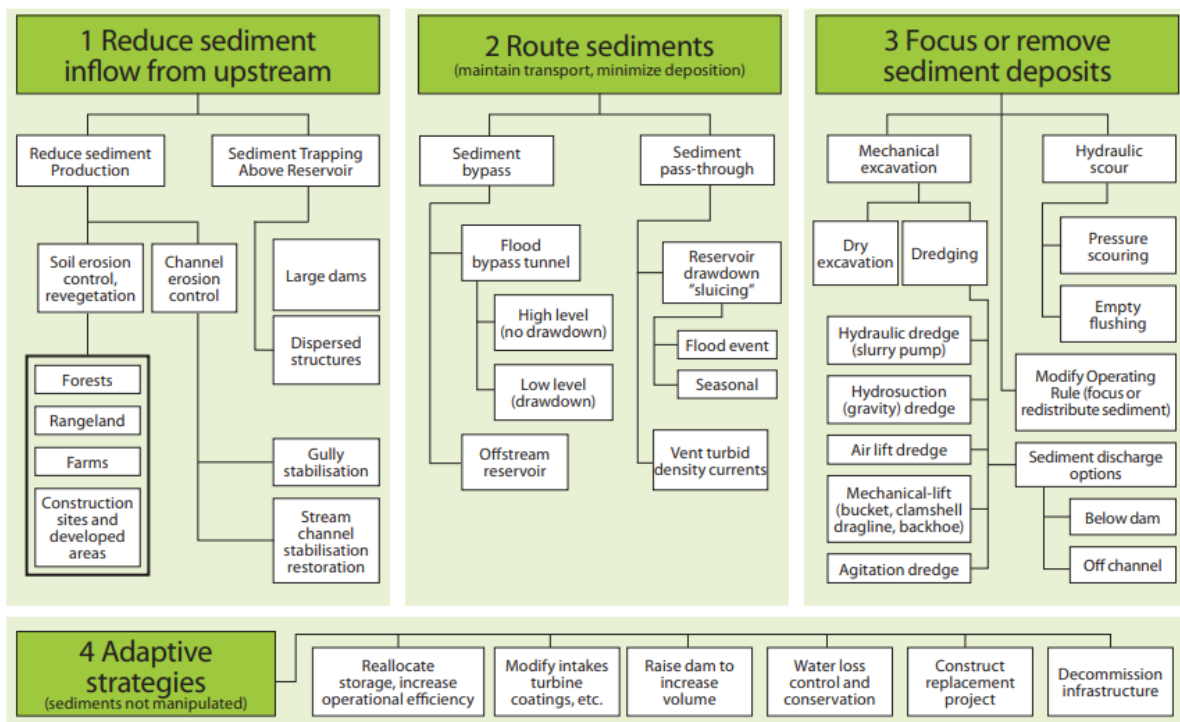


Figure 9. Strategies for sediment management in dam reservoir (International Hydropower Association 2019)

The first two approaches act on both the maintenance of reservoir storage capacity and delivery of sediment to downstream, whereas the third method focus only on storage capacity. The fourth approach is not aimed to adjust sediment balance but instead, to address the techniques to mitigate the storage loss (Morris, 2020). It has been estimated that the building of by-pass channel can exclude 90 – 95 % of total sediment load and extent the reservoir life by ten folds (Morris, 2020). The implementation of sluice and drawdown flushing involves in the freely passing of sediment through the dam without upstream impoundment and transport to the downstream (Kondolf et al., 2014). However, the sediment that has been excluded from reservoir can induce significant environmental risks such as pollutant transfer. The sediment flushing flow results in a drastic decrease of dissolved oxygen concentration due to the hyper-concentrated sediment load up to hundreds of thousand mg/L of suspended solid concentration (SSC) (Baoligao et al., 2016; Buermann et al., 1995); the increase of biological oxygen demand (BOD) concentration in downstream river due to the resuspension of organic matter (Chung et al., 2008); and the recorded release of contaminants that were previously retained in reservoir sediment, such as some hydrophobic organic contaminants (Lepage et al., 2020), trace elements (Bretier et al., 2019; Palanques

et al., 2020) and other heavy metals (Peter et al., 2014). The remobilization of contaminants associated to flushing sediment can induce bioaccumulation of contaminants by aquatic organisms and plants, increase damage and mortality by the toxicity of contaminants, river-ocean transport of contaminants especially in colloidal forms (Wildi et al., 2004).

1.2.4. Internal loads of phosphorus in reservoir

Internal loading of P is coming from the accumulation of sediment during high external nutrient input events (Jeppesen et al., 2005; Søndergaard et al., 2003) (Fig. 10). The high internal loading of P may delay or prevent aquatic ecosystem from recovery after experienced algal bloom (Parsons et al., 2017). The internal P loads are driven by two major opposite fluxes: downward flux due to sedimentation of particulate P coming from external input and particulate P produced in water column; upward flux due to organic matter decomposition and reductive dissolution of P-bearing minerals (Jeppesen et al., 2005; Orihel et al., 2017).

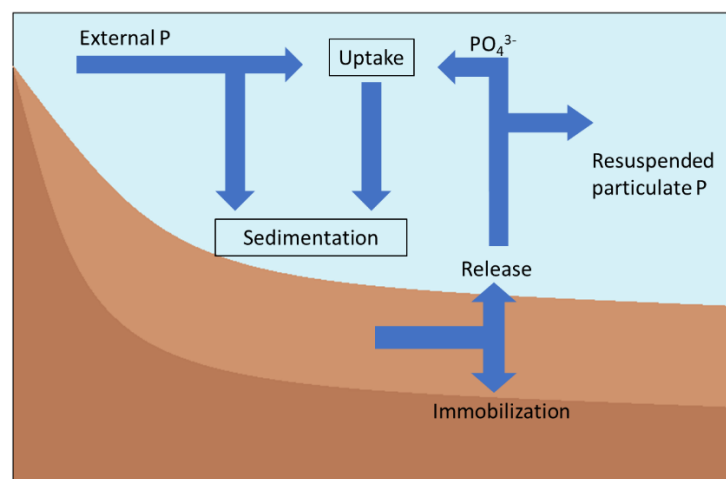


Figure 10. Simplified internal P cycle in reservoir adapted from (Cavalcante et al., 2018a).

The bottom sediment typically become anoxic at a few millimeters below the surface (Köster et al., 2000). Once P reach bottom sediment, it will become a part of complex and interexchange redox reactions to be either permanently buried or released back to overlying water. The redox potential, pH and the concentrations of organic matters, iron, aluminum, calcium are some of the main parameters influencing the P mobility at sediment-water interface. The sequential extraction of sediment has shown different constituents of sedimentary P depending on the deposit location of sediment. In granitic catchment or the catchment that has luvisols, the sedimentary P in deep reservoir was dominantly associated to amorphous Fe/Mn oxy(hydr)oxides (Cavalcante et al., 2018; Rapin et al., 2019), whereas in riverine section, P was mainly bound to calcium and amorphous Fe/Mn oxy(hydr)oxides (Rapin et al., 2020). Iron and manganese are redox-sensitive elements; hence under anoxic condition at bottom sediment, associated P is released through the dissolution of Fe/Mn oxy(hydr)oxides and migrate to surface water. Therefore, the variability in P dynamic in reservoir is strongly depending on the hydrological dynamic upon reservoir management.

Conclusion

Overall, dam construction, functioning and management have led to significant change in hydrology of the river, biogeochemical cycles of various elements of the reservoir and thus increase the risk of

eutrophication. To better understand and monitor P mobility, it is substantial to pay attention to the physical, chemical and biological parameters that can drive the transformation and migration of P from sediment to water column. Consequently, redox potential, pH, temperature, microbial activities, dry/wet cycles, and composition of P pools should be studied. Since P has high affinity to solid phase, the transfer of P to downstream river is not limited to soluble form but also in solid and colloid forms. Special attention should be paid to colloidal P which remains suspended and potentially labile to be uptaken by phytoplanktonic species.

I.3. Why do we focus on colloidal fraction?

I.3.1. Colloids

I.3.1.1. Definition and functional behaviours

Colloids, which are abbreviation of colloidal systems, originated from a Greek word “kolla” means “glue” and refers to a glue-like two-phase system constituted of a dispersed phase, of fine and evenly distributed particles, and a dispersion medium as a whole (Ho, 2013; Shchukin et al., 2001). Even though, through common usage, the term colloids became an acronym for the dispersed particles themselves, especially in environmental aspect. According to IUPAC Recommendations 2011, colloidal is the state of subdivision such that the molecules or polymolecular particles dispersed in a medium have at least one dimension between approximately 1 nm and 1 μm , or that in system discontinuities are found at distances of that order.

In natural water system, the behavior of contaminants is generally defined by three-phase systems. Their occurrence and distribution depend strongly on the partitioning between stationary solid material, solute phase, and the suspended matters. Certain portion of suspended matters will settle through time, whereas half of them will remain in suspension even over long period of time in the absence of aggregation and represent “colloids” (Wilkinson and Lead, 2007). Colloids are generally suspended particles that do not settle through time under ideal condition. The stability of colloids depends largely on electrical charges of individual particles and thus depends on presence of dissolved electrolytes (Mahmood et al., 2014). In stable dispersion, the collisions between particles do not lead to aggregation because interparticle repulsion forces dominate, thus the colloids remain dispersed indefinitely although the colloids bigger than about 0.1 μm should sediment depending on their density (Mahmood et al., 2014). In unstable dispersion, collisions lead to aggregation and large aggregates sediment depending on their relative density (Mahmood et al. 2014). The fundamental interaction between colloidal particles is often explained through DLVO theory (developed by Derjaguin and Landau (1941) and Verwey and Overbeek (1948) independently). According to DLVO theory, the stability of colloidal dispersion is driven by the balance between the long-range repulsion of the double layer and the short-range attraction due to Van der Waals forces (Biermann, 1996; Hamad-Schifferli, 2014; Ohshima, 2014) (Fig. 11).

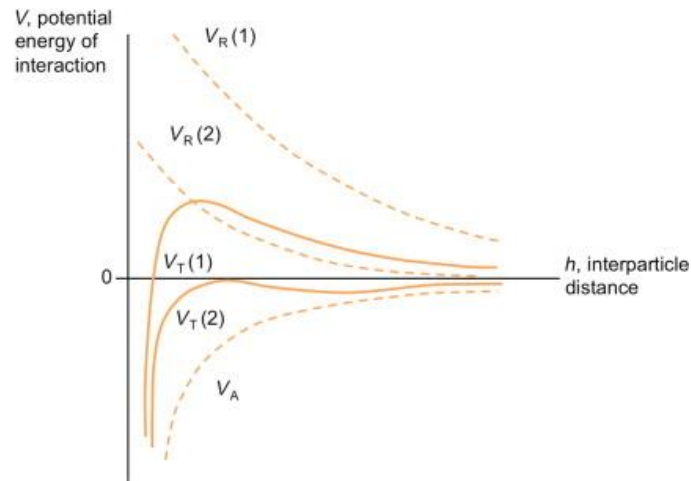


Figure 11. The interaction between two colloids described by DLVO theory with the total potential energy (V_T), repulsive energy due to electric double layer (V_R) and attractive energy due to Van der Waals (V_A). (1) corresponds to long Debye length at low electrolyte concentration. (2) corresponds to short Debye length at high electrolyte concentration. (Hamad-Schifferli, 2014).

The Van der Waal interactions are non-ionic in nature (Roy et al., 2015) and are purely interparticle attraction between fluctuating dipoles at close distance (Ohshima, 2014). Whereby, the double-layer repulsive forces between two colloidal particles is due to the overlap of double layers of particles at very long or very short distances (Hamad-Schifferli, 2014). The surface potential of colloid become negatively charged when negative ions in solution are adsorbed to its surface. To maintain the electrical neutrality, this negatively charged colloid eventually attracts positive counterions (Stern layer) and an electric double layer is formed surrounding the colloid (Park and Seo, 2011) (Fig. 12). The concentration of counterions declines exponentially from the stern layer and results in an ionic cloud called diffuse region of the electric double layer (Mahmood et al., 2014).

When colloid moves in solution, the overlapping of similar charged electric double layer between colloids give a repulsive force that pushes the colloids apart (Mahmood et al., 2014; Shaw, 1992). The double layer interactions depend on the variation in ionic strength of the dispersed medium (Adair et al., 2001). The determination of the total interaction energy via addition of these two forces can predict the stability of colloidal solution. At low electrolyte concentration, the repulsive forces dominate, resulting in positive total potential energy, referring to stable colloidal suspension. Meanwhile, at high electrolyte concentration, the Van der Waals attractive forces are dominant and there is no barrier energy for colloid to be coming in short contact with each other and lead to fast colloid aggregation (Hamad-Schifferli, 2014).

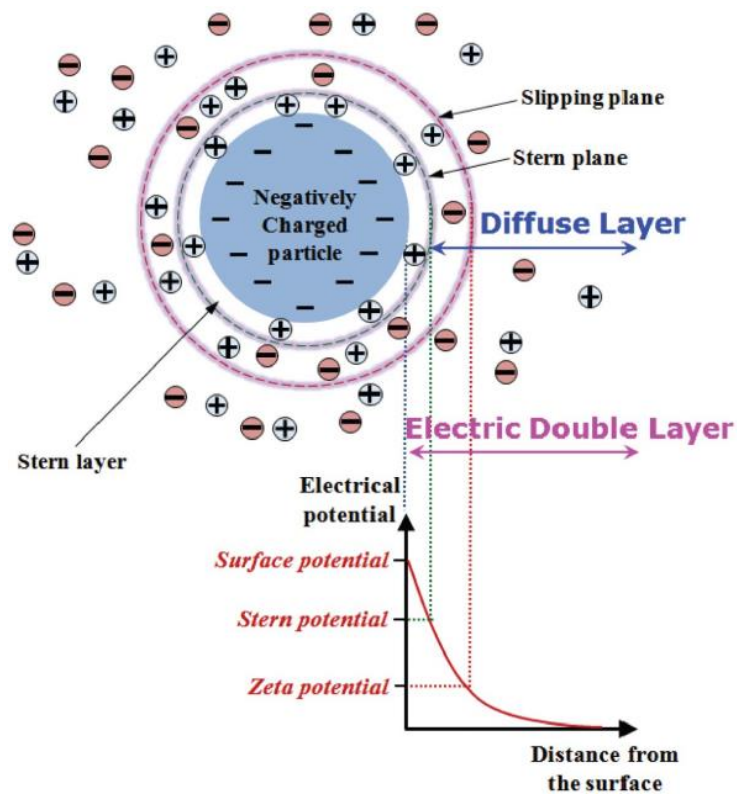


Figure 12. Electric double layer of colloidal particle (Park and Seo, 2011)

The size of colloids is very small (1 nm to 1 μm) (Mahmood et al., 2014), but they are large enough to scatter the light beam and make visible light pathway (Tyndall effect) that allow them to be visible under electron microscope (Bajpai, 2018). However, in some extents, the upper size threshold can be considered to be 2 μm (Tulve and Young, 1999) or even 10 μm (Sepehrnia et al., 2018). Thanks to their small size, colloids have a high surface area relatively to their volumes (Dukhin and Goetz, 2017) (Table 3). The proportion of colloids in total particulate mass and volume is small (less than 2 %) but they represent importantly a high available surface area to adsorb contaminants (Gaillardet et al., 2003; Perret et al., 1994). Most of colloids have negatively/positively charged surface due to their anionic/cationic functional groups, respectively (Bajpai, 2018). Colloids can thus adsorb opposite charge ionic contaminants to their surfaces. The examples are many minerals and solid phases such as clays, iron, manganese, aluminum oxy(hydr)oxides and humic colloids. For instance, the hydroxyl groups of inorganic colloids will be dissociated when in contact with water and develop surface charge that electrostatically attracts charged ions in surrounding liquid on its surface, whereby the organic colloids can adsorb non-ionic compounds via protonation, ligand exchange and hydrogen bonding (Berkowitz et al., 2008). Another property of colloids is their Brownian movement due to the collision of dispersed colloids with molecules in dispersion medium and results in zigzag chaotic movement of colloidal particles in suspension (Chhabra and Basavaraj, 2019). This Brownian movement also contribute partially to the stability of colloids in aqueous medium.

Table 3. Particle and colloidal properties of a mole of water versus spherical particle size. The specific area is applicable for spherical particles of specific gravity of 1.0, for other materials, divide this number by the specific gravity of the solid material for the given particle radius (Bajpai, 2018; Biermann, 1996)

Particle Radius	Particle Number	Particle Volume (cm ³)	Particle Area (cm ²)	Total Area (cm ²)	Total Surface ^a Energy (J/mol)	Specific Area ^b (m ² /g)
1.63 cm	1	18	33.2	33.2	0.00048	1.8 · 10 ⁻⁴
1.00 mm	4300	4.19 · 10 ⁻³	0.126	540	0.00619	3.0 · 10 ⁻³
0.10 mm	4.30 · 10 ⁶	4.19 · 10 ⁻⁶	1.26 · 10 ⁻²	5400	0.0619	3.0 · 10 ⁻²
0.01 mm	4.30 · 10 ⁹	4.19 · 10 ⁻⁹	1.26 · 10 ⁻⁵	5.4 · 10 ⁴	0.619	3.0 · 10 ⁻¹
1.00 μm	4.30 · 10 ¹²	4.19 · 10 ⁻¹²	1.26 · 10 ⁻⁷	4.3 · 10 ⁵	6.19	3.0
0.10 μm	4.30 · 10 ¹⁵	4.19 · 10 ⁻¹⁵	1.26 · 10 ⁻⁹	4.3 · 10 ⁶	61.9	3.0 · 10 ¹
0.01 μm	4.30 · 10 ¹⁸	4.19 · 10 ⁻¹⁸	1.26 · 10 ⁻¹¹	4.3 · 10 ⁷	619	3.0 · 10 ²
1.00 nm	4.30 · 10 ²¹	4.19 · 10 ⁻²¹	1.26 · 10 ⁻¹³	4.3 · 10 ⁸	6192	3.0 · 10 ³
0.1925 nm	6.02 · 10 ²³	2.98 · 10 ⁻²³	4.66 · 10 ⁻¹⁵	2.8 · 10 ⁹	40,300	3.0 · 10 ⁴

Nowadays, the definition of colloids is mostly established based on the size range and thereby, throughout this thesis: **“The term colloids are regarded to any entities that have at least one dimension ranging from 1 nm to 1 μm.”** (Buffle and Leppard, 1995, Stumm, 1993, Xu et al., 2018, Yan et al., 2017). By this definition, the term colloid also includes nanoparticles which is defined to have at least one dimension lower than 100 nm (American Society for Testing and Material, 2012).

I.3.1.2. Types of colloids in natural environment

Colloids are comprised of extremely complex and diverse materials: organisms, biological debris, organic macromolecules, clays, minerals, oxides, particularly coated with organic matter. Though, the vast variety of colloidal systems can be categorized into four commonly found types (Table 4): inorganic colloids, biocolloids, natural macromolecular organic matter and the association of minerals with organic matter (Stumm, 1993; Sen and Khilar, 2006).

Table 4. The classification and some common examples of colloids in natural environment (Kretzschmar et al., 1999)

Inorganic colloids	<ul style="list-style-type: none"> • Rock and mineral fragments, such as clay minerals, quartz, muscovite <hr/> <ul style="list-style-type: none"> • Mineral precipitates: <ul style="list-style-type: none"> - Oxy(hydr)oxides of iron (III) and manganese (III, IV) - Aluminum hydroxides - Carbonate minerals (calcite CaCO_3, dolomite $\text{CaMg}(\text{CO}_3)_2$, siderite FeCO_3, etc.) - Phosphate minerals (apatite $\text{Ca}_5(\text{F,Cl,OH})(\text{PO}_4)_3$, vivianite $\text{Fe}_3(\text{PO}_4)_2(\text{H}_2\text{O})_8$, etc.) - Sulfide minerals (pyrite FeS_2, gypsum $\text{CaSO}_4 \cdot 2\text{H}_2\text{O}$)
Organic colloids	Hydrocellulose, lignin, proteins Humic acids
Biocolloids	Microorganisms, bacteria, viruses Structural biological fibrils
Inorganic-organic colloids	Inorganic colloids coated with organic material Organic colloids associated with inorganic species

The inorganic colloids are mainly the fragments of rock and secondary minerals that are naturally present in aquifer, such as clay minerals, and the precipitation of inorganic species. The aluminosilicates are the most common colloids in aquatic systems due to the mobilization and transport from fractured rocks and soils (Degueldre et al., 1996; Weisbrod et al., 2018; Wilkinson and Lead, 2007). The aluminosilicates are important colloidal materials due to their cation-exchange capacity and the variety in charge types lead to different ways of aggregation, such as the plane-to-plane, edge-to-edge and edge-to-plane interactions (Wilkinson and Lead, 2007). For example, the flocculation of clay particles can occur through electrostatic attraction of positive edge charges to negative plane charges (Das and Sobhan, 2013). The adsorption of anion or desorption of proton due to change in pH of clay particles alters the charge reversal of the edge and can lead to spontaneous aggregation through edge-to-plane interaction (Tajana, 2016). Other forms of inorganic colloids in water is the mineral precipitates due to the chemical reaction upon the perturbation in solution chemical composition or the aeration of anoxic water (Zaenker et al., 2005; Zänker and Hennig, 2014) including insoluble oxides of iron (III) and manganese (III, IV), hydroxides of iron and aluminum, iron oxy(hydr)oxides and carbonate minerals. The cycling of colloidal minerals is generally in great concern because of their role in many relevant transports of contaminants through soil, freshwater and groundwater (Bollyn et al. 2019, Chadwick et al., 2006; Chen et al., 2015; Chotpantarat and Kiatvarangkul, 2018; Wolthoorn et al., 2004). With large specific surface area, mineral colloids have strong capacity to sorb various cationic/anionic and non-ionic contaminants depending on the nature of colloid (Sen et al., 2002; Wikiniyadhanee et al., 2015). A vast variety of toxic metal ions (examples of Pb, Cu, Cd, Ni, Zn), metalloids (Sb, As), radionuclides (Cs, Ce, U) and anionic nutrients (examples of phosphate, organic phosphate, polyphosphates) have been demonstrated to be adsorbed and migrated with inorganic colloids (Zhao et al., 2020; Bollyn et al., 2019; Islam et al., 2018; Tran et al., 2018; Baken et al., 2016a; Cheng and Saisers, 2015; Jiang et al.,

2012; Usman et al., 2005; Sen et al., 2002; House and Donaldson, 1986). The investigation for colloid-enhanced transport of non-ionic compounds has been reported for a common hydrophobic organic pollutant of phenanthrene (Roy and Dzombak, 1998).

The living microorganisms (viruses and some bacteria) are considered as biocolloids. The viruses and bacteria, which have size falling in colloidal range, are potentially pathogenic contaminants themselves or as pollutant carrier (Kim et al., 2003; Kretzschmar et al., 1999; McCarthy and McKay, 2004). Indeed, the virus and bacterial cells can either accumulate contaminants through uptake process or sorb contaminants on their surface, corresponding to biosorption. The cell wall of bacteria is more complex and heterogeneous than the surfaces of inorganic colloids (McCarthy and McKay, 2004). The exopolymers secreted at the cell surface of microbes are mainly constituted of polysaccharides (Chatterjee et al., 2019) and are able to bind with metals through covalent bonding between metal cations and negatively charged ligands of the polysaccharides (Miao et al., 2018). Furthermore, the hydrophobic organic contaminants can be sorbed on the surface of both dead and live cells of most bacteria, thus accelerate the transport of contaminants in natural environment (Tsezos and Bell, 1989).

The organic colloids are mainly the macromolecules of organic compounds derived from the decomposition of plant and soil organic matters, the exudates and biological structure of microbes such as fibrils secreting at organism-water interface and exopolymer substances (EPS) (Gaillardet et al., 2003; Stumm, 1993; Thurman, 2012). The organic colloids can account until 10 % of the dissolved organic carbon in fraction lower than 0.45 μm (Thurman, 1985). In the range of colloids, these organic macromolecules are dominantly the aggregates of humic acids that have a diameter between 2 – 50 nm (Thurman, 2012). In the presence of multivalent cations (Ca^{2+}), the flocculation of humic acids occurs at all pH condition, because the binding of cations to humic acids leads to the decrease in the zeta potential and formation of bridges that eventually initiates the attachment of humic molecules together and further aggregation into various size aggregates (from 1 – 5 μm) depending on the pH and concentration of divalent cations (Kloster et al., 2013). In addition, at near neutral pH (6 - 8), humic acids can dissociate protons from functional groups (carboxyl and phenol) and get negatively charged. Therefore, the binding of positively charged ions to these carboxylic and phenolic sites of organic colloids can play crucial role in the retention and mobility of these substances in terrestrial and aquatic environments (Thurman, 2012; Weber et al., 2018). On the other hand, the humic acids also show high affinity to bind with organically hydrophobic pollutants (De Paolis and Kukkonen, 1997). Whereby, the fibril is the structural biogenic packing of acid polysaccharides; these polysaccharides have multifunctional attribution in productive freshwater as floc formers, colloid scavenger based on hydrophobicity and facilitating microbial adhesion to surfaces (Leppard, 1997).

The anionic characteristic of organic macromolecules upon the proton dissociation of functional groups, allows them to bind with minerals and clays to form the inorganic-organic colloids (Gaillardet and Dupré, 2003; Wilkinson and Lead, 2007). Indeed, in natural environment, the coating of minerals with natural organic matter is more abundant than the bare minerals (Doucet et al., 2007; Gaillardet et al., 2003) and this association occurs via several mechanisms: hydrophobic interaction, hydrogen bonding, electrostatic interactions, cation bridging and ligand exchange (Wilkinson and Lead, 2007). In particularly to the formation of iron-organic matter (OM) colloids, the OM in soils and water tends to adsorb on the surface of metal oxides and oxy(hydr)oxides through surface ligand exchange between OM, carboxylic groups and mineral surface, hydroxyl groups at acidic pH or through hydrophobic force at neutral pH (Wu et al., 2008). Furthermore, the coprecipitation of insoluble iron (III) with OM at high C/Fe molar ratios (> 2.8) can lead to the complete coating of mineral surface sites and the desorption of

coprecipitated OM is in less extent than adsorbed OM (Chen et al., 2014). The OM adsorption capacity increases with increasing ionic strength and decreases with increasing pH (Wilkinson and Lead, 2007). Whereas the association of OM to clay minerals, which generally have lower cation exchange capacity and smaller surface area (Al-Essa and Khalili, 2018), is dominated by the cation bridging, the surface sorption can also occur through CH₂ groups of aromatic compounds (Feng et al., 2005). High number of carboxyl functional groups and hydrophobicity of organic coated on mineral colloids increases stability and enhances the surface reactivity to sorb toxic metal cations and metalloid contaminants (Hu et al., 2010; Li et al., 2019). In the eutrophic lakes with presence of phytoplankton EPS, which contains various types of organic compounds including proteins, polysaccharides, humic and fulvic acids, the EPS–Ca²⁺ bridging was the predominant mechanism for the enhanced heterogeneous aggregation mechanisms to form the EPS-colloid in both the absence and presence of electrolytes, enhancing the knowledge on the behaviors and fates of inorganic colloids in aquatic systems (Xu et al., 2016).

I.3.1.3. Natural sources of colloids in environment

In natural systems, colloids can derive from three major sources: (1) fragmentation from parent materials by physical disturbance (tectonic activity, freeze-thaw cycles...) of the fragile materials, (2) in-situ precipitation of inorganic species and disaggregation of large aggregates due to changes in solution chemistry and (3) biological activities.

(1) Fragmentation from parent materials by physical disturbance (tectonic activity, freeze-thaw cycles...) of the fragile materials

The detachment of colloids from fragile materials occurs under influence of tectonic activity, temperature, as well as the act of surface and subsurface water movement (Degueldre et al., 1996, 1989; Lelong et al., 1976). The alternation of expansion and contraction of rocks upon difference in temperature and water content establishes internal tension, weakening the surface of rocks and gradually resulting in fragmentation and mobilization of minerals from parent material (Channarayappa and Biradar, 2018). The freeze-thaw cycles of soil are also a potential mechanism to release colloids since the frozen of pore water creates pressure on pore walls, disintegrating the fragile material of soil aggregates and widening the flow path for latter colloid mobilization during thawing (Mohanty et al., 2014). Depending on the nature of parent materials, the mineralogical of colloids are inherently varied in the proportion of silica, alumina, iron, calcium, etc. to present as smectite, illite, muscovite, quartz, chlorite, calcite, pyrite, etc. (Chattopadhyay and Chattopadhyay, 2003; Wilson, 2004). The organic content in these colloids is low (Degueldre et al., 2000). The movement of surface and subsurface water acts a shear stress on soil matrix and release colloids whose composition is similar to the fine fraction of the bulk (Kretzschmar et al., 1999; Missong et al., 2018). The content of organic matter in colloids enhance their leaching with soil solution. The coating of organic matter increases the dispersibility of colloids by shifting the surface charge to be more negative and prevent colloids from coagulation and fixation to soil matrix (Kalbitz et al., 2005; Kretzschmar et al., 1995). The size and composition of leached colloids varying depends on the soil texture and soil profile properties (de Jonge et al., 2004; Missong et al., 2018). However, the size of leached colloids from soil are generally small, the maximum size in many studies is lower than 450 nm, which cannot thus be removed by filtration at 0.45 μm (de Jonge et al., 2004; Kaplan et al., 1993). Soil with sandy texture showed higher colloid leaching in comparison to soil with higher clay proportion because the clay fraction can form strong surface complexes with organic matter (Missong et al., 2018). Newly detached colloids are then translocated with infiltrating water through soil and sediment profile (Mohanty et al., 2015).

(2) In-situ precipitation of inorganic species and disaggregation of large aggregates due to changes in solution chemistry

Another common mechanism for colloid generation is the precipitation of secondary minerals due to chemical reaction upon the aeration of anoxic waters or the perturbation in water chemistry (Zänker et al., 2006). The evaporation or dissolution of primary minerals can result in the highly concentrated solution and is essential for the nucleation and growth of colloids (Lasaga, 1981). The high concentration of divalent cations, such as iron, magnesium and calcium, can react with carbonate ions to form carbonate minerals, such as calcite (CaCO_3), dolomite ($\text{CaMg}(\text{CO}_3)_2$), magnesite (MgCO_3), siderite (FeCO_3) (Gislason et al., 2010). The acidic condition, for example due to mineralization of organic matter, lead to the dissolution of carbonate minerals, releasing cations and carbonate ions that increase the solution alkalinity (Steiner et al., 2019). The divalent cations of Fe and Mn can get oxidized and precipitated to oxide minerals, but they are rapidly dissolved under reducing condition induced by microbial activities (Scheinost, 2005). Iron oxy(hydr)oxides (FeOOH) can be formed by the oxidation of iron(II) mineral such as pyrite (Opdyke and Channell, 1996), whereas the Al^{3+} and Si^{4+} tend to form aluminosilicate clay minerals. In general, the common secondary mineral colloids formed by in-situ precipitation include aluminosilicates, amorphous Al hydroxide, Fe/Mn oxy(hydr)oxides, Fe/Al silicates (Zänker et al., 2006) and at usual soil pH of 6 – 7, they have low solubility (Scheinost, 2005). However, the dissolution and precipitation of mineral colloids are strongly influenced by changes in solution chemistry, such as the alternation of inundation and desiccation in soil and sediment or the transient flow in subsurface zone. Many soils, riparian zones and shallow river sediments experience change in water level due to seasonal/annual hydrological pattern or human actions, such as flood monitoring, water withdrawal and drainage (Gu et al., 2018; Kinsman-Costello et al., 2016). Fluctuation of water level can expose or inundate large area of sediments, lead to changes in redox potential and thus affecting biogeochemical processes including sorption-desorption, precipitation/coprecipitation, biological dissimilation, organic matter decomposition. The exposure of redox-sensitive species to oxygen can change their mineral form. For example, the drying of immersed sediment can cause a decrease in amorphous Fe/Al oxides content (de Vicente et al., 2010). The precipitation of reduced iron and sulfur to form pyrite is observed in the subsoil experiencing desiccation (Lucassen et al., 2002). The drying and rewetting of soil and sediment do not only lead to the formation of colloids but also impact on the diffusion/advection transport of colloids by altering the flow path permeability (Mohanty et al., 2015).

(3) Biological activities

The growth/death and metabolism activities of microorganisms are another source for colloidal particles through the presence of viruses, bacteria, protozoa as well as the production of fibrils, organic skeletons and protein-rich cell fragments (Keller and Auset, 2007; Wang et al., 2015). In addition, the respiration of microorganisms, particularly the anaerobic respiration, is well-known for its roles in the reductive dissolution of mineral species, such as iron oxides and oxy(hydr)oxides (Arnold et al., 1988; Suter et al., 1991; Peiffer and Wan, 2016). The dissolution of Fe cementing agent can release colloids from the bulk soil aggregates (Henderson et al., 2012). Moreover, the production of CO_2 during aerobic decomposition of organic matter liberates proton and organic acids altering solution pH impacting on the precipitation/dissolution of pH-sensitive species according to the partial pressure of CO_2 and alkalinity of soil solution (Heberling et al., 2014). In addition, colloids and associated contaminants can be resuspended from sediment to water via bioturbation of benthic fauna and macroinvertebrates (Brownawell, 1986; Andrade et al., 2020; Gautreau et al., 2020).

I.3.1.4. Association of phosphorus to colloids

As shown in chapter I.1.3, phosphorus is present in aquatic environment as free orthophosphate ions, polyphosphates, in organic compounds, but also in association with particulates (Van Moorleghem et al., 2011; Baken et al., 2016). The finer fraction of particles, which comprised of colloids and nanoparticles, have a great interest for acting as P carrier. Indeed, due to their high mobility and high specific surface area, colloids may carry and facilitate the transport of P in the ecosystem (Buffle and Leppard, 1995; Lead and Wilkinson, 2007; Rick and Arai, 2011; Zang et al., 2013; Châtellier et al., 2013; Gottselig et al., 2014; Baken et al., 2016; Gu et al., 2018; Gottselig et al., 2017a; Missong et al., 2018; Nomoto et al., 2019; He et al., 2019; Bollyn et al., 2019; Warrinnier et al., 2019). The environmental effects of P associated to colloidal particles are different from those of free phosphate (Baken et al., 2014; 2016). In natural ecosystems, vast heterogeneous mechanisms can contribute to association of P to colloidal particles, changing according to water composition and physico-chemical conditions (Baken et al., 2016; Gottselig et al., 2017a). The associated partner of P at colloidal scale can be either single component: mineral or organic matter; or organo-mineral complexes (Klitzke and Lang, 2007; Gottselig et al., 2017b).

Colloidal P is mostly associated with Fe oxy(hydr)oxides (Baken et al., 2016) since phosphates are highly adsorbed to Fe oxy(hydr)oxides and oxides through bridging binuclear complex of Fe – O – P (Parfitt et al., 1976) and the precipitation of Fe(III)-phosphate occurs at acidic pH (Châtellier et al., 2013). The adsorbed phosphate on amorphous Fe hydroxide surface can further react with other reactive sites and become occluded inside the structure of Fe minerals, whereby the crystalline iron oxy(hydr)oxides, such as goethite, have lower specific surface, thus, lower adsorption capacity and allows only surface adsorption (Chen and Arai, 2020).

Though, P also associates with colloids constituted of other elements such as OM, Al, Ca, Si, Mn. In arable topsoil, colloidal P are dominantly present in association of OM and amorphous Fe/Al oxides in nano fraction < 20 nm and in aggregates of fine clay, whereas P in association with OM and more crystalline Fe oxides is found in fine colloid fraction 170 – 225 nm (Jiang et al., 2015). In forest stream water, colloidal P are potentially linked to Fe oxy(hydr)oxides in nano fraction 1 kDa - 20 nm, in the intermediate size 20 – 60 nm colloidal P have organo-mineral composition and in large colloid 60 – 300nm, P is sorbed to clay mineral surface by ligand exchange with metal hydroxides (Gottselig et al., 2017b).

In slightly alkaline soil (pH of 7.5 - 8), P is mainly found in precipitated form with calcium though calcium phosphate occurs in all soil pH (Beauchemin et al., 2003). The coprecipitation reaction between phosphate and the calcite surface can occur during the growth of crystal, some of dissolved phosphorus may also be entrapped or occluded into the bulk structure during rapid crystal growth (Danen-Louwerse et al., 1995; House and Donaldson, 1986). The presence of Ca can also enhance phosphate sorption via phosphate-Ca interaction coupled with Fe precipitation and lead to the coprecipitation of amorphous Ca-Fe(III)-phosphate (Senn et al., 2015).

The cations Ca, Mn, Al and Mg are well-known as ideal ligands to form bridges between negative charged particles and are essential bonds between organic compounds or between organic matter with minerals (Missong et al., 2018; Tipping et al., 1995). The bonding between organic molecules and minerals/metal cations occurs through direct ligand exchange via hydroxyl group of organic substrates (Rowley et al., 2018). Dissolved humic substances interact with metal via functional groups that will in-turn support phosphate sorption (Chen and Arai, 2020). In slightly acidic soil with high organic content

(pH lower than 5.7), humic acid can form phosphate-Meⁿ⁺-humate complexes, for example a complex of RCOO–Ca²⁺–phosphate, through the binding between the oxygen atom of carboxylic ligands with the calcium ion (acting as a bridge) and phosphate binding to calcium ions (Alvarez et al., 2004).

Generally, the association of P to colloidal particles is principally constituted of various building blocks: aluminosilicates (clay), organic matter, oxides and hydroxides of Fe, Al and Mn (Lyven, 2003; Hartland, 2013; Baken et al., 2016; Gottselig et al., 2017b) (Figure 13).

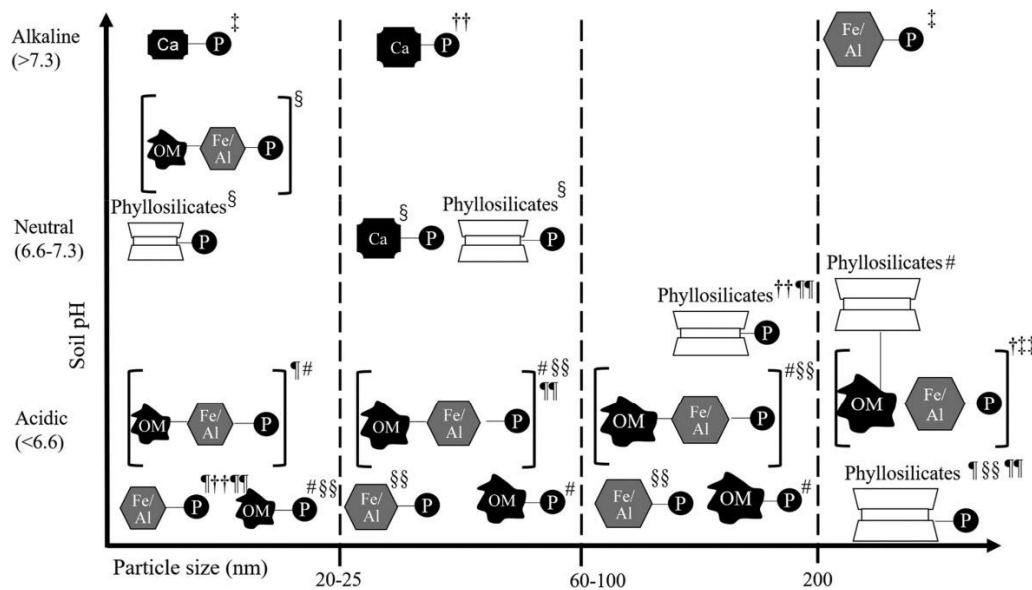


Figure 13. The distribution of different types of P-carrying colloids as function of pH and size in soil (Chen and Arai, 2020).

I.3.2. Evidences on release of colloidal phosphorus at sediment-water interface

It has been well-known that colloids contribute importantly to the transport of P in soil (Haygarth et al., 1997, Kretzschmar, 1999; VandeVoort et al., 2013), however almost zero literature studies concerning colloid-facilitated transport of P has been established at sediment-water interface.

Clay minerals, metal oxy(hydr)oxides, humic substances and microorganism can carry P at colloidal size at the subsurface environment (Kretzschmar et al., 1999; Hens, 2001; Ulén and Snäll, 2007). At sediment-water interface, P-bearing colloids are potential to migrate through sediment porous medium to the overlying water by hydrodynamic disturbance, bioturbations or changes in pH and redox condition (Buffle et al., 1989; Hens and Merckx, 2002; Sun et al., 2007). In the study of He et al., (2019), the content of colloidal P (difference between TP in fraction 2.0 μm and DIP in ultra-centrifuged aliquot) in sediment in agricultural land is relatively low, 0.5 %, in comparison to total sedimentary P; however, these P-colloids are the main component of the water-dispersible P fraction of sediment. Once mobilized to overlying water, this form of P remains stable in water column thanks to their small size, though colloidal P might be less available than orthophosphate (Baken et al., 2014). However, there are more mobile than particulate P, and thus can be transported for far longer distance. In lakes and reservoirs with long retention time, the resuspension of bottom sediment leads to release of colloidal P to water column and those released P-colloids can resettle only after 1 day without hydrodynamic perturbation

(Sun et al., 2007). The transportation of sedimentary colloidal P from sediment solution to the receiving water can be probably in comparative quantity with truly dissolved phosphorus (Zhang et al., 2020).

However, the mechanisms for P-colloid generation or mobilization from sediment have not been demonstrated. In contrary, mobilization mechanisms of P-colloids have been reported in many researches for various types of soils, leachate and forest stream water. For example, in riparian soil, Gu et al., (2018) found strong evidence on subsurface leaching of colloidal/nanoparticulate P during drying and rewetting events (DRW). The draining of leachate through a soil column was proceed for 30 hours and followed by drying by flushing O₂ for 2 days, this process was repeated for 3 times. The organic-rich and Fe/(Al)oxide-rich colloids contributed up to 70 % of total P in fraction lower than 0.45 µm released from soil leachate immediately after rewetting. The alternation between drying and rewetting of soil induces both physical (disruption of soil aggregates) and biological (microbial cell lysis) disturbance on soil that stimulates the mobility of colloidal/nanoparticulate P to soil solution. The increases in shear forces and capillary stress during drying pore walls and rewetting cause fragmentation of macropore walls and soil aggregates, that lead to mineral colloids release. Meanwhile, the osmotic shock upon rewetting of dried soil causes cell lysis and releases organic P to solution. These two independent P releasing processes can interact to form P-bearing organo-mineral colloids via the interaction between organic-P molecules and P-poor Fe oxyhydroxide colloids. The similar co-activation of physically and biologically release of P-colloids might also occur at sediment-water interface, which is often subjected to water level fluctuation and drying/rewetting alternance (Kerr et al., 2010; Cavaliere and Homann, 2012).

Furthermore, the released P-colloids from surface and subsurface runoff can migrate to rivers, lakes and reservoirs. Similar observation of colloidal P transport in runoff was pointed out by He et al., (2019). They monitored P-bearing colloids in runoff transfer from sloped farmland to sediment during rainfall event; they showed the content of colloidal P counted for 64.3 % of P loss in runoff and this content was linearly related to the sediment yield rate. The retained colloidal P within waterbodies having long retention times would latterly become a source of P to surface water in forms of resuspended P-colloids or anoxic-derived dissolved P (He et al., 2019; Moura et al., 2020; Zhang et al., 2020). Additionally, the release of dissolved P from sediment pore water can quickly precipitate with Fe, Ca, Al to form P-mineral colloids or be adsorbed to colloids upon the oxidation during resuspension (de Vicente et al., 2010).

1.3.3. Is colloidal phosphorus bioavailable to organisms?

P is an essential nutrient for growth and metabolism of organisms and accounts for approximately 3 % of the dry weight of all living organisms (White and Metcalf, 2007; Jin et al., 2019). However, not all forms of P are equally ready for algal uptake (Yang et al., 2018). The bioavailable P (BAP) is the fraction of P that plant and algae can use for growth and is defined as the sum of immediately available P for biological uptake and the P species that can be easily transformed into available forms by naturally occurring processes (Boström et al., 1988; Van Moorlegem et al., 2013; Li and Brett, 2015; Yang et al., 2018). The most bioavailable form of P is the free orthophosphate ions that are readily for algal uptake, whereas, the majority of other P forms can become available conditionally (eg., P bound to colloids and amorphous phosphate mineral forms) or are not available (insoluble and crystalline phosphate minerals) (Reynolds and Davies, 2001).

The colloidal P can be available at long-term scale and their bioavailability would vary depending on the speciation, therefore, the structural properties of P-colloids shall be well determined (Baken et al.,

2014). Meanwhile most of organic P can be converted into inorganic phosphate by biomineralization, chemical decomposition and photodegradation (Björkman and Karl, 2003; Guo et al., 2020); the liberation of bioavailable phosphates from inorganic species occurs via the chemical or biological dissolution of P-rich precipitation and desorption from metal oxides and hydroxides (Reynolds and Davies, 2001; Litchman and Nguyen, 2008; Van Moorlehem et al., 2013). The variability in the affinity of phosphate to mineral surfaces plays an important role in determining its P bioavailability. Guzman et al., (1994) found that the availability of adsorbed phosphate to iron minerals decreases with increasing relative affinity for phosphate. For instance, the adsorbed phosphate was more available in hematite and ferrihydrite than goethite. The amorphous Al oxides are shown to have higher availability than the more crystalline minerals (goethite) (He et al., 1994). The desorption of P can be driven by changes in pH in which the increasing pH to above 6.0 would enhance P desorption by increasing competition between hydroxyl and phosphate ions for specific sorption sites on mineral surfaces (Sato and Comerford, 2005).

According to the series of studies on Fe-rich colloids and their ability to associate with P (Baken et al., 2014; 2016), the P-saturated Fe-colloids (molar P:Fe ratio of above 2) contain mostly labile P which can be released within 7 days. Therefore, even though the associated P in the natural Fe-P-bearing colloids is not immediately available (within 1 hour), its availability for the longer term (days and weeks) should be examined (Baken et al., 2014). For this long-term BAP, their potential to deliver nutrient for algae growth can be observed after several weeks of culturing compared to the immediately BAP fraction (Van Moorlehem et al., 2013).

Additionally, according to Poirier et al., (2012), the fine fraction of sediment sized 0.05 – 1 μm , which was accounted for 50 – 68 % of particulate P in soils, contained more BAP (on average of 0.46 g P/kg, determined by 0.1 M NaOH extraction) than in coarser fraction of sediment sized 1-100 μm (0.22 g P/kg). This finding provides an evidence that colloids sizes lower than 1 μm contain more BAP than coarser particles (> 1 μm).

In general, though colloid-bound P is indeed having high mobility in aqueous environment, their bioavailability remains a disputed issue, therefore, requires acute evaluation in order to elucidate their role in delivering nutrients in regard to environmental problems such as harmful algal blooms.

Conclusion

In environmental sciences, colloids have been receiving increasingly interest thanks to their critical role in (i) carrying and facilitating transport of nutrients and contaminants in aquatic systems (Chotpantararat and Kiatvarangkul, 2018; Gottselig et al., 2014; Gu et al., 2018; Tran et al., 2016; Zänker and Hennig, 2014), (ii) their contribution to contaminant speciation in natural environment (Baken et al., 2016, Li et al., 2019; Liang et al., 2016; Xu et al., 2018) and (iii) the bioavailability of colloid-bound elements (Bollyn et al., 2019, Wang and Guo, 2000). However, many studies did not differentiate between dissolved and colloid-bound species. The filtration through 0.45 μm or 0.2 μm pore size for separation of dissolved and particulate species were widely used but this conventional separation ignored the presence of colloids.

The colloidal systems are generally heterogeneous mixture in terms of size and physico-chemical components. The finer colloidal fraction might have higher surface area and be composed by materials that are different than in larger colloidal fraction, thus, lead to different behaviors. Therefore, it is important to characterize the entire colloidal fraction but so is the distinction of colloidal fraction into different sub-divisions. In this study, we would like to investigate the fate of phosphorus present in

fraction sub-micron ($< 1 \mu\text{m}$), which is now called water-mobilizable fraction in this manuscript. As a result, a subset of nano/small colloids, intermediate/large colloids were performed based on size (Table 5).

Table 5. The classification of colloids based on size ranges

Label	Size range (nm)
Small/nano colloids	< 200
Large/intermediate colloids	$200 - 1000$

I.4. Current states of natural colloid extraction, separation, fractionation and characterization

A wide range of techniques have been applied to collect and analyze colloids from natural matrices. This chapter presents common methods used to extract, separate, fractionate and characterize colloids.

I.4.1. Colloid extraction

Mobilization of colloids can be induced by both physical and chemical condition. Colloids are generally electrical charged on their surface (Khilar and Fogler, 1998), therefore the major factors inducing colloid release are changes in solution pH and ionic strength. Numerous researches have elucidated the increase detachment and release of colloids under low ionic strength and high pH (Klitzke et al., 2008; Liang et al., 2010; Shang et al., 2008). However, change in ionic strength do not always stimulate colloid release, for instance, in case colloids and attached grains are oppositely charged, the low ionic strength provides no impact on colloid mobilization due to the strong electrostatic attraction (Sen and Khilar, 2006). The more common mobilization of colloids in natural environment is found to be relied on hydrodynamic forces. The act of hydrodynamic forces is complex and multi-dimensional, including lifting, surface sliding and rolling of colloids (Sen and Khilar, 2006).

To extract colloids from natural matrices, the most employed method is based on physical perturbation to disturb the balance between colloidal and hydrodynamic forces: agitation and sonication. Both techniques generate mechanical energy to overcome attraction forces between colloids and grains, promoting colloid dispersion and liberation. Agitation provides turbulence through the movement of solution according to air volume inside container to accelerate colloid dispersion and a kinetic energy to disrupt aggregates (So et al. 1997). However, the energy induced by agitation often impacts on unstable structure and barely lead to physical disruption of structure smaller than $2 \mu\text{m}$ (Mentler et al., 2004, So et al., 1997). In contrast, sonication is more abrasive technique, working by generating powerful ultrasound vibration amplitudes and cavitation which stress and break aggregate bonds (Schomakers et al., 2015). The high acoustic pressure emitted to solution caused by sonication can accelerate the disruption of stable particles with dimension of $2 \mu\text{m}$ (Schomakers et al., 2015). At energy range of as low as 60 J/mL , ultrasound energy can easily disrupt unstable aggregates sized $250 \mu\text{m}$ or smaller, those stable aggregates in smaller size class (clay) can be breakdown under energy of 700 J/mL (Kaiser and Berhe, 2014). Therefore, a question remains to be elucidated is that how sonication impact on the liberation of colloids and does sonication generate colloids according to its abrasive energy.

In addition, the diversification among existing colloid extraction methods encounters also differences in types and characteristics of material (soils, sediment, surface and ground water) as well as the treatments of raw material (moist, air-dried, oven-dried at various temperature, lyophilized) (see Table 6). The drying of soil was demonstrated to increase soil aggregation due to evaporation of water and precipitation of salts and minerals acting as cementing agent (Majdalani et al., 2008; Munkholm and Kay, 2002). Meanwhile the sublimation of ice during lyophilization can enlarge pore structure and facilitate transport of colloids in porous media (Dagesse, 2011). Due to these possible modifications in physicochemical properties of raw materials when subjected to different drying conditions, differences in sample storage could induce variation in quantity and quality of colloids to be extracted compared to fresh moist sample.

I.4.2. Colloid separation

The separation of colloidal fraction from particulate and truly dissolved fractions has been performed by several methods such as sedimentation, membrane filtration and centrifugation. Among them, filtration and centrifugation are more widely used than sedimentation.

I.4.2.1 Sedimentation

Sedimentation is a process that Brownian particles attain a certain settling velocity due to an external field (Dhont, 1996). A common sedimentation is based on gravitational field, which is an effective and economic means to clarify particles from suspension. Depending on the size and density of particle, a settling velocity can be used to characterize and separate different species of Brownian particles. During sedimentation, according to designated settling velocity and time, to separate particles at 1 μm , a long detention time would be required. Therefore, sedimentation is often coupled filtration or centrifugation in which particles that do not deposit and remain in suspension will be carried out to further treatment such as filtration or centrifugation to obtain colloidal size fraction.

I.4.2.2 Membrane filtration

Membrane separation is a versatile method for isolation of colloids from natural materials due to its feasibility for field operation, simplicity and low cost (Morrison and Benoit, 2001). In general, the sample solution is put under vacuum or pressure to flow through membrane surface. All the particles larger than pore size of filter paper are retained, while small particles and solutes pass through the filter. The accuracy of filtration is considered being high in case of no retardation, though in reality, its accuracy is often limited by formation of filter cake, membrane clogging (Zirkler et al., 2012), but also due to interaction with membrane. The foulant layers formed during filtration of colloidal solution exhibit the transition characteristic between concentration polarization and deposition (Chen et al., 1997). The concentration polarization refers to an increase in local concentration at near membrane surface compared to the bulk concentration that is caused by retention of particles (Bowen and Jenner, 1995). This significant mass polarization leads to a phase transition of matter from dispersed to condensed states (Bacchin et al., 2006; Bessiere et al., 2008). At sufficient concentration at polarized layer and weak repulsive forces between colloids, colloids can flocculate, deposit and form a cake layer that causes decreasing permeate flux (Tang et al., 2011). Meanwhile the filter clogging refers to the entrapment of colloids within the net of multilayered and complicated membrane structure (Zirkler et al., 2012). The increase of filtration volume can easily lead to overload membrane filter and decrease effective pore size due to colloids got lost or attached in/to pore structure and increase amount of colloids being retained (Morrison and Benoit, 2001). The recommendation for routine practices with filtration is

to pass small sample volume, terminate the collection of filtrate when permeate flow decreases and use multiple filters for large sample volume (Morrison and Benoit, 2001). Many factors are assumed to impact the colloid retention during membrane filtration including the characteristic of membrane and colloidal particles as well as solution chemistry.

One of the pronounced characteristics playing role during filtration of colloids is the membrane morphology (Fig. 14). The polymer track-etched membranes with straight cylindrical pores, such as polycarbonate and polyester (Fig. 14-3A and 3B), has lower abundance of pores at filter surface thus colloids deposit more in the space between pores (Iritani et al., 2017; Zirkler et al., 2012). The tortuous path membranes such as glass fiber (Fig. 14-2A and 2B), cellulose acetate, cellulose nitrate (Fig. 14-1A and 1B), are recommended for colloid fractionation because they are not easily clogged as track-etched membrane (Morrison and Benoit, 2001). However, the colloids often get lost within their multilayered and interconnected structure (Zirkler et al., 2012).

The surface charges and hydrophobicity of colloids involve in the interactions of colloid-colloid and colloid-membrane. If the filter and colloids have opposite charges, colloids are then attracted to the pore surface of filter due to the electrostatic adsorption (Lee , 1998). The increase in ionic strength will decrease the Debye length of electrical double layer, causing lower energy barrier and enhance aggregation of colloids or attachment of colloids to filter surface (Tang et al., 2011). The increase ionic strength, in general, leads to higher membrane fouling for small pore size membrane filter (Boussu et al., 2007). Furthermore, the difference in hydrophobicity between colloid and filter surface is another factor to determine the attraction (retention) or repulsion of colloids to pore walls (Brant and Childress, 2004).

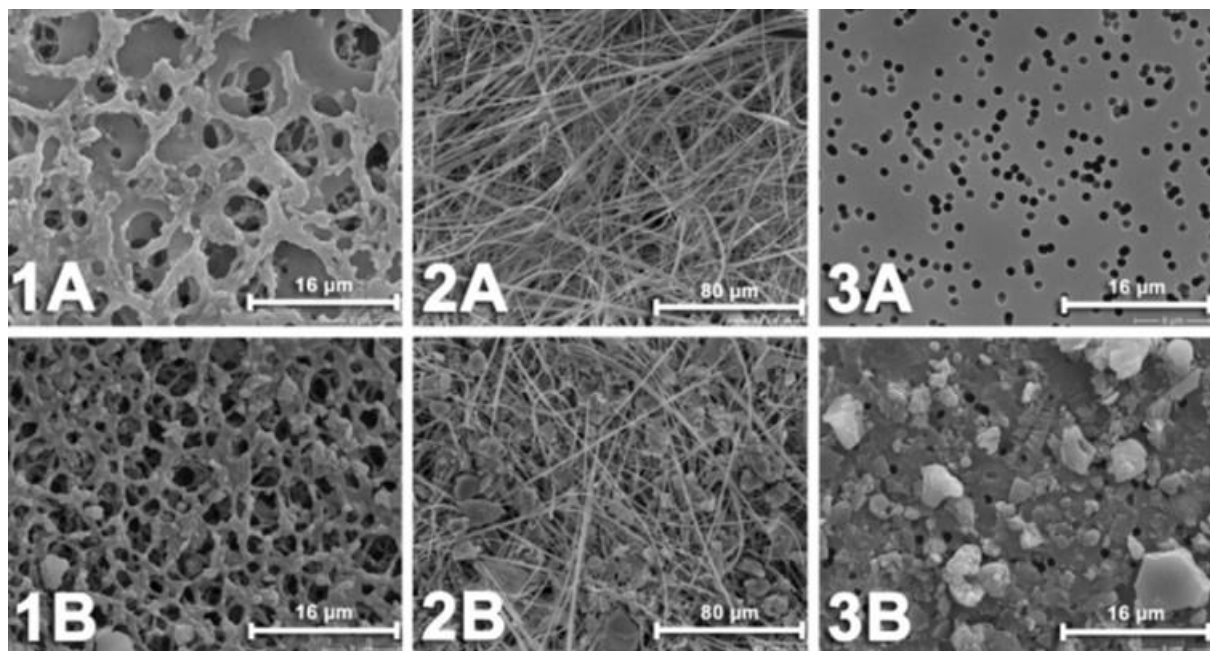


Figure 14. The surfaces of tortuous path membranes (1) 1.2 µm cellulose nitrate filter, (2) 1.0 µm glass fiber filter and polymer track-etched membrane (3) 1.0 µm polycarbonate filter. A: before filtration. B: after filtration of 10 mL soil suspension (S/L of 1/10). Images are taken from the work of Zirkler et al., (2012).

I.4.2.3 Centrifugation

Centrifugation is an accelerated sedimentation method with the application of intensive g-force (Ermolin and Fedotov, 2016). The problems of clogging and interaction of colloids with membrane filter during separation by filtration can be minimized when using centrifugation. Colloids are settled based on size at a given centrifugal force and time depending on particle density. Therefore, the accuracy of this technique depends greatly on particle material, size and shape (Shard et al., 2018). However, in natural samples, particle densities encounter a wide range from less than 1.0 g/cm³ for organic particles to more than 5 g/cm³ for iron oxide particles (Teja and Koh, 2009; Mankasingh and Gísladóttir, 2019). This diversity in particle density, concomitant with the polydispersity in size of natural colloidal material, will consequently lead to the difficulty in the achievement of precise size separation when using centrifugation (Zirkler et al., 2012). In addition, the assemblage of colloids into large particles can occur during centrifugation if the centrifugal force exceeds the interparticle electrostatic repulsion (Salim and Cooksey, 1981; Fan et al., 2015). Due to the infeasibility to obtain homogeneity in size or particle density of colloids from heterogeneous natural samples by centrifugation and to avoid the clogging of filter by large particles during filtration, the filtration at higher porosity or combination of both centrifugation and filtration can be a solution to obtain a precise size-separated colloidal fraction (Shand et al., 2000, Séquaris et al., 2013).

Other rarely encountered methods are listed in Table 9 including continuous flow centrifugation (CFC) and hollow fiber filtration (Hart et al., 1993) as well as straining through soil column (Kaplan et al., 1993).

I.4.3. Colloid characterization

The size, quantity and chemical properties of colloids has been characterized using various techniques and detailed discussion is provided in the following.

The size distribution and chemical composition are important properties in order to evaluate environmental colloids fate and behavior. The common methods used in measurement of size distribution include laser diffraction (LD), multiangle laser light scattering (MALLS) and dynamic light scattering (DLS). The LD and MALLS share similar principle by measuring size distribution based on the Fraunhofer and Mie diffraction theory in which the diffraction patterns (intensity and angle of scattering light) of a particle is proportional to its size (Ermolin and Fedotov, 2016; Varga et al., 2019). The difference between these two methods is that the MALLS allows measurement at several angles of scattered laser beam (Ermolin and Fedotov, 2016), whereas the DLS is based on the fluctuation in light intensity caused by Brownian motion of particles in suspension (Derkachov et al., 2020). The intensity fluctuation is linked to velocity of Brownian movement and allows calculation of particle size following Stokes-Einstein equation (Ermolin and Fedotov, 2016). Image analysis by scanning electron microscopy (SEM), environmental SEM or transmission electron microscopy (TEM) allows the visualization of precise size and morphology of individual colloids (Luo et al., 2013).

The analysis of colloid chemical composition can be done by a wide range of analytical methods. The examples are inductively coupled plasma optical emission spectrometry (ICP-OES) (Mills et al., 2017) and inductively coupled plasma mass spectrometry (ICP-MS) (Gottselig et al., 2017a, Missong et al., 2018, Maria et al., 2020).

The quantification of colloids is usually employed by gravimetric methods to measure dry mass of colloidal suspension (Table 6) but sometimes the dry mass does not exclude mass of dissolved salts

(Tulve and Young, 1999). Another method for colloid quantification is its estimation based on turbidity of colloidal suspension (Zirkler et al., 2012; Yan et al., 2017; 2018).

Conclusion

Overall, from literature survey, the isolation and characterization of colloids were mainly proceeded for soil and water sample, meanwhile sediment matrix has been rarely studied. For this reason, the knowledge on characteristics of sedimentary colloids as well as the method to extract and characterize them remains limited and requires further evaluation. The assessment of colloid isolation from sediment would confront the effects of sample storage modes, extraction and separation protocols on both quantity and properties of recovered colloids.

Table 6. Colloid separation using filtration, centrifugation, and the combination.

Note: CNA: composite cellulose nitrate/acetate membrane, DI: deionized water, nd: not determined, OM: organic matter, S/L: solid-liquid ratio by dry weight per volume, UC: ultra-centrifugation, UF: ultrafiltration, UPW: ultra-pure water

Authors	Matrix	Storage	Extraction method	Separation method		Colloid size	Colloid quantitative method	Colloid quantity
Kretzschmar et al., (1995)	Georgeville clay loam soil Fraction: nd	24 h - soaked soil	S/L: nd Dispersant: DI Mode: agitation (2 h)	Wet sieving Centrifugation	nd	0.05 - 0.5 μm	nd	nd
Haygarth et al., (1997)	River and soil waters Fraction: nd	Store at 4°C	nd	Filtration	Membrane filtration: 0.45, 0.22, 0.1 and 0.025 μm (CNA) UF: 10 kDa and 1 kDa at 276 kPa	nd	nd	nd
Bergendahl and Grasso, (1998)	Soil Fraction: < 6 mm	Store at 4°C	S/L: 1/20 Dispersant: acetate buffer (pH 5); UPW Mode: agitation at 30 rpm (6, 18, 24 and 36 h)	Filtration	Membrane filtration: 0.7 μm (glass fiber filter)	0.47 - 0.95 μm (peak at 0.65 μm)	nd	nd

Sinaj et al., (1998)	Soil Fraction: nd	nd	S/L: 1/10 Dispersant: nano pure water Mode: agitation (17 h)	Centrifugation combined filtration	Centrifugation: 2500 g (15 min) Filtration: 0.45, 0.2 or 0.025 μm	0.025 - 0.45 μm	Air dry	260 - 1320 mg/kg soil
Shand et al., (2000)	Soil rich in OM Fraction: < 6 mm	Air-dry	nd	Centrifugation and successive filtrations	Centrifugation: 1000 g (60 min) Filtration: 1.6 μm , 1.2 μm , 0.7 μm , 0.45 μm and 0.22 μm UF: 100, 10 and 1 kDa	0.22 - 1.2 μm	nd	nd
Turner et al., (2004)	Soil Fraction: < 2 mm	Air-dry (7 days)	S/L: 1/100 Dispersant: DI Mode: sonication at 650 W (5 min)	Centrifugation, filtration, UF	Centrifugation: 3000g (15 min) Filtration: 1, 0.4, 0.2 and 0.1 μm UF: 100, 10, 3 and 1 kDa	1 kDa - 1 μm	nd	nd
Klitzke et al., (2008)	Soil Fraction: < 2 mm	nd	S/L: 1/10 Dispersant: water Mode: agitation (12 h)	Filtration and UC	Filtration: 1.2 μm UC: particle diameter 4 and 10 nm	250 - 900 nm	nd	nd

Liang et al., (2010)	Soil Fraction: < 2 mm	Air-dry	S/L: 1/8 Dispersant: DI Mode: agitation at 160 rpm (24 h)	Centrifugation, filtration and UC	Centrifugation: 3000 g (10 min) Filtration: 1 µm UC: 300,000 g (2h)	nd	nd	nd
Murali et al., (2012)	River sediment Fraction: nd	Air-dry	S/L: 1/5 Dispersant: distilled water Mode: agitation (24 h)	Centrifugation	750 rpm (15 min)	20 - 300 nm	Dry at 100 °C	200 - 2400 mg/L
Zirkler et al., (2012)	Soil Fraction: < 2 mm	nd	S/L: 1/10 Dispersant: DI Mode: agitation at 15 rpm (16 h)	Filtration, centrifugation, UC	Filtration: 1.2 and 1 µm Centrifugation: 78 g UC: 124,000 g (1 h 17 min)	< 1 µm	Turbidity	Maximum: 1200 NFU
Séquaris et al., (2013)	Ruptic and silty soil Fraction: < 2 mm	Air-dry	S/L: 1/10 Dispersant: DI Mode: agitation at 150 rpm (6 h)	Sedimentation and centrifugation	Sedimentation: 12 h Centrifugation: 10,000 g (90 min)	499 - 790 nm	nd	nd

VandeVoort et al., (2013)	Sandy loam soil Fraction: < 2 μm	Air-dry	S/L: 1/20 Dispersant: nd Mode: agitation (48 h)	Centrifugation and filtration	Centrifugation: 2300 g (3 min) Filtration: 0.2 μm	0.2 - 0.41 μm	nd	nd
Zang et al., (2013)	Gleyed paddy soil Fraction: < 2 mm	Air-dry	S/L: 1/20 Dispersant: DI Mode: agitation (16 h)	Centrifugation, filtration and UC	Centrifugation: 3000 g (10 min) Filtration: 1 μm UC: 300,000 g (1h)	nd	nd	nd
Buettner et al., (2014)	Mineral soil Fraction: nd	Store at 4°C	S/L: 1/10 Dispersant: 2 mM KCl Mode: agitation at 120 rpm (2 h)	Successive centrifugation and UF	Centrifugation: 3195 g (3 min); 21,169 g (24 min) UF: 10 kDa (14,000 rpm, 10 min)	2.3 - 430 nm	nd	nd
Liu et al., (2014)	Ultisol soil Fraction: nd		S/L: 1/8 Dispersant: DI Mode: agitation (24 h)	Centrifugation, filtration and UC	Centrifugation: 3000 g (10 min) Filtration: 1 μm UC: 300,000 g (2 h)	0.02 – 1 μm	Dry at 100°C	nd

Missong et al., (2016)	Cambisol soil Fraction: < 2 mm	Fresh sample	S/L: 1/8 Dispersant: UPW Mode: agitation at 150 rpm (6 h)	Sedimentation, centrifugation and UC	Sedimentation: 15 - 20 min Centrifugation: 4000 g (4 min) UC: 14,000 g (60 min)	350 - 400 nm (average size)	Freeze drying	nd
Lou et al., (2017)	Soil Fraction: < 2 mm	Air-dry	S/L: nd Dispersant: nd Mode: agitation (2 h); sonication (30 min)	Sedimentation	Settle 24 h	96 - 181 nm (mean diameter)	nd	nd
Ma et al., (2017)	Forest land soil Fraction: 11.5 µm	nd	S/L: nd Dispersant: UWP Mode: sonication	Sedimentation and filtration	Sedimentation: nd Filtration: 1.2 µm	257.4 nm (Average size)	nd	nd
Mills et al., (2017)	Ground water and soil Fraction: nd	nd	S/L: nd Dispersant: DI Mode: agitation (1 h)	Filtration and centrifugation	Filtration: 0.45 µm Centrifugation: 8000 rpm (4.5 h)	0.02 - 0.45 µm	nd	nd

Yan et al., (2017)	Soil Fraction: < 0.05 mm	Air-dry	S/L: 1/10 Dispersant: DI Mode: agitation (24 h); sonication (15 min)	Successive centrifugation	Centrifugation: 221 g (8 min); 884 g (10 min); 22,095 g (8 min)	< 0.1 µm 0.1 - 0.45 0.45 - 1 µm	Dry at 105°C	nd 46.9 mg/L 29.2 mg/L
Gu et al., (2018)	Luvisol soil (leachate) Fraction: < 2 mm	Air-dry	S/L: nd Dispersant: 10 mM NaCl Mode: agitation (24 h); sonication (15 min)	Filtration and UF	Filtration: 0.45 µm UF: 30 kDa and 5 kDa (3400 g, 15 and 25 min, respectively)	5 kDa - 30 kDa 30 kDa - 0.45 µm	nd	nd
Xu et al., (2019)	Lake sediment Fraction: < 2 mm	Freeze-dry	S/L: 3/20 Dispersant: NaHCO ₃ Mode: sonication	Sedimentation, UF and UC	Sedimentation: nd UF: 1 kDa (concentration factor: 25) UC: 15,000 g (10 min)	30 - 200 nm	nd	nd

Table 7. Colloid fractionation using field-flow fractionation.

Note: FFF: field-flow fractionation, SdFFF: Sedimentary field-flow fractionation, FIFFF: flow field-flow fractionation, AF4: asymmetric flow field-flow fractionation, TSPP: sodium pyrophosphate, UF: ultrafiltration, UPW: ultra-pure water

Authors	Matrix	Storage	Extraction method	Separation method		Colloid size	Colloid quantitative method	Colloid quantity
				Principal	Operation			
Lee, (1998)	River water Fraction: nd	Store at 7°C	S/L: nd Dispersant: nd Mode: agitation (1h), sedimentation (20 min), sonication (5 min)	FFF	Channel: 26.5 cm x 2 cm (length x breadth) Channel void volume: 90 mL Carrier fluid: various composition Channel flow: 2 mL/min Microfiltration: 0.02 µm and 0.03 µm UF: nd	185 ± 30 nm 481 ± 113 nm 734 ± 149 nm	nd	nd
Stolpe et al., (2013)	River water Fraction: < 0.45 µm	Store at 8°C	nd	FFF	Membrane: 1 kDa Channel flow 0.5 mL/min Cross flow 3 mL/min	1 kDa - 0.45 µm	nd	nd
Chittleborough et al., (1992)	Sandy loam soil Fraction: < 2 µm	nd	S/L = 1/500 Dispersant: nd	SdFFF	Channel void volume: 5.3 mL Channel void thickness: 0.0266 cm Carrier fluid: UPW	0.04 – 0.5 µm	nd	nd

			Mode: sedimentation		Relaxation: 1000 rpm, $t_1 = 10$ min, $t_a = -80$ min Channel flow: 2 mL/min			
Ranville et al., (1999)	Soil Fraction: <1 μm	nd	nd	SdFFF	Channel void volume: 2.5 mL Channel void thickness: 0.0127 cm Carrier fluid: 1mM TSPP Relaxation: 800 rpm, $t_1 = 4$ min, $t_a = -33$ min Channel flow: 1 mL/min	0.08 - 1 μm	nd	nd
Chen et al., (2001)	Soil Fraction: < 1.2 μm	Air-dry	S/L: 1/24 Dispersant: water Mode: sonication at 650 W (5 min)	SdFFF	Channel void volume: 2.5 mL Channel void thickness: 0.0127 cm Carrier fluid: 1mM TSPP Relaxation: 700 rpm, $t_1 = 5$ min, $t_a = -40$ min Channel flow: 1 mL/min	< 1.2 μm	nd	nd
Lyven et al., (2003)	Freshwater Fraction: < 0.45 μm	Store at 4 °C	nd	FIFFF	Carrier fluid: 5 mM borate buffer (pH 8.1) and 10 mM NaCl Membrane: 1 kDa Channel flow: 0.5 mL/min Cross flow: 2.96 mL/min	1 kDa - 0.45 μm	nd	nd

Regelink et al., (2014)	Agricultural soil Fraction: < 2 mm	40°C-dry	S/L: 1/500 Dispersant: 5 mM NaHCO ₃ (pH 8.3); 10 mM TSPP (pH 8.5) Mode: agitation at 60 rpm (20 h), sonication at 106 W	Centrifugation, filtration and AF4	Centrifugation: 2100 g (10 min) Filtration: 0.45 µm AF4: - Membrane: 1 kDa - Cross flow: 0.2 mL/min	1 kDa - 0.45 µm	nd	nd
Gottselig et al., (2017b)	Stream water Fraction: < 5 µm	nd	S/L: nd Dispersant: nd Mode: agitation	AF4	Membrane: 1 kDa Tip flow: 0.3 mL/L Cross flow: 3 mL/min Focus flow: 3.2 mL/min (30 min)	nd	nd	nd
Kim et al., (2017)	Ground water Fraction: 10 kDa – 0.45 µm	nd	nd	AF4	Membrane: 10 kDa Pump flow: 0.2 mL/min (60 s) Focus flow: 1.5 mL/min	20 - 700 nm	nd	nd
Cuss et al. (2018)	River water rich in OM and Fe Fraction: < 0.45 µm	Store at 4°C	nd	AF4	Membrane: 300 kDa Focus flow: 0.2 mL/min (6 min) Crossflow: 2.1 mL/min	300 kDa - 0.45 µm	nd	nd

					Channel flow: 0.7 mL/min			
Missong et al., (2018)	Cambisol soil (leachate) Fraction: nd	Store at 4°C	S/L: nd Dispersant: 10 mM NaCl Mode: sonication	AF4	Membrane: 1 kDa Carrier fluid: 25 μM NaCl Cross flow: 3 mL/min Focus time: 25 min	0.6 – 20 20 – 70 70 - 400 nm	nd	nd

Table 8. Colloid fractionation using cross-flow ultrafiltration (CFF).

Note: CFF: cross-flow ultrafiltration, DI: deionized water

Authors	Matrix	Storage	Extraction method	Separation method		Colloid size	Colloid quantitative method	Colloid quantity
Dai et al., (1998)	Sea water Fraction: < 0.2 µm	nd	nd	CFF	Membrane: 1 kDa (Amicon) Pressure: 14 – 16 psi	nd	nd	nd
Ran et al., (2000)	River waters Fraction: < 25 µm	nd	nd	CFC and CFF	CFC flow: 4 L/min CFC speed: 5260 g Filtration: 1 µm, 0.2 µm, 100 kDa, 10 kDa	0.2 – 1 µm 100 kDa – 0.2 µm 10 – 100 kDa	Dry 103-105°C (16 h)	nd
Wang and Guo, (2000)	Sea water Fraction: < 0.2 µm	nd	nd	CFF	Membrane: 1 kDa Concentration factor: 40 L	1 kDa - 0.2 µm	nd	nd
Hasselov et al., (2007)	Ground water Fraction: < 0.22 µm	N ₂ purge	nd	CFF	Membrane: 1 kDa Cross pressure: 0.4 bar Permeate flow rate: 120 mL/min	1 kDa - 0.22 µm	nd	nd
Tang et al., (2009)	Soil Fraction: < 250 µm	Air-dry	S/L: 1/20 Dispersant: DI	Sieving, sedimentation, centrifugation and CFF	Sieving: 50 µm Sedimentation: 1 h 14 min	635 nm 76 nm	nd	nd

			Mode: sonication (10 min)		Centrifugation: 433 g (5 min); 3900 g (54 min) CFF: 0.1 µm membrane	(mean diameters)		
Baken et al., (2016)	Stream water Fraction: < 0.45 µm	Reduce hardness: Dowex HCR-S/S softening resin	nd	CFF	Membrane: 30 kDa	30 kDa - 0.45 µm	nd	nd
Wang et al., (2018)	Ground water Fraction: < 1 µm	nd	nd	CFF	Membrane: 100 kDa Permeate flow rate: 650 mL/min	50 - 1100 nm	nd	nd

Table 9. Application of other separation methods

Note: CFC: continuous flow centrifuge

Authors	Matrix	Storage	Extraction method	Separation method		Colloid size	Colloid quantitative method	Colloid quantity
Hart et al., (1993)	Flooded materials Fraction: nd	nd	nd	CFC and hollow fiber filtration	CFC speed: 8200 rpm CFC rate: 4 L/min Hollow fiber filtration: 0.1 µm and 0.015 µm	0.015 - 0.1 µm 0.1 - 1 µm	Dry at 103-105°C (16 h)	0.7 - 1.2 mg/L 5.5 - 8.6 mg/L
Kaplan et al., (1993)	Blanton soil Fraction: < 2 mm	nd	nd	Straining through soil profile	Lysimeter: 3 m x 3m x1.5m (Length x width x depth) Simulated rain event: Effluent: tap water (pH = 6.1, conductivity = 0.6mS/m) Rainfall rate: 5.1 cm/h, 2 h Effluent collection period: 2 - 28 h	0.1 – 1 µm	Dry at 373K (100°C)	0.3 - 1.7 g/L
Tulve and Young, (1999)	River sediment Fraction: < 63 µm	Air-dry	S/L: 1/1000 Dispersant: DI	nd	nd	< 10 µm (95%)	Dry at 105°C	122 mg/L (TSS)



			Mode: agitation, sedimentation (2 min), sonication (> 24 h)					
--	--	--	--	--	--	--	--	--

I.5. Global conclusion for literature review

One of the largest pools of P in global cycles is aquatic benthic sediment. With human intervention on hydrological transport system, sediment is retained in man-made dam reservoirs. It is estimated that river damming would retain 17 % of global riverine TP in 2030s (Maavara et al., 2015), therefore, dam reservoirs can attribute a potentially important pool of P.



Figure 15. Schema for the mobility of water-mobilizable P (sized below 1 μm) in reservoir bottom sediment.

Sediment accumulation in dam reservoir can act as both a sink and a source of P (Fig. 15) depending on physical, chemical and biological parameters that can induce the transformation and migration of P from sediment to water column. Consequently, the parameters such as redox potential, pH, temperature, microbial activity, dry/wet cycles and composition of P pools should be considered. Unlike the input of external P that can be effectively reduced and mitigated, the control of internal P is more complex (Wen et al., 2020). Furthermore, since P has high affinity to solid phase, the transfer of sedimentary P to water column is not limited to soluble form but also in particulate and colloidal forms. To better understand and monitor P mobility, special attention should be paid to colloidal P which remains suspended and potentially labile to be uptaken by phytoplanktonic species.

The natural colloids are heterogeneous in size and chemical composition. Different size class of colloidal fraction might exhibit different surface area and composed by different materials, thus, can behave differently. Therefore, the characterization of colloidal fraction should take into account also the fractionation and characterization of sub colloidal size classes. In this study, we would like to investigate the fate of phosphorus present in fraction sub-micron ($< 1 \mu\text{m}$), which will be called water-mobilizable fraction.

The isolation and characterization of colloids were mainly performed on soil/water matrices and rarely encountered for sediment matrix. To better isolate and characterize sedimentary colloids, it is important to determine the proper method to extract and characterize them, considering sample storage modes, extraction and separation protocols on quantity and quality of recovered colloids.

The questions we propose to investigate are:

- How to isolate colloids from sediment matrix?
- What is the role of colloids in P mobility?
- How do colloids and associated P vary along dam reservoir?
- How do colloids and associated P behave in anoxic bottom sediment?

Part II. Materials and methods

II.1. Studying area and sampling method

II.1.1. Characteristics of Champsanglard reservoir

Champsanglard hydroelectric dam reservoir is located on Creuse river (Fig. 16), in central France. It belongs to the Age complex, composed of the cascade of three dams which can supply electricity for a population of 21,000 inhabitants. The river source is from the Mas-D'Artige, in the south of Creuse department, Plateau de Millevaches (890 m above the sea level) and extends north-west toward the Col du Massoubre before flowing into the Vienne river at Port-de-Piles, Indre department (at 44 m above sea level) (Despriée et al., 2004). The Creuse river flows through 264 km length and receives water from a 10,279 km² watershed.

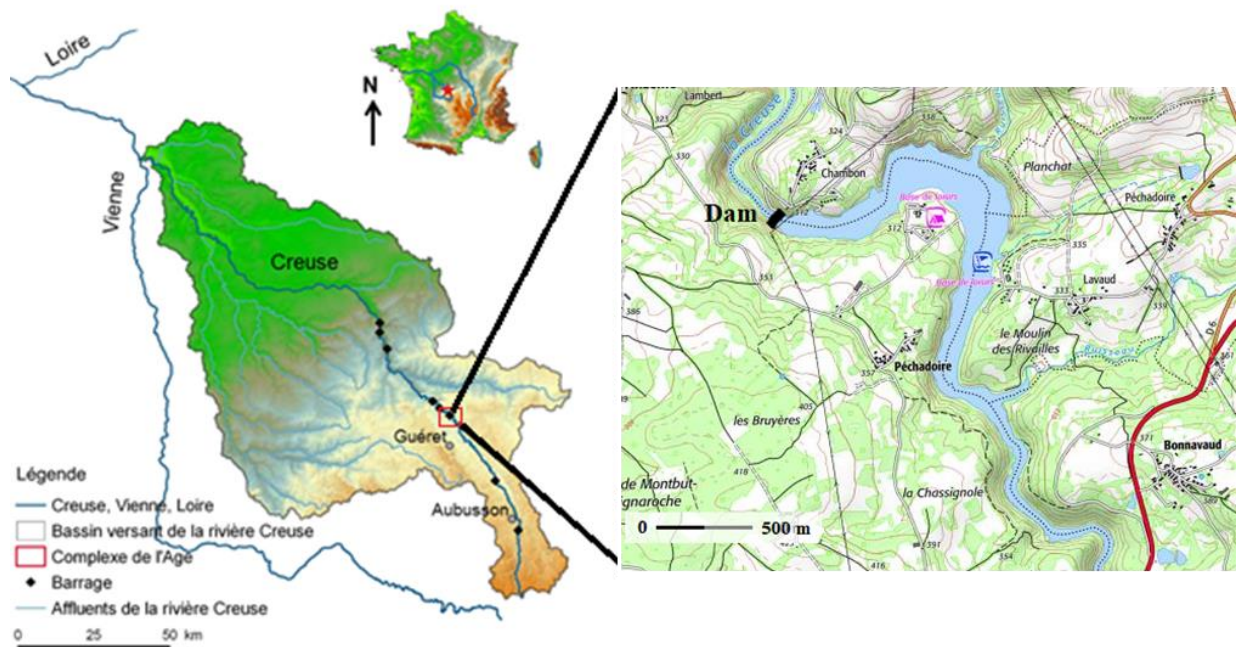
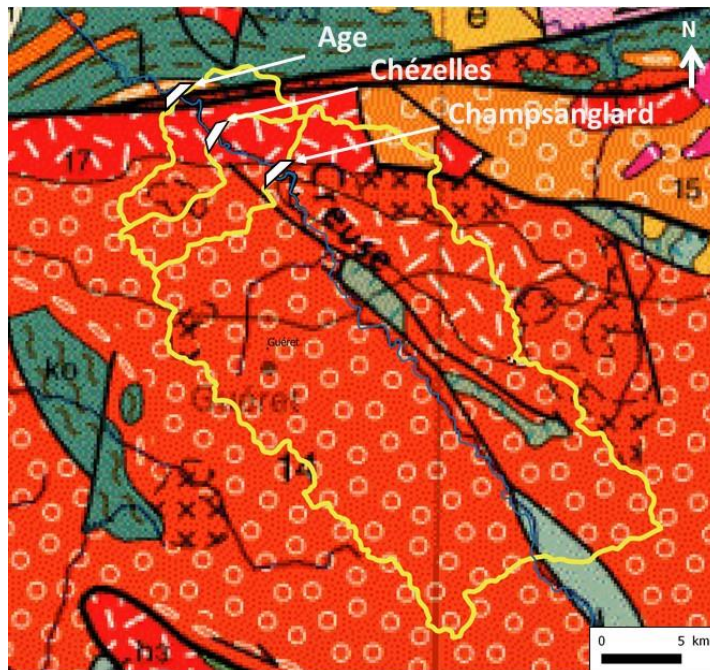


Figure 16. Watershed for Creuse river and location of the Age complex and Champsanglard reservoir.

The Champsanglard dam was first commissioned in 1984 with 19-meter height and 102-meter width. The EDF company takes over the rights to exploit and monitor Champsanglard dam. The reservoir covers an area of 0.55 km² and has a length of 2.36 km. The annual mean inflow is 13.8 m³/s, varying between 0.46 and 74 m³/s, at the Glenic station, at the upstream of Champsanglard dam. In reservoir, the residence time is 3 days and the average longitudinal terrain slopes is 0.37 %. The 406-km² watershed is covered by 65 % agriculture land, 30 % forest and semi-natural environment and 4 % of artificial use (Corine Land Cover data). The watershed stratum is characterized by the crystalline granitic rock that is composed of mainly quartz, feldspar and mica (Fig. 17). The Creuse water was not classified to be good ecological condition due to development of cyanobacteria and silting up of channel morphology (baignade.gouv.fr). During flooding period, water flows from the upstream to the downstream through the overflow crest with man-made operation. Reservoir receives suspended sediment mainly from Creuse river and two tributary (Dauge

and Pechadoire streams) inputs. Champsanglard dam retains certain part of water even during a flood depending on the filling state of the reservoir and avoid flooding the downstream. Hydrological condition in Champsanglard are influenced mainly by the regional climate. The climate on Creuse department is continental with atmospheric perturbation from the west. The climate is warm and temperate with annual precipitation of 1059 mm and average annual temperature of 11.3°C (donneespubliques.meteofrance.fr). In 2018, the temperature in Creuse region varies from 0 to 28°C with maximum rainfall level of 196 mm per month and the minimum of 14 mm per month.



Légende simplifiée associée au bassin versant du complexe de l'Age

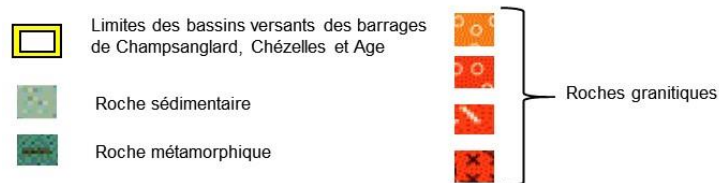


Figure 17. Geological map of Age complex watershed.

II.1.2. Sampling methods

Surface sediments were collected from Champsanglard reservoir during three campaigns to serve for three main objectives of this research. Each campaign carried out in short time (a day) before the following laboratory experimentation to assure fresh sediment could be used. Overall, thirteen sampling locations was selected starting from Champsanglard dam, going upstream toward the riverine section and across lateral sections (Fig. 18). Two campaigns were performed in the middle of reservoir on the 17 Mai 2018 and the 15 March 2019. For the first one, sediment was collected in the middle of the reservoir (Site 4, Figure 18) at the depth of 9 m, which was latterly subjected to the investigation on the influence of extraction/separation protocols and sediment storage modes on the quantity and quality of isolated colloids. The second one on the 15th March 2019 took place at site 2 that has higher depth (14 m) and is closer to the

dam. This last sediment was sampled to handle laboratory redox oscillation experiment. For these two campaigns, sediments were collected in surface of bed sediment up to 10 cm by using Ekman grab sampler. After excavated, sediments were homogenized using plastic spade before putting into HDPE bottles.

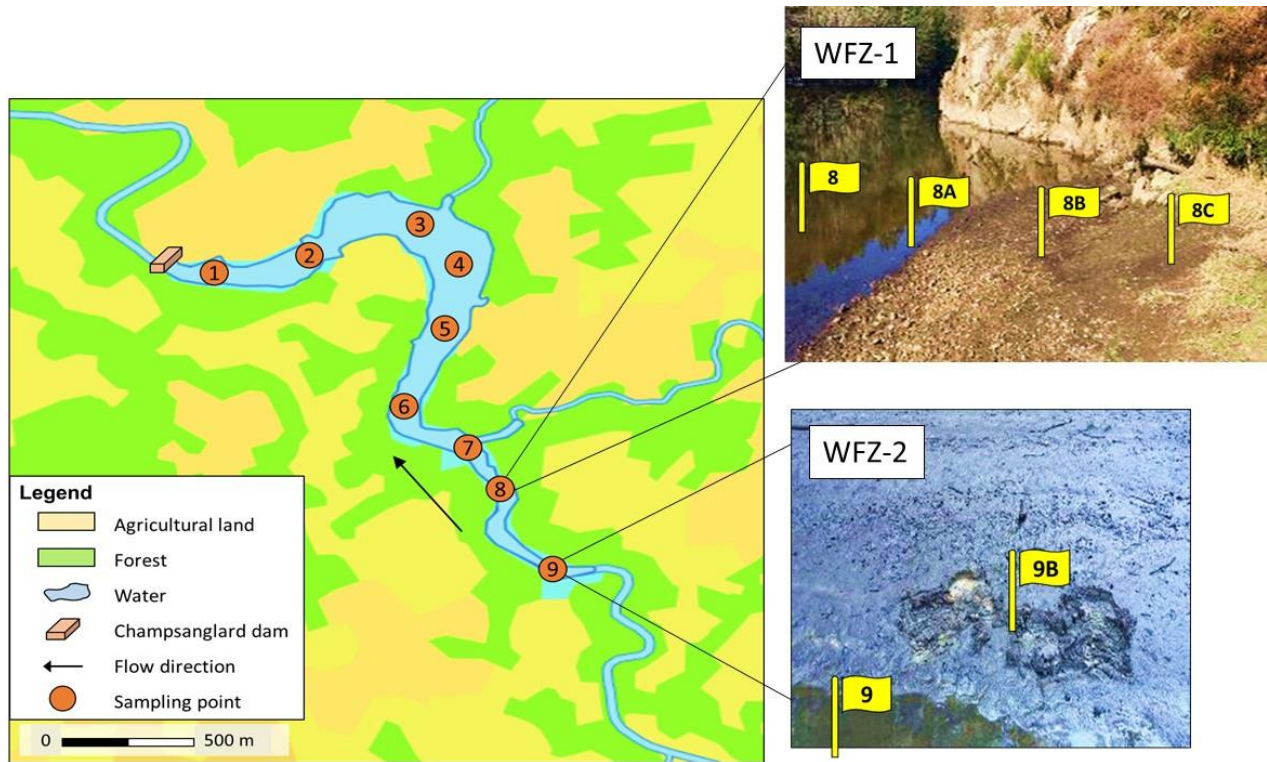


Figure 18. Localization of sampling sites in Champsanglard reservoir

To investigate longitudinal and lateral variability, a sampling campaign on 13 sites was performed on 25 February 2019, through the longitudinal of the reservoir (from site 1 to site 9) and at the cross-sections of site 8 and site 9. Those sites from locations 1 to 5 were located in lacustrine zone with deeper depth, meanwhile those sites from locations 6 to 9 were located in the transitional zone (tail of reservoir) and upstream riverine zone characterized by shallower depth and higher water velocity. Due to the changes in hydraulic condition, sediment deposited at higher altitude and near the bank at site 8 and site 9 were prone to air exposure and desiccation. Additionally, two small tributaries enter the main channel of reservoir at site 3 and site 7, featuring flow confluences. In upstream riverine region, samplings were performed at sites 8 and 9. At the shoreline of these two sites, where an important water-level fluctuation was observed, a series of samples were collected across the lateral axis from the deeper zone to the zone gradually exposed to air (Fig. 18). Three samples along the transect of site 8 (namely WFZ-1) and one sample along the transect of site 9 (namely WFZ-2). They were annotated “A” for the sediments sampled at the shoreline and assumed to be frequently submerged sediment. The annotation “B” and “C” were given to the sediments sampled at drier surface and higher elevation than water level that were assumed to be temporary and occasionally submerged sediments, respectively. The two water-level fluctuation zones at site 8 and site 9 (WFZ-1 and WFZ-2, respectively) exhibited different river morphology and toposequence. The WFZ-1 was similar to “bank of the river” and more soil-like, whereas the WFZ-2 was similar to a deposition area

of the transported river material and covered by thin organic layer (Fig. 18). Because of limited sedimentation (rocky shores), additional lateral sampling in the sites 1-7 was not allowed.

Sediments were preserved in icebox during transport. Once arrived in laboratory, all samples were immediately sieved through a 2-mm mesh to remove coarse particulates and large organic debris, stored at 4°C in dark room. All bottles and apparatus used during sampling were previously clean thoroughly by ultra-pure water in laboratory and by in-situ reservoir surface water.

II.2. Laboratory experimentation

II.2.1. Isolation of colloids from sediment matrix

II.2.1.1. Examination and validation of sediment storage modes, colloid extraction and separation protocols for fraction 0.2 – 1 µm

In order to determine the potential variability in the quantity and characteristics of extracted colloids in fraction 0.2 - 1 µm derived from the variation in applied isolation protocols, several sediment storage modes, colloid extraction protocols and finally separation modes were examined (Fig. 19).

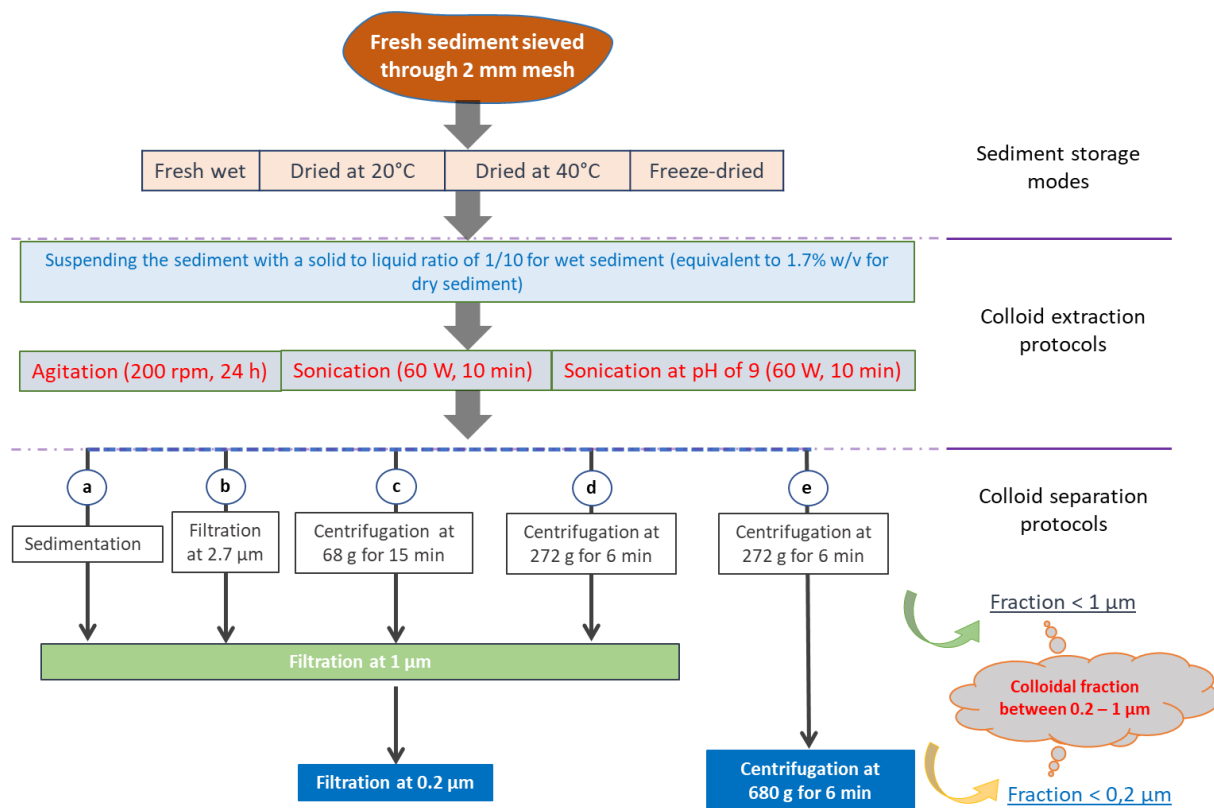


Figure 19. Diagram for the examination of various sediment storage modes, colloids extraction and separation protocols

Sediment was divided into four portions subjected to four different storage modes that are commonly encountered in literature references (Table 6). A first portion was kept in moisture at 4°C in dark room, corresponding to “wet sediment”. A second portion was air dried at constant room temperature of $20 \pm 1^\circ\text{C}$ for 2 weeks. A third portion was oven dried at 40°C for 5 days. The last portion was freeze-dried for 4 days using a lyophilizator (Cryotec, COSMOS-80).

To isolate colloids, both dried and wet sediments were suspended in 150 mL of ultrapure water at a humid solid-liquid ratio of 1/10, which was equivalent to 1.7 % of dry weight solid-liquid ratio. All dried sediments were not harshly crushed into powder to avoid the generation of colloids by mechanical grinding process that could subsequently involve in the overestimation of naturally occurring sedimentary colloids. However, the drying at 20°C and 40°C provided intensively consolidated sediments, therefore, a gently smash of consolidated sediment into smaller pieces was carried out. Further fragmentation and dispersion of dried sediment were performed on re-humidified and soften sediment after immersion in ultrapure water for 2 days and by gently crush using stainless spoon in concomitant with continuous manual shaken until obtaining homogenous suspension.

The most common techniques used to extract colloids from raw matrices are agitation and sonication (Table 6-9). Furthermore, colloids mobilization is favored at high pH, because the negative charge of hydroxyde group enhances the electrostatic repulsive force between colloids and attached surface. Herein, three extraction protocols were tested: agitation, sonication and sonication at pH 9. Agitation was set up during 24 hours at the speed of 200 rpm using IKA KS 501 digital agitator. Sonication was performed using ultrasonic probe (Bandelin, Sonopuls GM70) at 100 % power (60 W) for 10 minutes. For the third protocol, sample pH adjustment to 9 was done by addition of 1 M NaOH solution before sonication using similar program.

For colloid separation, five tested protocols were (a) direct filtration, (b) successive filtrations, (c) low-speed centrifugation and filtration, (d) high-speed centrifugation and filtration, and (e) successive centrifugations. All calculation was wade considering average density of sediment of 2.417. The details of each protocol are presented as below:

- a) Direct filtration: Sediment suspension was decanted for 2 h by gravitation which allow to settle down large particles larger than 42 μm . The supernatant was filtered through a 1- μm filter. The cut-off size was calculated from Eq. 1.

Equation 1. Formula to determine particle diameter after gravitational sedimentation.

$$d = \sqrt[2]{\frac{18 \times \eta \times v}{g \times \Delta\rho}}$$

where:

d: particle diameter (cm)

$\Delta\rho$: difference in particle volumic mass and suspension medium ($\rho_{\text{water}} = 1.0 \text{ g/cm}^3$)

η : dynamic viscosity of the suspension medium ($\eta = 0.01 \text{ g/(cm.s)}$)

v: settling velocity (cm/s)

g: gravitational acceleration ($g = 9.81 \text{ cm/s}^2$)

- b) Successive filtrations: Sediment suspension was filtered through $2.7 \mu\text{m}$, and the filtrates were then passed through a $1\text{-}\mu\text{m}$ filter.
- c) Low-speed centrifugation and filtration: Sediment suspension was centrifuged at 68 g for 15 min to separate particles larger than $2.0 \mu\text{m}$ ($d = 2.417$). The centrifugates were then carefully pipetted out and filtered through a $1\text{-}\mu\text{m}$ filter. The centrifugation speed and time were calculated using Eq. 2, according to Gimbert et al., (2005):

Equation 2. Formula to determine centrifugation speed and time.

$$t = \frac{18\eta \ln(R/S)}{\omega^2 d^2 \Delta\rho}$$

where:

d: particle diameter (cm)

$\Delta\rho$: difference in particle volumic mass (g/cm^3), herein $\rho_p = 2.417 \text{ g/cm}^3$, and volumic mass of suspension medium, here in $\rho_{\text{H}_2\text{O}} = 1.0 \text{ g/cm}^3$

η : viscosity of suspension medium (g/cm.s), herein $\eta = 0.01 \text{ g/cm.s}$

t: settling time (s)

R: distance from the axis of rotation to the settling level in the tube ($R = 10.8 \text{ cm}$)

S: distance from the axis of rotation to the suspension surface in the tube ($S = 5.5 \text{ cm}$)

ω : angular velocity of the centrifuge (rad/s), calculated according by Eqs. 3 and 4 with rotor radius of 108 mm :

Equation 3. Formula to determine angular velocity of centrifuge.

$$\omega = \frac{2\pi}{60} \times rpm$$

Equation 4. Formula to convert revolution per minute (rpm) to relative centrifugal force (g).

$$g = 1.118 \times R \times \left(\frac{rpm}{1000}\right)^2$$

- d) High-speed centrifugation and filtration: Sediment suspension was centrifuged at 272 g for 6 min to remove particles larger than $1 \mu\text{m}$. The centrifugates were then carefully pipetted out and filtered through a $1\text{-}\mu\text{m}$ filter.

- e) Successive centrifugations: Sediment suspension was first subjected to centrifugation at 272 g for 6 min to remove the fraction greater than 1 μm (Gimbert et al., 2005). The supernatant was then gently pipetted out and submitted to the second centrifugation at 680 g for 6 min to settle the particles greater than 0.2 μm . The pellets after the second centrifugation were resuspended in UPW by agitation for 30 min in order to obtain colloidal suspension of 0.2 – 1 μm . The supernatants were also gently pipetted out and represented the fraction smaller than 0.2 μm .

For the four protocols (“a” through “d”), an aliquot of obtained suspension (fraction smaller than 1 μm) was passed through a 0.2 μm cellulose nitrate membrane filter (Whatman) to obtain fraction lower than 0.2 μm . The glass microfiber (VWR) was chosen for separation at upper threshold of colloidal fraction due to high chemical resistance, pH resistance and biological inertia. All centrifugations were performed using a centrifuge (Thermo Scientific, Multifuge X3 FR) and a rotor (Thermo Scientific, FIBERLite F14-6x250LE). All experiments were run in triplicate.

Quantity of extracted colloidal particles, in the range 0.2 – 1 μm , was determined by the difference between drying mass of 0 – 1 μm solution and 0 – 0.2 μm solution at 40°C (see section II.3).

II.2.1.2. Colloid extraction for investigation of spatial distribution of colloidal P along Champsanglard reservoir

To investigate the spatial distribution of colloids and colloidal P in dam reservoir, 13 samples of surface sediment were collected along the length and at bank of riverine region of Champsanglard reservoir (see Section II.1.2). In laboratory, freshly sampled wet sediments were used to extract colloids. Sediments were suspended in ultrapure water at a wet solid-liquid ratio of 1/10 and were agitated for 24 h at the speed of 200 rpm using orbital shaker (IKA-WERKE, KS 501 digital).

Then, colloids were separated by using high-speed centrifugation at 272 g for 6 min, followed by a filtration at 1 μm (WVR, glass fiber) (protocol 4, see section II.2.1). Further separation between large colloidal and fraction lower than 0.2 μm (containing truly dissolved phase and nano/small colloids) was performed with filtration at 0.2 μm using cellulose nitrate filter membrane (Sartorius). After separation, two fractions were obtained as intermediate/large colloids with size from 0.2 - 1 μm and the fraction lower than 0.2 μm comprised nano/small colloids and truly dissolved species.

II.2.3. Incubation of sediment in anoxic/oxic alternation for investigation of colloidal P dynamic at sediment-water interface

The objective of this experiment was to elucidate the impacts of anoxic/oxic condition on the mobilization of colloids and associated P at the sediment-water interface. The experiment was conducted by the incubation of sediment suspension in synthetic water under controlled cyclic redox condition. The sediment suspension was prepared from 10 g of fresh wet sediment (sampling at site 2, figure 23) and completed by 200 mL of synthetic water (wet S/L of 1/20). The preparation of synthetic water is presented in Table 10 simulating major elemental composition of bottom water in Champsanglard reservoir.

Table 10. Composition of synthetic water simulating the major elemental composition of bottom water in Champsanglard reservoir

Ions	Concentration (mg/L)	Salts
Ca ²⁺	5.4	CaCl ₂ (Prolabo, 96 %), Ca(NO ₃) ₂ .4H ₂ O (Normapur, 98 %)
Mg ²⁺	1.6	MgSO ₄ .7H ₂ O (Sigma, 99 %)
K ⁺	8.6	KHCO ₃ (Normapur, 100 %)
Na ⁺	9.2	NaNO ₃ (Fluka, 99 %), NaHCO ₃ (Normapur, 100 %)
SO ₄ ²⁻	6.3	MgSO ₄ .7H ₂ O (Sigma, 99 %)
NO ₃ ⁻	4.9	NaNO ₃ (Fluka, 99 %), Ca(NO ₃) ₂ .4H ₂ O (Normapur, 98 %)
Cl ⁻	8.5	CaCl ₂ (Prolabo, 96 %)
HCO ₃ ⁻	34.7	KHCO ₃ (Normapur, 100 %), NaHCO ₃ (Normapur, 100 %)

Before the incubation, sediment solution was allowed to equilibrate under oxic condition for 2 days. The whole experiment was performed through a 63-days period composed of oxic/anoxic/oxic conditions with sacrifice samplings. The initial numbers of batches was 24 of 250-mL glass bottles. Regularly, bottles were shaken manually once a day, five days per week and different physico-chemical parameters were monitored: dissolved oxygen concentration, temperature, pH and redox potential (see II.3.2.2). During the whole experiment, each sampling was conducted with a sacrifice of 2 or 3 bottles for replicates.

The closing of bottles marked the beginning of incubation and was aimed to develop anoxic condition meanwhile the opening of bottles was aimed to reach oxic condition. To enhance the development of anoxic condition, on day 15, all bottles were purged with N₂ gas to remove O₂, then closed by septic silicon cap and covered by parafilm. All bottles were then transferred into a glovebox (PLAS LABS, 830-ABD/EX) maintained at 0.18 mg O₂/L in the dark. Subsequently, the redox potential induced by the N₂ purging and closing dropped gradually to reach anoxic condition after 23 days. For oxic condition, all bottles were transferred out of the glovebox, the silicon cap was removed but remained covering by parafilm to limit evaporation. The sediment incubation included a 23-day Oxic-1 phase, 22-day Anoxic phase, 23-day Oxic-2 phase (Figure 20).

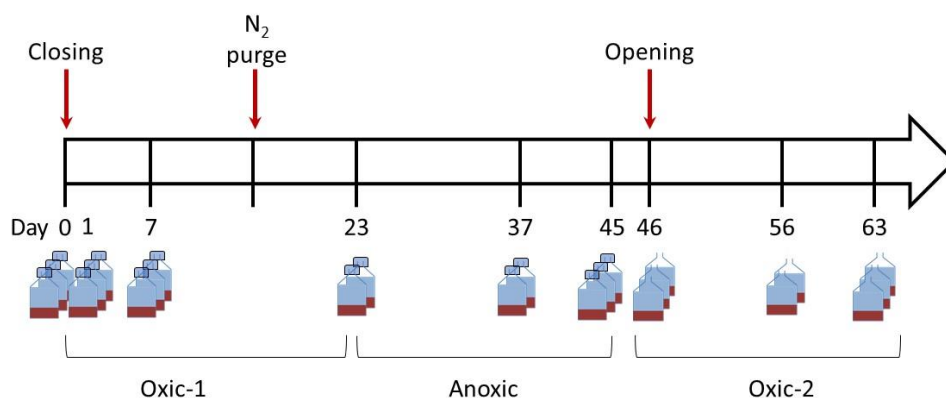


Figure 20. Schema for sediment incubation under oscillation between anoxic (closed system) and oxic (opened system) conditions

Sediment suspension was sampled 9 times, on days 0, 1, 7, 23, 37, 45, 46, 56, 63 to have, at least, one sampling date at the beginning, one sampling in the middle and one sampling at the end of each half cycle. On the day of sampling, sacrificed bottles were let settled for 30 min before the separation between supernatant and deposited solid. The supernatant was fractionated using successive filtrations to obtain four different size fractions of colloids: large colloids 0.45 - 1 μm , intermediate colloid 0.2 - 0.45 μm , small colloid 300 kDa - 0.2 μm , nano colloid 10 - 300 kDa and a fraction lower than 10 kDa considered as truly dissolved fraction (Fig. 21). For samples collected during anoxic half-cycle, the extraction and fractionation of colloids along with measurements were performed in anoxic glovebox (0.18 mg O₂/L).

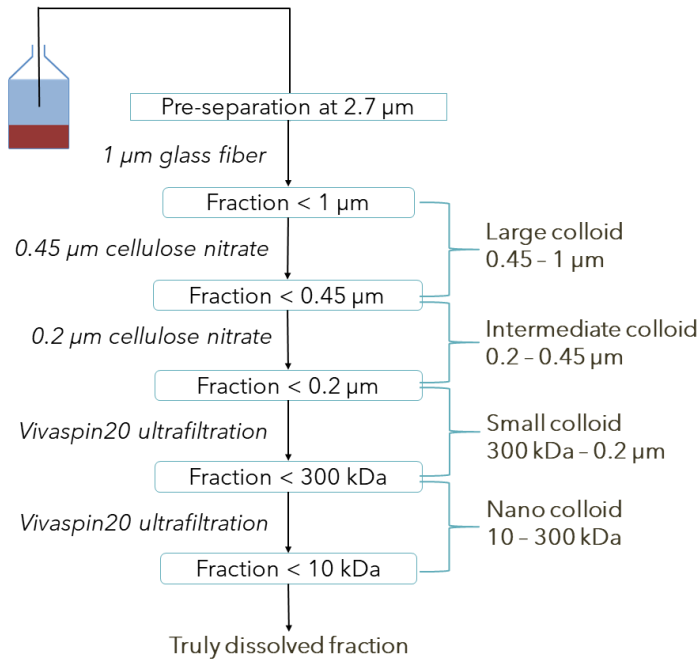


Figure 21. Size separation of water-mobilizable fraction (smaller than 1 μm) using successive filtrations

The five extracted colloidal and dissolved fractions were separately divided into small portions of aliquots serving for different measurements (Table 11). Four aliquots were immediately set aside for the analysis of alkalinity, ferrous iron (Fe(II)), total phosphorus (TP), dissolved inorganic P (DIP), and colloidal size distribution. The other aliquots were freeze dried in 10-mL polypropylene tubes for further analysis of total Fe, Al, Ca, Mn and Mg, organic carbon, and major ions (Ca²⁺, Mg²⁺, Na⁺, K⁺, NH₄⁺, Cl⁻, NO₃⁻, NO₂⁻ and SO₄²⁻).

Table 11. List of analysis for each fraction during one sampling day for redox oscillation experiment

	< 1 µm	< 0.45 µm	< 0.2 µm	< 300kDa	< 10KDa	Method	Status
Alkalinity		x				Acid titration to pH 4.3 (see section II.3.2.1)	Immediate
Fe (II)					x	Ferrozine (see section II.3.2.6)	Immediate
TP	x	x	x	x		Hach LCK 349 (see section II.3.1.2.1.2)	Immediate
DIP	x	x	x	x	x	Murphy and Riley (1962) (see section II.3.2.3)	Immediate
Colloids Size	x	x	x	x	x	Dynamic light scattering (see section II.3.1.1.3.2)	Immediate
Total Fe, Al, Ca, Mn and Mg with acid digestion	x	x	x			US EPA 3015a (2007) (see section II.3.1.2.2)	Frozen
Fe, Al, Ca, Mn and Mg without acid digestion			x	x	x	MP-AES (see section II.3.2.5)	Frozen
TOC	x	x	x	x	x	TOC analyzer (see section II.3.2.4)	Frozen
Major ions concentration			x			Ionic chromatography (see section II.3.2.6)	Frozen
Dry mass	x					Lyophilisation (see section II.3.1.1.6.2)	Frozen

II.3. Analytical methods

II.3.1. Particulate phase

II.3.1.1. General physicochemical characteristics

II.3.1.1.1. Siccidity

The loss on drying is determined as the percentage of weight remaining after drying at 105°C. To determine the siccidity, the balance should be able to weight 0.0001 mg (Ohaus). About 20 g of wet sediment were added on porcelain crucible and placed in an oven preheated at 105°C until the unchanged mass. The porcelain crucible was cooled at room temperature in desiccator before weighting with a precision balance with an accuracy of 0.0001 g (Ohaus) The percentage of loss on drying is calculated using Eq. 5.

Equation 5. Calculation of sediment Siccidity.

$$Siccidity (\%) = \frac{m_2 - m_0}{m_1 - m_0} \times 100$$

Where:

m₀: weight of supporter (aluminum cup or porcelain crucible)

m₁: weight of wet sediment with supporter

m₂: weight of dried sediment at 105°C with supporter

II.3.1.1.2. Particle density

Particle density is the mass per unit volume of sediment particles over the mass per unit volume of solvent, (without unity). A certain volume of wet sediment (V_{sediment}) was weighted before drying to obtain the mass of wet sediment (M_{Total}). The sediment was then dried at 40°C in preheated oven until unchanged mass and weighted to have the mass of solid (M_{Solid}). The particle density was calculated with following Eqs. 6 to 8:

Equation 6. Formula to determine bulk density.

$$\text{Bulk density (g/cm}^3\text{)} = \frac{M_{\text{Solid (g)}}}{V_{\text{sediment (cm}^3\text{)}}$$

Equation 7. Formula to determine porosity.

$$\text{Porosity} = \frac{M_{\text{Total (g)}} - M_{\text{Solid (g)}}}{V_{\text{sediment (cm}^3\text{)}}$$

Equation 8. Formula to determine particle density.

$$\text{Particle density (g/cm}^3\text{)} = \frac{\text{Bulk density (g/cm}^3\text{)}}{1 - \text{Porosity}}$$

II.3.1.1.3. Particle size distribution

II.3.1.1.3.1. Sediment grain size

The grain size of sediment was measured by the laser diffractometer (MasterSizer 3000, Malvern) on wet dispersion under ultrasonic field in ultrapure water that is purified through Milli-Q system (Sartorius). The MasterSizer 3000 apparatus allow the measurement of particle size ranging from 10 nm to 3.5 mm. The dispersion of sediment in ultrapure water decreases the particle-particle adhesive force via surface wetting, promoting aggregation of particles to be dispersed with lower adding energy input. The suspension has obscuration level lower than 10 % to avoid the blocking or multiple scattering of laser light due to high particle concentration. The stirring speed of 2000 rpm and 100 % sonication were applied during each measurement (30 to 60 seconds). Each sample was passed three times for measurement. Samples were replicated three times to obtain reproducibility and consistency in medium grain size D50 (μm). For all the measurement, the relative standard deviation between replicates and measurements were low (less than 10 %).

II.3.1.1.3.2. Colloidal size

Particle size distributions of colloid extracts were determined based on dynamic light scattering technique (ZetaSizer NanoZS, Malvern) on the 0 - 1 μm solution and 0 - 0.2 μm solutions. This device working based on classical single-scattering to calculate particle size in a range from 0.3 nm to 10 μm using a 633-nm laser. Material refraction index was set to be 0.18 and material absorption was 0.001. Ultrapure water was selected for dispersion medium and have refractive index of 1.330. Angle of measurement was 173° backscatter. Measurement started with 120-second equilibration, followed by 3 measurements with automatic selection of run and optimum position. The size measurement of colloidal suspension was

manipulated during 24 h after the extraction to avoid the destabilization of colloidal particles. Measurements were conducted without stirring.

II.3.1.1.4. pH

The pH of sediment was measured according to Method 9045D (US EPA, 2004). The wet sediment is suspended in ultrapure water at a ratio of 1/1 (w/v), covered and stirred for 5 min. Then, the suspension was let stabilized for about 1 h before the pH measurement. A glass electrode was immersed deep enough in clear supernatant solution for good electrical contact through the capillary hole. The pH measurement was performed using a CRISON GLP22 pH meter and a CRISON 5221 probe. The calibration was performed daily using buffer solution at pH 4 and 7.

II.3.1.1.5. Loss on ignition (LOI)

The sediment placed in a support (mass m_0) was dried at 105°C until unchanged mass (m_2) measurement and was then calcined at 550°C for 2 hours. The mass of calcined sediment in support was recorded as m_3 . The content of OM is calculated in mass percentage associated to the mass loss during calcination using Eq. 9.

Equation 9. Formula to estimate organic matter content (in %) from loss on ignition.

$$OM (\%) = \frac{m_2 - m_3}{m_2 - m_0} * 100$$

II.3.1.1.6. Intermediate/large colloid quantification

II.3.1.1.6.1. Gravimetry

The quantification of intermediate/large colloidal concentration (fraction 0.2 – 1 μm) was carried out according to gravimetric method through the measurement of dry mass at 30°C of colloidal suspension. An adequate volume (V) of suspension (< 1 μm) was passed through the 0.2 μm filter (Whatman, cellulose nitrate membrane) to separate colloids (0.2 – 1 μm). The filter was then dried at 30°C until unchanged mass and cooled to room temperature in desiccator. The colloid concentration was determined as Eqs. 10 and 11:

Equation 10. Determination of colloid concentration in extracted solution (in mg/L).

$$Colloid\ concentration\ (mg/L) = \frac{M_{30^\circ C}\ (mg) - M_{Filter}\ (mg)}{V\ (L)}$$

Equation 11. Determination of colloid concentration in dry weight of sediment (in mg/g_{DW-Sed}).

$$Colloid\ concentration\ (mg/g_{DW-Sed}) = \frac{Colloidal\ concentration\ (mg/L) * Volume\ (V)}{Dried\ weight\ of\ sediment\ (g)}$$

where:

M_{Filter} : dry mass of supporter, herein supporter is 0.2 μm cellulose nitrate membrane

$M_{30^\circ C}$: dry mass of colloid suspension at 30°C with supporter (filter)

V : initial volume of colloid suspension

II.3.1.1.6.2. Lyophilization

Fraction smaller than 1 μm in redox oscillation experiment was freeze-dried using lyophilizator (Cryotec) for 3 to 4 days until achieving constant weight. Colloid suspension was collected in 60-mL HDPE flask and frozen. Before lyophilization, the flasks were covered with parafilm with small holes to avoid mass loss during vacuum. The colloid concentration was reported by the difference between total dry weight of water-mobilization fraction (smaller than 1 μm) and the total dissolved salts.

II.3.1.2. Total contents of P, Fe, Al, Ca, Mn, Mg and Si

II.3.1.2.1. Total P

II.3.1.2.1.1. P content in sediment

Total P in sediment was measured according to Ruban et al., (2001) protocol. A 200-mg of sediment dried at 105°C was calcinated at 450°C for 3 h to break organic bonds and allow P extraction from OM. To avoid mass loss upon the transfer of calcinated sediment to centrifuge tube, both weight of sediment after calcination and actual weight of transferred sediment in centrifuge tube were well recorded. Calcinated sediment was then immersed in 20 mL of 3.5 M HCl for 16 h before centrifugation at 2000 g for 15 min. The supernatant was filtered through a 0.45 μm cellulose acetate membrane (LLG Labware). The filtrate was adjusted to pH between 2 to 7 by 5 M NaOH and/or 0.1 M HCl before being subjected to the measurement of dissolved inorganic phosphorus (DIP) by spectrophotometry (according to Murphy and Riley, (1962) protocol). The final concentration of sedimentary TP was calculated by Eq. 12.

Equation 12. Determination of total sedimentary phosphorus.

$$TP \text{ (mg/g}_{\text{DW-Sed}}) = \frac{DIP \left(\frac{\text{mg}}{\text{L}} \right) * V_{\text{HCl } 3.5 \text{ M}} \text{ (L)}}{M_c}$$

Where:

- DIP: final concentration of dissolved inorganic phosphorus (mg P/L), calculated by multiplying dilution factor (Df) with measured concentration of DIP, according to Eqs. 13 and 14:

Equation 13. Measurement of dissolved inorganic phosphorus according to method of Murphy and Riley, (1962).

$$DIP \text{ (mg/L)} = DIP_{\text{measured}} \text{ (mg/L)} \times Df$$

Equation 14. Dilution factor used in measurement of total phosphorus.

$$Df = \frac{V_{\text{water}} \text{ (L)} + V_{\text{sample}} \text{ (L)} + V_{\text{NaOH } 5 \text{ M}} \text{ (L)} + V_{\text{HCl } 0.1 \text{ M}} \text{ (L)}}{V_{\text{sample}} \text{ (L)}}$$

- $V_{\text{HCl } 3.5 \text{ M}}$: volume of HCl 3.5M used for extraction (L), herein $V = 0.02 \text{ L}$
- M_c : Corrected dry mass of sediment subjected to acid addition (g), calculated by Eq. 15:

Equation 15. Determination of sediment dry mass to calculate total sedimentary phosphorus.

$$M_C(\text{g}) = M_{450^\circ\text{C}}(\text{g}) \times \left(1 + \frac{M_{105^\circ\text{C}}(\text{g}) - M_{450^\circ\text{C}}(\text{g})}{M_{105^\circ\text{C}}(\text{g})} \right)$$

II.3.1.2.1.2. P content in colloidal extract

The total P concentration in colloidal extract and in water-mobilizable fraction (0 - 1 µm) was determined after persulfate digestion according to Method 365.1 (US EPA, 1993). For 10 mL of sample, 0.625 mL of a working digestion was added in prior to the autoclave for 30 minutes at 121°C and 1 bar of pressure. The working digestion solution was the combination of sulfuric acid 5.6 M and sodium persulfate, prepared daily. The digested solution needed to be adjusted to the pH between 2 and 7 for the phosphate analysis by spectrophotometric method (See section II.3.2.3). All forms of phosphorus were converted to orthophosphate and can be measured by the method of Murphy and Riley, (1962).

The TP was also measured using kit HACH LANGE LCK 349 with hydrolysis based on principle described in section II.3.2.3. Sample was digested with concentrated H₂SO₄ for 1 h at 100°C. This method provides a measurement of P over a range of concentration from 0.05 – 1.50 mg P/L.

II.3.1.2.2. Fe, Al, Ca, Mn, Mg and Si analysis

The determination of total element contents was based on a digestion procedure for analysis according to method 3015a (US EPA, 2007). The principle of this method is to dissolve sample in concentrated nitric and hydrochloric acid using microwave heating.

For sediment sample, a 250-mg of sediment dried at 105°C was put in Teflon tubes. The degradation of organic matter was done by adding 2 mL of concentrated peroxide (Merck, 30%) and let to degas overnight. In next step, a combination of 6 mL HNO₃ (Fisher, 65 %) and 3 mL HCl (Normapur, 37 %) was placed into vessel. After 4 h of reaction and degas, vessels were sealed and placed into microwave (Multiwave Go, Anton Paar) for 40 min at 180°C. After cooling, contents inside vessels were filtered through 0.45 µm cellulose acetate (LLG Labware), then diluted to 50 mL.

For colloidal extracts, 5 mL of solution were digested with aqua regia (of 6 mL HNO₃ (Fisher, 65 %) and 3 mL HCl (Normapur, 37 %)) in microwave (Multiwave Go, Anton Paar) operating with similar program. The pressure inside sealed Teflon vessel can reach 12 atm for the using of acid combination meanwhile the sample containing high organic matter can create 25 atm pressure inside vessel. Therefore, sample needs to be degassed overnight before heating in the microwave to avoid excessive increase in pressures inside Teflon vessels. Each microwave run included two blank samples and 3 replicates for each sample.

The contents of Fe, Al, Ca, Mn, Mg and Si in digested solution were latterly determined by microwave plasma atomic emission spectroscopy (Agilent, MP-AES 4100) (See section 3.2.5).

II.3.2. Dissolved phase

II.3.2.1. Alkalinity

Alkalinity in filtrate at 0.45 µm was determined according to acid titration by 0.001 M HCl until the pH of solution dropped to 4.3 to neutralize completely the hydrogen carbonate ions (ISO, 1994). The pH

monitoring was performed using a CRISON GLP22 pH meter and a CRISON 5221 probe. The results were reported in mg HCO₃⁻/L. The limit of quantification is 0.4 mmol/L and the quantification range is up to 20 mmol/L (ISO, 1994).

II.3.2.2. pH, conductivity, oxygen level and redox potential

The pH was monitoring using pH meter (Crison, GLP22) and a pH probe (Crison, 5221) which was calibrated daily by buffer solution at pH 4 and 7. The conductivity was measured using conductivity meter (MeterLab, CDM210). The oxygen concentration was measured by a multi-parameter (HACH, HQ40D). The redox potential was recorded using platinum band combined Ag/AgCl electrode (WTW, Portable Multimeter 3210). The Eh values were corrected according to standard hydrogen electrode following Eq. 16.

Equation 16. Formula to correct redox potential according to standard hydrogen electrode.

$$Eh_{Corrected} (mV) = Eh_{measured} (mV) + 230 - 0.76 \times (T(^{\circ}C) - 25) + 60 \times (pH - 7)$$

II.3.2.3. Dissolved inorganic phosphorus

Concentration of dissolved inorganic P (consistently in orthophosphates) in the solution was measured by colorimetric method according to the standard method NFT90-023 (Murphy and Riley, 1962).

In acid condition, orthophosphate ions (H₃PO₄, H₂PO₄⁻, HPO₄²⁻) react with molybdate ions to form a phosphomolybdic complex. After reduction with ascorbic acid, and in the presence of antimony, this complex turns into a blue molybdenum complex (McKelvie et al., 1995). The two pronounced wavelengths used to read the absorbance of blue molybdenum complex are 700 nm and 880 nm. The maximal absorbance was observed at 880 nm for different matrices obtained from different extraction and was used throughout the thesis. DIP concentration was calculated from regression equation by plotting absorbance response versus standard concentrations.

The pH of the samples must be adjusted to be between 2 and 7 by dilution or addition of acid/base before dosing using 5 M NaOH and/or 0.1 M HCl. The detection limit of this method is 20 µg P/L and has an error percentage of 5 %. The calibration curve is determined through the series of standards ranging from 0, 0.025, 0.05, 0.1, 0.25 to 0.5 mg P/L. The correlation coefficient of calibration curve needs to be at least 0.995 to be able to provide accurate results. Phosphate ion concentration was then measured by colorimetry at 880 nm using 1-cm cuvettes, and results were expressed in mg P/L.

The DIP was also measured using kit HACH LANGE LCK 349 without hydrolysis based on similar principle described above. This method provides a measurement of DIP over a range of concentration from 0.05 – 1.50 mg P/L.

II.3.2.4. Total organic carbon

For the determination of total organic carbon (TOC), a 7-mL solution was introduced into the TOC analyzer (Analytik Jena, multi N/C 2100S) with the measuring range of 0 – 30 mg C/L, LQ of 1 mg C/L. The measurement was carried out after acidification by 50 µL of phosphoric acid H₃PO₄ 2 M and bubbling to

remove inorganic carbon. Then, 500 μL of sample was injected to the oven and combusted at 800°C . The high temperature provides sufficient energy to break the stable C – C, C – O, C – N bonds. The released CO_2 gas was detected through infrared radiation.

II.3.2.5. Fe, Al, Ca, Mn, Mg and Si analysis

Elemental concentrations of Fe, Al, Ca, Mn, Mg, Si in dissolved fraction were directly measured by MP – AES. Principally, the element atom is excited by external energy and emits radiation with distinct wavelength pattern, forming emission spectrum when it returns to ground state. The MP-AES provides microwave energy to produce plasma discharge using N_2 gas. Sample is nebulized and come into interaction with plasma. The aerosol is subsequently dried, decomposed and atomized, promoting excited state and emitted light. The spectrum and intensity of each emission line are recorded. Concentration of element in sample was quantified by comparing with known concentration established on calibration curve. The limit of quantification (LQ) were 20 $\mu\text{g Al/L}$, 30 $\mu\text{g Fe/L}$, 12 $\mu\text{g Ca/L}$, 7 $\mu\text{g Mn/L}$, 1 $\mu\text{g Mg/L}$ and 15 $\mu\text{g Si/L}$.

II.3.2.6. Cations and anions

Concentrations of major anions (NO_3^- , NO_2^- , SO_4^{2-} , Cl^-) and cations (Na^+ , NH_4^+ , Ca^{2+} , Mg^{2+} , K^+) were measured in filtrates at 0.45 μm and 0.2 μm using ionic chromatography (Metrohm, 930 Compact IC Flux). The column for IC is packed with resin having opposite charge to analytes. The separation of analytes works based on the electrostatic interaction between molecules and fixed charges on stationary phase. The LQ for NO_3^- , NO_2^- , SO_4^{2-} , Cl^- , Na^+ , NH_4^+ , Ca^{2+} , Mg^{2+} and K^+ were 0.45, 0.075, 0.075, 0.25, 0.1, 0.3, 0.25, 0.25 and 0.15 mg/L , respectively.

Part III. Results and discussions

III.1. Impact of methods of sediment preconditioning, extraction and separation methods of colloids for sediment matrix

III.1.1. Introduction

The investigation of natural colloidal particles in the transport of contaminants, nutrients and their impact on the environment is a common research topic for aquatic systems and soils. In natural environments colloids occur with heterogeneous composition and diverse size classes. Prior to any assessment of the source, behavior, mobility and fate of colloids in the environment, the preliminary task is the extraction and separation of colloids from their natural matrices.

Common methods for extracting colloids include agitation and sonication (Table 6-9). According to the different input energy that agitation or sonication provide, and hence the varying interactions, it can induce between colloids and between colloids and soil/sediment particles, differences in the quantity and quality of colloids could be expected. However, the effect of these extraction methods on the recovered colloids characteristics has not been investigated. In addition, the extraction of the colloid can be performed on fresh wet sediment or on dried sediment. This also raises the question of the impact of different modes of sediment preservation (fresh, air-dry, oven-dry, freeze-dry) on the nature of colloids and their quantification.

Concerning colloids separation in the extracted solution (containing both colloids as well as particulate and dissolved fraction), there are several methods based on the different principles and providing different size ranges of colloids. The most common separation techniques to recover colloids from soil and water samples are gravitational sedimentation, filtration and centrifugation (Table 6). As the whole, the impact of those methods on the variation in sedimentary colloid recovery and characteristics is missing because very few researches were subjected to study them.

In this section, the impacts of extraction, separation of colloids from the sediment as well as the sediment preconditioning were targeted as follow:

- How the agitation and sonication of the sediment suspension during colloids extraction affect the quantity and quality of the recovered colloids?
- Do the separation protocols used (filtration, centrifugation and various degree of combination) affect the quantity and characteristics of the recovered colloids?
- Do different modes of sediment preservation (fresh, air-dry, oven-dry, freeze-dry) influence the nature of colloids and their recovery?
- If there are effects of sediment storage, extraction and separation, what changes in chemical properties of colloids could be induced?
- What is the more appropriate extraction and separation methods to recover colloids from sediment sample?

To answer these questions, a surface sediment was collected in Champsanglard reservoir and submitted to various sediment preservation (wet, air-dry, oven-dry, freeze-dry), colloid extraction (agitation, sonication) and separation methods (direct filtration, prefiltration before filtrations, low-speed centrifugation prior to

filtration, high-speed centrifugation prior to filtration, and successive centrifugations. The results were focused on quantity of extracted colloids and their characteristics (chemical composition and size distribution)

Results were presented in form of two articles:

- **Article 1: How do colloid separation and sediment storage methods affect water-mobilizable colloids and phosphorus? An insight into dam reservoir sediment**

The article was published in Journal of Colloids and Surfaces A: Physicochemical and Engineering Aspects (Nguyen et al., 2020)

- **Article 2: Comparison of three methods of colloid extraction for characterization of mobilizable colloids from Champsanglard sediment.**

This article will to be submitted to Chemosphere journal.

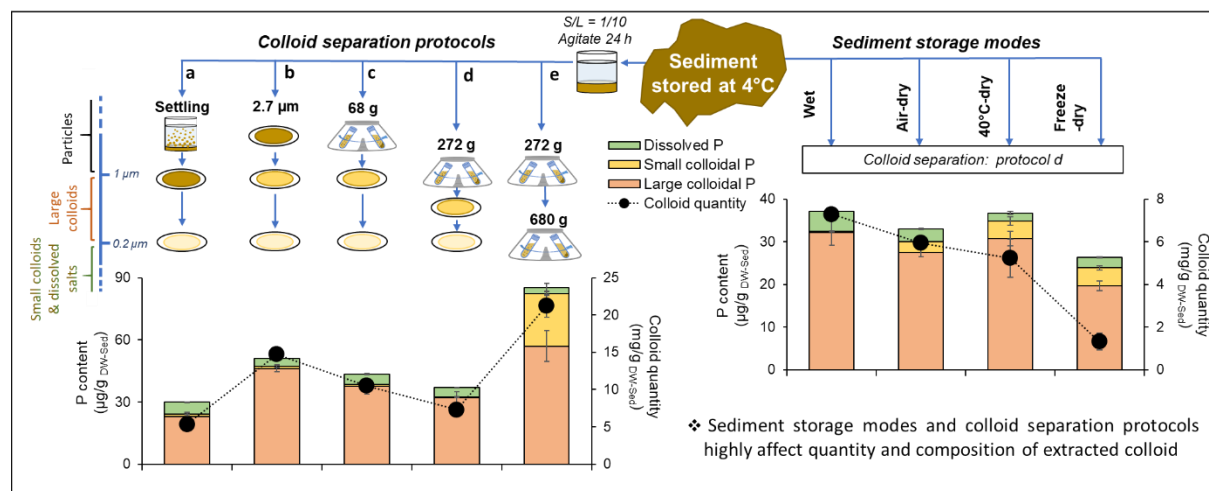
III.1.2. How do colloid separation and sediment storage methods affect water-mobilizable colloids and phosphorus? An insight into dam reservoir sediment

Article is accepted for Journal of Colloids and Surfaces A: Physicochemical and Engineering Aspects.

Diep N. Nguyen, Malgorzata Grybos, Marion Rabiet, Véronique Deluchat

Limoges University, PEIRENE EA 7500, 123 Av. Albert Thomas, 87060 Limoges Cedex, France

Graphical abstract



Abstract

Despite the significant role played by colloids in determining the fate of contaminants in aquatic systems, obtaining knowledge about the mobilizable colloids from bottom sediments of dam reservoirs has not yet received sufficient consideration. A major obstacle to understanding the role of colloids in aquatic systems is the limited comparability of results with the literature due to the vast number of methods practiced for colloid extraction/separation and the various sample storage conditions used for colloid extraction purposes. This work presents the effects of five colloid separation methods (namely direct filtration, successive filtrations, low-speed centrifugation and filtration, high-speed centrifugation and filtration, and successive centrifugations), combined with four sediment storage modes (wet, air-dried at 20°C, oven-dried at 40°C, freeze-dried), on the characteristics (mass, size distribution, composition) of water-mobilizable colloids from the bottom sediment of an eutrophic reservoir (Champsanglard, France). Special attention has been paid to phosphorus (P), an element that occupies a predominant place in the study of eutrophication process. Results showed that Champsanglard sediment contained a relatively high stock of water-mobilizable colloids (over 5.4 g/kg_{DW-Sed}), along with the associated colloidal P constituted of approximately 4% total sedimentary P and 81 - 93 % total water-mobilizable P (fraction < 1 μm). The mass and size distribution of released colloids, as well as the amount of colloidal and dissolved P, C_{org}, Fe, Ca, Mn, Al and Mg, differed by a factor of up to 26 depending on colloid separation protocols. The loss in colloidal mass upon membrane clogging during direct filtration was mitigated by means of a preliminary separation of particles through filtration and centrifugation, while successive centrifugations led to the potential overestimation of colloid quantity due to incomplete separation caused by presence of organic matter. Sediment storage impact at a

greater extent on extracted colloidal mass. In comparison with fresh sediment, drying decreased up to 40 folds the amounts of colloidal and dissolved elements. Special attention should be paid to sediment storage and separation protocols. According to our results, the characterization of colloids shall be done on fresh sediment and with separation by successive filtrations or combination of centrifugation and filtration. The comparison between sediment of different reservoirs should be based on similar application of sample storage and colloid separation protocol, the definition of normalized protocol would be thus required. It is strongly advised to avoid using solely centrifugation for colloid recovery and sediment freeze-drying for long-term storage when working with sediments.

Keywords: Dam reservoir sediment, colloidal size distribution, colloidal composition, colloid quantity, phosphorus, separation, centrifugation, filtration, drying, freeze-drying.

Abbreviations:

AF4	Asymmetric flow field-flow fractionation
ANOVA	One-way analysis of variance
CFC	Continuous flow centrifugation
CFF	Cross-flow ultrafiltration
DIP	Dissolved inorganic phosphorus
FFF	Field-flow fractionation
ICP-MS	Inductively coupled plasma mass spectrometry
LQ	Limit of quantification
MP-AES	Microwave plasma-atomic emission spectrometer
P	Phosphorus
P _{WM}	Water-mobilizable P
S/L	Dry weight solid-liquid ratio
TOC	Total organic carbon
TP	Total phosphorus
UC	Ultra-centrifugation
UF	Ultra-filtration
UPW	Ultrapure water

III.1.2.1. Introduction

Natural colloids (operationally defined as particles within the size range from 1 nm to 1 µm) play a key role in the fate and behavior of nutrients and contaminants in aquatic and terrestrial ecosystems, given their ubiquity and reactivity (Buffle and Leppard, 1995a, 1995b; Lead and Wilkinson, 2006; Baken et al., 2016; Gottselig et al., 2017a; Gu et al., 2018; Yan et al., 2017). Despite the significance of colloids in the balance of mobile nutrients in natural environment, the state of knowledge is rather poor regarding colloids in dam reservoirs and, more specifically, colloids being mobilized from the bottom sediments of these systems. It should be noted that reservoir sediments are generally enriched in biogenic elements since they are receptors of elements from both the surrounding catchments and internal recycling in the column water (Wildi et al., 2004; Teodoru and Wehrli, 2005; Maeck et al., 2013; Maavara et al., 2015; North et al., 2015; Orihel et al.,

2017; Hahn et al., 2018; Pestana et al., 2019; Palanques et al., 2020). In addition, their specific hydrodynamics, which depends in part on the type of dam and how it is managed, can cause sediment resuspension and thus contribute to the release of particles, colloids and ions through vertical distribution to the overlying water (Gálvez and Niell, 1992; Buermann et al., 1995; Effler and Matthews, 2004; Filstrup and Lind, 2010; Cavaliere and Homann, 2012; Zhang et al., 2012; Cervi et al., 2019).

The colloids in lake and reservoir water can be derived from several pathways, including inlet water, the detachment and/or resuspension from bottom sediments, breakdown of larger aggregates (biological and inorganic debris) and/or in situ formation of mineral precipitates or organo-mineral associations. In such systems, the increasing retention time promotes the entrapment and settling of fine and colloidal material, which for example in large lakes and reservoirs accounts for 30% of the inflowing suspended materials (Vörösmarty et al., 2003). The mobilization of colloids from bottom sediments to overlying water (i.e. internal colloid load) is associated with natural mechanical disturbances of sediment, or bioturbation (Pokrajac et al., 2007; Valipour et al., 2017; Phillips et al., 2019; Schroeder et al., 2019; Gautreau et al., 2020). Mobilizable colloids from sediment may contain the colloids settled from the water column and/or colloids generated within the sediments. Many processes occurring within sediments may contribute to colloid generation, e.g. incomplete decomposition of organic debris (Wilkinson and Lead, 2007), mineral precipitation in sediment pore water (Lewandowski and Hupfer, 2005; Rothe et al., 2015; Rothe et al., 2016; Woszczyk, 2016; Steiner et al., 2019; Vuillemin et al., 2019) or aggregate disintegration by the dissolution of cementing agents (Newman, 2008; Henderson et al., 2012). Colloids might also be continuously generated at the surface sediment-bottom water interface due to, for example: the mixing of reducing sediment porewater with overlying oxic water, and the oxidation of iron and manganese (Pakhomova et al., 2007; Châtellier et al., 2013; Corzo et al., 2018).

Several protocols for extracting and separating colloids from various matrices (soil, sediment and water) have been proposed in the literature, including centrifugation and filtration (see Table 6). Sedimentation, membrane filtration and centrifugation are simple methods that have been used in many researches for studying aquatic colloidal particles over a long period and continuing through today (Table 6). Each approach has distinct advantages but also drawbacks. For example, conventional filtration with a 1- μm membrane may underestimate the mass of colloids and cause a serious error in the colloidal size class evaluation. A progressively clogged membrane during filtration involves a decrease in effective membrane pore size and thus retains colloids (Morrison and Benoit, 2001). On the other hand, centrifugation has been recommended for separating colloids due to its advantages in overcoming the entrapment or interaction of colloids with the filter membrane (Gimbert et al., 2005). However, when operated properly in a way that avoids membrane overload and introduces multiple filters for large sample volumes (Morrison and Benoit, 2001), filtration can compromise high recovery.

Moreover, the differences in techniques used for colloid extraction, separation and characterization, plus the applied cutoff size could lead to differences in the colloidal size determination over the dissolved fraction. Conventional colloidal size separation has often been carried out at 1 μm for the upper colloidal fraction threshold, while the lower threshold for isolating colloids from the dissolved fraction has varied from one author to the next (Table 6). For example, Liu et al. (2014) considered a colloidal fraction of between 0.02 μm and 1 μm , whereas Tang et al. (2009) placed the size of this fraction at from 0.1 - 1.0 μm . In some instances, no distinction lies between dissolved and colloidal fractions (Gimbert et al., 2006; Zirkler et al., 2012; Yan et al., 2017).

Regarding the widespread use of filtration, the problem of membrane clogging has been minimized by proceeding with the pre-removal of large particles, e.g. by: sedimentation (Tang et al., 2009; Missong et al., 2016), filtration at higher pore sizes (Gottselig et al., 2017a), centrifugation (Sinaj et al., 1998; Turner et al., 2004; Liang et al., 2010; Zang et al., 2013), and a combination of various techniques (Shand et al., 2000). In addition, a wide range of colloid extraction methods are available; these comprise: the choice of solid-liquid ratio (w_{DW}/v) such as 1/8 (Missong et al., 2018), 1/10 (Buettner et al., 2014) and 1/20 (VandeVoort et al., 2013), matrix type (soil, sediment, surface, groundwater) and its characteristics, and raw matrix treatment for storage before colloid extraction such as wet (Missong et al., 2018), air-dried (Yan et al., 2017), oven-dried (Regelink et al., 2014) and lyophilization (Xu et al., 2019). The quantity of colloids in extracts varies from 0.03 to 1.7 g/L (Kaplan et al., 1993; Yan et al., 2017) and from 260 to 1,320 mg/kg (Sinaj et al., 1998) in soil; from 122 mg/L (Tulve and Young, 1999) to 200-2,400 mg/L (Murali et al., 2012) in sediment; and 0.7-8.6 mg/L (Hart et al., 1993) in water. Nonetheless, it remains unclear whether the differences in quantity of extracted colloids across studies have been induced by differences in sample characteristics or by the colloid extraction/separation/characterization protocols and raw matrix conditioning.

The majority of available studies have focused on surface and groundwater, porous media and soils (Grolimund et al., 1998; Kretzschmar et al., 1999; Ran et al., 2000; Bradford et al., 2002; Wolthoorn et al., 2004; Murali et al., 2012; Baken et al., 2016; Yan et al., 2016; Gottselig et al., 2017a; Missong et al., 2018). Much less attention has been paid to lake and river sediments (Seaman et al., 1997; Tulve and Young, 1999; Murali et al., 2012; Xu et al., 2019) and among them, no identical protocol is observed.

The objective of this paper is twofold: 1) evaluate the role of various sediment storage modes (wet, air-dried at 20°C, oven-dried at 40°C, freeze-dried) and various colloid separation protocols (direct filtration, successive filtrations, low-speed centrifugation and filtration, high-speed centrifugation and filtration, successive centrifugations) on the characteristics (mass, size distribution and composition) of water-mobilizable colloids from reservoir sediment; and then 2) propose recommendations for future studies. All tests were performed on organic P-rich sediment sampled in a hydroelectrical dam reservoir located in a granitic catchment and periodically impacted by eutrophication (Champsanglard, France). Special attention was paid to the dissolved and colloidal P, by virtue of its key role in the algal bloom process (Zhang et al., 2019).

III.1.2.2. Materials and methods

III.1.2.2.1. Sediment sampling and preconditioning

Sediment was collected in the middle channel of the Champsanglard dam reservoir (46°15'41.69"N, 1°53'30.49"E) on the Creuse River (France). This reservoir, with a surface area of 0.55 km², a total storage volume of 3.56 hm³ and a water depth of up to 19.4 m, exhibits thermal and oxygen stratification along with a significant bloom of microalgae during the summer period (Rapin et al., 2019). Surface sediment (up to 10 cm) was collected from the reservoir bottom (approx. 9 m) during mid-May 2018 using an Ekman grab. The sediment was manually homogenized and preserved in polyethylene bottles previously rinsed with reservoir surface water. All bottles were kept in an icebox during transportation. In the laboratory, the wet sediment was immediately sieved through a 2-mm mesh and separated for four different conditionings: 1) one portion was kept at 4°C (denoted "wet"), 2) another portion was air-dried at ambient temperature (20° ± 1°C) for 2 weeks (denoted "air-dried at 20°C"), 3) another portion was dried in an oven at 40°C for

5 days (denoted "oven-dried at 40°C"), and 4) the last portion was freeze-dried using a lyophilizator (Cryotec, COSMOS-80) for 4 days (denoted "freeze-dried"). Table 12 presents the general physicochemical characteristics of this sediment.

Table 12. Characteristics of sediment collected in the Champsanglard dam reservoir.

pH	D ₅₀	Particle density	Water loss on drying	OM*	P	Fe	Al	Ca	Mn	Mg
	µm	g/cm ³	%	%			mg/g _{DW-Sed}			
6.4 ± 0.2	19 ± 1	2.417	81.6	19 ± 1	1.43 ± 0.01	79 ± 1	136 ± 4	8.5 ± 0.5	1.5 ± 0.1	17.2 ± 0.0

The water loss on drying of sediment was determined as the percentage of mass loss after drying at 105°C until unchanged mass. The pH of sediment was measured on a suspension of wet sediment in ultrapure water with ratio of 1/1 (w/v) according to Method 9045D (US EPA, 2004). The grain size (D50) of sediment was measured by laser diffractometer (MasterSizer 3000, Malvern) on wet dispersion under ultrasonic field in ultrapure water. Particle density was determined by drying a certain volume of wet sediment at 105°C until unchanged mass. The particle density was then calculated as bulk density minus the pore spaces occupied by air and water according to following equation:

$$\text{Bulk density (g/cm}^3\text{)} = \frac{M \text{ dry sediment (g)}}{V \text{ sediment (cm}^3\text{)}}$$

$$\text{Porosity (\%)} = \frac{M \text{ moist sediment (g)} - M \text{ dry sediment (g)}}{1000 * V (L)} * 100\%$$

$$\text{Particl density (g/cm}^3\text{)} = \frac{\text{Bulk density (g/cm}^3\text{)}}{1 - \text{Porosity (\%)}}$$

The organic matter (OM) content was calculated by percentage of mass loss during calcination at 550°C for 2 h. The measurement of total P in sediment was performed according to the method of Ruban et al., (2001) in which calcinated sediment was digested with HCl 3.5 M for 16 h. Digested solution was centrifuged at 2000 g for 15 min, filtered through 0.45 µm cellulose acetate membrane (LLG Labware) and measured of dissolved phosphate by spectrophotometry (see part 3.2). The determination of total contents of Fe, Al, Ca, Mn and Mg was based on a microwave-assisted digestion procedure with concentrated peroxide (Merck, 30 %), HNO₃ (Fisher, 65 %) and HCl (Normapur, 37 %) (Multiwave Go, Anton Paar) for 40 min at 180°C according to method 3015a (US EPA, 2007). The contents of Fe, Al, Ca, Mn and Mg in digested solution were determined by microwave plasma atomic emission spectroscopy (Agilent, MP-AES 4100) (See section 3.2).

III.1.2.2.2. Colloid extraction and separation

Throughout this study, the focus will be placed on the fraction of large colloids with a size ranging between 0.2 and 1 µm.

III.1.2.2.2.1. Extraction

Colloid extraction was carried out from sediment suspension prepared by adding 150 mL of ultrapure water (UPW) to a 15-g equivalent of wet sediment. The ratio of dried solid/liquid (S/L) equaled 1.7% (w_{DW}/v). Sediment suspensions were agitated for 24 h at 200 rpm using an orbital shaker (IKA-WERKE, KS 501 digital). Since drying involved significant sediment consolidation, before colloid extraction, the dried sediments were submerged in UPW for 2 days to soften, then gently hashed using a stainless spoon and shaken manually to disperse sediment particles. Dried sediments were not powdered so as to avoid a grinding process that would generate new colloidal particles.

III.1.2.2.2. Separation

The effect of the various colloid separation protocols was solely assessed on wet sediment.

Five such protocols were applied on the wet sediment in order to isolate the fraction smaller than 1 μm from sediment suspension. The separation protocols were selected according to reviews found in the literature (Gimbert et al., 2005, 2006; Liang et al., 2010; Murali et al., 2012; Liu et al., 2014; Regelink et al., 2014; Séquaris et al., 2013; Yan et al., 2017), consisting of sedimentation, filtration, centrifugation or the combination of two techniques, as presented in Figure 22.

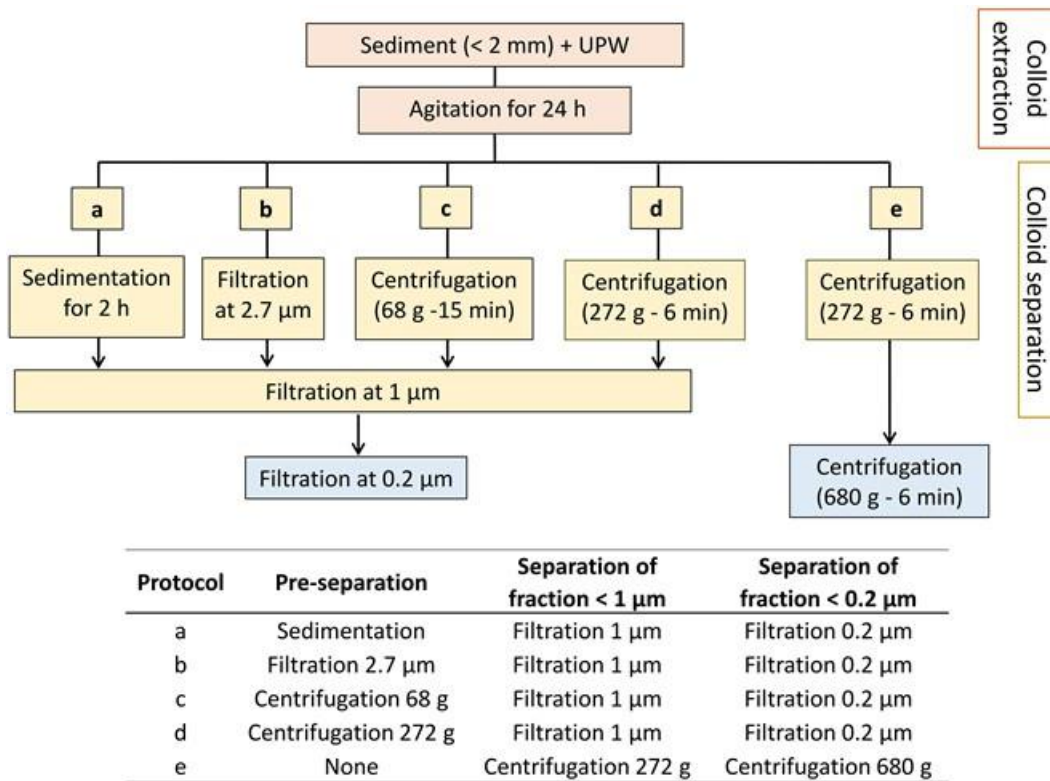


Figure 22. Colloid extraction and separation protocols applied on wet sediment.

- a) Direct filtration: Sediment suspension was decanted for 2 h by gravitation which allow to settle down large particles. According to the quality of decanting or centrifuging matters (mineral, organic or mix), the size cut-off would be different (Klitzke et al., 2012). Considering average density of sediment, 2 h of decantation would settle the particles larger than 42 μm ($d = 2.417 \text{ g/cm}^3$); for organic particles ($d =$

1.2 g/cm³), the cut-off size would be 112 μm. then, the supernatant was filtered through a 1-μm filter. The cut-off size was calculated from equation (1):

$$d = \sqrt[2]{\frac{18 \times \eta \times v}{g \times \Delta\rho}} \quad (1)$$

where:

d: particle diameter (cm)

Δρ: difference in particle density and suspension medium (ρ_{water} = 1.0 g/cm³)

η: dynamic viscosity of the suspension medium (η = 0.01 g/(cm.s))

v: settling velocity (cm/s)

g: gravitational acceleration (g = 9.81 cm/s²)

- b) Successive filtrations: Sediment suspension was filtered through 2.7 μm, and the filtrates were then passed through a 1-μm filter.
- c) Low-speed centrifugation and filtration: Sediment suspension was centrifuged at 68 g for 15 min to separate particles larger than 2.0 μm (d = 2.417 g/cm³). In case of organic particles (d = 1.2 g/cm³), the cut-off size was 5.23 μm. The centrifugates were then carefully pipetted out and filtered through a 1-μm filter. The centrifugation speed and time were calculated using the equation (2), according to Gimbert et al., (2005):

$$t = \frac{18\eta \ln(R/S)}{\omega^2 d^2 \Delta\rho} \quad (2)$$

where:

d: particle diameter (cm)

Δρ: difference in particle density and suspension medium (ρ_p = 2.417 g/cm³) (ρ_{water} = 1.0 g/cm³)

η: dynamic viscosity of the suspension medium (η = 0.01 g/(cm.s))

t: settling time (s)

R: distance from the axis of rotation to the settling level in the tube (R = 10.8 cm)

S: distance from the axis of rotation to the suspension surface in the tube (S = 5.5 cm)

ω: angular velocity of the centrifuge (rad/s) as calculated by the following equation:

$$\omega = \frac{2\pi}{60} \times rpm$$

- d) High-speed centrifugation and filtration: Sediment suspension was centrifuged at 272 g for 6 min to remove particles larger than 1 μm (d = 2.417 g/cm³). In case of organic particles (d = 1.2 g/cm³), the cut-off size was 2.62 μm. The centrifugates were then carefully pipetted out and filtered through a 1-μm filter.
- e) Successive centrifugations: Sediment suspension was first subjected to centrifugation at 272 g for 6 min to remove the fraction greater than 1 μm (d = 2.417 g/cm³) (Gimbert et al., 2005). The supernatant was then gently pipetted out and submitted to the second centrifugation at 680 g for 6 min to settle the particles greater than 0.2 μm (d = 2.417 g/cm³). In case of organic particles (d = 1.2 g/cm³), the cut-off size would be 2.62 μm and 0.52 μm for the first and second centrifugation, respectively. The pellets after the second centrifugation were resuspended in UPW by agitation for 30 min in order to obtain colloidal suspension of 0.2 - 1 μm. The supernatants were also gently pipetted out and represented the fraction smaller than 0.2 μm.

For the four protocols (“a” through “d”), an aliquot of obtained suspension (fraction smaller than 1 μm) was passed through a 0.2- μm filter.

All filtrations at 2.7 μm and 1 μm were conducted with glass microfiber (VWR), which features a higher chemical resistance, pH resistance and biological inertia, and at 0.2 μm with a cellulose nitrate membrane (Whatman). All centrifugations were performed using both a centrifuge (Thermo Scientific, Multifuge X3 FR) and a rotor (Thermo Scientific, FIBERLite F14-6x250LE). All experiments were run in triplicate.

Protocol “d” (combining centrifugation at 272 g and filtration at 1 μm , see Fig. 22) was selected for investigating the various sediment storage modes (wet, air-dried, oven-dried at 40°C, freeze-dried).

III.1.2.2.3. Colloid characterization

III.1.2.2.3.1. Colloid concentration and size distribution

The quantity of colloids was determined by gravimetric method. The filtrates at 1.0 μm (protocols “a” to “d”) and suspension 0.2 - 1 μm (protocol “e”) were passed through a 0.2- μm filter to retain the large colloidal fraction (0.2 - 1 μm), and the filters were oven-dried at 30°C until the mass remained unchanged. The colloidal concentration was quantified as a dry mass of colloid divided by the dry mass of sediment ($W_{\text{DW-Colloid}}/W_{\text{DW-Sed}}$). The particle size distribution of colloids was determined based on a dynamic light scattering technique using ZetaSizer NanoZS (Malvern) on the 0 - 1 μm (protocols “a” to “d”) and 0.2 - 1 μm (protocol “e”) suspensions. The material refraction index was set at 0.18 and the material absorption equaled 0.001. The angle of measurement was 173° backscatter; measurements started with a 120-second equilibration, followed by three measurements with an automatic selection of running times and optimal measurement position. The size distribution was presented according to number-based DLS data.

III.1.2.2.3.2. Chemical analysis for TP, Fe, Al, Mn, Ca, Mg, TOC

All chemical analyses were conducted on two fractions: 0 - 1 μm and 0 - 0.2 μm . The 0.2 - 1 μm fraction was determined by the difference between these two fractions across all separation methods, except for protocol “e” since the resuspended solution had already presented colloids sized 0.2 - 1 μm .

Total organic carbon (TOC) was measured using a TOC analyzer (Analytik Jena, multi N/C 2100S) with an LQ of 1 mg C/L. The organic content analysis was carried out with onboard magnetic stirring in order to avoid colloid aggregation and decantation.

Measurements of Fe, Al, Mn, Ca and Mg contents were recorded using MP-AES (Agilent, MP 4100). The LQ were: 30 $\mu\text{g/L}$, 20 $\mu\text{g/L}$, 7 $\mu\text{g/L}$, 12 $\mu\text{g/L}$ and 1 $\mu\text{g/L}$, respectively. For the fraction smaller than 1 μm , prior to analysis the samples were acid digested with *aqua regia*, as presented in Method 3015a (US EPA, 2007) using a microwave digestion system (Anton Paar, Multiwave GO).

Total released phosphorus (TP) was analyzed after persulfate digestion according to Method 365.1 (US EPA, 1993). This method converts all forms of P into orthophosphate by autoclaving at 121°C for 30 min with ammonium persulfate and sulfuric acid. The content of digested orthophosphate, or dissolved inorganic phosphorus (DIP), was then measured by means of spectrophotometry using ammonium molybdate and antimony potassium tartrate, according to the method described by Murphy and Riley,

(1962). The amount of DIP was determined by the absorbance of molybdenum blue P, in conjunction with a UV-visible spectrophotometer at 880 nm (Agilent 8453 UV-visible spectrometer), using 1-cm cuvettes. Results were expressed in mg P/L. The limit of quantification (LQ) for this method is 0.01 mg P/L.

Four fractions of P could be determined: water-mobilizable P (P_{WM} : TP in the fraction smaller than 1 μm), large colloidal P (TP content in the 0.2 - 1 μm fraction, as identified by subtracting $TP_{< 0.2 \mu\text{m}}$ from P_{WM}), small colloidal P (TP in the fraction smaller than 0.2 μm minus the dissolved P, as found by subtracting $DIP_{< 0.2 \mu\text{m}}$ from $TP_{< 0.2 \mu\text{m}}$), and dissolved P (evaluated by DIP in the fraction smaller than 0.2 μm). By this fractionation step, the small colloidal P covers P-colloids less than 0.2 μm , whereas large-colloidal P includes P-colloids from 0.2 to 1 μm .

III.1.2.2.4. Statistical analysis

A one-way analysis of variance (ANOVA) and two-tail t-test were used to analyze the significance of the differences between colloid separation methods and sediment storage modes at a 0.05 level of significance. The possible correlation between colloidal P and other colloidal elements was measured by means of the Pearson correlation coefficient R^2 . All statistical analyses were run on Microsoft Excel, enhanced with Analysis ToolPak, XLSTAT and XL Toolbox NG.

III.1.2.3. Results and discussion

III.1.2.3.1. Separation protocols

III.1.2.3.1.1. Effects on the quantity of separated colloids and their size distribution

The mass of water-mobilizable colloids (0.2 - 1 μm) obtained according to five separation protocols is presented in mg colloid/ g_{DW-Sed} of sediment (Fig. 23). The colloid quantity varied between $5.4 \pm 0.6 \text{ mg}/g_{DW-Sed}$ for direct filtration (protocol “a”) and $21.2 \pm 1.5 \text{ mg}/g_{DW-Sed}$ for successive centrifugation (protocol “e”), which corresponds to a factor of 4 across the tested assays.

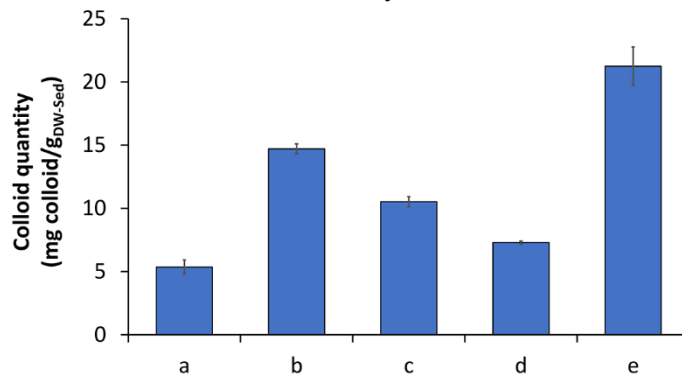


Figure 23. Variation in dry mass of the colloidal fraction sized 0.2 - 1 μm by means of different colloid separation protocols. The error bar depicted 1 SD.

When comparing protocol “a” with pre-separation filtration protocols “b” through “d”, the introduction of a pre-separation step by filtration or centrifugation prior to filtration at 1 μm induced an increase of 1.5 to 2 times the mass of obtained colloids (from 7.3 ± 0.2 to $14.7 \pm 0.4 \text{ mg}/g_{DW-Sed}$) relative to direct filtration at 1 μm ($5.4 \pm 0.6 \text{ mg}/g_{DW-Sed}$). The lower mass of colloids obtained by direct filtration, compared to “pre-

treated” separation methods, is typically associated with membrane fouling, which decreases the flow rate due to an accumulation of particles at the surface (cake layer formation) or inside the membrane pores (Speth et al., 2000; Gimbert et al., 2005; Tang et al., 2009). Cake layer formation is driven by both particle diameter and filter porosity with larger flocs/particles creating a thicker cake (Shirazi et al., 2010). Introduction of the pre-separation step therefore helped reduce the deposition of coarser particles and resulted in an increase of colloid quantity passing through the 1- μm membrane. The decantation carried out prior to filtration in protocol “a” was insufficient to limit this phenomenon. However, the quantity of isolated colloids could also be decreased by colloid interaction with the filter or by attachment to larger particles retained by the membrane during filtration or aggregation to larger floc (Buffle and Leppard, 1995a; Stumm and Morgan, 1995). These interactions are not well understood, and more studies are needed to reveal the complex interactions taking place between colloid and membrane.

Application of a pre-centrifugation step (protocols “c” and “d”) showed lower colloid recovery when compared with protocol “b” (pre-filtration at 2.7 μm), 10.5 ± 0.5 and 7.3 ± 0.2 against 14.7 ± 0.4 $\text{mg/g}_{\text{DW-Sed}}$, respectively. The mass of colloids further decreased by approximately 30% as the centrifugal force increased from 68 g (protocol “c”) to 272 g (protocol “d”) yet remained at least 1.4 times higher than direct filtration (protocol “a”). Separation by centrifugation could bring particles into closer contact and enhance aggregate formation (Vauthier et al., 2008). An increase in centrifugal force likely resulted in greater colloid collision and aggregation. Colloidal aggregates larger than 1 μm would be eventually separated in the subsequent filtration and could explain the lower mass observed in pre-centrifugation protocols. However, aggregate formation upon pre-centrifugation cannot be demonstrated in this study since no significant size discrimination for large colloids in the colloidal fraction (0.2 - 1 μm) were observed between two centrifugal speeds; moreover, for large aggregates, the size distribution of the particle fraction (i.e. above 1 μm) was not recorded herein. Although pre-centrifugation induced important mass loss of recovered colloids in subsequent filtrations compared to the successive filtration protocol, pre-centrifugation did remain a good solution for overcoming membrane clogging during direct filtration without any significant change in size distribution.

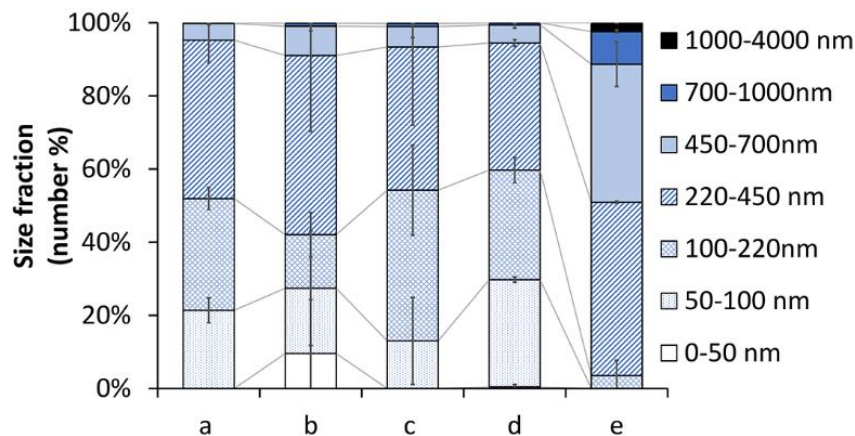


Figure 24. Effect of colloid separation protocols on the size distribution of the water-mobilizable fraction smaller than 1 μm , except for protocol "e", which presents the 0.2 - 1 μm fraction size. The error bar depicted 1 SD.

For successive centrifugation without filtration at 0.2 μm (protocol “e”), the colloid quantity was considerably higher than for the other protocols (by a factor ranging from 1.4 to 5), and the size distribution of obtained colloids revealed the presence of particles larger than 1,000 nm (Fig. 24). Meanwhile, the expected size was between 200 and 1,000 nm. During two successive centrifugations, the first aimed to remove particles larger than 1 μm and the second to separate colloidal from the conventional “dissolved fraction” at 0.2 μm . The appearance of particles larger than 1 μm after two successive centrifugations could be ascribed to an incomplete separation, caused by the heterogeneity of particle density and/or colloid aggregation/flocculation under high centrifugal forces. Particle density has an important role on the cut-off of colloidal particles separated by centrifugation using Stoke’s law. The particles with lower density (for example organic particles) travel at a lower rate and at some point, will be separated from particles with higher density. Therefore, organic matter dominated particles would give a larger size cut-off than the particles dominated by minerals when subjected to the same centrifugation procedures (Klitzke *et al.*, 2012). According to our calculation, at the centrifugation speed of 272 g and 680 g and considering density of 1.2 g/cm^3 (for organic particles), the size of separated colloids was estimated to be 2.62 μm and 0.52 μm , respectively. The presence of particles larger than 1000 nm (Fig. 24) is a hint for presence of organic colloids. Moreover, as shown in figures 25a and 25b, the major component of separated colloids was organic carbon (9-12 %). Thus, the colloids separated from studied sediment contained high amount of organic matter (estimated as 15-21 % by a factor of 1.72 of total organic carbon). The incomplete separation of colloids during successive centrifugation (protocol “e”) and associated higher size cut-off of separated colloids could be related colloid composition (with high organic content).

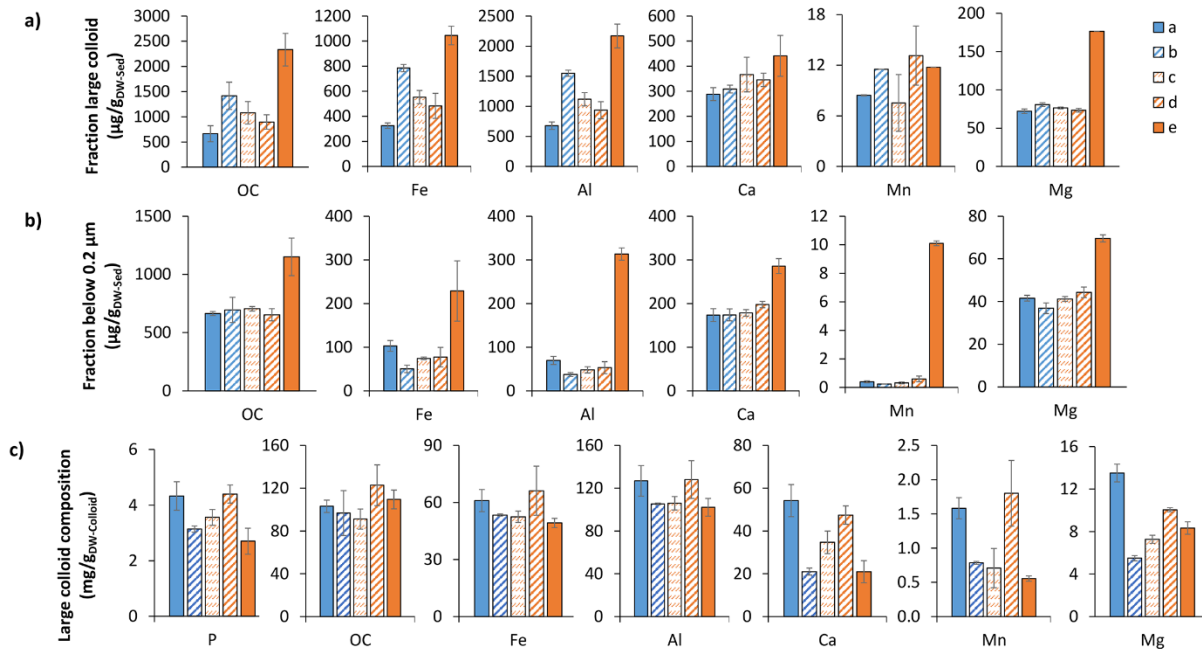


Figure 25. Impacts of colloid separation methods on the elemental composition, expressed per dry mass of sediment for: a) large colloidal fraction (0.2 - 1 μm), and b) fraction below 0.2 μm ; versus c) the concentration per dry mass of large colloids (0.2 - 1 μm). The error bar depicted 1 SD.

On the other hand, high density of colloids could favor colloid assemblies. Aggregation/flocculation may occur in the pellets or through colloid collision/agglomeration within supernatant (Salim and Cooksey, 1981; Baalousha, 2009; Maria et al., 2020) to form large aggregates/flocs. In general, the supernatant obtained from the first supernatant could contain particles, colloidal and dissolved fractions.

When considering incomplete separation and aggregation with respect to the second-centrifuged supernatant, the presence of colloids larger than 0.2 μm could be expected even after the second centrifugation step. This has been confirmed by means of a size analysis of the fraction assumed to be smaller than 0.2 μm , in which $19 \pm 15\%$ of particles were in the range of greater than 200 nm for successive centrifugations, compared to $6 \pm 3\%$ for the other protocols (Fig. 31). Nevertheless, the presence of larger particles due to this incomplete separation has notably increased the expected mass of colloids (Fig. 23) and can lead to overestimating the colloidal fraction. This finding highlights the importance of considering not only the weight of extracted colloids but also their size distribution.

The large colloidal and dissolved fractions separated by all tested protocols contained high amounts of organic, Al and Fe and lower contents of Ca, Mg and Mn (Figs. 25a and 25b). Chemical composition of extracted colloids and dissolved fractions was related to composition of sediment (Table 12) which was related to local geological context (mainly granitic). As shown in figures 4 and 5a, the masses of P, OC, Fe, Al, Ca, Mn and Mg recovered in fraction lower than 1 μm were respectively: from 30.1 ± 2.1 to 85.3 ± 7.8 $\mu\text{g P/g}_{\text{DW-Sed}}$, 1330 ± 160 to 3500 ± 400 $\mu\text{g C/g}_{\text{DW-Sed}}$, 430 ± 30 to 1300 ± 100 $\mu\text{g Fe/g}_{\text{DW-Sed}}$, 750 ± 70 to 2500 ± 200 $\mu\text{g Al/g}_{\text{DW-Sed}}$, 460 ± 30 to 730 ± 90 $\mu\text{g Ca/g}_{\text{DW-Sed}}$, 8.8 ± 0.1 to 21.9 ± 0.2 $\mu\text{g Mn/g}_{\text{DW-Sed}}$ and 115 ± 5 to 250 ± 2 $\mu\text{g Mg/g}_{\text{DW-Sed}}$. Water-mobilizable fraction (below 1 μm) represented 2.1 – 6 %, 0.7 – 1.8 %, 0.5 – 1.6 %, 0.5 – 1.9 %, 5.4 – 8.6 %, 0.5 – 1.5 % and 0.7 – 1.4 % of total sedimentary P, OC, Fe, Al, Ca, Mn and Mg contents. The percentages were obtained under experimental gentle agitation with UPW and probably did not represent all the mobilizable P-colloids in natural system. The large colloids (0.2 – 1 μm) represented 67 – 90 %, 50 – 67 %, 76 – 94 %, 87 – 98 %, 61 – 67 %, 54 – 98 % and 62 – 72 % of P, OC, Fe, Al, Ca, Mn and Mg contents in water-mobilizable fraction (below 1 μm).

It is important to highlight that higher release of OC in large colloids (0.2 – 1 μm) by successive centrifugation protocol were concomitating with higher release of Al, Fe, Mg and P. In fraction below 0.2 μm , this release of OC was with Al, Ca, Fe, Mg, P and Mn. This suggesting the remaining colloids after centrifugation could be organo-mineral colloids.

Furthermore, there are difficulties in comparison potential of sediment to mobilize colloids with other terrestrial systems as most of the studies presented colloid concentration by volume of extract. Dissimilarities between the method used to extract and separate colloid, S/L ratio and cut-off size for colloidal fraction do not allow straight comparison. However, to some extents, the estimation of colloidal stock in sediment can be relatively determined. For example, Sinaj et al., (1998) showed colloid concentrations of 0.26 – 1.32 $\text{g/kg}_{\text{DW-Soil}}$ in Ap horizon soils for fraction 0.025 – 0.45 μm separated by centrifugation combining filtration and with similar S/L ratio of 1/10 to present work. Our sediment showed a colloid concentration of 7.29 – 10.52 $\text{g/kg}_{\text{DW-Sed}}$ for fraction 0.2 – 1 μm by similar separation protocol (protocols “d” and “c”). Hence, the amount of colloids in reservoir sediment is 7 – 10 times higher than in soil reported by Sinaj et al., (1998). This drastic variation might indicate the higher potential of reservoir sediment to release colloids than in soil. However, it should be noted a different in cut-off size can derive incomparable data; as taken into the work of Yan et al., (2017), large colloids (0.45 – 1 μm) contributed

lower proportion (approximately 38 %) than small colloidal in total soil colloids (0.1 – 1 μm) separated by successive centrifugation.

III.1.2.3.1.2. Effects on water-mobilizable phosphorus

The concentrations of water-mobilizable phosphorus (P_{WM}) obtained from five separation protocols are presented in three size-based forms: DIP; “small colloidal P” containing colloids sized below 200 nm; and “large colloidal P” containing P-colloids sized 0.2 μm - 1 μm . The concentration of P_{WM} is presented in μg of P per g_{DW} of sediment (Fig. 26).

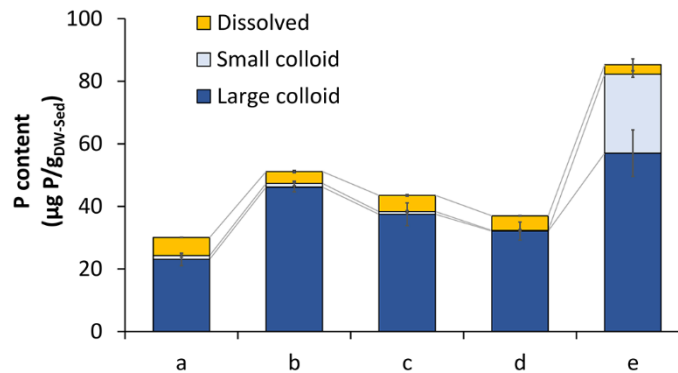


Figure 26. Distribution of water-mobilizable phosphorus extracted from wet sediment using five separation protocols. Large colloidal P sized from 0.2 – 1 μm . Small colloidal P sized smaller than 0.2 μm . Dissolved P represented dissolved inorganic phosphate in fraction smaller than 0.2 μm . The error bar depicted 1 SD.

The release of P_{WM} varied between 30.1 ± 1.6 (direct filtration) and 85.3 ± 9.6 $\mu\text{g P/g}_{\text{DW-Sed}}$ (successive centrifugations) in proportion with the mass of colloids released from the sediment ($R^2 = 0.88$). The P_{WM} distribution between dissolved, small and large colloidal fractions was relatively similar for all tested separation protocols, except successive centrifugations (protocol “e”). Generally, P_{WM} presented mainly in large colloids (> 0.2 μm ; 67% - 90%). The lowest quantity of large P-colloids was observed after direct filtration (protocol “a”, 23.1 ± 2.0 $\mu\text{g/g}_{\text{DW-Sed}}$), while the highest amount was obtained after successive centrifugations (protocol “e”, 57.1 ± 7.5 $\mu\text{g/g}_{\text{DW-Sed}}$) and varied proportionally to the mass of P_{WM} . The quantities of small colloidal P were less than 1.3 ± 0.6 $\mu\text{g/g}_{\text{DW-Sed}}$ and contributed up to 4% of P_{WM} for the separation protocols using filtration (protocols “a” to “d”). As opposed to other protocols, namely the successive centrifugations protocol, a significant contribution of small P-colloid was observed (30 ± 3 %). An increasing amount of small colloidal P in successive centrifugations might be due to the remaining large colloids due to incomplete separation in second-centrifuged supernatant. These colloids were organic or organo-mineral considering their chemical composition (Fig. 25b).

The quantities of dissolved P were not strongly impacted by any of the separation protocols, with an average of 4.5 ± 1.1 $\mu\text{g/g}_{\text{DW-Sed}}$, constituting 11 ± 6 % of P_{WM} and 0.3 ± 0.1 % of total sedimentary P. As such, the total colloidal P in both the small and large colloids accounted for 1.7 - 5.8 % of total sedimentary P, which

far exceeds dissolved P, thus highlighting the major contribution of P-colloids, beyond the focus on truly dissolved P.

In comparison to studies on soil samples, in the present work, the contribution of colloidal P in fraction lower than 1 μm represented 81 – 93 %, which is relatively higher than the contribution of colloidal P extracted from soils. For example, for agricultural soil, Liang et al., (2010) found that 25.5 % of total P in fraction below 1 μm came from colloidal form and Liu et al., (2014) reported proportions of 55.2 – 80.9 % for colloidal fraction between 0.02 – 1 μm . In study performed on wetland soils, Gu et al., (2018) found up to 70 % of nano and small colloidal P contributed to $\text{TP}_{<0.45\ \mu\text{m}}$ but in different size range 5 kDa – 0.45 μm . Even though, the important proportions of the colloidal P found in other studies and in our study highlight the significant contribution of this fraction to the potential mobilization of P from sediment to the water column and the interest to improve knowledge about this fraction.

III.1.2.3.1.3. Effects on the chemical composition of large colloids (0.2 -1 μm)

Figure 25c presents the elemental composition of P, OC, Fe, Al, Ca, Mn and Mg in separated large colloids. The P concentration obtained by successive centrifugations (protocol “e”) equaled $2.7 \pm 0.5\ \text{mg/g}_{\text{DW-Colloid}}$, which was similar to the successive filtrations (protocol “b”, $3.14 \pm 0.12\ \text{mg/g}_{\text{DW-Colloid}}$) and low-speed centrifugation-filtration (protocol “c”, $3.6 \pm 0.3\ \text{mg/g}_{\text{DW-Colloid}}$). However, these concentrations were less than those in colloids separated by direct filtration (protocol “a”) and high-speed centrifugation-filtration (protocol “d”), with 4.4 ± 0.6 and $4.4 \pm 0.4\ \text{mg/g}_{\text{DW-Colloid}}$, respectively. The concentrations of Ca, Mn and Mg in large colloids also varied across the separation protocols, with higher values being observed for protocols “a” and “d” (i.e. 54.2 ± 7.5 and $47.5 \pm 4.4\ \text{mg Ca/g}_{\text{DW-Colloid}}$, 1.6 ± 0.2 and $1.8 \pm 0.5\ \text{mg Mn/g}_{\text{DW-Colloid}}$, 13.6 ± 0.9 and $10.1 \pm 0.2\ \text{mg Mg/g}_{\text{DW-Colloid}}$, respectively). Therefore, the higher concentrations of P for protocol “a” and “d” can be linked to higher concentrations of Ca, Mn and Mg. On the other hand, the difference in separation protocols seems to exert no influence on the concentrations of OC, Fe and Al in large colloids (one-way ANOVA: $p > 0.05$ for OC and Fe, t-test for each pair of means for Al), with average values of 105 ± 6 , 56.5 ± 7.0 and $114 \pm 13\ \text{mg/g}_{\text{DW-Colloid}}$, respectively. For P, Ca, Mn and Mg elements, the low concentrations in large colloids after separation by means of successive centrifugations, in spite of the higher dry mass, may be caused by dilution due to the presence of large particles resulting from incomplete separation, because colloids have higher specific surface area than particles (Biermann, 1996).

On the whole, the successive centrifugations should be considered with caution since this technique introduces a high probability of incomplete separation, which in turn can lead to overestimating quantity and underestimating quality of the colloidal fraction. Special attention should be paid to organic rich sediment which could induce higher error in size separation by this method and overestimation of colloid mass and size. Among the four separation protocols using filtration, successive filtrations provided the highest recovery in colloid quantity, whereas high-speed centrifugation and filtration delivered lower colloid quantity, though with colloids richer in P content. In the next section, as regards the role of P in the aquatic environment, an assessment of several sediment storage modes will be conducted from the colloid separated by high-speed centrifugation and filtration (protocol “d”) in order to obtain colloids with elevated P contents.

III.1.2.3.2. Sediment storages

III.1.2.3.2.1. Effects on the quantity of extracted colloids and their size distribution

The mass of large colloids (0.2 - 1 μm) and the size distribution of the fraction smaller than 1 μm are presented in Figures 27 and 28, respectively. From here, the wet sediment will be considered as a reference when assessing the influence of various sediment drying on the quantity and quality of water-mobilizable colloids obtained according to protocol “d” (high-speed centrifugation and filtration, Fig. 22).

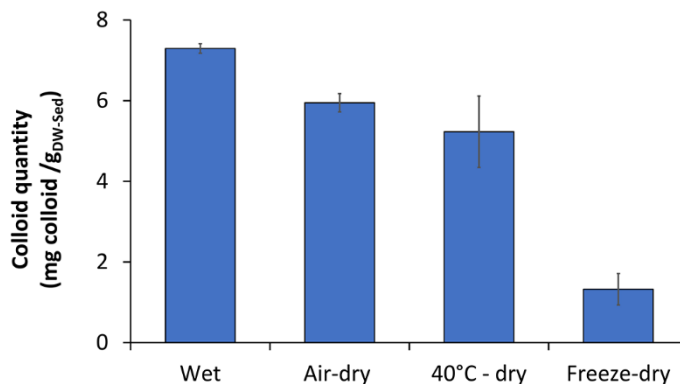


Figure 27. Effect of the rewetting of previously air-, oven-, and freeze-dried sediments on the dry mass of colloids sized 0.2 - 1 μm . The employed colloid separation protocol was high-speed centrifugation combined with filtration (i.e. protocol “d”, Fig. 1). The error bar depicted 1 SD.

As displayed in Figure 27, various modes of sediment storage prior to colloid extraction performed strong influence on the quantity of colloids actually yielded. The mass of colloids (0.2 - 1 μm) obtained from the wet sediment was 7.3 ± 0.2 mg/g_{DW-Sed}, as decreased by 18 % and 28 % after sediment drying at 20°C and 40°C, respectively, and by 82 % after freeze-drying. Sediment drying had also exerted an impact on the size distribution of water-mobilizable colloids (Fig. 28). In the first part of this study, we showed that when the “d” protocol was used for colloid separation, 94 % of the released colloids were sized smaller than 450 nm; also, colloids sized 0 - 50 nm did not appear in extracted supernatant from the wet sediment. We noted that even after sediment drying and rewetting, this fraction remained undetectable. We did however observe an impact of sediment drying on the 50 - 100 nm, 100 - 220 nm and 220 - 450 nm fractions. The percentages of colloids sized 50 - 100 nm declined significantly, i.e. from 29 ± 1 % in wet sediment to less than 5 % in dried sediment regardless of the drying mode, whereas the percentage of the 100 - 450 nm fraction increased from 65 ± 14 % for wet sediment to 95 ± 2 % for dried sediment.

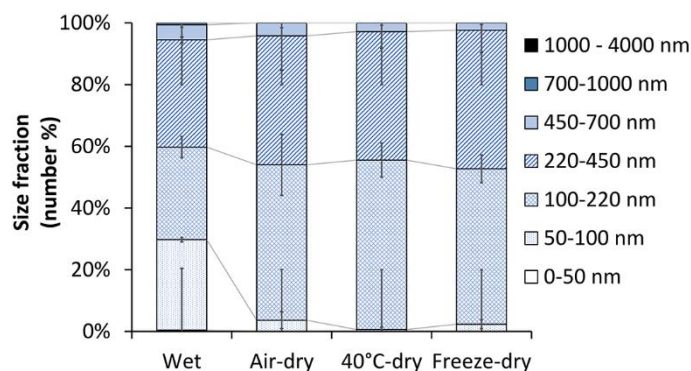


Figure 28. Effect of the rewetting of previously air-, oven-, and freeze-dried sediments on the size distribution of the water-mobilizable fraction smaller than 1 µm. The employed colloid separation protocol was high-speed centrifugation combined with filtration (i.e. protocol “d”, Fig. 1). The error bar depicted 1 SD.

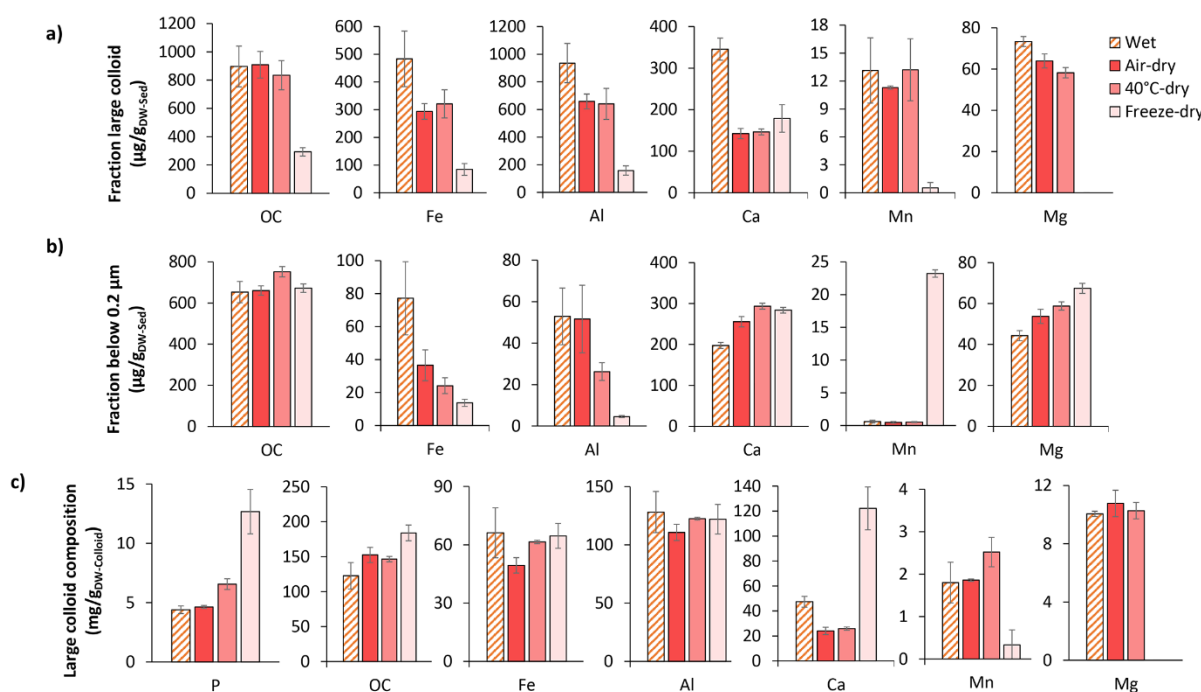


Figure 29. Impacts of the rewetting of previously air-, oven-, and freeze-dried sediments on the elemental composition, expressed per dry mass of sediment of: a) large colloidal fraction (0.2 - 1 µm), and b) fraction below 0.2 µm; versus c) the concentration per dry mass of large colloids (0.2 - 1 µm). Extraction using the high-speed centrifugation protocol combined with filtration (i.e. protocol “d”, Fig. 1). The error bar depicted 1 SD.

The observed decrease in colloidal mass and the change in colloidal size distribution may be due to two phenomena: (i) an increase in the hydrophobicity and/or (ii) an aggregation occurring during the evaporation of water by desiccation and freeze-drying. The first phenomenon concerns an increase in water repellency on solid surfaces during drying, which implies an increase in the hydrophobicity of solid phases (Dekker et al., 2001; Klitzke and Lang, 2007). The intensification of hydrophobicity involves the retention

of colloidal particles on the surface of solids, and thus affects their dispersibility after rewetting (Klitzke and Lang, 2007). It is also postulated that colloids become more hydrophobic during drying and become less mobile after rewetting (Klitzke and Lang, 2007; Wan and Wilson, 1994). Another possible explanation for the decrease in colloid recovery after drying is aggregation. During water elimination, the cohesive forces of capillary-bound water increase with the decrease in pore water pressure and thus increase the effectiveness of bridging and cementing materials (Munkholm and Kay, 2002). Especially during freeze-drying, through the sublimation of ice crystals, the water molecular layers in electrical double layers are limited, which in turn enhances short-range attractive forces and accelerates both colloid-colloid and colloid-particle flocculation (Dagesse, 2011). Moreover, the duration of drying process plays an important role in colloid mobility (Majdalani et al., 2008; Mohanty et al., 2015). Drying would initially enhance colloid release because during the early period of drying, pore walls are broken under capillary stress that favor colloids generation. However, after a critical period of 2.5 or 9 - 11 days, according to cases cited in Mohanty et al. (2015) and Majdalani et al. (2008), the quantity of mobilized colloid decreases. This phenomenon was explained by the precipitation of salts and minerals in pore water during evaporation, which according to the authors serves to bind colloids and prevent their mobilization during rewetting (Majdalani et al., 2008). Moreover, further drying can lead to the hydraulic disconnection of previously saturated pores and might limit the diffusive transport of colloids from matrix to solution (Mohanty et al., 2015). It is therefore possible that in our study the important decrease in mass of large colloids was associated with the precipitation of dissolved Fe and Al during drying (2 weeks for 20°C-dried sediment, 5 days for 40°C-dried sediment and 4 days for freeze-dried sediment). As shown in Figure 8b, in most cases, a lower release of Fe and Al in the fraction below 0.2 μm (generally defined as dissolved) was observed when using dried sediments as compared to wet ones. The release of Fe from wet sediment to the fraction smaller than 0.2 μm amounted to $78 \pm 22 \mu\text{g/g}_{\text{DW-Sed}}$, dropping to $37 \pm 9 \mu\text{g/g}_{\text{DW-Sed}}$, $25 \pm 22 \mu\text{g/g}_{\text{DW-Sed}}$ and $14 \pm 2 \mu\text{g/g}_{\text{DW-Sed}}$ ($p < 0.05$) in the experiments carried out on sediments dried at 20°C, 40°C and by freezing, respectively. For Al, the release from wet sediment was $53 \pm 14 \mu\text{g/g}_{\text{DW-Sed}}$ and significantly decreased after 40°C and freeze-drying to reach $27 \pm 4 \mu\text{g/g}_{\text{DW-Sed}}$ and $4.6 \pm 0.6 \mu\text{g/g}_{\text{DW-Sed}}$ respectively ($p < 0.05$). The drying of sediment at 20°C seems to exert no impact on the amount of dissolved Al. The lower release of dissolved Fe for all dry modes and Al for 40°C-dried and freeze-dried sediments suggested that Fe and Al precipitation may have played a role in the formation of cement bridges binding the colloids to one another and/or the colloids with sediment particles; moreover, the dissolved Fe and Al could interact with large colloids and promote their aggregation. Thus, colloids bound to sediment particles (by cementation or increased solid phases/colloid hydrophobicity) and/or contained in the aggregates larger than 1 μm were eliminated during the extraction and/or separation steps or else were not mobilized after rewetting. As shown in Figure 29a, a portion of large Al-, Fe- and Ca-colloids were impacted by the processes described above at an intensity varying by sediment drying mode. The lowest release of large Fe- and Al-colloids occurred after freeze-drying, with quantities of 80 ± 30 and $160 \pm 40 \mu\text{g/g}_{\text{DW-Sed}}$ respectively, corresponding to 0.11 % and 0.12 % of total sedimentary Fe and Al, against 480 ± 110 and $940 \pm 150 \mu\text{g/g}_{\text{DW-Sed}}$ respectively (corresponding to 0.61 % and 0.69 % of total sedimentary contents) found in colloids separated from wet sediment. The Ca quantities in large colloids were similar across three sediment drying modes ($p > 0.05$), with an average value of $160 \pm 20 \mu\text{g/g}_{\text{DW-Sed}}$ which were two-times lower than for the wet one, and composed of 1.8 ± 0.2 % of total sedimentary Ca. In contrast, it seems that large water-mobilizable OC-, Mn- and Mg-colloids were not impacted by sediment drying at 20°C and 40°C, but only by freeze-drying. Their colloid quantities in 20°C- and 40°C-dried sediments were: 870 ± 60 , 12 ± 2 and $61 \pm 4 \mu\text{g/g}_{\text{DW-Sed}}$, respectively, representing 0.45 %, 0.82 % and 0.36 % of total sedimentary OC, Mn and Mg.

These quantities of OC, Mn and Mg in large colloids dropped to 290 ± 30 , 0.6 ± 0.6 and zero $\mu\text{g/g}_{\text{DW-Sed}}$ when the sediment was freeze-dried, thus representing lower proportions in total sedimentary contents (0.15 % and 0.04 % for OC and Mn). Several studies have reported an increase in the solubility of organic matter following drying, as attributed to microbial lysis and the disruption of organic matter coatings on mineral particles (e.g. Bartlett and James, 1980; Turner et al., 2003). A greater release of dissolved and/or colloidal OC would thus be expected, but as presented in Figures 29a and 29b, differences in the OC pool in the 0 - 0.2 μm and 0.2 - 1 μm fractions remained relatively small (except for large OC colloids in the freeze-drying assay) and lied within the error expected for replicate analyses. This finding indicates that air-drying and oven-drying cause no systematic changes in OC release; furthermore, if the disruption of organic matter coatings on the mineral particles occurred during drying pretreatment, then this step shall produce OC in the fraction larger than 1 μm and hence was not evaluated herein. Our results indicate the preferential immobilization of inorganic colloids during air and oven drying comparing to organic colloids, which underline their different mobility after drying. This result is consistent with the observations reported by Klitzke and Lang, (2007) suggesting that the dispersibility of colloids after drying depends on their composition and that organic colloids are more mobile than organo-minerals colloids. In addition, we observed a decreasing release of large OC colloids in freeze-dried sediment, most likely due to the formation of larger particles (or more hydrophobic) and their retention during the extraction and/or filtration step. Freeze-drying is a common method employed to avoid microbial and chemical degradation in samples (Sun et al., 2015; Weißbecker et al., 2017; Wu et al., 2018). However, the use of freeze-dried sediment instead of fresh sediment can result in a significant underestimation of water-mobilizable OC, Fe, Al, Ca, Mn and Mg.

III.1.2.3.2.2. Effects on water-mobilizable phosphorus

The variation in P_{WM} quantities induced by the different sediment drying modes is presented in Figure 30, in comparison to the reference (wet sediment). We observed that P_{WM} recovery during colloid extraction was significantly altered by the freeze-drying pretreatment step. The amounts of P_{WM} extracted from wet, 20°C- and 40°C-dried sediments were comparable, at $36 \pm 3 \mu\text{g/g}_{\text{DW-Sed}}$, whereas with freeze-drying, P_{WM} recovery decreased by a quarter compared to the initial value, reaching $27 \pm 1 \mu\text{g/g}_{\text{DW-Sed}}$. A lower release of P_{WM} from freeze-dried sediment is primarily due to the decrease in large P-colloids and probably due to the same processes explaining colloidal OC retention (see previous section). On the other hand, the sediment drying pretreatment step led to an alteration in the size-based forms of P_{WM} , regardless of drying mode, by increasing small-sized colloidal P from $0.35 \pm 0.17 \mu\text{g/g}_{\text{DW-Sed}}$ for wet sediment to reach $2.5 \pm 0.7 \mu\text{g/g}_{\text{DW-Sed}}$ for the 20°C-dried and $4.2 \pm 0.7 \mu\text{g/g}_{\text{DW-Sed}}$ for the 40°C-dried and freeze-dried modes. The small-sized P-colloids only contributed $1.0 \pm 0.4 \%$ of total P_{WM} in wet sediment, while this P fraction rose to $8 \pm 3 \%$ for 20°C-dried, $11 \pm 3 \%$ for 40°C-dried and $16 \pm 2 \%$ for freeze-dried sediments. Thus, air-, oven- and freeze-drying generated small-sized colloidal P, probably in the range of 100 - 200 nm, in accordance with an increase in the 100 - 220 nm sized fraction (Fig. 28). In sediments, P can be associated with the organic fraction and with primary and/or secondary minerals, which are mostly composed of Fe, Mn and Al oxi-hydroxides and Ca phases (Pettersson et al., 1988). According to the literature, drying may induce the solubilization of small-sized P-colloids because of microbial cell lysis and/or organic matter solubilization through disrupting the mineral particle organic coating (Turner et al., 2003). However, as indicated in Figures 29a and 29b, the expected increase in OC release was not observed for dried sediments. A greater release of Ca and Mg in the 0 - 0.2 μm fraction from all dried sediments (Fig. 29b) suggests that

small P-colloids released from dried sediments originated rather from inorganic particles and were or still are associated or generated along with Ca and/or Mg. It is also possible that a portion of small-sized P colloids was produced by the (co)precipitation of DIP during drying. As shown in Figure 30, the amount of dissolved P decreased from $4.7 \pm 0.1 \mu\text{g/g}_{\text{DW-Sed}}$ for wet sediment to $3.0 \pm 0.1 \mu\text{g/g}_{\text{DW-Sed}}$, 2.0 ± 0.4 and 2.6 ± 0.2 for 40°C-dried, 20°C-dried and freeze-dried sediments, respectively. Thus, across all sediment storage modes, the principal fraction of P_{WM} came from large-sized colloidal P (i.e. larger than $0.2 \mu\text{m}$), which varied from $75 \pm 4 \%$ to $87 \pm 8 \%$ of P_{WM} , against $5 \pm 1 \%$ to $13 \pm 1 \%$ for truly dissolved P. Therefore, the large-size colloidal fraction plays a substantial role in the mobilization of P from sediment to aqueous phase. The P_{WM} recovered from wet and dried sediments represented $2.4 \pm 0.3 \%$ of total sedimentary P.

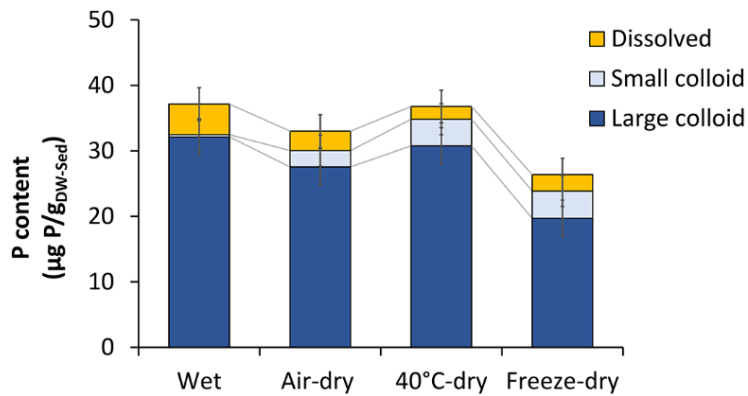


Figure 30. Distribution of water-mobilizable phosphorus extracted from wet and rewetted previously air-, oven-, and freeze-dried sediments using the high-speed centrifugation protocol combined with filtration (i.e. protocol “d”, Fig. 1). Large colloidal P sized from $0.2 - 1 \mu\text{m}$. Small colloidal P sized smaller than $0.2 \mu\text{m}$. Dissolved P represented dissolved inorganic phosphate in fraction smaller than $0.2 \mu\text{m}$. The error bar depicted 1 SD.

III.1.2.3.2.3. Effect on chemical composition of colloids

The total mass of recovered elements (P, OC, Al, Fe, Ca, Mg and Mn) in $0.2 - 1 \mu\text{m}$ fraction represent $37 \pm 2 \%$ of the mass of large water-mobilizable colloids released from wet, 20°C-dried and 40°C-dried sediments and 51% of the mass of colloids released from freeze-dried sediments. Taking into account the local geological context of Champsanglard reservoir (i.e. mainly granitic (Rapin et al., 2019), the missing mass is probably due to Si, Na, K and other elements (not evaluated in this study). When considering the measured elements, we can conclude that the major components of large colloids mobilized from wet sediment were: Al ($128 \pm 18 \text{ mg Al/g}_{\text{DW-Colloid}}$) and OC ($123 \pm 19 \text{ mg C/g}_{\text{DW-Colloid}}$), followed by Fe ($67 \pm 13 \text{ mg Fe/g}_{\text{DW-Colloid}}$) and Ca ($48 \pm 5 \text{ mg Ca/g}_{\text{DW-Colloid}}$), with a smaller share ascribed to Mg ($10.1 \pm 0.2 \text{ mg Mg/g}_{\text{DW-Colloid}}$), P ($4.4 \pm 0.3 \text{ mg P/g}_{\text{DW-Colloid}}$) and Mn ($1.8 \pm 0.5 \text{ mg Mn/g}_{\text{DW-Colloid}}$). Sediment drying affected differently the release of individual elements in colloidal form, so the chemical composition of recovered colloids depended on the sediment drying mode. For example, sediment drying at 20°C (compared to wet sediment) favored the release of colloidal OC and lowered the release of colloidal Ca, whereas drying at 40°C favored the release of colloidal P (1.5 times higher) and decreased the release of colloidal Ca. Freeze-drying drastically favored the release of colloidal P (3 times higher), Ca (2.6 times) and OC (1.5 times) while decreasing by a factor of 5 the release of colloidal Mn and by 10 the release of Mg (Fig. 29c). Freeze-

drying resulted in releasing the lowest quantity of colloids compared to wet and 20°C-dried or 40°C-dried sediments. However, it is noticeably that freeze-drying led to enriching large colloids by P and Ca.

III.1.2.4. Conclusion and Recommendations

Based on our experimental data, it can be concluded that diversification in applied separation and sample storage induce significant variation in quantity and physicochemical characteristics of recovered colloids. Apart from confirmation that loss of colloids by membrane fouling during filtration can be improved by introducing a pre-separation step via filtration at a greater pore size or with centrifugation. The successive centrifugations, a usual alternative protocol for filtration, also showed obstacle in size accuracy. The incomplete separation between colloids and particles under centrifugal forces in our cases highlights the participation of colloid aggregation/flocculation and of heterogeneity in particle density. The latter one refers to difference in density of organic and inorganic particles, hence, chemical composition of sediment strongly affected the colloid separation. Those sediments rich in organic matter like our case could result in overestimation of colloid quantity obtained with these successive centrifugations.

As opposed to the impact of varying separation protocols on colloid quantity, changing the sediment storage modes (drying at 20°C, at 40°C and by lyophilization) led to a critical modification in both quantity and characteristics of recovered colloids (size and chemical composition). The drying of sediment decreases colloids quantity and altered their size distribution by increasing small/intermediate-sized colloids and decreasing nano-colloids. Furthermore, organic colloids behave differently to mineral-rich colloids upon drying. Mineral or organo-mineral colloids could be prone to immobilization in sediment structure after drying than organic colloids due to cementation and increase of sediment/colloid hydrophobicity. Therefore, the common storage by drying at 20°C is not appropriate for sediment's colloid characterization.

From these considerations, effect of colloid separation and sample storage on colloid recovery are specific to sample characteristics and experimental approaches. Dissimilarities in colloid quantity and characteristics are at a factor up to 40 depending on sample storages and up to 26 according to colloid separation protocols. Hence, this may drastically alter the interpretation of how sedimentary colloids behave in situ. No standard methods currently exist for either sediment storage or colloid separation prior to the quantification of water-mobilizable colloids. Straight comparison of colloid composition in sediment or soils cannot be done unless special care should be paid to solid composition, solid storage and colloid separation protocol.

Based on our findings, we recommend working with fresh moist sediment and eluding the use of successive centrifugation protocol for colloid separation.

Apart from an insight to the heterogeneity between colloid extraction protocols, this study also shed a light on the strong potential of bottom sediment to release colloids and associated contaminants/nutrients to surface water which has been rarely investigated in dam reservoir context. To some extent, our data can enrich current knowledge on mobility of colloidal P in reservoir context. Dam reservoir sediment exhibited a relatively high potential of water-mobilizable colloids, with over 5.4 g/kg_{DW-Sed} and those colloids could deliver approximately more than 25 mg P/kg_{DW-Sed}.

Acknowledgments

The authors would like to thank France's Nouvelle-Aquitaine Regional Council, the EDF electric utility company and the "Dam and Water Quality" Chair of Excellence with the "University of Limoges Partnership Foundation" for financially supporting this research work.

Supplementary material

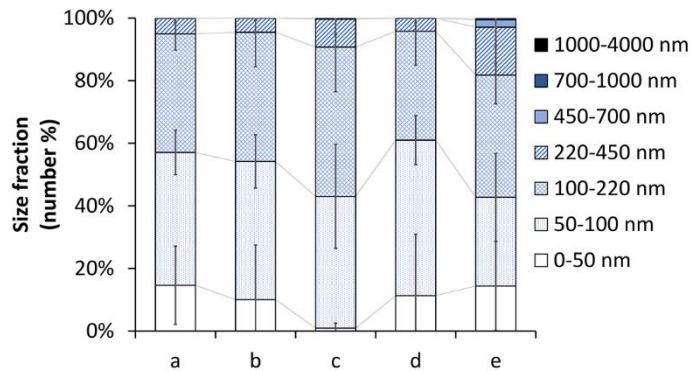


Figure 31. Effect of colloid separation protocols on size distribution of fraction smaller than $0.2 \mu\text{m}$: protocols "a" through "d" were separated by filtration, whereby protocol "e" was separated by centrifugation. *The error bar depicted 1 SD.*

III.1.3. Comparison of three methods of colloid extraction for characterization of mobilizable colloids from Champsanglard sediment.

Article to be submitted to Chemosphere journal.

Diep N. Nguyen, Malgorzata Grybos, Marion Rabiet, Véronique Deluchat

Limoges University, PEIRENE EA 7500, 123 Av. Albert Thomas, 87060 Limoges Cedex, France

Abstract

Water mobilizable colloids from bottom sediment of lakes and reservoirs contain nutrients and contaminants and thus may affect water quality once being released. A major obstacle to evaluate the quantity and quality of mobilizable colloids in natural system located in the using of appropriate method for colloid extraction from sediment and their separation from dissolved and particulate phases. This work evaluates the role of extraction methods (agitation, sonication at sediment pH (6.6 with studied sediment), and sonication at pH of 9) on the characteristics (mass, size distribution, shape and composition) of water-mobilizable colloids from the bottom sediment of Champsanglard dam reservoir (France). Special attention has been paid to phosphorus (P), an element playing an important role in eutrophication process. Compared to agitation, both sonication protocols impacted significantly on recovered colloids. The less aggressive agitation liberates low-energy water dispersible colloids without physical damage and probably with less modification in colloidal chemical composition and shape. Whereas sonication released 10-20 times higher colloid quantity and colloids were in lower size, probably due to physically disruption of fragile and organic-rich sediment structure or aggregated/agglomerated colloids. On the other side, the alkaline pH intensified colloid release by fortified repulsive forces between colloids and dissolution of organic coat. For all protocols, extracted colloids were composed of organo-mineral composition. Concerning phosphorus, the competition with OH⁻ for sorption site or dissolution of phosphate minerals in alkaline pH caused release of dissolved P to solution and decrease of P content in recovered colloids. In conclusion, agitation is recommended for the extraction of colloids from sediment matrix to limit any destruction in sediment aggregates and unwanted generation of new colloids under robust ultrasonic field.

Keywords: *Colloids composition, colloids size distribution, reservoir sediment, ultrasonic extraction, phosphorus, organic matter, pH*

II.1.3.1. Introduction

Due to small size (1 nm - 1 µm) and high specific surface area, colloids are able to carry and transport nutrients (N, P) through various surface and subsurface environment, thus, they affect the surface water quality (Miller and Karathanasis, 2014; Gavrilescu, 2014; Judy et al., 2018). Therefore, understanding the fate and behavior of mobilizable colloids from sediment to overlying water is an important issue. In surface water, the behavior of colloids is distinct from dissolved substances since they are susceptible to aggregation and to evolve in suspended particles and further sedimentation. Colloids are heterogenous in size and composition (organic, mineral, organo-mineral), and generally have a charged surface that allows association with dissolved elements, other colloids and/or organic and minerals particles. In general, the negatively charged colloids have higher electrostatic affinity with positively charged mineral surfaces (for example Fe-oxy(hydr)oxides) and/or adsorb dissolved cationic species. In contrast, positively charged

colloids possess higher electrostatic affinity with a negatively charged mineral surfaces (for example clay minerals) and may adsorb dissolved organic matter and other dissolved anionic species (including phosphates). Sedimentary colloids are multiphasic entities either originated from water column or formed as a result of biophysiochemical reactions occurring in sediment (Ryan and Gschwend, 1992; Zänker et al., 2006; Quik et al., 2012; VandeVoort et al., 2013; Xu et al., 2019). They could be present in individual or aggregated form (flocs) in interstitial porewater or be attached to pore surface (Buffle and Leppard, 1995).

The release of colloids from sediment to overlying water could be induced by hydrodynamic disturbance, bioturbation, changes in pH, ionic strength or under reducing condition (Buffle et al., 1989; Hens and Merckx, 2002; Liang et al., 2010; Sun et al., 2007; VandeVoort et al., 2013; Valipour et al., 2017; Gautreau et al., 2020). Thus, the definition of an appropriate method to extract colloid is prerequisite for ensuring no impact on the physico-chemical nature of water-mobilizable colloids from sediment, because sediment matrix is complex, heterogeneous and sensitive to external forces. According to the literature (Tables 7-10), several techniques are currently employed to recover colloids from natural matrices (soils, sediment). While the recovery of colloids in sediment pore water could be accomplished by simply mixing sediment with water, the extraction of colloids attached to sediment pore surface or in loosely aggregated forms can require more specific treatments. From numerous instances, we can list here three main treatments: (i) dispersion of raw material in extracting dispersant (water, NaCl, KCl, NaHCO₃) (Buettner et al., 2014; Mills et al., 2017; Gu et al., 2018; Xu et al., 2019), (ii) extraction of colloids from raw material to dispersant by providing sufficient energy to disintegrate bonds between colloids and attached surface (e.g. agitation, sonication) (Gu et al., 2018; Mills et al., 2017; Xu et al., 2019), and (iii) extraction of colloids from sediment exposed to a solution at high pH that can increase negative charges of both colloids and sediment matrix, thus, favor colloids detachment (Klitzke et al., 2008). Since colloids are comprised of complex and diverse materials (biological debris, organic matter, clays, oxo(hydr)oxydes, carbonates, silicates, etc.), and the colloids mobilization can be triggered both physically and chemically, it is likely that the mass, size and chemical composition of extracted colloids would vary according to employed protocol. Therefore, the proper choice for extraction of colloids from raw material could be an important step during colloid isolation from natural matrices.

From literature survey, the most common techniques applied to withdraw colloids are agitation and sonication (Tables 6-9). Both techniques aim to establish mechanical vibration to overcome the attractive energy due to van der Waal forces and initiate the disruption of linkage bonds between colloids and attached surface, promoting liberation of colloids. The energy generated by ultrasound has been considered as more powerful than the one produced by agitation and is sufficient to breakdown not only larger (< 250 µm) unstable aggregates but also the smaller (< 2 µm) and more stable aggregates composed of clay-metal-organic particles (Mentler et al., 2004). Sonication is efficient technique to liberate natively-born colloids, but at the same time, risks to generate new colloids through disruption of aggregates, therefore requires to be evaluated in comparison with the less robust agitation protocol in terms of the quantity and properties of recovered colloids.

Furthermore, the stability of colloids is strongly impacted by changes in solution chemistry such as pH and ionic strength, since the adsorption of similar charged ions from surrounding solution can enhance repulsive forces that inhibit colloid aggregation and attachment (Hamad-Schifferli, 2014; Liang et al., 2010). Organically enriched colloids under elevated pH conditions usually exhibit a negatively charged surface

that enhance electrostatic repulsion and colloidal stability (Calero et al., 2017; Kretzschmar et al., 1997). Therefore, a change in solution pH can induce a change in quantity of extractable colloids.

The objective of this study was to elucidate the impacts of different extraction protocols on the quantity and quality of recovered colloids from reservoir sediment. Three modes of colloid extraction including (i) agitation, (ii) sonication and (iii) sonication at pH 9, were examined on wet sediment collected from Champsanglard dam reservoir.

III.1.3.2. Materials et methods

III.1.3.2.1. Sediment sampling and characteristics

The sampling was carried out in Champsanglard dam reservoir (surface area of 0.55 km², storage volume of 3.56 hm³) which exhibits thermal and oxygen stratification along with repeatedly bloom of microalgae during the summer period (Rapin et al., 2020).

Surface sediment (up to 10 cm) was collected during mid-May 2018 from the middle channel (9-m depth) of Champsanglard reservoir using an Ekman grab (Creuse River, France). Sediment was manually homogenized, preserved in polyethylene bottles previously rinsed with surface water and transported under cool and dark condition. In laboratory, sediment was sieved through a 2-mm mesh and stored at 4°C until experimentation. Champsanglard sediment was rich in P (1.4 ± 0.2 mg P/g_{DW-Sediment}) that was mainly associated to ascorbate fraction (Rapin, 2018) and contained high amount of organic matter ($19 \pm 1\%$). Total concentrations of Al, Fe, Ca, Mn and Mg were 79 ± 1 , 136 ± 4 , 8.5 ± 0.5 , 1.5 ± 0.1 and 17.2 ± 0.1 mg/g_{DW-Sediment}, respectively. The median grain size (D₅₀) of the sediment was 19 ± 1 µm and the pH_{H2O} was 6.4 ± 0.2 (Nguyen et al., 2020). Inorganic particulate fraction was dominated by quartz, felspar, clay minerals (kaolinite, chlorite) and mica (Rapin et al., 2019).

III.1.3.2.2. Colloid extraction

Sediment suspensions were prepared by dispersion of 15 g of wet sediment in 150 mL of ultrapure water, corresponding to a wet solid-liquid ratio of 1/10 (w/v). Suspensions were subjected to three different modes of colloid extraction: agitation, sonication at sediment pH (pH_{sed}), and sonication at pH of 9 (pH₉). Agitation in 250-mL cylindrical flask was performed at 200 rpm for 24 h using an IKA-WERKE KS 501 digital orbital shaker. Sonication was performed using Bandelin Sonopuls GM70 ultrasonic probe at 100 % power (60 W) for 10 minutes, which provides equivalently an energy of 240 J/mL. This duration of sonication was selected to avoid the heating of sediment solution during prolonged period. Preliminary test had shown an increase of approximately 10°C when increase sonication time from 10 to 60 min. For sonication at high pH, 300 µL of 1 M NaOH was added to solution sediment solution, in order to reach pH of 9 in prior to sonication.

After sediment dispersion, obtained suspensions were let settle for 2 h and supernatants were afterward gently pipetted out for further colloid separation. A high-speed centrifugation combined with filtration was chosen according to higher recovery of P-rich colloids (See section III.1.2, Nguyen et al., 2020). Supernatants were firstly centrifuged at 272 g for 6 min to remove particles larger than 1 µm. The centrifugates were passed through 1 µm glass fiber membrane (WVR) to ensure an accurate size separation of colloids by removal of particles remaining in centrifugate due to heterogeneous sediment particle density.

A portion of filtrates at 1 μm was filtered through 0.2 μm cellulose nitrate membrane (Sartorius). The fraction below 1 μm was considered as the water-mobilizable fraction, meanwhile the fraction below 0.2 μm was composed of dissolved species and small colloids sized between 1 nm and 0.2 μm . The large colloids sized from 0.2 to 1 μm were then estimated by the difference between these two fractions.

III.1.3.2.3. Colloid characterization

The particle size distribution of water-mobilizable fraction was performed using dynamic light scattering at 173° backscatter (see section II.3.1.1.3.2). Quantity of extracted large colloids was determined by gravimetric method. Large colloids retained on 0.2 μm cellulose nitrate membrane were dried at 30°C until unchanged mass. TOC concentration was quantified using TOC analyzer (Analytik Jena, multi N/C 2100S) with an LQ of 1 mg C/L. Concentrations of Fe, Al, Mn, Ca and Mg were measured using MP-AES (Agilent, MP 4100) with LQ of 30 μg Fe /L, 20 μg Al/L, 7 μg Mn/L, 12 μg Ca/L and 1 μg Mg/L, respectively. Concentration of DIP was measured by spectrophotometry according to the method of Murphy and Riley (1962) using 1-cm cuvettes and a UV-visible spectrophotometer at 880 nm (Agilent 8453 UV-visible spectrometer). LQ for this method is 0.02 mg P/L.

Prior to analysis of Fe, Al, Ca, Mn and Mg, filtrates at 1 μm were acid digested with nitric and hydrochloric acids, as described in Method 3015a (US EPA, 2007) using a microwave digestion system (Anton Paar, Multiwave GO). Particularly for TP measurement, both filtrates at 1 μm and 0.2 μm were digested with ammonium persulfate and sulfuric acid according to Method 365.1 (US EPA, 1993) (see section II.3.1.2.1.2).

Therefore, P was quantified into four fractions: water-mobilizable P (P_{WM}), large colloidal P including P-colloids from 0.2 to 1 μm , small colloidal P covering P-colloids less than 0.2 μm and truly dissolved P (Table 13).

Table 13. Determination of colloidal and dissolved P through size fractionation of PWM

Fraction of P	Corresponding size fraction	Determination
Water-mobilizable P (P_{WM})	< 1 μm	Total P in filtrate at 1 μm
Large colloidal P	0.2 – 1 μm	Difference in TP between filtrates at 1 μm and 0.2 μm
Small colloidal P	< 0.2 μm	Difference between TP in filtrate at 0.2 μm and DIP in filtrate at 0.2 μm
Dissolved P	< 0.2 μm	DIP in filtrate at 0.2 μm

III.1.3.2.4. Scanning electronic microscope investigation

Microscopic observations were conducted onto 0.2-1 μm fraction. This fraction was prepared by filtering 5 – 10 mL of filtrates < 1 μm on a 0.2- μm cellulose nitrate filter (Whatman) and let dry in desiccator at room temperature (20 \pm 1°C). All filters were coated with thin Au-Pd layer of 15-nm to create conductive surface for morphology image or with 12-nm layer of C for chemical analysis. Colloids were analyzed with

scanning electron microscope coupled with energy dispersive X-ray spectroscopy (SEM-EDS, LEO 1530VP,) at EHT = 5 kV for image processing and EHT = 15 kV for EDS analysis.

III.1.3.3. Result and discussion

III.1.3.3.1. Variability in mass and size distribution of recovered colloids

Figure 32 presents the dry mass of colloidal fraction sized 0.2 – 1 μm according to colloid extraction protocol.

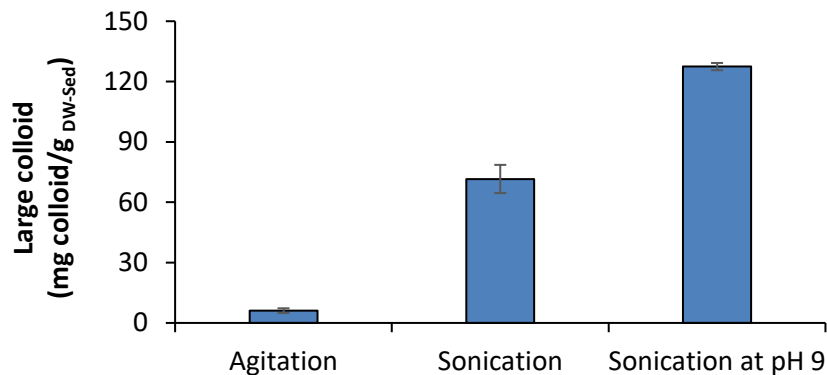


Figure 32. Variation in dry mass of colloidal fraction sized 0.2 – 1 μm recovered from three modes of extraction

Among three extraction protocols, the lower mass of large colloids (0.2-1 μm) was obtained by agitation ($6.1 \pm 1.2 \text{ mg/g}_{\text{DW-Sed}}$) and the highest by sonication at pH_9 ($128 \pm 2 \text{ mg/g}_{\text{DW-Sed}}$). In the case of sonication at pH_{sed} , the mass of large colloids was $72 \pm 8 \text{ mg/g}_{\text{DW-Sed}}$ (Fig. 32). As shown in Fig. 33A, the three modes of colloid extraction also impacted the size distribution of recovered colloids (< 1 μm). The $96 \pm 1 \%$ of water-mobilizable colloids was smaller than 450 nm regardless of extraction protocols. However, the relative proportion of nano colloids (< 50 nm) was similar between agitation and sonication at pH_{sed} , considering standard deviation, but this fraction was absent after sonication at pH_9 . Colloids extracted by agitation showed highest proportions for two size fractions 220-450 nm ($33 \pm 16 \%$) and 450-700 nm ($4 \pm 2 \%$). Sonication at pH_9 looked to induce an increase in the size fraction 100-220nm.

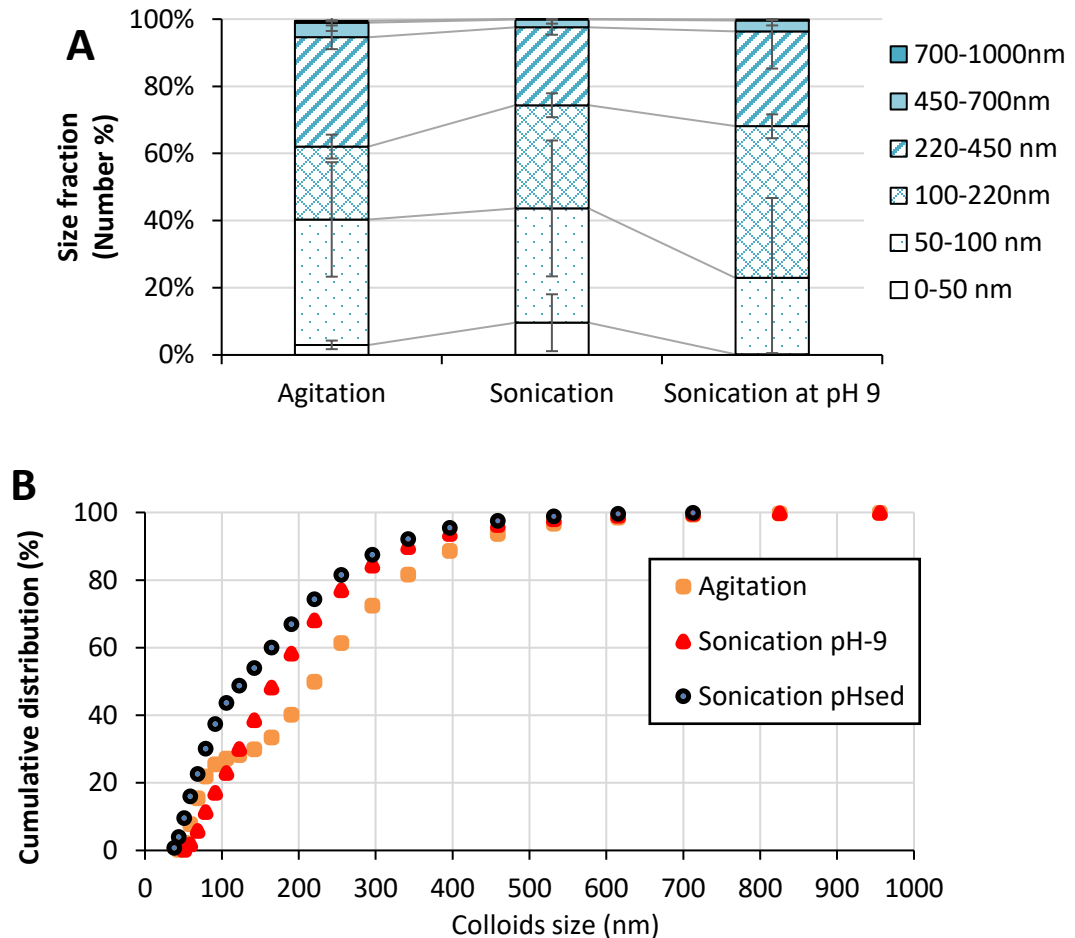


Figure 33. Effect of extraction protocols on the size distribution of water-mobilizable colloids: (A) size fractionation and (B) cumulative distribution.

Extraction of colloids from a natural material by agitation and/or sonication is often used for soils. It has been shown that both techniques provide sufficient mechanical energy to overcome attractive forces between colloids and soil grains to release loosely attached colloids, and that vigorous stirring or high-power ultrasound can disrupt soil aggregates and subsequently release colloid-size fragments without using chemical agents (So et al, 1997; Raine and So, 1997; Kaiser and Berhe, 2014; Schomakers et al., 2015; Luo et al, 2017; Ma et al., 2017). It has been also shown that agitation is generally less efficient than sonication in disrupting micro-aggregates smaller than 2 μm (Raine and So, 1997). However, sonication due to ballistic impact and higher shear stress, can physically damage soil particles and, depending on the energy used, affect the degree of particle/aggregates fragmentation thus generating new colloids (Mentler et al., 2004). In the case of permanently submerged sediments, the breakdown of the cohesive bonds between the colloids and the sediment grains as well as the disruption of the sediment aggregates upon agitation and/or sonication could contribute to the release of a low-energy-required fraction of water-mobilizable colloids and the colloids freely present in the interstitial water of sediments. As shown in Fig. 33B, presenting the cumulative size distribution of recovered colloids upon the three tested methods, the sonication at pH_{Sed} provided the highest percentages of small colloids (< 300 nm) than agitation and sonication at pH_9 .

protocols. Particularly, the proportion of colloids below 300 nm in case of agitation was about 20 % lower than upon two modes of sonication and the fraction 100-150 nm were nearly absent (Fig. 33B). These results show that the size of colloids extracted by agitation is larger than those extracted by the two modes of sonication and that concerns mainly the colloids between 100-500 nm. Therefore, it can be concluded that higher release of sedimentary colloids upon sonication is related to the additional release of small sized colloids. It could be related to more disruptive action on the structure of large colloids and/or induced by the fragmentation of sediment particles/aggregates into smaller pieces. Agitation mobilizes low-energy water dispersible colloids (for example dispersion of pre-existing colloids in sediment porewater and/or detachment of labile colloids on pore surfaces), whereby, sonication produces additional portion of colloids via disintegration of flocs and/or by breakdown of sediment particles/aggregates. As shown on SEM images (Fig. 34), the extracted colloids from Champsanglard sediment consisted of aggregated/agglomerated small and nano-colloids. The colloids extracted by sonication at pH_9 exhibited more globular shape and larger size comparing to those extracted by sonication at pH_{sed} . The colloids extracted by agitation exhibited much less globular shape and appear to be chained. This observation suggests that different modes of colloids extraction imply not only variation in the quantity of recovered colloids and their size but also play important role in modification of colloid' shape.

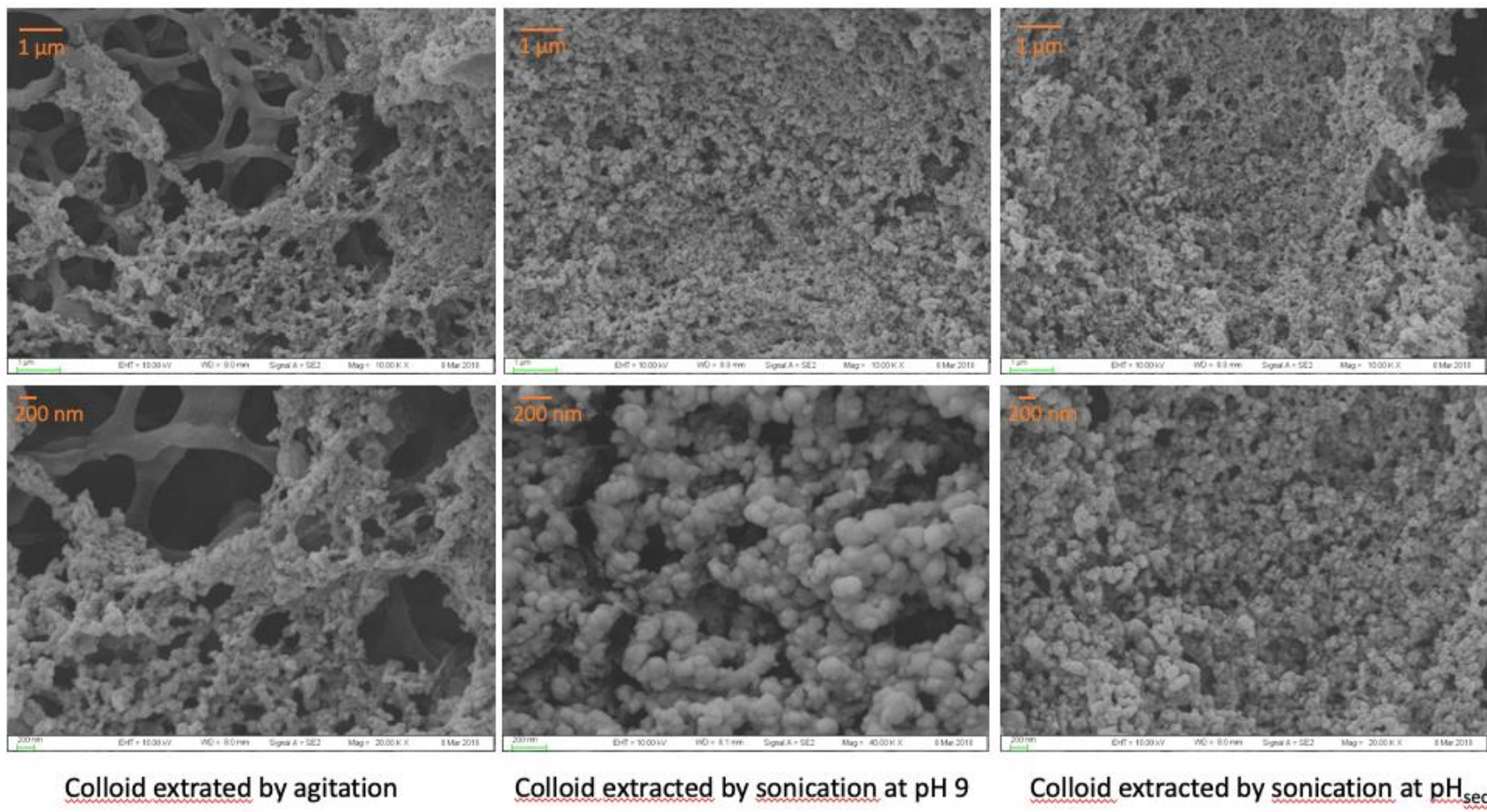


Figure 34. Scanning electronic microscopic images of extracted colloids from Champsanglard sediments.

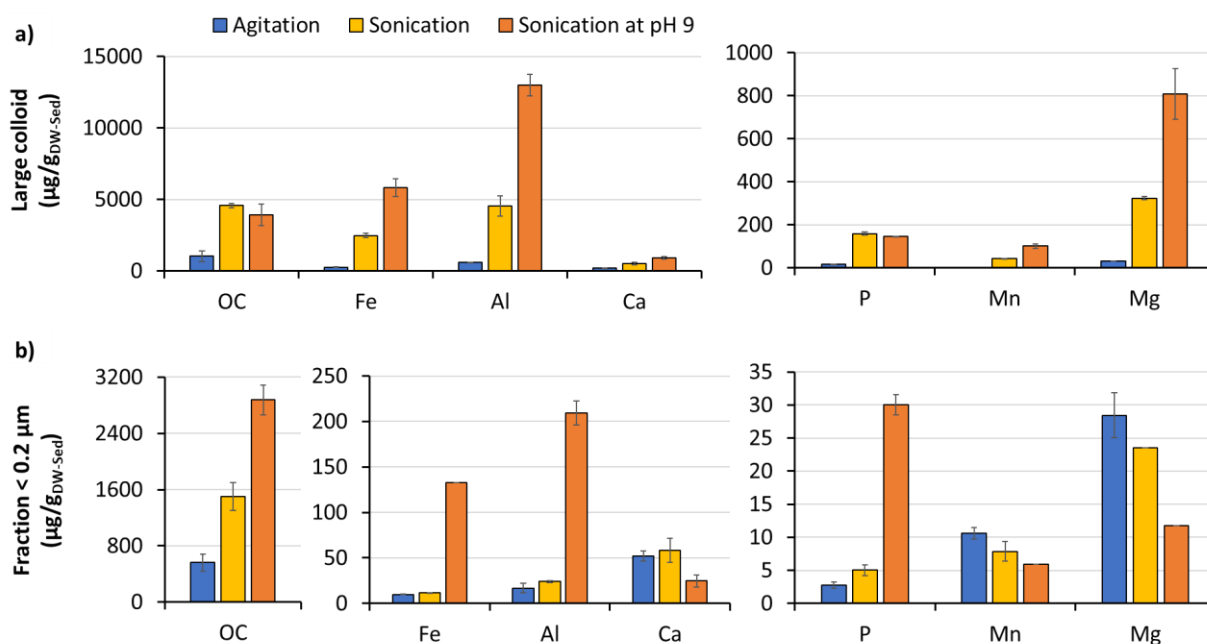


Figure 35. Impacts of extraction protocols on elemental masses of P, OC, Fe, Al, Ca, Mn and Mg in (a) large colloids sized 0.2 – 1 µm and (b) fraction smaller than 0.2 µm.

Champsanglard sediment is silty and contain important amount of OM ($19 \pm 1\%$). It was shown that sand and silt-sized mineral particles can be disrupted under ultrasound energy exciding 700 J/mL (Kaiser et al., 2012), whereas the disintegration of organic particles, which are less dense and cohesive, could be observed under the application of much lower ultrasound energy (60 or 90 J/mL) (Balesdent, 1991, Amelung and Zech, 1999; Kaiser and Berhe, 2014). Particles within clay-size fraction of soils ($< 2\ \mu\text{m}$) are shown not to be disintegrated by sonication despite that the application of ultrasound energy superior to 12,000 J/mL reveals breakage of pure minerals such as kaolinite (Kaiser and Berhe, 2014). According to these literature data, considering the far lower energy used in this study (240 J/ml, 10 min), a 12-fold increase in mass of recovered colloids upon sediment sonication at pH_{sed} compared to agitation cannot be explained by the disintegration of the crystalline mineral particles, but rather by the breakdown of organic particle or breakdown of sediment aggregates.

Considering Champsanglard sediment, the breakdown of organic particles under sonication could occur due to an important stock of OM available for mechanical disruption. As shown in Figure 35a, the amount of OC in 0.2 – 1 µm fraction was 4.4-fold higher by sonication at pH_{sed} than by agitation. However, along with increase in mass of colloids extracted by sonication at pH_{sed} the 26-fold increase in Mn, 10-fold increase in Mg, 9.4-fold increase in Fe, 9.2-fold increase in P, 7.2-fold increase in Al, and 2.5-fold increase in Ca were observed in fraction 0.2-1 µm (Fig. 35a). These releases of both organic and inorganic species in large colloidal fraction suggests that sonication of sediment was able to disrupt both organic particles, organic coating minerals or organo-mineral aggregates, and lower increase of OC in this fraction suggest that organic matter played binding role in the formation of organo-mineral aggregates or flocs. In addition, surface sediments from lake and reservoir are unconsolidated and not as highly aggregated as soils due to the presence of water that prevents desiccation and aeration. Surface sediments are also less compacted than deeper sediments. Hence, surface sediments exhibit finer and fragile structure compared to soils and a 30 % contributes of total sedimentary material is amorphous material (Chirinos et al., 2005; Sheppard et al., 2020). Thus, another hypothesis could be the breakdown

of amorphous mineral phases under ultrasonic treatment. However, this hypothesis is not solid due to shortage in available literature data concerning the impact of ultrasonic force on amorphous structures.

Particularly, for fraction below 0.2 μm (Fig. 35b), compared to sonication at the pH_{sed} , the sonication at pH_9 resulted in 2-time higher OC in concomitant with 12-time higher Fe, 9-time higher Al, implying that an increase in pH strongly influence organic coat of Fe/Al mineral than sole sonication and lead to higher release of Fe/Al colloids in fraction below 0.2 μm . On one hand, at pH of 9, the mineral particles are deprotonated, the concentration of negative charge on colloids also increased and enhanced repulsive force between colloids or between colloids and sediment solids, thus promoted colloids mobilization. On another hand, the effect of increasing pH in enhancing colloid release has been already well demonstrated for increasing OM degradation, dissolution of organic coating or organic binding agent (Krachler et al., 2009; Liang et al., 2010). Higher release of Fe and Al together with OC by sonication at pH_9 suggests their association with negatively charged organic compounds. It is well known that Al release is highly promoted at high pH (considering extraction protocols for instance, Paludan and Jensen, (1995)), and that multivalent cations induce aggregation process of organic molecules involving the aggregates of several small organic matter moieties (Iskrenova-Tchoukova et al., 2010; Kalinichev and Kirkpatrick, 2007; Piccolo, 2002). In general, effect of cation bridging is higher for trivalent ions than for divalent ions (Ghosh and Schnitzer, 1980). As shown in Fig 35b, the bivalent elements (Ca, Mg and Mn) are not shown higher release in the fraction below 0.2 μm .

III.1.3.3.2. Variability in water-mobilizable phosphorus

Figure 36 illustrates the variation in quantities of water mobilizable P (P_{WM}) and its three size-based subfractions (large colloids, small colloids and dissolved).

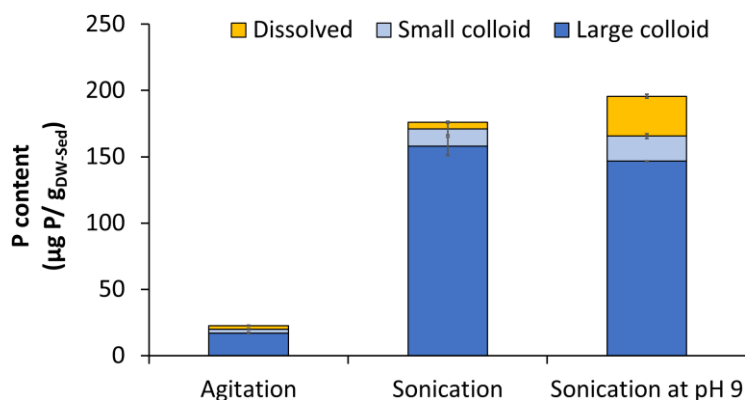


Figure 36. Distribution of water-mobilizable phosphorus extracted from wet sediment using three colloid extraction protocols.

Due to the impact of sonication on the physical properties and the redistribution of OC across water-mobilizable subfractions presented in previous section, agitation protocol was considered herein as reference. Quantities of P_{WM} released by sonication at pH_{sed} and sonication at pH 9 were respectively 176 ± 4 and 196 ± 1 $\mu\text{g P/g}_{\text{DW-sed}}$, equivalent to 8 times higher than that recovered from agitated sediment, 22.5 ± 0.3 $\mu\text{g P/g}_{\text{DW-sed}}$. For all three modes of colloid extraction, a major portion of P_{WM} (more than 85 %) was released under colloidal forms. For agitation, P_{WM} was composed of 12.6 % dissolved P, 0.6 % small colloidal P and 86.8 % large colloidal P. This P distribution was modified when applying sonication protocols. Sediment sonicated at pH_{sed} and sonicated at pH_9 , released higher portion of small

colloidal P, 7.4 % and 9.7 % of P_{WM} , respectively. In comparison with agitation protocol, the portion of dissolved P decreased to 2.9 % upon sonication at pH_{sed} but increased up to 15.4 % upon sonication at pH_9 . In contrast, the release of large colloidal P from sonicated sediment at pH_{sed} and at pH_9 was comparable and was 9.2 and 8.6-fold, respectively, higher than for agitated sediment.

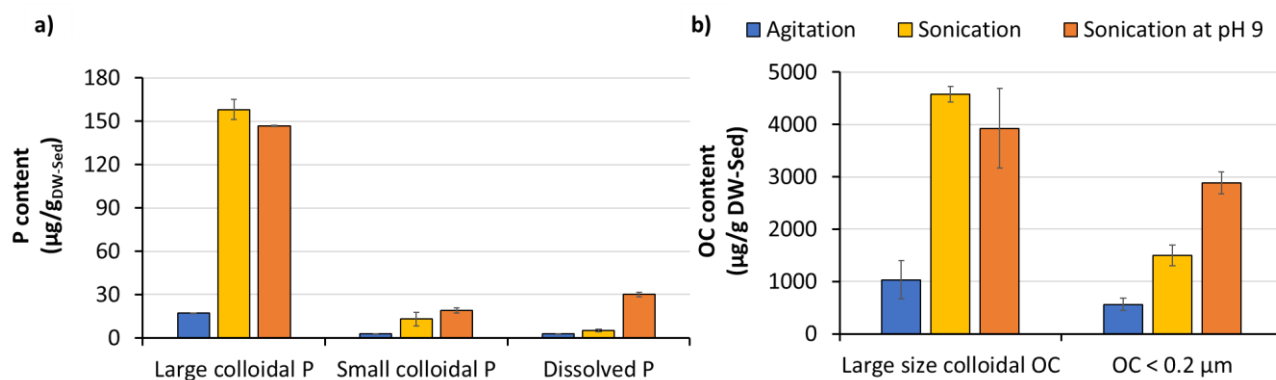


Figure 37. Distributions of (a) phosphorus (P) and (b) organic carbon (OC) in three size classes of water-mobilizable fraction smaller than 1 μm .

In general, sonication protocols resulted in significantly higher amounts of both small and large colloidal P (averages of 16 and 152 $\mu\text{g P/g}_{DW-sed}$, respectively) compared to agitation protocol (2.9 ± 0.5 and 17.2 ± 0.5 $\mu\text{g P/g}_{DW-sed}$) (Fig. 37a). According to comparable quantity of both large and small colloidal P obtained by two sonication protocols (Fig. 37a) indicates that the increase of the pH did not influence the release of colloidal P but did highly increase the release of dissolved P (Fig. 37a). In surface sediment, dissolved P is mainly present as orthophosphates and various organic forms (Wan et al., 2020). As shown in Fig. 37b the increase of dissolved P was correlated to the increase in OC content in fraction lower than 0.2 μm . However, the increased pH upon sonication did not increase the release of P in large and small colloidal fractions (Fig. 37b). This suggests the sonication at pH_{sed} resulted in the disruption of larger organic aggregates/flocs into large and small colloidal P, whereas the increase in solution pH caused additional release of dissolved P due to competition with OH^- for sorption sites and release of dissolved organic P.

III.1.3.3.3. Chemical composition of extracted colloids

As shown in Fig. 38, according to the mass of released elements by mass of colloids, regardless of extraction modes, the nature of recovered colloids from sediments was organo-mineral, with similar range amount for Fe, Al and Mg whereas colloids released by agitation contained significantly higher organic carbon content. The total mass of analyzed elements (P, OC, Fe, Al, Ca, Mn and Mg) in large colloidal fraction (0.2 – 1 μm) represented only 32 % of dry mass of recovered large colloids for “agitation” and about 18 % for the two sonication protocols. It indicates that recovered colloids contained also other elements and that sonication involved their higher release. In Table 14, the qualitative evaluation of chemical composition of colloids by SEM-EDS analysis demonstrated that, besides the elements previously presented (P, C, Al, Fe, Ca, Mn and Mg), the recovered colloids contained also Si, Na, K and S and, some of them, N.

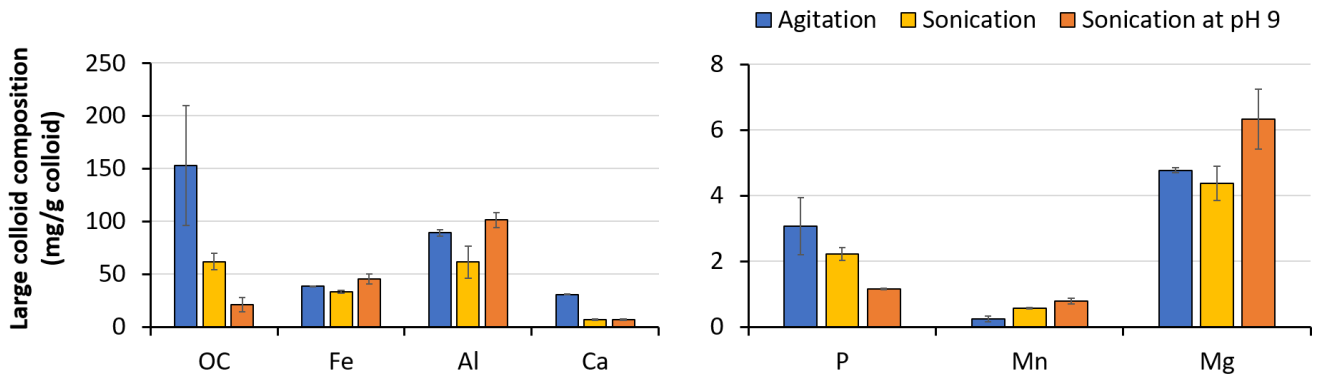


Figure 38. Impacts of extraction protocols on elemental composition of recovered large colloids sized 0.2 – 1 μm , expressed by dry mass of colloids.

In comparison with agitation, the application of two sonication protocols showed major impacts on P and OC concentrations of large colloids (t-test, $p < 0.05$). The relative proportion of OC to mass of colloids decreased by 60 % for sonication at pH_{sed} and 86% and sonication at pH_9 in (Fig. 43). Via chemical composition of recovered colloids determined by chemical analysis (Fig. 35a) and SEM-EDS (Table 14), it can be suggested that both sonication and increasing pH caused by drastic release of colloidal Al, Si or Mg (in case of pH_{sed}) that could be associated to mobilization of aluminosilicate colloids during sonication. The presence of kaolinite, K-feldspar, plagioclases and chlorite in Champsanglard sediments had been illustrated by X-ray diffraction (Rapin et al., 2019). Therefore, a significant quantity of these minerals introduced to colloidal fraction by both sonication protocols attributed to lower contribution of OC in colloidal mass.

%	C	N	Na	Mg	Al	Si	P	S	K	Ca	Fe
Agitation	100	5	82	5	18	18	18	68	18	23	0
Sonication pH_{sed}	100	0	83	17	92	100	17	92	17	0	0
Sonication pH_9	100	2	100	17	98	100	17	100	17	45	64

Table 14. The percentage of analysis detecting the presence of a given element in recovered sedimentary colloids. Chemical composition of colloids was determined by SEM-EDS analysis based on the number of total independent analysis of 22 for colloids recovered by agitation, 12 by sonication at pH_{sed} and 47 by sonication at pH_9 .

For P concentration, in comparison with agitation, a 4-fold decline in P content of colloids (Fig. 38) was observed in case of sonication at pH_9 , meanwhile, considering standard deviation, no difference observed between agitation and sonication at pH_{sed} . After sonication, the solution pH decreased from 9 to 8.0 ± 0.1 (Table 15), this pH decrease could be explained by hydroxide sorption onto colloids, and further, the lower P content in colloids extracted by this method was likely to be caused by competition with OH^- for sorption site on mineral surface and possible P desorption from colloids. Another mechanism can also explain this result, the dissolution of phosphate minerals (Al-P especially) is expected in alkaline solution. As a consequence, the sonication at pH_9 caused important increases in the levels of Fe (12-fold), Al (9-fold) and P (6-fold) in fraction below 0.2 μm compared to sonication at pH_{sed} (Fig. 35b).

Table 15. The variation in solution chemistry before and after extraction by three different modes: agitation, sonication at pH_{sed} and sonication at pH9.

Extraction mode	Before extraction						After extraction					
	pH		Temperature (°C)		Conductivity (µs/cm)		pH		Temperature (°C)		Conductivity (µs/cm)	
	Mean	SD	Mean	SD	Mean	SD	Mean	SD	Mean	SD	Mean	SD
Agitation	6.8	0.1	20.0	0.1	20.7	0.3	6.7	0.1	23.0	0.1	28.3	1.8
Sonication at pH _{sed}	6.8	0.1	20.0	0.1	18.4	0.2	6.6	0.1	38.0	0.1	36.0	4.9
Sonication at pH 9	9.1	0.1	20.0	0.1	29.8	1.0	8.0	0.1	37.8	0.3	72.6	0.9

III.1.3.4. Conclusion

Compared to agitation, both sonication protocols provided drastic increase in the quantity of colloids to be extracted from sediment with a factor of 10 to 20 times, accordingly. Agitation provides less aggressive mechanical stresses on sediment structure than sonication and liberate colloids that pre-exist in sediment porewater and/or detachment of labile colloids on pore surfaces without physical damage and probably with less modification in colloidal chemical composition and shape. On the other hand, sonication provides amplified vibration that could physically disrupt low fractal sediment structure or aggregated/agglomerated colloids into smaller colloidal size classes which is responsible to the critical release of colloids by this method. Organic compartment of sediment seems to be the major target of disruption by sonication due to its low density and fragile structure than mineral particles. The increase in pH might intensify the release of colloids due to enhancing repulsive forces between colloids, dissolution of organic binding agents. Regardless of extraction modes, recovered colloids showed an organo-mineral composition. Sonication released superior quantity of recovered colloids compared to agitation and therefore higher quantity of colloidal P. However, in alkaline pH (at 9), the competition with OH⁻ for sorption site or dissolution of phosphate minerals caused release of dissolved P to solution and decrease P content in recovered colloids.

Overall, according to physically disruption of sediment structure and diminution in P content of colloids caused by sonication and increasing pH, the application of low-power agitation looks to be the most appropriate to extract colloids from sediment matrix.

Acknowledgement:

This work was financially supported by the France's Nouvelle-Aquitaine Regional Council; the EDF Electric utility company; and the "Dam and Water Quality" Chair of Excellence, University of Limoges Partnership Foundation.

III.1.4. Conclusion

All sediment drying modes tested (air-dry, oven-dry, freeze-dry) show an important impacts on lowering the quantity of colloid recovery and modification their size class and chemical composition comparing to the colloids extracted from wet sediment.

→ The work with sedimentary colloids is advised to be carried out on wet sediment to preserve the natural physico-chemical properties of the colloids.

Concerning the extraction protocols, extraction by sonication will derive from 10 to 20-times higher recovery of colloids depending on applied pH, although these colloids may contain both the labile/freely-dispersed in the porewater and colloids that are presents in flocs and/or agglomerates.

→ Agitation is recommended to avoid changing in size and shape of colloids as well as modification in colloidal composition.

The colloid separation by centrifugation did not allow the correct size separation of recovered colloids due to the heterogeneity in particle density of natural colloids. The use of centrifugation to separate colloids needs to be accompanied with a filtration step to ensure size integrity. Successive centrifugations is not recommended for colloid separation from heterogenous matrices.

→ The most suitable colloids separation methods is filtration with pre-separation step filtration or centrifugation at higher cutoff size.

→ The separation of colloids by filtration should be done in an appropriate manners: filtrate a small volume (about 10 -15 mL) of sample per filter to avoid membrane fouling.

III.2. Impacts of reservoir management on the size partitioning and mobilization of phosphorus from sediment

III.2.1. Introduction

River plays an important role in the Earth's system and the transport of materials from continental surfaces to the oceans. Most of rivers around the world are regulated by dam, there is 70,000 large dams worldwide (Maavara et al., 2015). The impacts of river damming are well-known for changing flow continuity and disrupting sediment transport. The sedimentation pattern of suspended material exhibits longitudinal variability upon the change in flow regime with the accumulation of fine fraction towards low-energy lacustrine zone of reservoirs and in front of the dams (Kondolf et al., 2014, López et al., 2016).

Sediment is one of the sinks for biogenic compounds/substances, including phosphorus. However, only a part of sequestered P remained permanently buried in the sediment, meanwhile a part can be released as an internal P load support primary production in the water column and thus cause eutrophication.

Most of studies on the internal P load in reservoirs focus on particulate or dissolved P and neglect colloidal P fraction. Colloidal P has been proved to be abundant in soil water, leachate and runoff and to contribute to the external non-point source P loads (Heathwaite et al., 2005, Liang et al., 2016, Missong et al., 2018). However, the spatial distribution, mobility and fate of colloidal P in reservoirs has not yet been demonstrated.

Therefore, this study was dedicated to providing a preliminary view concerning the distribution of sedimentary water-mobilizable colloidal P in a dam reservoir. The questions we attempted to answer in this chapter are as below:

- How the sediment potential to release colloids and P in the reservoir change spatially?
- What are the relationships between the physical and chemical characteristics of sediments and the distribution and chemical composition of water mobilizable colloid?
- What are the factors influencing the mobility of water-mobilizable colloids and P in the reservoir?

To answer these questions, surface sediments were collected along the Champsanglard dam reservoir, at the bottom of lacustrine and riverine zones of reservoirs as well as in the banks. As a first step, the main physical and chemical characteristics of sediments were analyzed. Then, for each collected sediment, colloids were extracted to determine the quantity and physico-chemical properties (mass, size, chemical composition). The results were presented in the form of an article to be submitted to the journal Science of The Total Environment.

III.2.2. Spatial distribution of water-mobilizable colloids from dam sediment and the risk of water-level fluctuation on phosphorus release

Article to be submitted to Science of The Total Environment.

Nguyen Ngoc Diep, Grybos Malgorzata, Rabiet Marion, Deluchat Véronique

Limoges University, PEIRENE EA 7500, 123 Av. Albert Thomas, 87060 Limoges Cedex, France

Abstract

The hydrodynamics of dam reservoirs favor the accumulation of phosphorus (P) in sediments as it has a strong affinity for the sedimenting particles. The release of sedimentary P may occur in dissolved, colloidal or particulate forms. Despite the well-known internal flux of dissolved P from the sediment, little is known about the release of colloidal P. The aim of this study was (i) to evaluate the potential of sediments, accumulated in the bottom of Champsanglard reservoir and in the area of water level fluctuation, to release colloids and (ii) to investigate of the impact of sediments quality on the release of colloids and their characteristics. A sampling campaign was carried out for 9 locations along the main channel of reservoir from riverine to lacustrine area (bottom sediments) and 4 locations across riverine transects where the sediments were impacted by significant water-level fluctuation. The results showed that colloids are intrinsic component of reservoir sediment and contribute up to 2.3 % of sediment mass. Colloidal P attributed up to 6 % of total sedimentary P and 80 % of water-mobilizable P (fraction < 1 μm). The stock of water-mobilizable colloids and associated P varied according to sediment size distribution and was strongly dependent to channel morphology, hydrodynamics and inlet of tributary. Particularly, the water-level fluctuation in riverine regions strongly impacted on potential of bank sediments to release water-mobilizable colloids and P. Bank sediment contained high amount of the more bioavailable P (dissolved P and small/nano P-colloids) than bottom sediment. Therefore, special attention should be paid to this area of reservoir as one of the nutrient sources to be manage in the context of eutrophic water system.

Keywords: Dam reservoir, sedimentary colloids, phosphorus form, spatial variability, water-level fluctuation zone, drying, organic matter, iron

III.2.2.1. Introduction

The management of water resources and demand of renewable energy production have led to the increasing construction of dams along rivers. One of the consequences of river damming is trapping of sediments in reservoirs due to the reduction in flow velocity and therefore in transport capacity. Sediment enters reservoirs because of soil erosion of upstream watershed, erosion of riverbed and banks, and transport through the river system. The amount of sediment trapped in the reservoirs depends on the quantity and type of entering transported material, as well as the characteristics of the reservoir and the way how the dam is managed. In general, the distribution of sediments is associated to the variations in the intensity and location of the energy-controlled process and the fine-grained particles preferentially accumulate in low-energy zones that usually corresponds to deeper zones and the quiet water in shoreline areas (Rose et al., 1993; Kirk and Bradley, 1995). However, in reservoirs, the proportion of fine-grained particles in deeper zones may be diluted by the influx of coarse-grained sediments derived from tributaries at different points

in the reservoir or by secondary distribution of sediments linked to steep slope in reservoir (Abraham et al., 1999; Curran et al., 2015; Tang et al., 2018). Therefore, spatial distribution of the sediments within the reservoir is complex, not uniform, and site dependent. Consequently, knowledge about sediment distribution in natural lakes may not be comparable to the reservoir because of its more river-like hydrodynamic characters (Abraham et al., 1999).

Many natural and anthropogenic compounds, including phosphorus (P), have a strong affinity for fine-grained particles (Heathwaite and Dils, 2000; Lopez et al., 2009; Fonseca et al., 2010; Rapin et al., 2019; Rapin et al., 2020) including colloids (Doucet et al., 2007; Baken et al., 2016; Bol et al., 2016; Gottselig et al., 2017b; Cuss et al., 2018; Nguyen et al., 2020). Therefore, their behavior in surface water is largely regulated by transport, dispersion and sedimentation of fine-grained materials (Effler and Matthews, 2004; Cieřła et al., 2020; Wang et al., 2020). Because the hydrodynamic of reservoirs favors the trapping of fine-grained sediments, it also promotes the formation of internal sedimentary P stock (Maavara et al., 2015). However, only a portion of P is permanently buried in sediments and under favorable conditions an important amount of sedimentary P is mobilized to pore- and overlying waters (Søndergaard et al., 2003). Internal P load becomes thus a source of P for reservoir waters and, together with nitrogen, can promote primary production and eutrophication (Smith and Schindler, 2009; Schindler et al., 2016; Le Moal et al., 2019). Therefore, in recent years, the biogeochemistry of sedimentary P has been a subject of particular attention since internal sedimentary P load is supposed to delay eutrophication recovery time and prevents improvement of water quality in such systems (Søndergaard et al., 2003; Jeppesen et al., 2005; Filippelli, 2008; North et al., 2015; Baker et al., 2019).

In sediment, P is associated to inorganic and organic materials (Pettersson et al., 1988; Lopez et al., 2009; Cavaliere and Homann, 2012; Cavalcante et al., 2018b; Rapin et al., 2020). The release of sedimentary P is related to the availability of mobilizable P as well as activated mechanisms/factors facilitating such release (*e.g.* sediment resuspension, anoxia, temperature, bioturbation...) (Kim et al., 2003; Surridge et al., 2007; Parsons et al., 2017; Chen et al., 2019; Rapin et al., 2019; Gautreau et al., 2020; Taguchi et al., 2020). In general, internal P load originates mainly from redox-sensitive iron compounds (redox-P) or from the more or less labile organic forms (labile organic P) (Søndergaard et al., 2003; Cavalcante et al., 2018; Rapin et al., 2020). The mobilization of sedimentary P from redox sensitive mineral phases is somewhat site-specific and favored in the reservoirs characterized by temporary or permanent oxygen depletion (anoxia) (Cavalcante et al., 2018; Norgbey et al., 2020). In fully aerated reservoirs, the release of sedimentary P via redox-driven internal loading is limited (Zhang et al., 2017; Moura et al., 2020) and can be relied on change in pH (Gaoa, 2012; Jin et al., 2006). The release of labile organic P, on the other hand, could be limited under anoxic conditions because low oxygen level inhibits organic matter decomposition. Other important factors affecting internal P load are: (i) shifting from a clear to a turbid state of water, *e.g.* the resuspension of bed sediment (Filstrup and Lind, 2010; Gautreau et al., 2020) and (ii) fluctuations in the water level causing sediment emersion, desiccation and re-inundation (Tang et al., 2018; Zhang et al., 2012). The turbid flow can lift up fine particles from sediment accumulated throughout the reservoir, whereas the water level fluctuation impacts mainly the sediments accumulated in the proximity of shores and in the banks. The frequency and magnitude of sediment drying and rewetting (SDW) is variable and site-specific. Inundation and desiccation may alter sediment redox, pH, physical and biological characteristics and thus sedimentary P speciation, transformation and release (Baldwin and Mitchell, 2000; Forber et al., 2017; Gu et al., 2018; Sun et al., 2018). Thus, the sediment impacted by water-level fluctuation of dam reservoir can induce a

pulse release of P in different manner than the sediment accumulated in deeper part of reservoir through a suit of different biogeochemical processes.

The release of sedimentary P may occur in dissolved, colloidal or particulate forms. Despite mechanism for release of dissolved P (orthophosphate ion) are well known via diffusion and advection (Darke and Walbridge, 2000), few attentions have been paid to the release of colloidal P, particularly its exchange between bottom sediment and water. However small/nano P-colloids (sized 3 kDa – 240 nm) are considered bioavailable for living organisms (Montalvo et al., 2015) and should be thus taken into account to better evaluate eutrophication risks. The mobility of colloids has been elucidated to keep an important role as P carriers across vast environmental matrices such as soils, vadose zones, riparian zone, rivers and groundwater (Turner et al., 2004; Wolthoorn et al., 2004; Séquaris et al., 2013; Jiang et al., 2015; Baken et al., 2016; Gottselig et al., 2017b; Missong et al., 2018; Gu et al., 2018). Nonetheless, the role of sedimentary colloids in P dynamic in dam reservoir context is not yet studied.

Considering that the heterogeneous spatial distribution of fine-grained sediments in dam reservoir is responsible for the uneven distribution of P in the deposited sediments (Rapin et al., 2020), the aims of this study was to (i) evaluate the colloids release potential of bottom sediments accumulated at different zones of the reservoir (lacustrine/riverine zones, at confluence with tributary, in the area impacted by water level fluctuation) (ii) to investigate the role of the physico-chemical properties of the sediment on the characteristics of released. The study was conducted on the sediment deposited in Champsanglard dam reservoir impacted by water-level fluctuation and characterized by the presence of tributaries. Sediments were sampled at 9 sites along the longitudinal pathway of the reservoir from the upstream riverine area downwards to the dam (permanently submerged bottom sediments) and at 2 complemented sites by lateral cross-sections (bank sediments impacted by water level fluctuation).

III.2.2.2. Materials and methods

III.2.2.2.1. Description of studied site

The study was carried out in Champsanglard hydroelectric dam reservoir, located on Creuse river (France). Champsanglard belongs to the Age complex which is constituted of three cascade dams and supplies electricity for a population of 21,000 inhabitants. The Champsanglard dam was commissioned in 1984 with 19-meter height and 120-meter width. In the middle channel near to the dam, the water depth can reach up to 17 m. The Champsanglard covers an area of 0.55 km², has a length of 2.36 km and receives an annual average inflow of 13.8 m³/sec. During flooding period, the water flows through the overflow crest with man-made operation. The Champsanglard watershed (406 km²) is composed of 65 % of agriculture land, 30 % forest and semi-natural environment and 4 % of artificial use (CORINE Land Cover data). The underlying lithology is mainly granitic (<http://infoterre.brgm.fr>). Thus, agricultural activity is a principal source of P for aquatic system. The Champsanglard is periodically subjected to thermal stratification and oxycline as well as to recurrent development of cyanobacteria (<http://baignades.sante.gouv.fr>). Champsanglard reservoir receive the sediment mainly by Creuse river and two tributaries (Fig. 39). The hydrological conditions in Champsanglard are influenced by oceanic continental climate with annual precipitation of 1059 mm and average annual temperature of 11.3°C (Météo France meteorological data). In 2019, the temperature in Creuse region varies from 1 to 27°C with maximum monthly rainfall level of 177 mm and the minimum of 44 mm. The precipitation height is lowest during summer (July to September)

and at the end of winter (February) with an average of 50 mm per month, compared to autumn and winter (October to December) of 155 mm per month averagely (Historique-meteo). The Creuse flow is maximum in winter (up to 70 m³/s) and minimum at the end of summer.

III.2.2.2.2. Sediment sampling, pretreatment and characterization

III.2.2.2.2.1. Sediment sampling and pretreatment

The sediments (up to 10-cm depth) were collected in high-flow period but during a month with low precipitation (February 2019), from nine sites along the longitudinal pathway from lacustrine region to riverine region (up to 3.3 km away from dam) (Fig. 39).

In lacustrine region, samplings were performed: near the dam (sites 1 and 2), in the middle of the reservoir (sites 3 to 5), and in the tail of reservoir (sites 6 and 7). The sites 3 and 7 were located near tributaries.

In upstream riverine region, samplings were performed at sites 8 and 9. At the shoreline of these two sites, where an important water-level fluctuation was observed, a series of samples were collected across the lateral axis from the deeper zone to the zone gradually exposed to air (Fig. 39): 3 additional samples along the transect of site 8 (namely WFZ-1) and 1 additional sample along the transect of site 9 (namely WFZ-2). They were annotated as “A” for the sediments sampled right at the shoreline (frequently submerged sediment), “B” and “C” for the sediments sampled at drier and higher position than water level (namely temporary and occasionally submerged sediments, respectively). It should be noted that two water-level fluctuation zones (WFZ-1 and WFZ-2) exhibited different river morphology and toposequence. The WFZ-1 was likely “bank of the river” and soil-like, whereas the WFZ-2 was a deposition area of the transported river material and covered by thin organic layer (Fig. 39). The additional lateral sampling in the sites 1-7 was not feasible because of limited sedimentation (rocky shores).

From here, we named sediments collected at deep channel and permanently submerged, from site 1 to 9, as “bottom sediments” and the sediments collected in the shore and impacted by water level fluctuation (8A, 8B, 8C and 9B) as “bank sediments” (Fig. 39).

Sediments were collected using an Ekman grab, homogenized manually and preserved in polyethylene bottles previously rinsed with surface water. All samples were well kept under refrigerated and dark conditions during transportation. In laboratory, the sediments were immediately homogenized, sieved through a 2-mm mesh and stored at 4°C before experimentation and analyses.

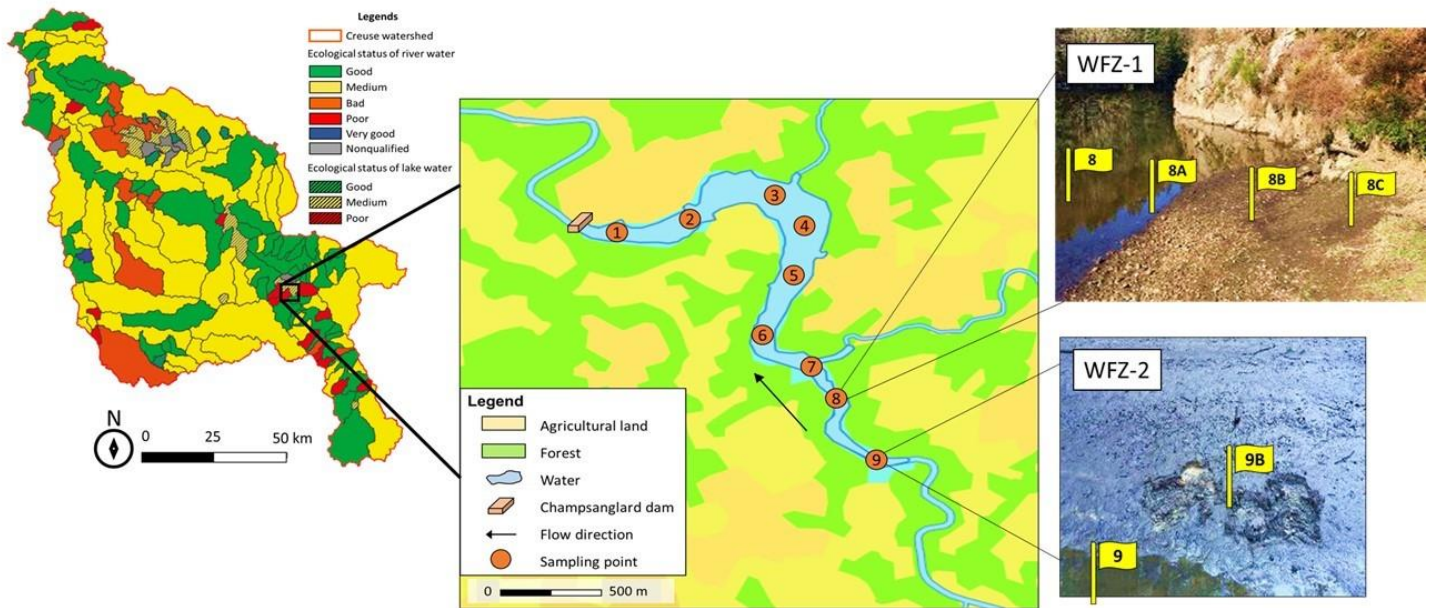


Figure 39. Sampling sites along Champsanglard dam reservoir (permanently submerged bottom sediments) and in two zones of water-level fluctuation (WFZ-1 and WFZ-2 areas; non-permanently submerged sediments) (source : Geoportail, EPTB Vienne 2018).

III.2.2.2.2. Sediment characterization

Granulometry analysis was done on wet sediment by the laser diffraction particle size analyzer (Malvern, MasterSizer 3000) after ultrasonically dispersion in ultrapure water (UPW). The $\text{pH}_{\text{H}_2\text{O}}$ was measured on a 1:1 wet sediment-water suspension using GLP22 pH meter (Crison) and a 5221-pH probe (Crison). Sedimentary organic matter (OM) was estimated by the loss on ignition at 550°C for 2 h.

For measurement of total contents of Fe, Al, Ca, Mn, and Mg, the sediments were dried at 105°C , crushed into powder, immersed in hydrogen peroxide (Merck, 30%) to degrade OM before the digestion according to US EPA 3051a (2007) method. Sediments were further digested by reverse aqua regia (HNO_3 65 %, HCl 37 %) and heated in a microwave for a duration of 40 min at 180°C (Anton Paar Multiwave Go). The digested solution was filtered at $0.2 \mu\text{m}$ cellulose acetate membrane (LLG Labware) and dissolved contents of Fe, Al, Ca, Mn, and Mg were analyzed by MP-AES (Agilent, MP 4100) (See part 2.3.2).

For the determination of total sedimentary P, sediments were calcinated at 450°C for 3 h and digested in HCl 3.5 M (VWR Prolabo Anala R Normapur) during 16 h (Ruban et al., 2001). The obtained solution was firstly centrifuged at 2000 g for 15 min, then filtered through $0.45 \mu\text{m}$ cellulose acetate membrane (LLG Labware). The concentration of dissolved inorganic phosphates (DIP) in digested solution was measured by spectrophotometric method at 880 nm after pH adjustment (between 2 and 7) (Murphy and Riley, 1962). Method for DIP measurement is presented in part 2.3.2

III.2.2.2.3. Extraction and characterization of water-mobilizable fraction (below 1 μm)

III.2.2.2.3.1. Method of extraction and separation for water-mobilizable fraction

Water mobilizable fraction was defined as dissolved and colloidal part in the fraction inferior to 1 μm . Colloids were extracted from fresh wet sediment resuspended in UPW. The wet solid/liquid (S/L) ratio was 1/10 corresponding a dry S/L ratio of 1.55 - 1.96 % (w_{DW}/v) according to different samples (water loss on drying at 105°C were ranging from 51 ± 6 % to 82 ± 2 %). Sediment suspensions were firstly agitated for 24 h at 200 rpm using orbital shaker (IKA-WERKE, KS 501 digital). Then, the separation for water-mobilizable fraction was performed by centrifugation (272 g for 6 minutes) to remove larger particles (theoretically larger than 1 μm considering average density of sediment) in coupling with filtration at 1 μm . The speed and time of centrifugation were calculated by equation (1), according to Gimbert et al., (2005).

$$t = \frac{18\eta \ln(R/S)}{\omega^2 d^2 \Delta\rho} \quad (1)$$

With d : particle diameter (cm)

$\Delta\rho$: difference in particle density (g/cm^3), herein $\rho_p = 2.417 \text{ g}/\text{cm}^3$, and density of suspension medium, here in $\rho_{\text{H}_2\text{O}} = 1.0 \text{ g}/\text{cm}^3$

η : viscosity of suspension medium ($\text{g}/\text{cm}\cdot\text{s}$), herein $\eta = 0.01 \text{ g}/\text{cm}\cdot\text{s}$

t : settling time (s)

R : distance from rotation axis to the settling level in the tube (10.8 cm)

S : distance from rotation axis to the surface of suspension in the tube (5.5 cm)

ω : angular velocity of the centrifuge (rad/s), calculated according by equations (2) and (3) with rotor radius of 108 mm:

$$\omega = \frac{2\pi}{60} \times rpm \quad (2)$$

$$g = 1.118 \times R \times \left(\frac{rpm}{1000}\right)^2 \quad (3)$$

The filtration through 1 μm was done with glass fiber filter (VWR). Filtration step is important to assure the accurate size of separated materials since the centrifugation can result in the presence of larger particles in supernatant due to the heterogeneity of sediment (Nguyen et al., 2020).

For organic carbon (OC), Fe, Al, Ca, Mn and Mg analysis, the separation between large colloidal fraction (0.2-1 μm) and fraction below 0.2 μm (including small/nano colloidal and truly dissolved species) was performed by filtration at 0.2 μm using cellulose nitrate membrane (Sartorius). For P, we distinguished truly dissolved, small/nano colloidal (0 - 0.2 μm) and large colloidal (0.2 - 1 μm) by an additional chemical step (see section 2.3.2).

III.2.2.2.3.2. Characterization of colloids and water-mobilizable fraction

Particle size distribution of water-mobilizable colloids was measured using dynamic light scattering technique performed by ZetaSizer NanoZS (Malvern). Material absorption and refraction index were 0.001 and 0.18, respectively. The backscatter angle of measurement was at 173°. The measurement was made

after 120-second of equilibration, through three measurements with automatic selection of working times and optimal measuring position.

The mass of large colloids (0.2 – 1 μm) was estimated by gravimetric method and determined as dry weight of the amount of colloids retained on the pre-weighted 0.2- μm filter at 30°C until unchanged mass.

Fraction lower than 1 μm was characterized for total organic carbon (TOC), total P (TP) and total contents of Fe, Al, Mn, Ca, Mn and Mg with acid digestion. Fraction lower than 0.2 μm was characterized for TOC, TP, dissolved inorganic phosphate (DIP) as well as total contents of Fe, Al, Mn, Ca, Mn and Mg without acid digestion.

Subsequently, the contents of OC, P, Fe, Al, Ca, Mn and Mg in large colloids were determined by the difference in total contents between fraction lower than 1 μm and fraction lower than 0.2 μm . Exclusively for P, a fraction namely small/nano colloidal P was further estimated by the difference between TP and DIP in fraction lower than 0.2 μm . In this study, four fractions of P were established: water-mobilizable P (P_{WM} : TP in the fraction lower than 1 μm), large P-colloids (P_{WM} minus $\text{TP}_{<0.2\ \mu\text{m}}$), small/nano P-colloids ($\text{TP}_{<0.2\ \mu\text{m}}$ minus $\text{DIP}_{<0.2\ \mu\text{m}}$) and truly dissolved P ($\text{DIP}_{<0.2\ \mu\text{m}}$).

Content of TP was determined in persulfate digested solution according to US EPA 365.1 method (1993). The digestion was performed by adding 625 μL of working digestion solution containing $(\text{NH}_4)_2\text{S}_2\text{O}_8$ 0.56 M and H_2SO_4 5.6 M into 10 mL of sample and heating for 30 minutes using autoclave at 121°C and 1 bar (LEQUEUX). Solution after digestion was filtered at 0.2 μm using cellulose acetate membrane (LLG Labware). The DIP levels in both digested and non-digested solutions were measured with molybdenum method according to Murphy and Riley, (1962) at 880 nm using 1-cm cuvettes with UV-visible spectrophotometer (Agilent 8453 UV-visible spectrometer). The LQ of method is 20 $\mu\text{g P/L}$. The TOC measurement was done using TOC analyzer (Analytik Jena, multi N/C 2100S) with LQ of 1 mg C/L. The analysis of TOC was carried out with onboard magnetic stirring to avoid colloids aggregation and decantation during analysis. The measurements of Fe, Al, Mn, Ca, Mn and Mg concentrations in both digested solution (for fraction lower than 1 μm , using US EPA 3015a method; see part 2.2) and in non-digested solution (for fraction lower than 0.2 μm) were analyzed using MP-AES (Agilent, MP 4100). The limits of quantification (LQ) are 20 $\mu\text{g Al/L}$, 30 $\mu\text{g Fe/L}$, 12 $\mu\text{g Ca/L}$, 7 $\mu\text{g Mn/L}$ and 1 $\mu\text{g Mg/L}$.

III.2.2.3. Results

III.2.2.3.1. Sediment characteristics

III.2.2.3.1.1. Grain size of sediments

For the bottom sediments, the median grain size (D_{50}) was largest in riverine region ($74 \pm 14\ \mu\text{m}$ at site 9 and $46 \pm 2\ \mu\text{m}$ at site 8) and decreased toward the dam ($18 \pm 2\ \mu\text{m}$, at sites 1 to 3) (Fig. 40A). The finer fraction (below 20 μm) of sediments was highest at site 2, and represented 65 % of particles, then decreased gradually to be at 27 % at site 9. The grain size patterns at site 3 and site 7 (entrances of tributaries) exhibited no difference than other sampling sites. It is notably that the coarsest grain fraction ($> 210\ \mu\text{m}$), was dispelled when approaching the deeper part of reservoir (from site 2 to site 4), “reappeared” in front of the dam (site 1) at about 4 %.

For bank sediments, the D_{50} showed a similar grain size pattern to bottom sediments in both WFZ-1 and WFZ-2 zones (Fig. 40A) with a variation of less than 11 % and 8 %, respectively.

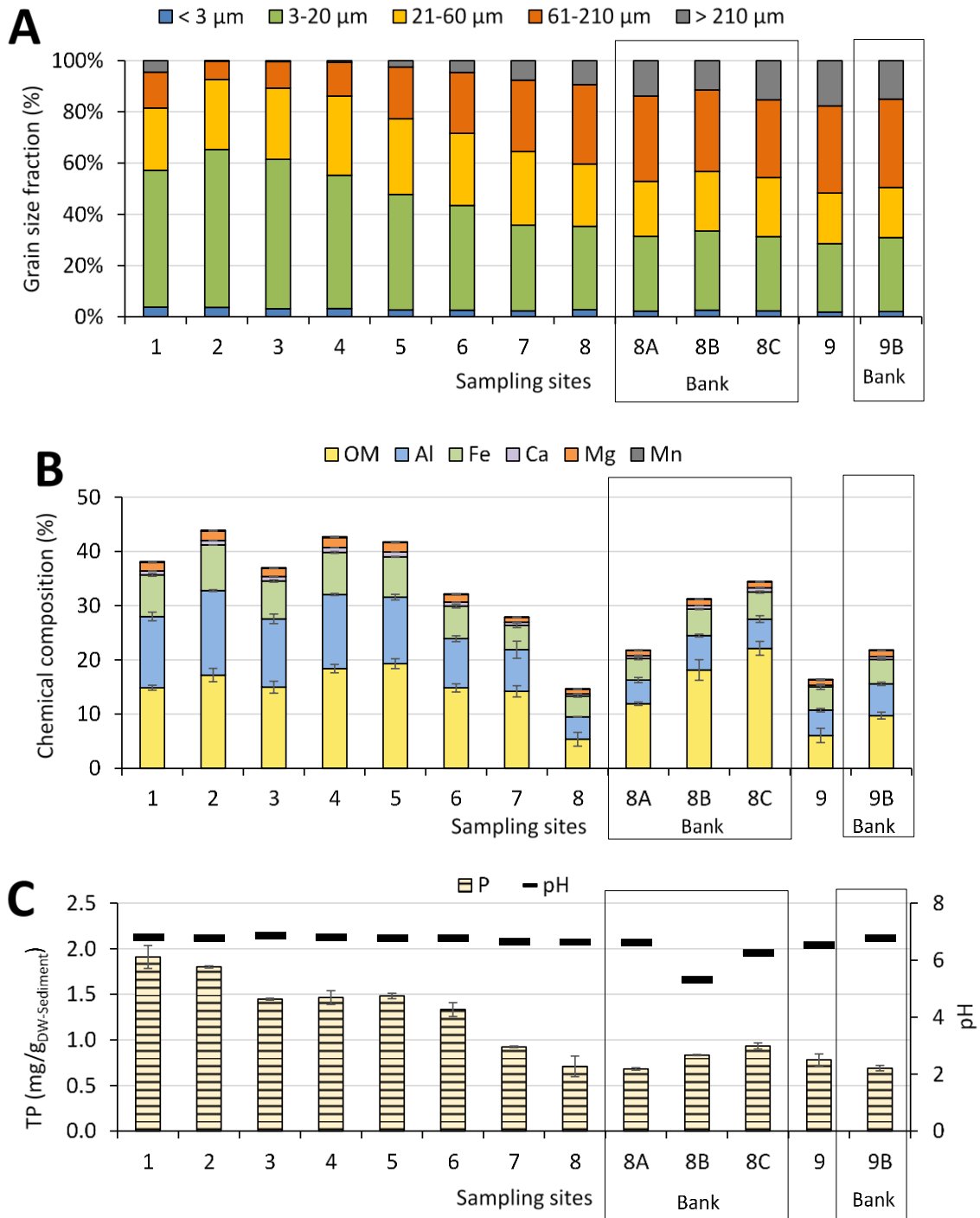


Figure 40. Sediment characteristics deposited along the reservoir (sites 1-9) and in WFZ-1 (8A, 8B, 8C) and WFZ-2 (9B) areas: (A) grain size distribution, (B) quantity of OM, Al, Fe, Ca, Mn, Mg and (C) amount of total phosphorus content and pH. WFZ - water-level fluctuation zone, OM – organic matter.

III.2.2.3.1.1. Chemical characteristics of sediments

The content of OM in lacustrine bottom sediments (at sites 1 to 7) ranged from $15 \pm 1 \%$ to $19 \pm 1 \%$ with the highest values found in the sediments deposited in the middle part (sites 2, 4, 5) of reservoir (Fig. 40B). The entries of two tributaries at site 3 and site 7 induced no significant variation in OM contents of bottom sediments. Riverine bottom sediments (site 8 and site 9) were characterized by lower amount of OM, with values of $5.4 \pm 1.3 \%$ and $6.0 \pm 1.3 \%$ respectively. Riverine bank sediments at WFZ-1 and WFZ-2 contained increasing concentration of OM with increasing elevation; for instance, from $11.9 \pm 0.3 \%$ (site 8A) to $22.1 \pm 1.3 \%$ (site 8C) and from $6.0 \pm 1.3 \%$ (site 9) to $9.7 \pm 0.6 \%$ (site 9B).

In Fig. 40B, the total concentrations of OM, Fe, Al, Ca, Mn and Mg in bottom sediments collected in lacustrine region (at sites 1 to 6) were higher than in the tail and riverine regions (at sites 7 to 9). We noted the decrease in concentrations of OM, P, Ca, Mn started from site 5 to site 8 and decrease in Al, Fe and Mg started at sites 4 to 8. At riverine region, concentration of Ca increased gradually from bottom sediments, $3.4 \pm 0.4 \text{ mg Ca/g}_{\text{DW-Sed}}$ (site 8) and $3.1 \pm 0.6 \text{ mg Ca/g}_{\text{DW-Sed}}$ (site 9), to be 1.6 - 2.3 times higher in bank sediments, $7.8 \pm 0.5 \text{ mg Ca/g}_{\text{DW-Sed}}$ (site 8C) and $5.1 \pm 0.6 \text{ mg Ca/g}_{\text{DW-Sed}}$ (9B). Similar tendency was observed for Al, Fe, Mg and Mn, but with slighter increases of up to 1.5, 1.3, 1.3 and 1.4 times, respectively (Table 16).

Table 16. Chemical composition of sediment along reservoir and at two zones of water-level fluctuation (WFZ-1 and WFZ-2).

Sampling site	P		OM		Fe		Al		Ca		Mg		Mn		pH	
	mg/g _{DW-Sediment}		%						mg/g _{DW-Sediment}							
	Mean	SD	Mean	SD	Mean	SD	Mean	SD	Mean	SD	Mean	SD	Mean	SD	Mean	SD
1	1.91	0.13	14.9%	0.5%	76.87	2.85	131.29	8.01	7.11	0.07	15.67	0.59	1.62	0.10	6.83	0.03
2	1.80	0.01	17.2%	1.2%	84.39	0.05	155.83	1.86	8.19	0.01	17.28	0.00	1.59	0.10	6.79	0.03
3	1.45	0.01	15.0%	1.1%	69.91	2.22	125.96	8.98	7.99	0.35	15.33	0.13	1.25	0.10	6.88	0.01
4	1.46	0.08	18.4%	0.8%	77.76	1.76	136.65	2.01	8.92	0.09	18.38	0.20	1.38	0.10	6.82	0.01
5	1.48	0.03	19.3%	0.9%	74.49	0.99	122.63	5.16	9.03	0.03	17.19	0.11	1.45	0.10	6.77	0.04
6	1.33	0.08	14.8%	0.8%	60.13	3.49	90.74	5.47	7.17	0.15	14.07	0.44	1.14	0.10	6.79	0.03
7	0.92	0.01	14.2%	1.0%	44.68	4.21	76.86	15.80	5.79	0.02	9.02	0.28	0.81	0.10	6.67	0.01
8	0.71	0.11	5.4%	1.3%	38.57	2.19	41.08	0.31	3.67	0.65	8.75	0.42	0.71	0.09	6.65	0.03
At WFZ-1																
8	0.71	0.11	5.4%	1.3%	38.57	2.19	41.08	0.31	3.67	0.65	8.75	0.42	0.71	0.09	6.65	0.03
8A	0.68	0.01	11.9%	0.3%	39.86	2.25	43.75	4.59	5.14	0.90	9.45	0.49	0.81	0.20	6.63	0.01
8B	0.83	0.01	18.1%	1.9%	48.85	0.81	63.49	2.49	6.74	0.03	11.50	0.04	0.99	0.10	5.32	0.03
8C	0.93	0.03	22.1%	1.3%	49.76	2.00	53.95	6.28	7.82	0.49	10.79	0.19	0.92	0.10	6.26	0.06
At WFZ-2																
9	0.78	0.06	6.0%	1.3%	42.99	4.66	46.86	3.42	3.11	0.59	9.75	1.31	0.85	0.20	6.55	0.01
9B	0.69	0.03	9.7%	0.6%	45.13	1.69	58.58	2.84	5.08	0.65	11.31	0.00	1.21	0.06	6.79	0.02

As shown in Fig. 40C, the highest quantity of TP ($1.8 \pm 0.1 \text{ mg/g}_{\text{DW-Sed}}$) was observed in bottom sediments deposited near the dam (at sites 1 and 2). Between the site 3 and 6, TP concentration in bottom sediments remained comparable with about $1.5 \pm 0.1 \text{ mg/g}_{\text{DW-Sed}}$. In contrast, riverine bottom sediments (sites 8 and 9) contained lower TP level ($0.7 \pm 0.1 \text{ mg/g}_{\text{DW-Sed}}$) and were in the same range than TP concentration in bank sediments ($0.8 \pm 0.2 \text{ mg/g}_{\text{DW-Sed}}$).

Along the reservoir, pH of bottom and bank sediments were in the range of slightly acidic to neutral pH with values from 6.5 ± 0.1 to 6.9 ± 0.1 . However, particularly at riverine regions, bank sediment (site 8B) had a notably lower pH of 5.3 ± 0.1 .



III.2.2.3.2. Water-mobilizable fraction

II.2.2.3.2.1. Geochemical of water-mobilizable fraction

The chemical composition of fraction below 0.2 μm , containing both dissolved and small/nano colloidal species, varied according to sampling site (Table 17). For bottom sediment, in lacustrine regions (at sites 1 to 7), the contents of Fe, Ca, OC and Mn were higher (by 1.5 to 9 times) than in riverine regions (site 8 and 9). For Fe and OC, the values at site 8 were 30 and 40 % lower than at site 9 (Table 17). The content of Mg was lowest at site 9 ($0.008 \pm 0.001 \text{ mg Mg/g}_{\text{DW-Sed}}$) then increased by 4-fold to be relatively stable in lacustrine zone (at sites 1 to site 7). Content of Al was slightly higher near the dam ($0.07 \pm 0.01 \text{ mg Al/g}_{\text{DW-Sed}}$ at site 1) than at other sites ($0.05 \pm 0.01 \text{ mg Al/g}_{\text{DW-Sed}}$), except a peak of $0.09 \pm 0.01 \text{ mg Al/g}_{\text{DW-Sed}}$ at site 7 (corresponding to a tributary entrance). In contrast, the contents of P below 0.2 μm , fluctuated throughout the length of reservoir between $3.91 \pm 0.12 \mu\text{g P/g}_{\text{DW-Sed}}$ (site 8) and $15.33 \pm 0.8 \mu\text{g P/g}_{\text{DW-Sed}}$ (site 9) (Table 17). Bank sediments had higher contents of P, OC, Fe (except WFZ-2), Al, Ca, Mg and Mn than bottom sediments, with factors between 2 to 6 (Table 17).

The increasing tendency in elemental contents towards the dam was also observed for large colloidal fraction (0.2 – 1 μm) (Table 18). In riverine bottom sediments, the contents of P, Fe, Al, Ca and Mg were respectively 3 to 5-fold, 3.6 to 6.6-fold, 7 to 12-fold, 1.6 to 2-fold and 3.5 to 4-fold lower than in lacustrine bottom sediments, respectively. The contents of OC behaved differently; the highest values were found near the dam, with $1.5 \pm 0.3 \text{ mg OC/g}_{\text{DW-Sed}}$ (sites 2) and $1.1 \pm 0.1 \text{ mg OC/g}_{\text{DW-Sed}}$ (site 1), whereas these values were 3-fold lower at tributary (site 3) and from 3 to 25-fold lower at the tail and riverine regions (at sites 6 to 9). In bank sediments, the contents of OC, Fe, Al and Mg in large colloids were higher than in bottom sediments with factors between 2.8 to 10 (Table 18). In contrast, the contents of P in large colloids were higher for frequently submerged sediment (site 8A) and lower for temporary-occasionally submerged sediments (site 8B, 8C and 9B) than in bottom sediments.

Table 17. Chemical composition of the fraction below 0.2 μm (in mg per g dry sediment) along reservoir and at two zones of water-level fluctuation (WFZ-1 and WFZ-2).

Site	Dissolved and small colloidal P		OC		Fe		Al		Ca		Mg		Mn	
	$\mu\text{g/g}_{\text{DW-Sediment}}$		$\text{mg/g}_{\text{DW-Sediment}}$											
	Mean	SD	Mean	SD	Mean	SD	Mean	Mean	Mean	SD	Mean	SD	Mean	SD
1	10.13	0.93	0.49	0.06	0.08	0.01	0.07	0.01	0.15	0.01	0.033	0.002	2.96	0.40
2	9.55	0.36	0.43	0.05	0.06	0.01	0.06	0.01	0.13	0.01	0.029	0.002	1.00	0.49
3	7.72	0.44	0.39	0.03	0.05	0.01	0.05	0.01	0.14	0.01	0.033	0.001	0.39	0.13
4	5.97	1.24	0.47	0.09	0.05	0.02	0.05	0.02	0.15	0.01	0.034	0.001	0.79	0.27
5	7.74	1.54	0.44	0.05	0.05	0.02	0.05	0.02	0.16	0.01	0.036	0.001	0.41	0.06
6	8.28	0.50	0.39	0.06	0.07	0.01	0.07	0.01	0.15	0.01	0.035	0.002	ND	ND
7	12.97	1.01	0.50	0.02	0.07	0.01	0.09	0.01	0.12	0.01	0.029	0.001	ND	ND
8	3.91	0.12	0.20	0.04	0.03	0.01	0.05	0.01	0.04	0.01	0.011	0.001	ND	ND
9	15.33	0.74	0.29	0.01	0.05	0.01	0.05	0.01	0.04	0.01	0.008	0.001	ND	ND
At WFZ-1														
8	3.91	0.12	0.20	0.04	0.03	0.01	0.05	0.01	0.04	0.01	0.011	0.001	ND	ND
8A	16.87	1.55	0.32	0.02	0.06	0.01	0.08	0.01	0.07	0.01	0.021	0.001	1.20	0.07
8B	19.58	3.03	0.51	0.05	0.06	0.01	0.10	0.01	0.08	0.01	0.024	0.001	1.74	0.10
8C	22.49	2.33	0.56	0.03	0.06	0.01	0.09	0.01	0.10	0.01	0.027	0.001	1.23	0.08
At WFZ-2														
9	15.33	0.74	0.29	0.01	0.05	0.01	0.05	0.01	0.04	0.01	0.008	0.001	ND	ND
9B	17.46	1.61	0.35	0.01	0.05	0.01	0.07	0.01	0.10	0.01	0.028	0.001	0.85	0.06

Table 18. Chemical composition of large colloids (fraction 0.2 – 1 µm) in mg/g dry sediment along reservoir and at two zones of water-level fluctuation (WFZ-1 and WFZ-2).

*ND: not detected

Site	P		OC		Fe		Al		Ca		Mg		Mn	
	mg/g _{DW-Sediment}													
	Mean	SD	Mean	SD	Mean	SD	Mean	SD	Mean	SD	Mean	SD	Mean	SD
1	0.059	0.011	1.08	0.11	1.09	0.09	1.90	0.10	0.25	0.02	0.15	0.01	0.016	0.001
2	0.071	0.004	1.52	0.29	1.16	0.08	3.21	1.01	0.22	0.05	0.17	0.03	0.017	0.000
3	0.067	0.001	0.36	0.17	1.00	0.09	2.00	0.32	0.24	0.07	0.14	0.01	0.009	0.003
4	0.067	0.005	0.84	0.11	0.88	0.08	1.55	0.11	0.22	0.03	0.13	0.04	0.005	0.001
5	0.062	0.005	0.91	0.14	0.64	0.10	1.07	0.23	0.14	0.03	0.09	0.01	0.006	0.001
6	0.039	0.001	0.16	0.02	0.50	0.04	0.99	0.06	0.24	0.05	0.08	0.01	0.006	0.001
7	0.028	0.002	0.11	0.04	0.41	0.01	0.88	0.08	0.21	0.07	0.11	0.03	0.006	0.010
8	0.014	0.001	0.04	0.02	0.18	0.02	0.27	0.01	0.11	0.01	0.04	0.01	ND	ND
9	0.023	0.001	0.03	0.01	0.32	0.01	0.46	0.01	0.14	0.02	0.05	0.01	0.005	0.001
At WFZ-1														
8	0.014	0.001	0.04	0.02	0.18	0.02	0.27	0.01	0.11	0.01	0.04	0.01	ND	ND
8A	0.021	0.001	0.29	0.01	0.44	0.03	0.69	0.05	0.06	0.01	0.03	0.01	0.004	0.001
8B	0.007	0.003	0.40	0.18	0.76	0.09	1.61	0.20	0.09	0.01	0.11	0.03	0.010	0.001
8C	ND	ND	0.30	0.05	0.66	0.03	1.36	0.06	0.12	0.03	0.11	0.03	0.011	0.001
At WFZ-2														
9	0.023	0.001	0.03	0.01	0.32	0.01	0.46	0.01	0.14	0.02	0.05	0.01	0.005	0.001
9B	0.001	0.000	0.29	0.08	0.45	0.05	0.69	0.08	0.16	0.03	0.08	0.01	0.005	0.001

II.2.2.3.2.2. Size distribution of colloids

Figure 41 presents the particle size distribution of water mobilizable fraction. Fraction below 450 nm contributed approximately to 92 ± 2 % of total fraction below 1 µm regardless of the sediment analyzed. Between 40 and 70 % of released colloids were smaller than 220 nm. In bottom sediment, nano-colloids (smaller than 50 nm) were only detected in bottom sediment at sites 1, 4, 5 and 6. Meanwhile, the size of colloids at site 3 (meandering confluence) became enriched by large colloids (larger than 220 nm). In front of the dam (site 1), colloids were mainly composed of fraction 100 – 450 nm. No difference was observed in size class of bottom sediments between site 8 and site 9.

Concerning bank sediments, both WFZ-1 and WFZ-2 zones exhibited comparable size of water-mobilizable fraction and bank sediments showed no difference to bottom sediments. Up to 90 % of released colloids were sized below 450 nm, and about 50-60 % of them were inferior to 220 nm. Nano-colloids (below 50 nm) were observed only in temporarily submerged sediment for both site 8B and site 9B.

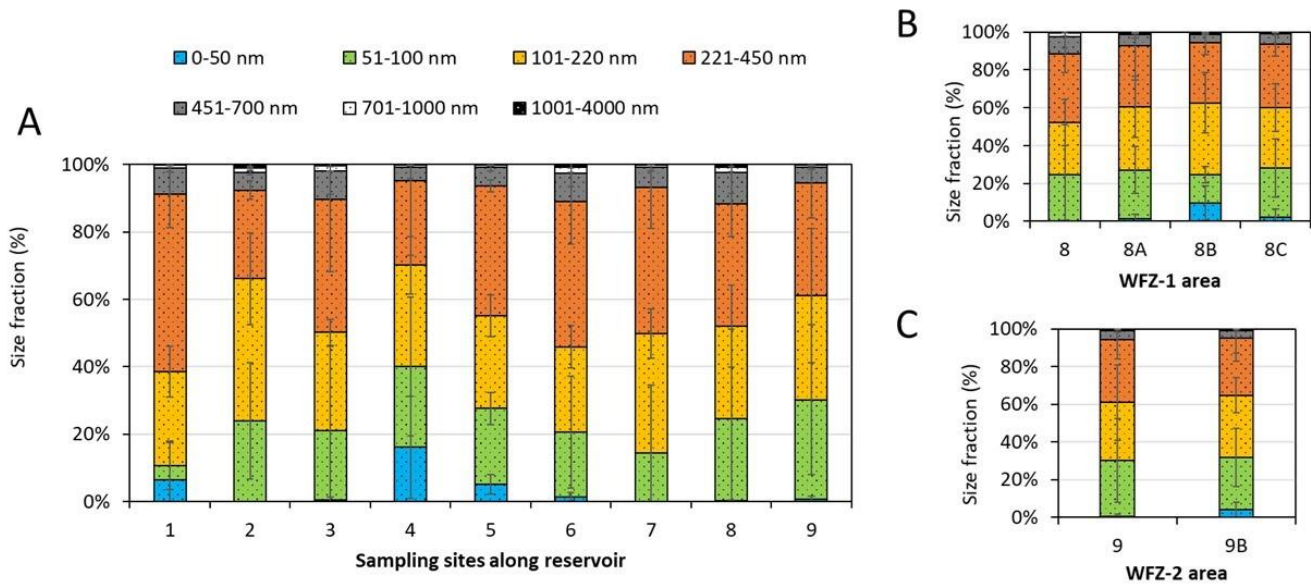


Figure 41. Size distribution of water-mobilizable colloids (< 1 μm): (A) along reservoir, (B) in WFZ-1 area and (C) in WFZ-2 area. WFZ stands for water-level fluctuation zone

II.2.2.3.2.3. Mass of large colloid (0.2 - 1 μm)

For bottom sediments, masses of large colloids (0.2-1 μm) increased from site 8 (at 2.8 ± 0.3 mg/g_{DW-Sed}) toward the dam, with a factor up to 8 to reach 22.8 ± 0.9 mg/g_{DW-Sed} at site 2 (Fig. 42A). Bottom sediment at site 9 contained 1.5-time higher level of colloidal mass than site 8. In front of the dam (site 1), colloidal mass was 22 % lower than in site 2. At site 2, right after entrance of tributary at site 3, mass of colloids increased by 30 %.

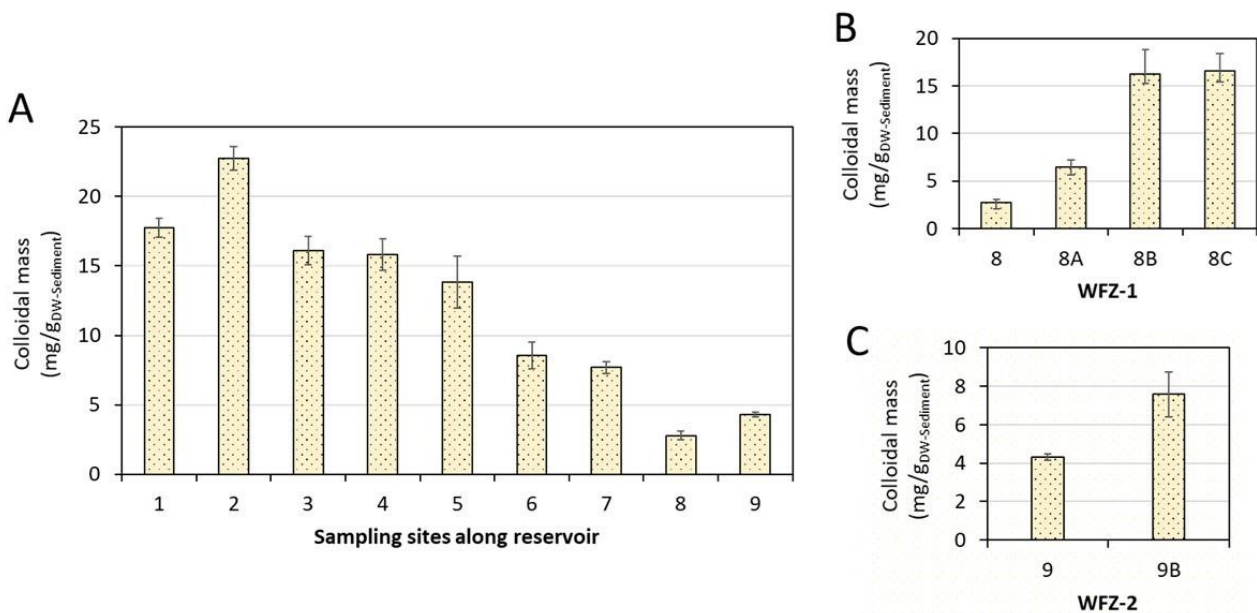


Figure 42. Spatial variability of large colloids (0.2 – 1 μm): (A) along reservoir, (B) in WFZ-1 area and (C) in WFZ-2 area. WFZ stands for water-level fluctuation zone.

In bank sediments, the amounts of large colloids were higher than in bottom sediments (Fig. 42B and 42C) and were comparable to the quantities released from lacustrine bottom sediments. At WFZ-1 area, the quantity of large colloids released from occasionally air-exposed bank sediment (site 8A) was $6.5 \pm$

0.7 mg/g_{DW-Sed} and raised up to 16.6 ± 1.8 mg/g_{DW-Sed} in frequently and temporary air-exposed sediment (sites 8B and 8C). These contents at WFZ-1 were 6 times higher than in bottom sediments that were never exposed to air drying. At WFZ-2 area, a higher quantity of released large colloids from bank sediment was also observed compared to bottom sediment, but with a lower increase amplitude, 1.8-fold, to reach 7.6 ± 1.2 mg/g_{DW-Sed} (site 9B).

II.2.2.3.2.4. Composition of large colloids

In the case of bottom sediments, the masses of analyzed elements (OC, P, Al, Fe, Ca, Mn and Mg) in large colloids (0.2-1 μ m) accounted for 0.06 - 0.63 % of total sediment mass (Fig. 43-A1) and 21 – 31 % of total colloidal mass (Fig. 43-B1). Among analyzed elements, large colloids contained high concentrations of Al, Fe, OC and Ca with the averages of 110 ± 20 , 60 ± 10 , 45 ± 27 and 22 ± 12 mg/g_{DW-Colloid}, respectively (Table 19). The amounts of Mg, P and Mg were in lower range with the averages of 10 ± 3 , 4.3 ± 0.9 and 0.6 ± 0.4 mg/g_{DW-Colloid}, respectively. Right after the entering of tributary at site 3, at site 2, higher OC was observed. No significant difference in composition of large colloids was detected for tributary entrance at site 7.

Table 19. Chemical composition of large colloids (0.2 – 1 μ m) expressed in mg per g dry colloids along reservoir and at two zones of water-level fluctuation (WFZ-1 and WFZ-2).

*ND: not detected

Site	P		OC		Fe		Al		Ca		Mg		Mn	
	mg/g dry colloid													
	Mean	SD	Mean	SD	Mean	SD	Mean	SD	Mean	SD	Mean	SD	Mean	SD
1	3.4	0.6	59.6	7.7	61.3	3.8	107.0	1.9	14.1	1.2	8.6	0.3	0.88	0.07
2	3.1	0.2	66.5	10.8	50.9	3.2	137.9	42.6	10.0	2.0	7.5	1.3	0.74	0.04
3	4.2	0.4	15.6	0.3	61.9	3.5	125.1	28.6	14.7	3.8	8.9	0.7	0.59	0.23
4	4.2	0.2	53.2	8.5	55.8	0.9	97.8	0.5	14.0	1.3	8.3	1.9	0.34	0.04
5	4.9	0.6	63.9	18.5	47.4	8.8	81.5	16.1	10.8	2.2	6.5	0.9	0.42	0.05
6	4.5	0.6	18.3	4.0	59.0	9.8	117.0	17.0	28.7	9.0	9.7	1.7	0.66	0.10
7	3.6	0.2	14.8	5.1	53.3	2.8	113.3	1.0	27.3	9.7	14.2	4.4	0.73	1.33
8	5.3	0.4	16.9	11.2	63.5	1.9	101.4	12.5	39.9	7.5	15.2	1.5	ND	ND
9	5.3	0.7	7.8	2.2	75.7	1.8	107.3	2.8	34.4	2.4	11.3	0.3	1.24	0.03
At WFZ-1														
8	5.3	0.4	16.9	11.2	63.5	1.9	101.4	12.5	39.9	7.5	15.2	1.5	ND	ND
8A	3.3	0.4	42.7	3.1	68.4	2.6	106.0	4.2	10.0	3.1	5.4	0.6	0.68	0.06
8B	0.4	0.2	24.5	6.1	46.9	2.1	99.3	3.6	5.3	0.8	6.6	1.0	0.60	0.10
8C	ND	ND	19.1	6.0	39.9	4.1	82.6	10.0	7.5	2.3	6.7	1.8	0.65	0.08
At WFZ-2														
9	5.3	0.7	7.8	2.2	75.7	1.8	107.3	2.8	34.4	2.4	11.3	0.3	1.24	0.03
9B	0.15	0.03	40.6	19.9	60.3	6.3	92.0	9.1	21.3	2.0	11.2	2.1	0.63	0.12

For the bank sediments, the total mass of analyzed elements in large colloids accounted for 0.06- 0.3 % of total sediment mass (Fig. 43-A2, A3) and 16 – 23 % of total colloidal mass (Fig. 43-B2, B3). Among analyzed elements, large colloids contained higher amount of Al, Fe, OC and Ca of averagely 100 ± 10 , 60 ± 2 , 30 ± 5 and 20 ± 3 mg/g_{DW-Colloid}, respectively. The concentrations of Mg, P and Mg in large colloids were in lower range, with the averages of 10 ± 1 , 2.4 ± 0.3 and 0.6 ± 0.1 mg/g_{DW-Colloid}, respectively.

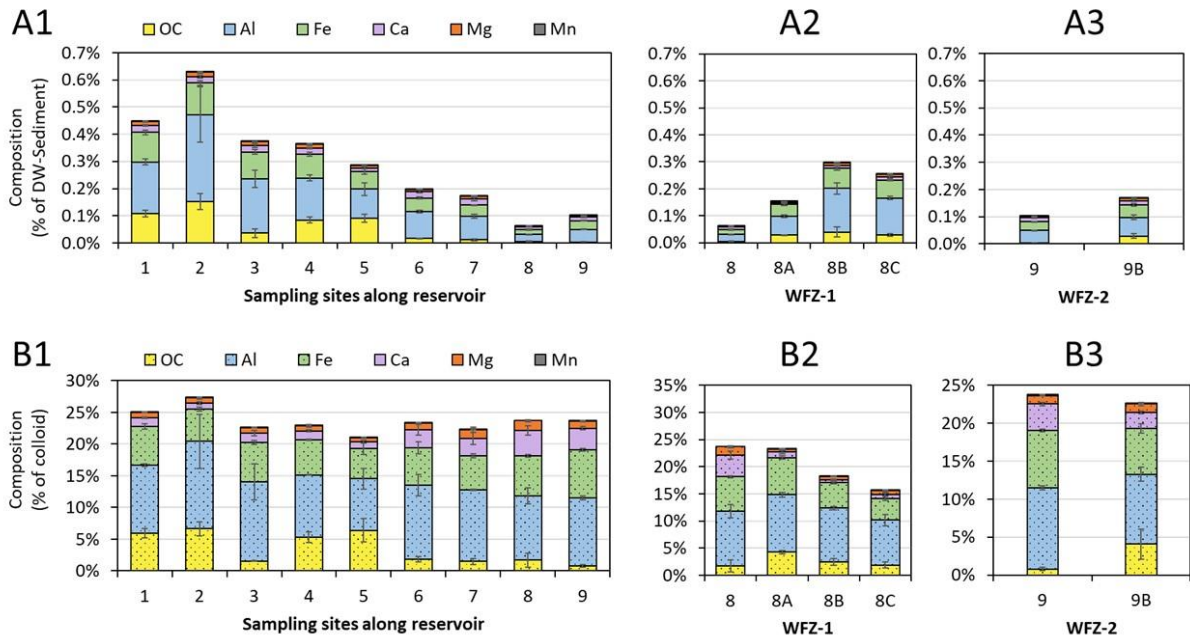


Figure 43. Chemical composition (OC, Fe, Al, Ca, Mg, Mn) of large colloids presented in % of dry sediment, mg/g_{DW-Sediment} (A1-A3) and in % of dry large colloids, mg/g_{DW-Colloids} (B1-B3). WFZ stands for water-level fluctuation zone.

II.2.2.3.2.5. Phosphorus

Fig. 44A illustrated that the quantity of water-mobilizable P (P_{WM}) extracted from bottom sediments varied longitudinally.

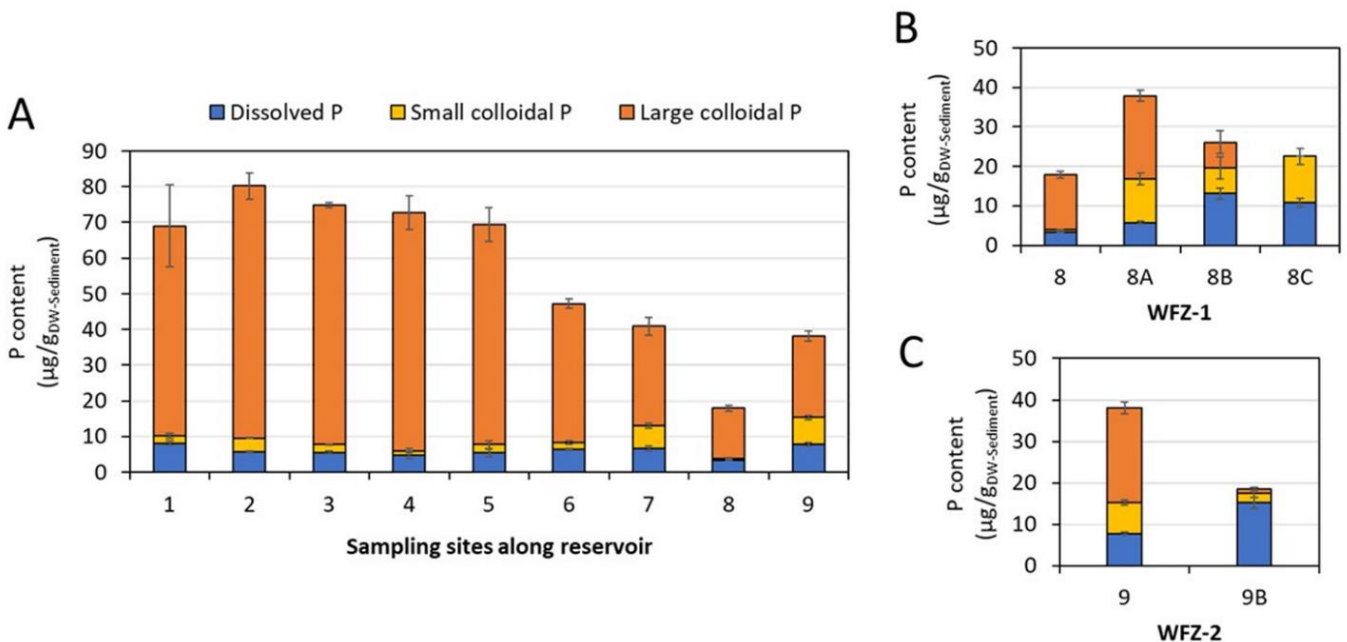


Figure 44. Distribution of water-mobilizable P: (A) along reservoir, (B) in WFZ-1 area and (C) in WFZ-2 area. WFZ stands for water-level fluctuation zone.

For bottom sediments, as observed for mass of colloids, higher concentrations of P_{WM} were observed in lacustrine regions ($74 \pm 6 \mu\text{g/g}_{DW-Sed}$, at sites 1 to 5) than in the tail and riverine regions ($43 \pm 4 \mu\text{g/g}_{DW-Sed}$, at sites 6, 7 and 9). The lowest P_{WM} level was recorded at site 8 ($15 \pm 1 \mu\text{g/g}_{DW-Sed}$) and the highest at site 2 ($71 \pm 4 \mu\text{g/g}_{DW-Sed}$).

The large colloidal P was the main component of P_{WM} (more than 75 %). In lacustrine region, bottom sediments (from site 1 to site 5) contained about $65 \pm 5 \mu\text{g/g}_{DW-Sed}$ of large colloidal P and it represented $88 \pm 4 \%$ of P_{WM} . Whereby, in the tail (sites 6 and 7), the amounts of large colloidal P released from bottom sediments were less important, at $33.4 \pm 7.8 \mu\text{g/g}_{DW-Sed}$ and represented approximately 77 % of P_{WM} . Lower large colloid P_{WM} levels were observed in riverine region (sites 8 and 9) than in lacustrine region. Between them, according to distinction in the context of the two sampling stations, P_{WM} at site 8 was composed by $14.0 \pm 0.9 \mu\text{g/g}_{DW-Sed}$ of large colloids (represented 78 % of P_{WM}), meanwhile this value increased by 1.6 time to reach $22.7 \pm 1.4 \mu\text{g/g}_{DW-Sed}$ at site 9 (represented 60 % of P_{WM}).

The difference in large colloids of P_{WM} between these two sampling sites was also observed for small/nano colloidal P. The amount of small/nano colloidal P_{WM} was $7.5 \pm 0.6 \mu\text{g/g}_{DW-Sed}$ at site 9 but was 15-time lower at site 8 ($0.51 \pm 0.07 \mu\text{g/g}_{DW-Sed}$, corresponding to 3 % of P_{WM}). The contents of small/nano colloidal P (0-0.2 μm) were lower for lacustrine bottom sediments ($2.2 \pm 0.9 \mu\text{g/g}_{DW-Sed}$, corresponds to $3 \pm 1 \%$ of P_{WM}) than in riverine bottom sediment ($7 \pm 1 \mu\text{g/g}_{DW-Sed}$, corresponding to $18 \pm 3 \%$ of P_{WM}), except for site 8.

The amount of dissolved P released from bottom sediment remained relatively constant longitudinally with an average of $6 \pm 1.5 \mu\text{g/g}_{DW-Sed}$ and accounted for less than 20 % of P_{WM} . Riverine bottom sediments (sites 8 and 9) contained higher proportion ($19 \pm 2 \%$) of dissolved P than lacustrine sediments (mean of 10 %, from site 1 to site 7).

For bank sediments, in WFZ-1 area, the amounts of P_{WM} were higher than bottom sediment (Fig. 44B). The frequently submerged sediment (site 8A) mobilized two-time higher P_{WM} levels ($38 \pm 1 \mu\text{g/g}_{DW-Sed}$) than bottom sediment ($18 \pm 1 \mu\text{g/g}_{DW-Sed}$), meanwhile the temporary and occasionally submerged sediment (sites 8B and 8C) also showed an increase in P_{WM} by 23 % and 32 %. In sediments exposed to air and desiccation, large colloidal P level was higher at site 8A for frequently submerged sediment (in WFZ-1 area) to reach $21 \pm 2 \mu\text{g/g}_{DW-Sed}$, but then it decreased with from site 8A to site 8C. In contrast, the amount of small/nano colloidal P was higher (factor of 10-25) compared to bottom sediment (site 8) to reach the maximum at $11.7 \pm 2.1 \mu\text{g/g}_{DW-Sed}$ at site 8C. In contrast, across the WFZ-2 (Fig. 44C), bank sediment mobilized 2 times lower P_{WM} amount compared to bottom sediment. The quantity of small/nano colloidal P was 3 times lower in sediment exposed to air (site 9B) than in bottom sediment (site 9). Similarly, a lower in large colloidal P amount was observed at site 9B (a factor of 21.5) in comparison to site 9.

In both WFZ-1 and WFZ-2, bank sediments released higher quantity of dissolved P than bottom sediments, especially by factor of 4 for the temporarily and occasionally submerged sediments (up to $13 \pm 3 \mu\text{g/g}_{DW-Sed}$) which represented up to 52 % (WFZ-1) and 83 % (WFZ-2) of P_{WM} .

III.2.2.4. Discussion

III.2.2.4.1. Sediment distribution and characteristics along the reservoir

The sedimentation of particles in an aquatic system is driven by various factors, including the characteristics of the sedimentary materials (especially size and density) as well as the hydrodynamic conditions. As expected, the presence of dam generated a noticeable spatial heterogeneity of sediment

in terms of grain size distribution and chemical composition. As shown in Fig. 40A, the sediments collected in all sites were fine grained, from 80 to 100 % corresponding to a fraction below 210 μm , but with very low content (less than 0.4 %) of clay (fraction below 2 μm). Such a low content of clay in comparison to natural lakes, where clay content often exceeds 50 % (Shah et al., 2019), is associated to specific hydrodynamic of dam reservoir, that is characterized by more river-like than lacustrine dynamic. The 13 sampled sediments presented heterogenous distribution of sand and silt fractions. Bottom sediments of lacustrine zone were siltier comparing to riverine zones and were dominated by 3-20 μm fraction (up to 60 %). Riverine bottom sediments as well as the sediments accumulated in the zone of water level fluctuation were sandy and dominated by 60-210 μm fraction (up to 50 %). Therefore, the median grain size (D50) of the bottom sediments deposited in the main channel (longitudinal axis) decreased from the riverine section toward the dam, that was related to a lower water flow velocity towards the dam (Rapin et al., 2020; Tang et al., 2018a). Therefore, the highest amount of the finest fractions (< 3 μm and 3-20 μm) was observed within the lacustrine zone of the reservoir (site 2). Sediments accumulated in the front of the dam (site 1) were coarser, possibly due to turbulent condition when water current approaches the dam (Bocaniov et al., 2014). Taking into account the obtained results, it was not possible to state whether the sediment deposited at the site 1 was depleted in the finest fraction due to the reservoir water outflow during the period of high-water level in the reservoir, or whether the sediments deposited at site 2 is enriched by the deposition of fine-grained sediment transported by tributary inflow. Champsanglard reservoir is characterized by two main tributaries whose the convergences are close to the sites 3 and 7. Since a confluence of two separated flows often plays an important role in sediment transport (Gualtieri et al., 2018; Best and Rhoads, 2008), we observed that the bottom sediments at site 2 and 6 (downstream of tributaries) contained higher, but not very significant contents of fine-grained particles (fraction below 20 μm). This may be due to the turbulent hydrodynamic condition in the boundary of mixing water (site 3 and 7), which induces shear stresses near or within the surface sediment and prevents the finest particles or low-density particles from settling down (Yuan et al., 2018). On the other hand, the bank erosion arising from the flow shear stress at the outside meander bends can remobilize sediment or transfer material to the channel, therefore, causing the delivery of particles downstream to be deposited in the further distance (Constantine et al., 2014). In our case, the entering of tributaries is located near meander bends, therefore, it is not possible to illustrate the appropriate function of each channel feature. Furthermore, it is remarkable that the inlets of two tributaries at sites 3 and 7 as well as fluctuation in water-level at the bank (sites 8 and 9) not significantly affected the grain size of the sediment.

The geochemistry of accumulated sediments was related to local geological context (mainly granitic). The sediments were rich in Al and Fe (averagely at 8.8 % and 5.8 % of total sedimentary mass respectively) but poor in Ca (at averagely 0.7 % of total sedimentary mass). Spatial distribution of sedimentary OM, Al, Fe Ca, Mg, Mn and P was more heterogenous compared to the size grain distribution (Fig. 40B). Lacustrine bottom sediments were organic rich (from 15 ± 1 % to 19 ± 1 % of total sedimentary mass) whereas riverine bottom sediments contained lower OM level (averagely 5.7 % of total sedimentary mass). This tendency was observed for all analyzed elements (Al, Fe and Ca, Mg, Mn and P) that is in concordance with observation of Rapin et al., (2020). Higher content of OM in reservoir bottom sediments could be a consequence of many overlapping factors. On the one hand, agricultural practices and low permeability of crystalline watershed substratum favor the loss of OM from soils while decreasing water velocity favors its accumulation within the reservoir. On the other hand, the hydrodynamic of the Champsanglard reservoir (16 m in deepest part) causes temporal stratification of water and oxycline (Rapin et al., 2019). The development of anoxic conditions slows down the mineralization of organic compounds favoring its accumulation. High primary production in the lacustrine zone may also contribute to increase the OM level in the sediments. In riverine section,

oxidative condition enhances OM mineralization and higher water flow promotes low density organic particles transport downstream.

Bank sediments in both water-level fluctuation zones of sites 8 and 9 showed higher contents of OM, Fe and Al than bottom sediments in these areas (Table 16). Especially at WFZ-1 (site 8), sedimentary OM content in bank sediments (18.1 ± 1.9 % and 22.1 ± 1.3 % at 8B and 8C respectively, Fig. 40B) were comparable and even higher than bottom sediment deposited within lacustrine region (from 14.2 to 19.3 %, Fig. 40B). Higher OM level in bank sediments compared to riverine bottom sediments was also observed at WFZ-2 (site 9). This indicate that bank sediments are the depositional area for organic matter along the channel. However, lower content of OM was observed in bank sediments at WFZ-2 (site 9B) compared to bank sediments at WFZ-1 (site 8B). In fact, site 9B is a deposition zone for materials transported by river and covered by a thin organic layer (accumulation of OM is mainly on the bank-top sediments) whereas site 8B is soil-like materials. In soils, pedogenic processes favor OM stabilization in the aggregates, that physically protect organic compounds from rapid decomposition by microorganisms (Berhe and Kleber, 2013) whereas in fluvial lateral banks, organic compounds are mainly stabilized mainly chemically by its adhesion to mineral particles (Martinez-Mena et al., 2019).

Inlets of both tributaries at site 3 and site 7 impacted mainly the contents of Fe and Al, with higher values in their associated downstream, at sites 2 and 6 respectively. Confluence of two separated flows is common phenomenon in river systems and often plays important role in sediment transport and thus in its composition (Gualtieri et al., 2018; Best and Rhoads, 2008). The turbulent hydrodynamic condition in this mixing interface causes the bed scouring and resuspension of bottom sediment, partially attributed to the delivery of low-density particles (as OM ones) downstream (Konsoer and Rhoads, 2014; Rhoads, 2014). Moreover, the counter downwelling helical flow can increase the hyporheic exchange and consequently enhance the adsorption of dissolved P (Yuan et al., 2018). Therefore, the reallocation of enriched sediment in downstream area of the confluence shall exhibit higher concentration of adsorbed P. As shown in Fig. 40C, the higher TP levels in sediment were observed in the downstream of tributary, in upstream transient zone (site 6) and at the confluent meander bends in lacustrine zone of the reservoir (site 2). The strongest positive correlation between the content of 3-20 μm sized sedimentary particles and the total of sedimentary P ($R^2 = 0.89$, Table 21) suggests that this particles size fraction is responsible for P accumulation within the sediments. This fraction also plays the role in the accumulation of Fe and Al (positive correlation between the content of 3-20 μm sized fraction and sedimentary Fe and Al was respectively $R^2 = -0.86$ and $R^2 = -0.92$). As shown in Table 21, much lower correlations were observed between sedimentary P, Fe and Al and the content of the 21 and 60 μm sized particles and negative correlations were revealed between sedimentary P, Fe and Al and 61-210 μm and > 211 μm sized particles content. It demonstrates different affinity of those elements to various size fractions of sediment. This in consequences could cause change in geochemistry of sediment during reallocation. In general, the longitudinal sharp observed increase in the quantity of both P, Fe and Al in surface sediment towards the dam is critically associated to the stronger affinity to fine-grained sediment and substantial settling of this sediment fraction in lacustrine region due to lower flow velocity, as well as mixing flow from tributary that additionally promotes P adsorption. This sharply increasing trend of P accumulation within surface sediment in the downstream of river impoundment has been long reported in many researches as consequences of low-velocity flow and/or P recycling by redox processes (Maavara et al., 2015; Van Cappellen and Maavara, 2016; Tang et al., 2018b; Rapin et al., 2019).

III.2.2.4.2. The distribution of water-mobilizable fraction along the main channel of dam reservoir: insight for bottom sediments.

III.2.2.4.2.1. Large/intermediate colloids

Our results demonstrated that all bottom sediments deposited in Champsanglard reservoir contained water-mobilizable colloids. Depending on site sampling, from 30 to 60 % of released colloids were in the size range of 220 – 1000 nm, and from 40 to 70 % were in the range below 220 nm which is often applied as a cutoff size for the evaluation of dissolved fraction (Fig. 41). Consequently, the colloids are intrinsic component of the sediment and should receive commensurate consideration in studying of water-mobilizable fraction. As shown in Fig. 4, the potential release of large colloids from sediments was heterogeneous at reservoir scale and was increased from the riverine section towards the dam, with the greatest release of large colloids found for the sediments accumulated at site 2 ($22.8 \pm 0.9 \text{ mg/g}_{\text{DW-Sed}}$). At this site, the sediment's potential to release large colloids was $22 \pm 5 \%$ and $29 \pm 6 \%$ higher compared to the sediments deposited downstream (site 1) and upstream (site 3) respectively. The sediment's potential to release large colloids was positively correlated with the content of fine-grained sediment particles and especially with for 3-20 μm fraction ($R^2 = 0.91$). Therefore, the size of sedimentary particles deposited along main channel of reservoir plays an important role in the amount of large colloids released from them.

The origin of sedimentary colloids in the aquatic system is usually twofold. On one hand, colloids are continuously delivered to surface sediment by the settling from column water. Gravitational settling is especially observed for the colloids with sufficient size and density that can settle during long residence time, and for the colloids able to flocculate/aggregate to form larger particles. However, it has been demonstrated that non perturbed natural water, the size and physico-chemical properties of colloids are instable in time and their transformation often take place after 2 days due to aggregation, biological and chemical reactions (Lead et al., 1997). On the other hand, colloids can be generated within the sediment and/or at sediment-water interface. The generation of new colloids within the sediment could be observed when anoxic condition develops in sublayer and initiate a series of reactions that can disintegrate sedimentary aggregates and/or while the infiltration of oxic water in anoxic sediment cause the precipitation of dissolved species, as metals oxy(hydr)oxides (Amirtharajah and Raveendran, 1993; Henderson et al., 2012; Liu et al., 2013).

Thus, the lower release of large colloids in the riverine part of Champsanglard reservoir (from site 6 to site 9) can be explained by the higher-velocity flow in steep part of the channel that involves in-channel bottom erosion and thus the redistribution of finer sediments downstream (Pacina et al., 2020). This part of reservoir is characterized by the presence of coarser sediment compared to lacustrine part of reservoir (Fig. 40A) and characterized by lower content of OM, Al and Fe, especially at site 8 and 9 (Fig. 40B). Meanwhile, lacustrine sediments of the reservoir were characterized by a higher potential colloid release, though, the amount of potentially mobilizable large colloids from bottom sediments was unevenly distributed with significant impact by tributaries. Both tributary convergence (sites 3 and 7) seems to take part in the increase of water-mobilizable colloids in downstream sediment (sites 2 and 6). As described above, the presence of two tributaries had an impact on the quality of deposited sediments at site 2 and 6 (downstream of tributaries); these sediments contained slightly higher content of fine-grained particles (fraction below 20 μm) as well as higher quantities of Al and Fe (Fig. 40A and 40B) but lower quantity of OM. It was because the finest particles or low-density particles could not settle down in more turbulent hydrodynamic condition imposed by mixing water (Yuan et al. 2018). Furthermore, the bank erosion (*e.g.* at the outside meander bends) and/or bottom sediment scouring can remobilize colloids causing its delivery and settle downstream (Konsoer and Rhoads, 2014; Constantine

et al., 2014). Thus, the significant occurrence of large colloids was observed in the deeper region of reservoir and in the downstream of tributary junctions and meander bends.

Chemical composition of released large colloids and the fraction below 0.2 μm was related to the composition of sediment. Because the chemical composition of sediments varied spatially (Fig. 40), we compared the chemical composition of large colloids (Table 19) to the chemical composition of the sediment (Table 16) to evaluate the effect of heterogeneous sediment distribution on the chemistry of released colloids. For each analyzed element, we calculated the ratio (R) corresponding to the amount of a given element in a large colloidal fraction (expressed in mg/g of dry weight colloids, Table 19) to the amount of a given element in the sediment (mg/g of dry weight sediment, Table 16). At the same sampling site and for an element, if the R was around 1, the concentration of this element in large colloids and deposited sediment was comparable. If the $R > 1$ or $R < 1$, the concentration of the element in large colloids is respectively higher or lower compared to the sediment and indicate an enrichment or an impoverishment of this element in large colloids. As shown in Table 20, the R varied spatially and differently for each element. The R_{Ca} and R_{P} decreased toward the dam and were about 10.9 - 1.2 for Ca and 7.5 - 1.7 for P. The R_{Fe} and R_{Al} also decreased toward the dam however varied from 1.8 to 0.6 for Fe and from 2.5 to 0.7 for Al. The R_{OC} and R_{Mg} were always lower than 1, except at site 9. It demonstrated that the quality of sediment is not the sole factor controlling the chemical composition of water mobilizable colloids, and that various complex interactions and transformations operating at different deposit sites impact their chemical and physical characteristics. For example, the lowest R_{OC} at tributary junctions (sites 3 and 7) and meander (site 6) could be related to preferential removal or non-deposition of lesser density organic colloids due to more turbulent flow. The low amount of organic matter can lower the flocculation/aggregation between colloids; thus, the inorganic colloids can be easily resuspended under turbulent condition and be transported downstream. Among all considered elements, none of them showed correlation between colloidal and sedimentary concentrations (Table 20), except for Ca which performed a correlation coefficient of - 0.61. This result confirmed that there might be other factors controlling chemical nature of sedimentary colloids rather than inheriting characteristics from sediment. For instance, the general decline of R_{Ca} from the upstream to the dam could be associated the formation of Ca-rich aggregates and its burial in the sediment. Meanwhile, in lacustrine zone, the low and variable R_{Fe} could be associated to Fe recycling under redox reactions, whereas in the more oxygenated riverine water is R_{Fe} is higher than 1.

As shown in Table 19, difference in concentration of P in large colloids between lacustrine sediments and upstream riverine sediments suggests that the reactivity of large colloids toward P was affected by the longitudinal deposition of sediment or river impoundment. Colloids contained higher P content from site 3 to site 6 in lacustrine region and highest P contents in riverine region. The richer in P of colloids in the downstream of tributary at site 7 could be due to the aeration at mixing confluence that increase affinity of P to colloids and these P-rich colloids were transported to further distance. At riverine region, the high-energy flow and fully aerated sediment can also result in higher P sorption onto colloids. The characteristics of large colloids are not uniform along the length of reservoir. Across the flatter and lower-energy flow regions, P performed strong association in large colloids to organic carbon ($R^2 = 0.73$) and Al, as with surface of aluminosilicates ($R^2 = 0.84$), but low correlation to Fe ($R^2 = 0.48$) (Table 22). Meanwhile, the large colloidal P at turbulent regions, such as high-energy upstream flow, confluences and meanders, contained heterogeneous inorganic composition but shows lower organic content (Figures 44A and 40-B1).

Table 20. Elemental colloid-sediment ratio (R) corresponding to the amount of an element in a large colloidal fraction (expressed in mg/g of dry weight colloids, Table 19) to the amount of a given element in the sediment (mg/g of dry weight sediment, Table 16).

*ND: not detected

Sampling site	P		OM		Fe		Al		Ca		Mg		Mn	
	Elemental colloid - sediment ratio													
	Mean	SD	Mean	SD	Mean	SD	Mean	SD	Mean	SD	Mean	SD	Mean	SD
1	1.76	0.31	0.68	0.09	0.80	0.06	0.81	0.05	1.98	0.16	0.55	0.03	0.54	0.05
2	1.69	0.08	0.66	0.12	0.60	0.04	0.89	0.27	1.20	0.25	0.43	0.08	0.47	0.04
3	2.92	0.28	0.18	0.01	0.89	0.06	0.99	0.24	1.84	0.48	0.58	0.04	0.47	0.19
4	2.87	0.18	0.49	0.08	0.72	0.02	0.72	0.01	1.57	0.14	0.45	0.10	0.25	0.03
5	3.28	0.40	0.56	0.17	0.64	0.12	0.66	0.13	1.19	0.24	0.38	0.05	0.29	0.04
6	3.36	0.43	0.21	0.05	0.98	0.17	1.29	0.20	4.00	1.25	0.69	0.13	0.58	0.10
7	3.85	0.14	0.18	0.06	1.19	0.13	1.47	0.30	4.72	1.68	1.57	0.49	0.90	1.64
8	7.41	1.27	0.53	0.37	1.65	0.11	2.47	0.30	10.88	2.80	1.74	0.19	ND	ND
9	6.84	0.96	2.35	0.59	1.76	0.20	2.29	0.18	11.07	2.24	1.15	0.16	1.46	0.34
At WFZ-1														
8	7.41	1.27	0.53	0.37	1.65	0.11	2.47	0.30	10.88	2.80	1.74	0.19	ND	ND
8A	4.78	0.57	0.61	0.05	1.72	0.12	2.42	0.27	1.95	0.69	0.57	0.07	0.85	0.22
8B	0.44	0.17	0.23	0.06	0.96	0.05	1.56	0.08	0.79	0.12	0.58	0.09	0.61	0.12
8C	ND	ND	0.15	0.05	0.80	0.09	1.53	0.26	0.96	0.31	0.62	0.17	0.71	0.12
At WFZ-2														
9	6.84	0.96	0.22	0.08	1.76	0.20	2.29	0.18	11.07	2.24	1.15	0.16	1.46	0.34
9B	0.22	0.04	0.71	0.35	1.34	0.15	1.57	0.17	4.19	0.66	0.99	0.18	0.52	0.10

III.2.2.4.2.1. Phosphorus

Phosphorous mobilized in fraction below 1 μm (P_{WM}) represented from 3 to 6 % of the total sedimentary P. Strong positive correlation between P_{WM} and total sedimentary P ($R^2 = 0.81$) as well as between P_{WM} and the content of fine grained (3-20 μm) sedimentary particles ($R^2 = 0.89$) confirm high affinity of P to finer sediment (Lopez et al., 2009; Rapin et al., 2020). In bottom sediments, the mass of P_{WM} increased towards the dam and higher content of P_{WM} in lacustrine sediments compared to upstream riverine sediments was associated to lower water flow at this part of the reservoir. As shown in Fig. 44A, P_{WM} in bottom sediments was composed of large P-colloids, small/nano P-colloids, dissolved P. Large colloidal P ($65 \pm 5 \mu\text{g/g}_{\text{DW-Sed}}$) was the principal component in P_{WM} fraction and accounted for approximately 80 % of P_{WM} in lacustrine part of reservoir. The level of dissolved P was minor but relatively constant ($6 \pm 1.5 \mu\text{g/g}_{\text{DW-Sed}}$) across the longitudinal channel of reservoir. The content of small/nano P-colloid ($< 0.2 \mu\text{m}$) was lower ($2.2 \pm 0.9 \mu\text{g/g}_{\text{DW-Sed}}$) than dissolved P in lacustrine part of reservoir, but it exhibited important augmentation in the upstream riverine area (up to $7 \pm 1 \mu\text{g/g}_{\text{DW-Sed}}$), except site 8. The uneven distribution within P_{WM} in the sediments (large P-colloids, small/nano P-colloids, dissolved P) may be associated to the morphological characteristics of reservoir and the process occurring within the deposited reservoir. Riverine region of the reservoir is shallower, has stronger water flow and coarser sedimentary particles than in the lacustrine region (Fig. 40A), thus riverine sediments are more oxygenated than in lacustrine region. Oxygen can prevent Fe-oxy(hydr)oxides from reductive dissolution, but also it can accelerate the mineralization of organic matter and induce the release of associated P (Orihel et al., 2017). Thus, higher content of small/nano P-colloids in riverine bottom sediments could be explained by hydrolysis of organic particles that induce transfer from large colloids to small/nano colloids. Meanwhile, in lacustrine zone, where anoxic condition can develop in deeper bottom sediment, OM degradation is limited and P could be recycled by redox transformation of redox-sensible elements, for example Fe, S (Rapin et al., 2019). The Fe cycling in couple with OM can result in release and then aggregation/flocculation of colloidal P towards larger size (see Part III.3.2).

At site 8, the P_{WM} was very low, and dominated by the release of dissolved and large colloidal P whereas the fraction of small/nano colloidal P became insignificant. This distinctive P_{WM} composition of site 8 could be related to channel morphology. Site 8 is located near a meander bend and thus characterized by more turbulent water flow than at upstream site 9 and downstream site 7. At the same time, large/intermediate colloids from both site 8 and site 9 contained higher P concentration than those in lacustrine sediments (Table 19). This higher P affinity of riverine sedimentary colloids probably caused by the lower OM contents. At low OM content, the surface charge of minerals can become more positive because of lower surface complexation with negatively charged organic compounds, therefore, increase P sorption.

On the whole, bottom sediments accumulated in the lacustrine zone of the reservoir typically accommodated stronger potential to release P_{WM} in colloidal form, meanwhile the sediment deposited in riverine section attributed a much lower potential to release P_{WM} but the released P_{WM} were composed of increasing proportion of the more bioavailable P: dissolved and small/nano colloidal forms.

III.2.2.4.3. Potential of bank sediment affected by water level fluctuation to release of water-mobilizable colloids and phosphorus

III.2.2.4.3.1. Large/intermediate colloids

At both water level fluctuation zones the potential of sediment to release large/intermediate colloids increased from permanently submerged to occasionally submerged sediment (1.7 to 6-fold increase in WFZ-2 and WFZ-1 respectively, Figs. 42B and 42C). For the bottom sediments accumulated in lacustrine part of the reservoir, the potential of the sediments to release colloids was positively correlated with the content of fine-grained materials. In the case of bank sediments, this correlation was very low ($R^2 = 0.06$) because fine-grained materials either did not have accumulation advantage toward the riverbank as shown in Fig. 40A or were impacted by changing in water-level. Although the distribution of water flow velocity cross channel is uneven and generally slower or stagnant at the bank (Yang et al., 2019); the sediment accumulated at WFZ-1 and WFZ-2 area revealed a very comparable particle size distribution. Therefore, increased potential of sediments accumulated towards the riverbank to release large colloids cannot be explained by the accumulation of finer sedimentary materials but rather as the result of repeated drying and rewetting of bank sediment related to the water level fluctuation. It has been shown for example, that in the case of soils, when water withdrawn during the first drying and wetting event, the aggregate stability is lowered by disruption from macroaggregates to microaggregates, whereas repetitive dry-wet cycles increase macroaggregates stability (Denef et al., 2001). In the case of Champsanglard reservoir, during the low flow period, bank sediments are exposed to the air and generally partially dried before their immersion during the next high flow. The drying process for short period of less than 2.5 (Mohanty et al., 2015) or 11 days (Majdalani et al., 2008) depending on sediment characteristics can initially promote colloids mobilization during re-inundation through the enlarged pore walls (Majdalani et al., 2008; Mohanty et al., 2015). By contrast, the extended drying times could cause precipitation of dissolved species, binding colloids together or to the sediment pore, thus the bank sediments subjected to longer exposure period are expected to have lower stock of mobilizable colloids (Bartlett and James, 1980; Majdalani et al., 2008; Munkholm and Kay, 2002). However, in Champsanglard system, the bank sediments were regularly submerged by river and/or surface runoff from surrounding catchment. The time of air exposure in this context shall be insufficient to reach the critical duration of colloid immobilization, but still be sufficient for pore wall expansion and subsequently favor colloid mobilization. Thus, the bank sediments in upstream riverine section remain a source of colloids in comparable concentration with lacustrine bottom sediments. On the whole, riverine sediments deposited at the bank and affected by water level fluctuation, contained important

amount of water mobilizable large colloids but exhibit no significant difference (considering important standard deviation) in colloid size distribution compared to permanently submerged bottom sediments.

In both WFZ-1 and WFZ-2 areas, according to chemical composition (Table 19, Fig. 43-A2 and 43-A3), large colloids accumulated in bank sediments were more organic but their content in Fe, Al, and Mn but they were poorer in P compared to bottom sediment. For both sites, the chemistry of recovered large colloids did not reflect the variation of the chemistry of deposited sediments (Table 20). At the WFZ-1 area, recovered colloids from all sediments were enriched in Al ($R > 1$) whereas Al-enrichment factor decreased toward the soil. The colloids recovered from permanently (site 8) and frequently submerged (site 8A) sediments were enriched in P, Fe, Al and Ca, and the colloids recovered from occasionally submerged sediments (site 8B and 8C) were impoverished in all (except Al) analyzed elements. It demonstrates that various processes are responsible for sedimentary colloids generation and reveals complex interactions between the colloids and other component of sediments (particles, colloids, dissolved fraction). For example, the sediment accumulated on the site 8B and 8C were characterized by lower pH, that could be related to increased microbial activity and the production of microbial metabolites. At site 8B, the lowest Ca level (Table 19) was recorded that was explained by low pH value (5.3, Fig. 40C) observed at this sampling station due to the fact that Ca precipitates dissolved when pH gets lower than 5.5 (Morse et al., 2007). At the site 8A, higher concentrations of Fe and Al in colloids (Table 19) could be due to the formation of Fe and Al hydroxides at site 8A (pH of 6.6) from the runoff of ionic species present at site 8B (pH of 5.3).

At the WFZ-2 area, at site 9B, OC concentration in large colloids was higher than in bottom sediment, whereas other elements contents were lower (Table 19), except for Mg (similar levels). The higher OC concentration could be explained by the fine organic layer observed at this sampling station.

III.2.2.4.3.2. Phosphorus

The fluctuation in water-level at the upstream riverine section influenced the quantity and the forms of P_{WM} . At WFZ-1, the bank sediments impacted by water-level fluctuation released more P_{WM} compared to bottom sediment (Fig. 44-B). The highest release of P_{WM} took place for frequently submerged sediment (site 8A). Among bank sediments, the level of large P-colloids in P_{WM} decreased toward the land (Fig. 44-B). In contrast, an increase in the level of P in fraction inferior to 0.2 μm (including small/nano colloidal and dissolved P) towards the land was observed (Fig. 44-B). This trend was also noticed in the study of Blackwell et al., (2009) when sediment was subjected to faster rewetting rate. In our case, the frequently submerged sediment (site 8A) located at a place receiving more frequent and rapid immersion compared to the sites 8B and 8C presented therefore the highest quantity of P_{WM} . The study of Blackwell et al., (2009) also showed that with slower rewetting time, phosphate can be re-adsorbed on soil, at the same time, the microorganism can revive and uptake higher P amount, thus causing decline in P concentration in fraction below 0.45 μm . At sites 8B and 8C, lower P_{WM} amounts were noted compared to site 8A. As presented in Fig. 40C, sediments at site 8B and 8C contained higher total sedimentary P level than site 8A, which could indicate higher P sorption at sites 8B and 8C. However, P_{WM} decline was mainly associated to a strong decline of large P-colloids and P_{WM} became dominated by dissolved and small colloidal P. Therefore, it is likely that there were other factors impacting on the transfer of large colloidal P to small/nano colloidal and dissolved P.

At WFZ-2 area, we observed the same trends, the quantity of P_{WM} decreased toward the land, together with large colloidal P whereas the amount of dissolved P increased notably (Fig. 44-C).

Frequent water fluctuation in WFZ involves in a series of biogeochemical processes, including microbial cell lysis during rewetting upon osmotic stress, the mineralization of organic P during drying phase (Turner and Haygarth, 2001) and non-microbial processes involved in transformation of redox- and pH-sensitive species (as Fe or Mn) with their associated P (Forber et al., 2017). The introduction of oxygen during prolonged drying period increases the sorption of phosphate on positively charged minerals (mainly Fe oxy(hydr)oxides) and improves the association of P to sedimentary colloids. However, in our cases, the concentration of Fe in large colloids decreased when sediment became exposed to the air (Figs. 43-B2 and 43-B3) and this lower content of Fe- could limit the adsorption of P to large colloids and probably to small/nano colloids. Furthermore, variation in the pattern and intensity of dry-wet events could cause the mineralogical transformation and thus impact on P sorption capacity (Zhang, Lin, and Werner, 2003). During drying, the crystallinity of Fe (hydr)oxides may increase, hence, the decrease in quantity of P associated to colloids can be related to irreversible loss of amorphous Fe minerals upon re-wetting of sediment (de Vicente et al., 2010; Darke and Walbridge, 2000). The poorly crystalline Fe (hydr)oxides often have a much larger and more reactive surface area than crystalline one (Duiker et al., 2003). As a consequence, the release of crystalline colloidal Fe mineral in sediment impacted by water-level fluctuation contributes to the increase of colloid quantity but with lower P amount in these colloids.

In fraction smaller than 0.2 μm , the increase in P and OC from sites 8A to 8C was observed and together with a significant positive correlation between them ($R^2 = 0.89$) could be explained by hydrolysis of organic matter. Furthermore, alternation of drying and rewetting had been shown to stimulate the indirect release of inorganic and organic P via microbial cell lysis (Turner and Haygarth, 2001) and the disruption of OC-Fe/ OC-Al associations during OM mineralization (Blackwell et al., 2009). In the case of soils, dry-wet events were claimed to cause the increase in nutrients availability transferring from soil leachate (Blackwell et al., 2009; Xu et al., 2011), similar observation could occur in sediment suggesting increasing transfer of P to the water bodies and migration of bioavailable P to the downstream flow (Forber et al., 2017; de Vicente et al., 2010).

In addition, higher quantity of small/nano P-colloids was observed at WFZ-1 (Fig. 44-B) for those bank sediments impacted by changes in water-level. The P enrichment in small/nano colloidal fraction could be due to the increase in calcium phosphate, as an increase of calcium amount was recorded in fraction smaller than 0.2 μm (Table 17) and a positive correlation ($R^2 = 0.65$) between P and Ca in this fraction was noted. The amount of Ca in fraction below 0.2 μm raised from 0.04 ± 0.01 to 0.10 ± 0.01 $\text{mg/g}_{\text{DW-Sediment}}$ when moving from the deeper channel to the bank (Table 17). The drying of sediment can promote degradation of organic matter and release of organic acids (sites 8B and 8C). Eventually, lower pH in bank sediment could drive the dissolution of Ca bridge, releasing P in forms of dissolved inorganic phosphates or in form of small/nano colloids. The physical process of slaking fortified in extending drying period can be another important mechanism in the formation of small/nano colloidal P as the disruption of sediment aggregate structure and integrity.

III.2.2.5. Conclusion

Colloids are intrinsic component of reservoir sediment and contribute up to 2.3 % of sediment mass. A 30-60 % of released colloids were in the size of large colloids 0.22-1 μm and thus this fraction should be taken into accounts when studying the behaviour of colloidal P. The potential of sediment to release colloids increased from river towards the dam and was positively correlated to distribution of fine-grained sediment. Lower release potential of colloids from riverine sediment is due to higher-energy flow that caused in-channel erosion and involved in transport of the finest particle including colloids downstream. This potential of colloid release was found to be higher in lacustrine region but was

unevenly distributed according to impact of tributary in which the role of mixing water at confluence may involve in both migration of low-density colloids downstream and delivery of bank eroded materials.

Chemical composition of colloids was related to local geological context with elevated contents of Al, Fe and OC and was controlled by geochemical processes rather than inheriting sedimentary properties. Colloids were enriched in Ca and P but poorer in OC and Mn than sediment particles though out the reservoir. The colloids recovered from riverine sediments were richer in P, Fe and Ca meanwhile the colloids recovered from lacustrine sediments were poorer in those elements, which could be related to the annual development of anoxic condition in deeper water .

The amount of P associated to colloids contributed up to 6 % of total sedimentary P and 80 % of water-mobilizable P. The variability of water-mobilizable P was uneven in sediments along reservoir and associated to channel morphology. Oxygenated riverine sediments contained higher amount of small/nano P-colloids, whereas lacustrine sediments were characterized by large P-colloids.

The water-level fluctuation was shown to impact on potential of bank sediments to release colloids as well as water-mobilizable P. Longer drying time and slower re-wetting of bank sediments resulted in significant elevation of water-mobilizable colloids to reach about 1.5 % of sediment mass which was comparable to the value obtained in lacustrine sediments. Large colloids found in bank sediments have lower P affinity than bottom sediment at the same latitude and also poorer in Fe, Al and Ca which could be a consequence of sediment drying and rewetting. Across the water-level fluctuation zones, high amounts of dissolved P and small/nano P-colloids in riverine bank sediments can be easily transferred from the sediment to channel flow during high water flow, supporting bio-uptake in the further distance of reservoir and causing higher potential of algal bloom in lacustrine zone. This finding could illustrate that a P reserve in bank sediments is another source of bioavailable P inside dam reservoir system in addition to the currently well-known catchment input and internal load of P.

Acknowledgement

This work was financially supported thanks to the France's Nouvelle-Aquitaine Regional Council, the EDF electric utility company and the "Dam and Water Quality" Chair of Excellence with the "University of Limoges Partnership Foundation".

Supplementary data

Table 21. Correlation coefficient (R^2) between elemental concentrations in sediment and various sediment size fractions.

Grain size fraction	P	Fe	Al	Ca	Mg	Mn	OM
< 3 μm	0.66	0.64	0.66	0.23	0.49	0.60	0.06
3-20 μm	0.89	0.86	0.91	0.43	0.73	0.73	0.12
21-60 μm	0.41	0.44	0.52	0.56	0.44	0.20	0.32
61-210 μm	-0.85	-0.86	0.92	-0.53	-0.76	-0.65	-0.22
> 211 μm	-0.73	-0.75	0.82	-0.66	-0.70	-0.51	-0.32

Table 22. Correlation coefficient (R^2) between element concentrations in large colloids (0.2 – 1 μm) for lacustrine regions (accounted for sites 1, 2, 4, 5 and excluded impacts of tributary entrance at site 3).

	<i>P</i>	<i>Fe</i>	<i>Al</i>	<i>Ca</i>	<i>Mn</i>	<i>Mg</i>	<i>OC</i>
P	1						
Fe	0.479	1					
Al	0.839	0.828	1				
Ca	0.18	0.888	0.504	1			
Mn	0.345	0.908	0.801	0.68693	1		
Mg	0.563	0.991	0.85	0.88403	0.85	1	
OC	0.73	0.785	0.969	0.41292	0.86	0.777	1

III.2.3. Conclusion

The study of the distribution of water mobilizable colloid and P, along the dam reservoir of Champsanglard, considering the impact of tributary and water fluctuation zones, leads to the following conclusions:

- Large colloids (0.2-1 μm) are an intrinsic component of reservoir sediments that can constitute up to 2.3 % of the sediment mass.
- Distribution of colloids in reservoir sediments largely depends on channel morphology and hydrodynamics.
- The content of water mobilizable colloids was positively correlated with fine-grained fraction of sediments (fraction < 20 μm).
- Chemical composition of colloids is not associated to chemical composition of sediment.
- The amount of P associated to colloids represent up to 6 % of total sedimentary P and 80% of water-mobilizable P.
- Sediments accumulated at the bottom of lacustrine area of the reservoir contain a higher content of large colloids, but lower concentration of associated P than in riverine region.
- Tributary inlets contribute to the redistribution of large colloids downstream, especially low-density and organic colloids, but did not appear to have a significantly effect on water-mobilizable P.
- Bank sediments accumulated in the zone of water-level fluctuations contained a higher amount of large colloids than corresponding bottom sediments. However, the large colloids in bank sediments contained lower concentration of P than in bottom sediments.
- Bank sediment exposed to repeated drying and rewetting have a strong risk to release the more bioavailable form of P (dissolved phosphates and small/nano colloids).

III.3. Effects of redox oscillation on the release of dissolved and colloidal phosphorus

III.3.1. Introduction

One of the factors controlling sedimentary P mobility in aquatic systems is redox condition. It is commonly known that anoxic condition promotes the release of dissolved P from sediment to water column (Niirnberg, 1994; Golterman, 2001). However, in many studies, the evaluation of dissolved P release was based on a conventional measurement of soluble reactive P (SRP) in fraction below 0.45 μm or 0.2 μm . This evaluation is not so accurate for two reasons. In one hand, the SRP is not only constituted of truly dissolved P but also contain a part of colloidal P (Shand et al., 2000; Filella et al., 2006; Zang et al., 2013). This could lead to misunderstanding of P mobility and possible overestimation of the internal flux of truly dissolved P to receiving water. In other hand, the SRP does not take into account the colloidal fraction in the range of 0.2 or 0.45 – 1 μm . Though, as truly dissolved P, colloids could be considered as a source of bioavailable P (Montalvo et al., 2015) and has been proved to be an efficient bearing phase of P in various environments such as soil and surface water (Gottselig et al., 2014; Bol et al., 2016; Gu et al., 2018).

In large reservoirs, according to temperature stratification in warm season, anoxia is often established in the bottom of lacustrine zone. Redox variations are responsible for alter redox-sensitive species such as iron/manganese (mainly included in oxy(hydr)oxides), organic matter decomposition and microbial activity and thus strongly impact on P mobility in bottom sediments (Rapin et al., 2019; Orihel et al., 2017, Parsons et al., 2017; Schönbrunner et al., 2012; Smith et al., 2011). As presented in Part III.2, the bottom sediments in lacustrine region of Champsanglard reservoir contained about 4-time higher colloid quantity in concomitant of 3-time higher water-mobilizable P than in riverine region but lower in the content of small/nano colloidal P. This finding highlights the possible role of anoxia in addition to channel hydrodynamics on distribution of water-mobilizable P in dam reservoir.

Therefore, this part of the thesis devoted to examining the mobility and behavior of P in association with colloids under redox dynamic condition. The following questions are attempted to be answered in this part:

- Does anoxic condition mobilize of colloidal P? If yes, how much of sedimentary P can be released under the form of colloidal P? What is the size class of released colloidal P in anoxic condition?
- Does oxic condition induce colloidal P mobilization? If yes, how much of sedimentary P can be released in colloidal form? What is the size class of released colloidal P?
- What is the key parameter influencing the mobility of colloidal P in changing redox conditions?

To do this, a surface sediment was collected in the deepest part of Champsanglard reservoir and subjected to laboratory incubation of oscillating oxic/anoxic/oxic condition. During the incubation, special attention was paid to the evolution of solution in term of physico-chemical parameters (pH, Eh, alkalinity, P, Fe, and OC) as well as size distribution of water-mobilizable fraction in 5 subfractions: large colloids (0.45-1 μm), intermediate colloids (0.2-0.45 μm), small colloids (300 kDa-0.2 μm), nano colloids (10-300 kDa) and truly dissolved fraction (below 10 kDa). This part was presented in form of an article to be submitted to the journal “Environmental Science and Technology”. Besides, an additional part was given to tackle the limitation in the use of freeze-drying as a pretreatment for colloid quantification.

III.3.2. How does anoxia promote mobilization of P-bearing colloids from dam reservoir sediment?

Article to be submitted to Journal Environmental Science and Technology.

Ngoc-Diep Nguyen, Marion Rabiet, Malgorzata Grybos, Véronique Deluchat

Limoges University, PEIRENE EA 7500, 123 Av. Albert Thomas, 87060 Limoges Cedex, France

Abstracts:

Purpose: In reservoir context, anoxia often developed at bottom sediment and has been proved to induce mobilization of dissolved phosphorus (P) to overlying water. Considering recent evidence on the important role of colloids in transportation of P in various environments, including soils solution and surface waters, and their bioavailability above particulate fraction, present study aimed to investigate the behavior of colloidal P in alternative oxic-anoxic-oxic conditions and elucidate possible processes that could be involved in colloidal P dynamic in water-sediment interface.

Principle results: The development of anoxic condition caused an important liberation of water-mobilizable P (below 1 μm) from sediment to water, whereas previous oxic condition contributed very fewer. The released P was composed mainly by colloidal form (about 90 % of water-mobilizable P). Truly dissolved P was released at the beginning of anoxia but then decreased over time. The main factors controlling dynamic of water-mobilizable P was (i) iron reductive dissolution that mobilizes both dissolved and colloidal P, (ii) organic matter release that involves in stability of released colloids. A half of water-mobilizable P liberated in anoxia stayed stable in further oxic condition and composed strictly of colloidal P, in the fraction 300 kDa-0.45 μm .

Major message: Anoxia induced a higher mobilization of colloidal P in comparison to truly dissolved P and a major portion of them remained in suspension when condition became oxygenated.

Keywords: colloid, phosphorus, sediment, redox, anoxic release, dam reservoir, mobility

III.3.2.1. Introduction

Phosphorus (P) has been long considered as a limiting nutrient for primary production in most of inland waters and thus is a critical factor to manage eutrophication in many freshwater systems (Conley et al., 2009; Schindler et al., 2016; Le Moal et al., 2019). With exponentially growing human population, the anthropogenic input of P intensified and responded in nuisance algal blooms, deteriorated freshwater ecosystems in particular lake system that are particularly sensible to eutrophication. Despite all the recent efforts in controlling P discharges since 2000 (Poikane et al., 2019) in order to reach the objectives of European environmental legislation, the P concentration remains high in aquatic system and continue to cause eutrophication in reservoirs. An explanation of this observation is that reservoirs have sequestered gradually since long time nutrients in accumulated sediment, which in turn can become a source of P for reservoir surface water, limiting the effectiveness of all regulatory measures (Nürnberg et al., 2012; Maavara et al., 2015; North et al., 2015).

Since then, many research groups have focused their attention on the P mobility at sediment-water interface (Parsons et al., 2017; Cavalcante et al., 2018; Rapin et al., 2019), showing that sediment–water P

interactions are controlled by several biogeochemical processes, including dissolution/precipitation, sorption/desorption and microbial organic matter (OM) mineralization/biotic assimilation, dependent on surrounding bio-physicochemical conditions (Anschutz et al., 2007; Smith et al., 2011; Orihel et al., 2017). P mobility is closely coupled to biogeochemical cycles of redox sensitive elements, in particular iron, organic carbon, but also sulfur (Søndergaard et al., 2003; Orihel et al., 2017; Cavalcante et al., 2018; Dadi et al., 2020). It has been nowadays widely demonstrated that the anoxic condition induced by complex hydrodynamic behavior of the lake and flow management enhances release of phosphorus from sediment through dissolution of and desorption from associated organo-iron phases. Subsequently released P can migrate to overlying water via physical or bioturbation-induced diffusion (Horppila and Nurminen, 2003; Zhang et al., 2019; Gautreau et al., 2020).

In most cases, study focusing on phosphorus cycle in environment (river, soil or reservoir contexts) used the classical soluble reactive P (SRP) measured by the molybdenum blue method in the fraction passing through a 0.45 μm or 0.2 μm filter (Björkman and Karl, 2003; Dupas et al., 2018; Dadi et al., 2020). Indeed, hitherto, SRP is usually considered to be the only bioavailable P species (Šimek et al., 2006; Kwak et al., 2018; Jin et al., 2019;). However, this view neglects an important set of interactions that occur between P and very highly mobile particles, colloids, limiting the understanding of phosphorus transport. Colloids with size range between 1 nm – 1 μm are small enough not to be subjected to gravitational forces, and their electrostatic charges induce repulsion that maintain them to be dispersed in water column (Mahmood et al., 2014). Therefore, colloids are highly mobile in aquatic environment and have been shown to be effective sorbents of trace/nutrient elements owing to their high specific surface area and charge density (Buffle and Leppard, 1995; Bol et al., 2016). Recent studies in various contexts (soil solution, soil water extract, lake freshwater) highlighted the important role of colloids as efficient carriers of P and potentially bioavailable P form (Reynolds and Davies, 2001; Hens and Merckx, 2002; Filella et al., 2006; Sun et al., 2007). For instance, in soil context, colloid-facilitated transport is recognized as an important pathway for the loss of soil phosphorus in agricultural systems (Jiang et al., 2015; Missong et al., 2018; Gu et al., 2018). Thus, in some cases, colloidal P can represent up to 70 % of total P in operationally defined dissolved fraction of soil solution (below 0.45 μm) (Filella et al., 2006; Blackwell et al., 2009; Henderson et al., 2012; Gu et al., 2018). These findings suggest that colloidal fraction is of preeminent importance in controlling the transport of phosphorus in aquatic system and in particular in lake system where the potential of P-bearing colloids to be produced and released from sediment are not well known.

The cause of colloid mobilization is complex according to their sensitive response to various laboratory and environmental conditions, though, main driven factors include pH, redox and ionic strength (VandeVoort et al., 2013). In natural environment, depending on the size-based fraction, colloidal P can be associated with iron, calcium, organic matter or clay mineral (Jiang et al., 2015; Baken et al., 2016; Missong et al., 2016; Gottselig et al., 2017a, 2017b). The variation in carrier phase of P among different colloidal size fraction implies different processes involved in P mobilization/immobilization. The preferential carrier phases in each size fraction of P-bearing colloids is site-specific, depending on hydrogeological, chemical and biological properties. A study from Henderson et al., (2012) suggested important mobilization (71 – 91 % of total released P) of P-bearing colloids sized 200 – 250 nm from soil under reducing conditions caused by reductive dissolution of iron-oxide cementing agent in soil aggregate structure. In contrast, the role of OM in association with P has not yet been investigated even though evidence on the formation of binary humic acid-metal colloids is well described at anoxic-oxic interfaces (Liao et al., 2017), therefore, a

formation of ternary complexes between humic acid-metal-P should be taken into account (Audette et al., 2020).

While the release of SRP from sediment is well documented in the literature (Jarvie et al., 2008; Dupas et al., 2018; Varol, 2020), colloidal P has not yet received adequate attention and is generally overlooked when assessing P mobility. Moreover, colloidal phosphorus studies concern mainly soil system whereas sediment system are rarely examined, particularly in reservoir context, leading to a lack of knowledge concerning mechanisms driving this P release.

Concerning the study of “dissolved” P release from dam reservoir sediment exposed to redox oscillation, Rapin et al., (2019) hypothesized that Fe(III) solubility increase was due to the possible formation of DOM-Fe-P complexes and/or the predominance of colloidal Fe(III) favoring the persistence of P in fraction lower than 0.45 μm . Moreover, a study from Nguyen et al., (2020) showed that reservoir sediment contained a relatively high stock of water-mobilizable colloids, associated to significant content of colloidal P, which represented 81 – 93 % of total water-mobilizable P. Thus, along with the growing number of publications showing colloid-facilitated transport of P, the study of colloidal fraction contribution in P release from sediment constitutes a main issue. For this reason, the present study aims (i) to investigate the behavior of water-mobilizable P released from sediment throughout controlled oxic and anoxic periods, (ii) to provide an insight characterization of multiple size fractions of colloidal P, and (iii) to elucidate the processes that could be prevalently responsible for total and colloidal P mobility.

III.3.2.2. Materials and methods

III.3.2.2.1. Site description and sediment sampling

Sediment was sampled in the Champsanglard hydroelectric dam reservoir, constructed in 1984 in Creuse River (France) and frequently observed for harmful cyanobacteria blooms during summertime, thermal stratification and oxycline (Rapin et al., 2019). The total catchment adjacent to Champsanglard reservoir covers a 406-km² area and are predominantly occupied by agricultural land (65 %) and deciduous forest (30 %) (Corine Land Cover data). Agricultural activities in this catchment are mainly meadow for cattle and sheep farming. Champsanglard reservoir is used for both hydroelectric production and recreation activities such as fishing and bathing, therefore its water quality requires a good ecological status according to Water Framework Directive 2000/60/EC. However, these recreational services are regularly banned since several years according to water quality deterioration by cyanobacteria growth.

Surface sediment was sampled in the middle of reservoir in March 2019 at the depth of 14 m (46° 15' 40" N, 1° 53' 02" E) using an Ekman grab sampler (up to 10 cm depth). Collected sediment was homogenized and transferred to polyethylene bottles. In laboratory, sediment was then sieved at 2 mm to remove large debris and stored at 4°C in the dark. The incubation of sediment started on a following day of sampling to avoid changes in biological and chemical properties due to long term storage.

III.3.2.2.2. Sediment characterization

The homogenized and wet sediment sample (fraction < 2 mm) was used to characterize physical and chemical characteristics. The water loss on drying was determined as mass loss after drying at 105°C until unchanged mass. The median grain size (D50) was measured by laser diffractometer (MasterSizer 3000,

Malvern) on wet dispersion in ultrapure water and under ultrasound. The pH of sediment was measured on a sediment suspension in ultrapure water with ratio of 1/1 (w/v) according to Method 9045D (US EPA, 2004).

The organic matter (OM) content was calculated as percentage of mass loss between calcination at 550°C for 2 h and drying at 105°C. Sediment P was measured by digestion of calcinated sediment with HCl 3.5 M for 16 h according to the method of Ruban et al., (2001). Digested solution was then centrifuged at 2000 g for 15 min, filtered through 0.45 µm cellulose acetate membrane (LLG Labware) and measured dissolved phosphate using spectrophotometry (see part 2.5). The measurement of total sediment concentrations of Fe, Al, Ca, Mn and Mg were performed according to method 3015a (US EPA, 2007) in which sediment was firstly digested with concentrated peroxide (Merck, 30 %) to degrade organic matter and then with reverse aqua regia (HNO₃ 65 % and HCl 37 %) in a microwave (Multiwave Go, Anton Paar) for 40 min at 180°C. The contents of Fe, Al, Ca, Mn and Mg in digested solution were then analyzed using microwave plasma atomic emission spectroscopy (Agilent, MP-AES 4100) (See section 2.5).

III.3.2.2.3. Sediment incubation

Sediments were suspended in synthetic water and incubated under controlled redox condition. The sediment suspensions were prepared from 10 g of freshly wet sediment and completed with 200 mL of synthetic water (wet S/L of 1/20). All incubation was carried out in acid-washed (HCl 10%, v/v) 250-mL glass bottles. The synthetic water, prepared to simulate major elemental composition of bottom water in Champsanglard reservoir (Rapin et al., 2019), contained 5.4 mg Ca²⁺/L, 1.6 mg Mg²⁺/L, 8.6 mg K⁺/L, 9.2 mg Na⁺/L, 6.3 mg SO₄²⁻/L, 4.9 mg NO₃⁻/L, 8.5 mg Cl⁻/L and 34.7 mg HCO₃⁻/L (ionic strength I = 1.28 mM).

Sediment solutions were let equilibrate under oxic condition for 2 days before starting incubation to revive microbial activity. The whole incubation was carried out through a 63-days period, composed of a closed and an opened period to mimic various redox conditions (oxic and anoxic). At the beginning, the anoxic condition was induced by closing bottles with septic plugs and maintained in the dark inside a glovebox (PLAS LABS, 830-ABD/EX) adjusted to low oxygen level (< 0.18 mg O₂/L). After the first 15 days, according to the real-time monitoring of redox potential, all bottles were then purged with N₂ gas to accelerate development of anoxic condition. Considering monitored Eh, the first 23 days corresponded to a first oxic condition and transition towards anoxia. The anoxic condition started from day 23 and lasted until day 45. Afterward, oxic condition was applied by transferring bottles to the outside of glovebox, removing septic plug but enfolding with a layer of parafilm, which limits evaporation but remains sufficient for air exchange. The second oxic phase lasted for 20 days, from day 46 to day 63. Regularly, bottles were shaken manually once a day, 5 days per week and the monitoring of oxygen level, temperature, pH, redox potential was performed. During the whole experiment, each sampling was conducted as a sacrifice of 2 or 3 bottles according to real-time monitoring for replicates. This sacrificial method allows constant solid-liquid ratio of 1/20 throughout the sediment incubation without any modification within system. Three sampling was made for each period: on days 0, 1, 7 for the first oxic phase, on days 23, 37, 45 for the anoxic phase and on days 46, 56, 63 for the second oxic phase. During closed phase, the sampling and colloid separation as well as chemical analysis were carried out inside glovebox under low oxygen level to avoid any oxidation.

III.3.2.2.4. Colloid separation

Sediment suspensions were let settle for 30 min before the separation. The supernatants were fractionated using successive filtrations to obtain four different size fractions of colloids: large colloids 0.45 - 1 μm , intermediate colloids 0.2 - 0.45 μm , small colloids 300 kDa - 0.2 μm , nano colloids 10 - 300 kDa and a fraction lower than 10 kDa considered as truly dissolved fraction (Fig. 45). Supernatants were first filtered through a glass fiber membrane at 2.7 μm (VWR) to remove large particles that could latterly enhance membrane clogging during colloid separation. Afterward, filtrates were then passed through a series of filtration and ultrafiltration steps using glass fiber membrane at 1 μm (VWR), cellulose nitrate membrane at 0.45 μm , 0.2 μm using cellulose nitrate membrane (Sartorius) and Vivaspin® 20 ultrafiltration units (Sartorius) at 300 kDa and 10 kDa. The ultrafiltrations were applied with centrifugation at 6,000 g for 15 min. At each filtration step, subsamples were collected for elemental analysis in prior to the following successive filtration.

Some samples were dedicated to immediate analyses (alkalinity, ferrous ions, total phosphorus (TP) and phosphates) while others were stored at - 20°C for later analyses (total Fe, Al, Ca, Mn, Mg and organic carbon).

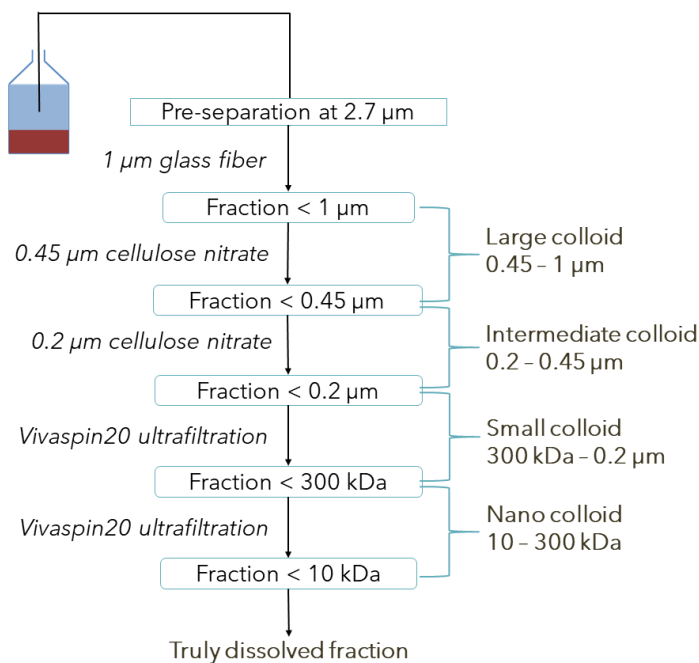


Figure 45. Size separation of water-mobilizable fraction (smaller than 1 μm) using successive filtrations.

III.3.2.2.5. Chemical measurement and analysis

The chemical analysis and measurement methods for each of five subsamples of water-mobilizable fraction (below 1 μm) are described in Table 23.

The monitoring of solution chemistry (pH, dissolved oxygen, Eh) was carried out on sediment suspension after 2-h of sedimentation. The pH was measured using pH meter (Crison, GLP22) and a pH probe (Crison,

5221) which was calibrated daily by buffer solutions at pH 7 and 4. The oxygen concentration was measured using an oximeter HQ30D flexi (HACH). The redox potential was measured using platinum band combined Ag/AgCl electrode (WTW, Portable Multimeter 3210). The Eh values were corrected according to standard hydrogen electrode (Bohn, 1971) following below equation:

$$Eh_{Corrected} (mV) = Eh_{measured} (mV) + 230 - 0.76 \times (T(^{\circ}C) - 25) + 60 \times (pH_{measured} - 7)$$

Alkalinity in filtrate at 0.45 μm was determined by acid titration using 0.001 M HCl until the pH of solution reached 4.3 and was reported in mg HCO_3^-/L .

The dissolved inorganic phosphorus (DIP) was quantified by spectrophotometry method (Murphy and Riley 1962) at a wavelength of 880 nm using Agilent 8453 UV-Vis spectrometer and a 1-cm cuvette (LoD of 20 $\mu\text{g}/\text{L}$). Total phosphorus (TP) was determined by HACH LANGE LCK 349 (LQ of 50 $\mu\text{g}/\text{L}$) including a digestion with concentrated H_2SO_4 acid for 1 h at 100 $^{\circ}\text{C}$ (HACH, LANGE LT200) and measured using portable spectrophotometer (HACH, DR1900). Organic carbon (OC) content was determined using Shimadzu TOC-L analyzer (LQ of 1 mg C/L). Contents of Fe, Al, Ca, Mn and Mg were analyzed on an Agilent MP4100 MP-AES. For those fractions ranging from 10 kDa to 1 μm , samples were previously subjected to microwave acid-assisted digestion using reverse aqua regia (USEPA 3015a 2007) before analysis with MP-AES. The LQ were 30 μg Fe/L, 20 μg Al/L, 12 μg Ca/L, 7 μg Mn/L, and 1 μg Mg/L. In addition, dissolved Fe(II) concentrations were also measured in fraction smaller than 10 kDa inside glovebox according to 1,10-phenantroline method (HACH LANGE 8146) with a LQ of 20 $\mu\text{g}/\text{L}$.

Elemental concentrations in colloidal fraction were determined as the difference between total concentration in fraction below 1 μm and dissolved concentration in fraction below 10 kDa. For each colloidal fraction (nano: 10 - 300 kDa; small: 300 kDa - 0.2 μm ; intermediate: 0.2 - 0.45 μm ; large: 0.45 - 1 μm), concentrations were calculated by differences between each phase successively.

Concentrations of major anions (NO_3^- , NO_2^- , SO_4^{2-} , Cl^-) and cations (Na^+ , NH_4^+ , Ca^{2+} , Mg^{2+} , K^+) were measured in filtrates at 0.2 μm using an ionic chromatography (Metrohm, 930 Compact IC Flux). The LQ for NO_3^- , NO_2^- , SO_4^{2-} , Cl^- , Na^+ , NH_4^+ , Ca^{2+} , Mg^{2+} and K^+ were 0.45, 0.075, 0.075, 0.25, 0.1, 0.3, 0.25, 0.25 and 0.15 mg/L, respectively.

Table 23. The chemical analysis of different size class subfractions of water-mobilizable extract.

Analysis	< 1 µm	< 0.45 µm	< 0.2 µm	< 300 kDa	< 10 KDa	Method
Alkalinity		x				Acid titration to pH 4.3
Fe(II)					x	Ferrozine
TP	x	x	x	x		Hach LCK 349
DIP	x	x	x	x	x	Murphy and Riley (1962)
Al, Fe, Mn, Ca, Mg (with acid digestion)	x	x	x			US EPA 3015a (2007)
Al, Fe, Mn, Ca, Mg (without acid digestion)			x	x	x	MP-AES
TOC	x	x	x	*	*	TOC analyzer
NO ₃ ⁻ , NO ₂ ⁻ , SO ₄ ²⁻ , Cl ⁻ , Na ⁺ , NH ₄ ⁺ , Ca ²⁺ , Mg ²⁺ , K ⁺			x			Ionic chromatography

III.3.2.2.6. Statistics and geochemical modelling

The chemical modeling was performed with Visual MINTEQ version 3.1 software to determine chemical speciation at equilibrium and saturation index toward certain minerals. The modeling was performed using the chemical composition (major anions and cations, P, Fe, Ca, Mn, Mg), pH and Eh in fraction below 10 kDa throughout the days 0 to 45, corresponding to first oxic and anoxic period, and between days 45 to 46, corresponding to transition point between anoxic to oxic phase, to evaluate which species were able to precipitate during incubation.

Pearson correlation coefficient was used to reveal possible correlation between colloidal elements that reinforce the precipitation/coprecipitation of colloids under biochemical redox changes. Statistical analysis was carried out using Microsoft Excel enhanced with Analysis ToolPak.

III.3.2.3. Results

III.3.2.3.1. Sediment characteristics

The physico-chemical characteristics of surface sediment in Champsanglard reservoir were presented in Table 24. Sediment contained a high percentage of water loss on drying (105°C) of 82 ± 2 %. The sediment pH_{H2O} was slightly acidic at 6.8 ± 0.1 . Sediment grain size was dominated by fine grained fraction, with 50 % of particles sized below 13.8 ± 0.6 µm. Sediment was rich in organic matter (190 ± 10 mg/g_{DW-Sed}), Al (156 ± 2 mg/g_{DW-Sed}), Fe (84 ± 1 mg/g_{DW-Sed}), but poor in Mg (17.3 ± 0.1 mg/g_{DW-Sed}), Ca (8.2 ± 0.1 mg/g_{DW-Sed}) and Mn (1.6 ± 0.1 mg/g_{DW-Sed}). Total sedimentary P content was 2.04 ± 0.02 mg/g_{DW-Sed}.

Table 24. Sediment characteristics.

Characteristics	Unit	Content
pH _{H2O}		6.8 ± 0.1
D50	µm	13.8 ± 0.6
Water loss on drying	%	82 ± 2
Organic matter	mg/g _{DW-Sed}	190 ± 10
Al	mg/g _{DW-Sed}	156 ± 2
Fe	mg/g _{DW-Sed}	84 ± 1
Mg	mg/g _{DW-Sed}	17.3 ± 0.1
Ca	mg/g _{DW-Sed}	8.2 ± 0.1
P	mg/g _{DW-Sed}	2.04 ± 0.02
Mn	mg/g _{DW-Sed}	1.6 ± 0.1

III.3.2.3.2. Biogeochemical redox dynamic of sediment solution

At the beginning of the sediment incubation, the redox potential was 630 ± 30 mV (Fig. 46a). After the closure of the batches, the Eh value decreased slowly to 352 ± 20 mV by day 7. After being purged with nitrogen gas at day 15 (aimed to accelerate the development of redox condition), the Eh dropped to 120 ± 5 mV at day 23 and maintained under 100 mV corresponding to anoxic condition. After the opening of the batches, redox potential increased quickly to reach 240 ± 10 mV within a day (day 46) and remained above 350 ± 10 mV until the end of experimentation (day 63). According to redox potential dynamic, we considered that from day 0 to day 7 sediment was submitted to a first oxic condition, to an anoxic condition from day 23 to day 45, and to a second oxic condition from day 46 to day 63.

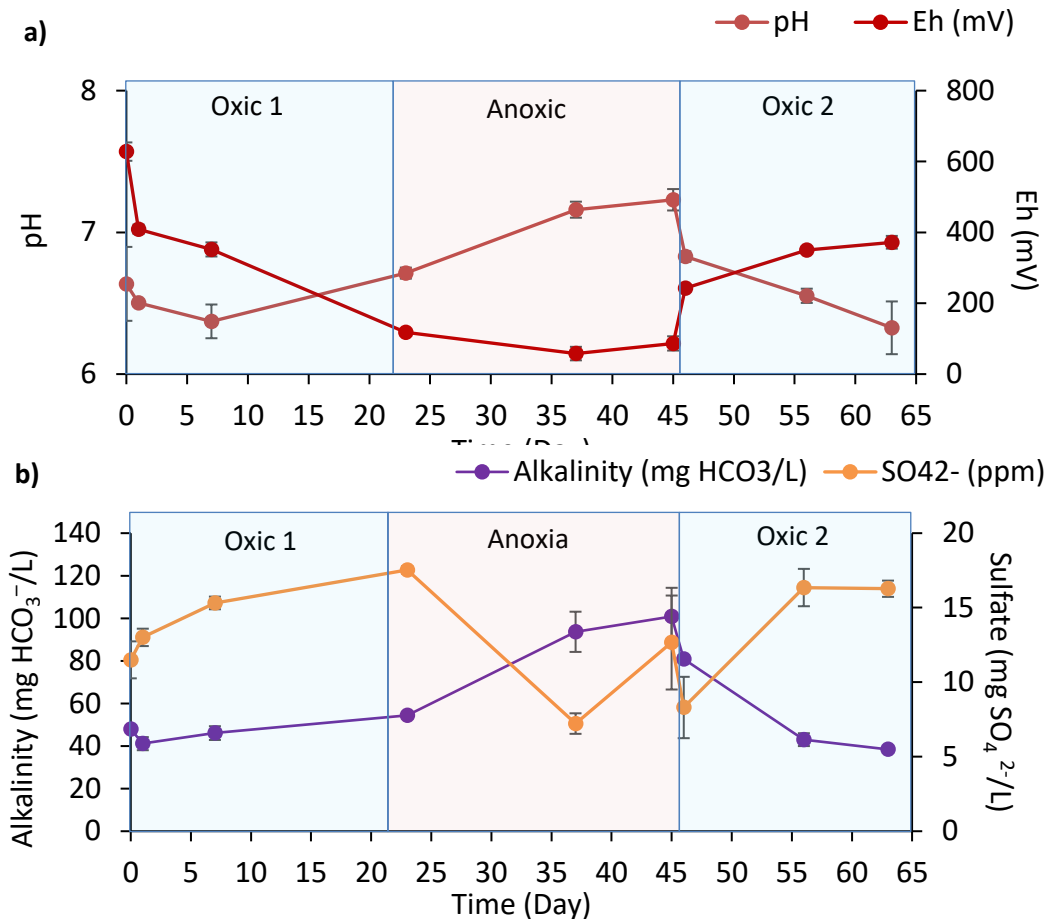


Figure 46. Evolution of redox potential, pH, alkalinity throughout the incubation.

As shown in figure 46a, the initial pH was 6.6 ± 0.3 and dropped to 6.4 ± 0.2 during first oxic condition (day 7). After being purged with nitrogen gas (day 15), pH started to increase from 6.7 ± 0.1 on day 23 to reach 7.2 ± 0.1 by the end of anoxic period (day 45). When opening the batches (day 46), pH dropped rapidly to 6.8 ± 0.1 and continued decreasing during oxic 2 to reach 6.3 ± 0.2 by the end of second oxic condition (day 63).

Similar tendency was observed for alkalinity (Fig. 46b). The alkalinity did not vary significantly during the first oxic condition, averagely at 45.0 ± 3.5 mg HCO₃⁻/L. Alkalinity began to increase after nitrogen gas purging, from 54.4 ± 0.7 mg HCO₃⁻/L to achieve the highest values of 101 ± 14 mg HCO₃⁻/L by the end of anoxic condition (day 45). During the second oxic condition, alkalinity dropped significantly from 80.9 ± 1.9 mg HCO₃⁻/L (day 46) to 38.4 ± 1.6 mg HCO₃⁻/L (day 63).

In contrast, sulfate concentration in sediment solution fluctuated along the incubation (Fig. 46b). Concentration of sulfate increased from 11.5 ± 1.2 mg/L at the start of experiment to 17.5 ± 0.2 mg/L on day 23, then declined by 2.4 times to be at 7.2 ± 0.7 mg/L on day 37. By the end of anoxic condition, sulfate level raised back to 12.7 ± 3.2 mg/L which was close to initial state. After batch opening, sulfate level

dropped quickly to 8.3 ± 2.1 mg/L, then increased to be stable at 16.3 ± 0.7 mg/L between day 56 and 63 of the second oxic period.

III.3.2.3.3. Evolution in elemental composition of water-mobilizable fraction

III.3.2.3.3.1. Nutrient dynamics

III.3.2.3.3.1.1. Phosphorus

Figure 47 presents the evolution of water-mobilizable P (P_{WM}) release along the incubation. The P_{WM} released from sediment to solution remained at low quantity of less than 0.02 ± 0.01 mg/g_{DW-sed} at the beginning experimentation corresponding to the first oxic period (from day 0 to day 7). At day 23, the quantity of P_{WM} started to increase by 4 times to reach 0.07 ± 0.01 mg/g_{DW-sed} (day 37), then 0.82 ± 0.10 mg/g_{DW-sed} at the end of anoxic condition (day 45). Right after the opening and thus re-oxygenation of the batches (day 46), P_{WM} quantity decreased by half and remained stable at 0.41 ± 0.1 mg/g_{DW-sed}.

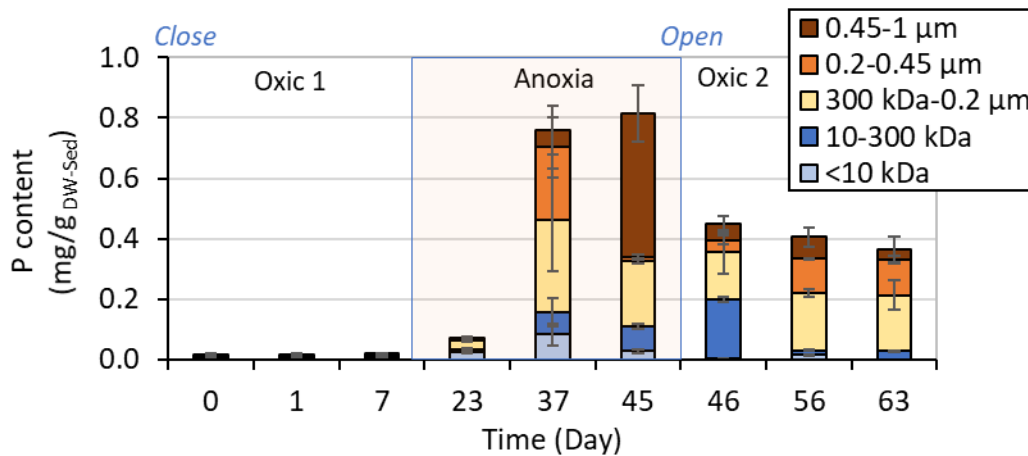


Figure 47. Evolution of water-mobilizable P release throughout the incubation.

The size fractionation of P shows that throughout the experimentation, colloidal form was predominant with variable proportions of between 70 ± 20 % and 100 ± 30 % of P_{WM} .

During first oxic period, the percentage that colloid P contributed to P_{WM} was remarkably very high (ranging from 80 ± 30 % to 90 ± 20 % of P_{WM}), meanwhile, the truly dissolved P was less than 0.003 μg/g_{DW-sed} and contributed less than 19 ± 8 %.

Once anoxic condition developed (from day 23), colloidal P increased strongly, particularly between day 23 and 37, with concentration passing from 0.05 ± 0.01 mg/g_{DW-sed} (day 23) to 0.7 ± 0.3 mg/g_{DW-sed} (day 37), corresponding to a 14-fold increase. At the end of anoxic period, colloidal P represented 100 ± 20 % of P_{WM} . On day 37, the colloid P consisted mainly of small and intermediate colloidal P (80 ± 40 %), large and nano colloids represented 20 ± 20 %. During this period, truly dissolved P increased also from 0.024 ± 0.001 mg/g_{DW-sed} to 0.08 ± 0.04 mg/g_{DW-sed}.

On day 45, P_{WM} did not continue to increase as much in concentration, but it did evolve in shift in colloid size classes from intermediate to large colloid. The P_{WM} contained lower amount of small and intermediate colloidal P (0.23 ± 0.02 mg/g_{DW-sed}, equivalent to 29 ± 4 % of colloidal P) and important amount of large colloidal P (0.48 ± 0.10 mg/g_{DW-sed}, equivalent to 60 ± 20 % of colloidal P). The quantity of nano colloidal P remained at 0.08 ± 0.01 mg/g_{DW-sed} and represented 10 ± 2 % of colloidal P. The truly dissolved P decreased and reached 0.027 ± 0.008 mg/g_{DW-sed}.

After batch opening and during the entire second oxic period, the proportion of colloidal P maintained at 100 ± 20 % of P_{WM} . Regarding P colloidal size fractionation, at the beginning of batch opening (day 46), quantity of nano colloidal P increased from 0.08 ± 0.01 mg/g_{DW-sed} to 0.20 ± 0.01 mg/g_{DW-sed} (representing 44 ± 8 % of colloidal P) whereas large colloidal P dropped from 0.48 ± 0.10 mg/g_{DW-sed} to 0.05 ± 0.01 mg/g_{DW-sed} (representing 12 ± 7 % of colloidal P). During the following days of second oxic stage (days 56 and 63), this amount of nano colloidal P fell to 0.015 ± 0.003 mg/g_{DW-sed} and became negligible regarding colloidal P. In contrast, fraction of small and intermediate colloidal P increased from 0.20 ± 0.08 mg/g_{DW-sed} (day 46) to 0.30 ± 0.01 mg/g_{DW-sed} and remained stable until the end of experimentation (day 63). The quantity of truly dissolved P decreased importantly at the opening of the batches down to approximately 0.002 ± 0.001 mg/g_{DW-sed} (day 46), then jumped up to 0.015 ± 0.001 mg/g_{DW-sed} on day 56. By the end of oxic second oxic period (day 63), no truly dissolved P was recorded.

III.3.2.3.3.1.2. Nitrate and ammonium

Figure 48 presents the evolution in ammonium and nitrate concentration along the incubation.

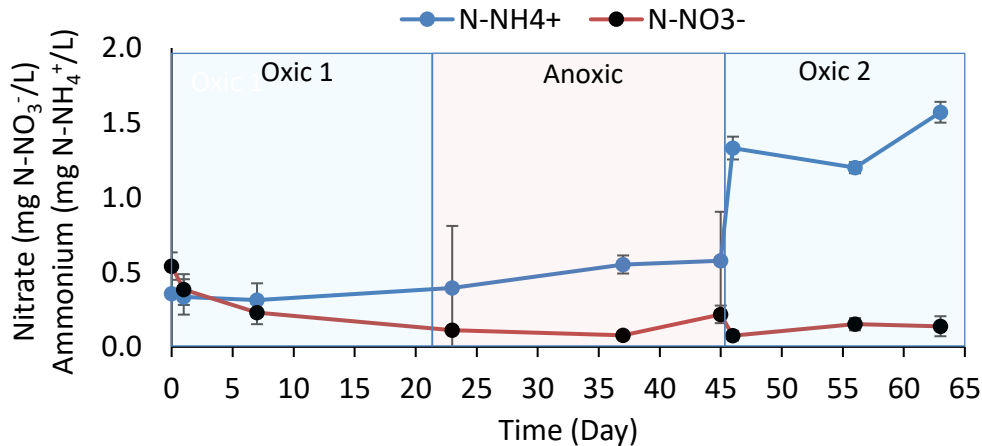


Figure 48. Evolution of $N-NH_4^+$ and $N-NO_3^-$ concentration throughout the incubation.

During the first oxic condition, the concentration of nitrate decreased from 0.54 ± 0.09 mg/L to 0.23 ± 0.08 mg/L, meanwhile the ammonium concentration varied between initial values of 0.36 ± 0.03 mg/L and 0.31 ± 0.11 mg/L on day 7 (Fig. 48). After the purging with nitrogen gas, the nitrate concentration dropped quickly to 0.11 ± 0.03 mg/L on day 23 and 0.08 ± 0.03 on day 37, but then increased up to 0.22 ± 0.06 mg/L on day 45 (end of anoxic condition). In the meantime, ammonium level increased slightly to 0.55 ± 0.06 mg/L on day 37 and remained stable at 0.58 ± 0.33 mg/L until the end of anoxic condition. During the second oxic condition, nitrate concentration remained stable between 0.15 ± 0.04 mg/L (day 56) and 0.14

± 0.07 mg/L (day 63), whereas ammonium concentration evolves significantly to reach 1.57 ± 0.07 mg/L on day 63.

III.3.2.3.3.1.3. Organic carbon

During the first 7 days, the water-mobilizable OC levels were stable at 0.74 ± 0.04 mg/g_{DW-sed} and OM was mainly in fraction below $0.2 \mu\text{m}$ (78 – 97 %) (Fig. 49a). When the batches underwent anoxic phase (day 23 to day 45), the levels of water-mobilizable OC increased gradually to reach 1.8 ± 0.1 mg/g_{DW-sed} on day 45, corresponding to an increase by a factor of 2, and the increase was observed for all fractions. At the end of the anoxic period, the content of colloidal OC was 0.26 ± 0.03 mg/g_{DW-sed} in fraction $0.2 - 0.45 \mu\text{m}$ (equivalent to 15 ± 2 % of water-mobilizable OC) and 0.36 ± 0.12 mg/g_{DW-sed} in fraction $0.45 - 1 \mu\text{m}$ (equivalent to 20 ± 6 % of water-mobilizable OC).

Once the batches were opened, we observed a quick decrease in the $0.45-1 \mu\text{m}$ fraction passing from 0.36 ± 0.12 mg/g_{DW} to 0.08 ± 0.09 mg/g_{DW-sed}, the other fractions remained unchanged. After that, throughout the remaining second oxic period, from day 46 to day 56, the water-mobilizable OC amounts decreased in the fraction inferior to $0.2 \mu\text{m}$ from 1.1 ± 0.1 mg/g_{DW-sed} to 0.53 ± 0.11 mg/g_{DW-sed} and seemed to remain stable until day 63.

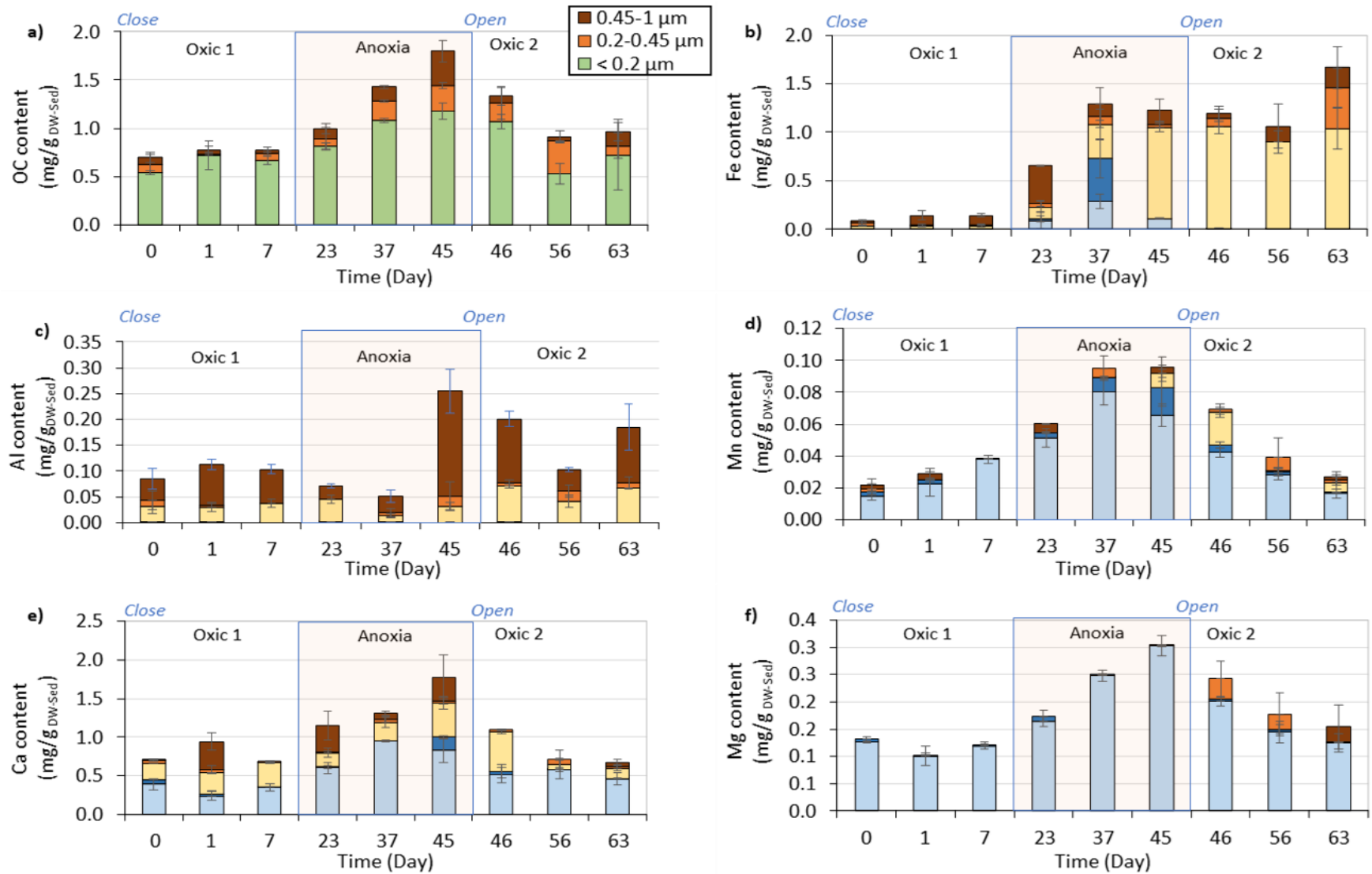


Figure 49. Evolution of OC, Fe, Ca, Mg and Mn in water-mobilizable fraction during anoxic and oxic conditions.



III.3.2.3.3.2. Metal dynamic

III.3.2.3.3.2.1. Iron

Throughout the experimentation, the iron content (Fe) in water-mobilization fraction (Fig. 49b) varied significantly between 0.09 ± 0.03 mg/g_{DW-sed} (day 0) and 1.7 ± 0.4 mg/g_{DW-sed} (day 63).

During the first oxic stage (from day 0 to day 7), the quantity of water-mobilizable Fe remained at low level (below 0.14 ± 0.03 mg/g_{DW-sed}, day 7) and was mainly in large colloidal fraction (up to $66 \pm 16\%$ of total water-mobilizable Fe). Truly dissolved Fe (fraction below 10 kDa) was under detection limit (Fig. 49b), however, as shown in Fig. 6, there were presence of Fe²⁺ in solution but at very low concentration and slightly increased on day 7 (at 14 ± 4 μg/g_{DW-sed}).

From day 23 (beginning of anoxic condition), water-mobilizable Fe amount increased by 9 times to reach 1.24 ± 0.06 mg/g_{DW-sed} on day 45. The concentration of Fe(II) or truly dissolved Fe showed similar tendency, increased on day 37 to about 0.35 mg/g_{DW-sed} but then slightly dropped on day 45 to be at 30 ± 10 μg/g_{DW-sed} and 0.11 ± 0.01 mg/g_{DW-sed}, respectively. At maximum, truly dissolved Fe represented only $22 \pm 7\%$ of total water-mobilizable Fe, the remaining existed in colloidal form, especially fraction above 0.2 μm. Similar observation was acquired for nano-colloidal Fe, in which the highest level recorded was 0.44 ± 0.20 mg/g_{DW-sed} on day 37 ($35 \pm 20\%$ of total water-mobilizable Fe) then dropped to not quantifiable value on day 45. In contrast, the small colloidal fraction evolved gradually through anoxic incubation to reach 0.94 ± 0.04 mg/g_{DW-sed} on day 45 (representing $84 \pm 10\%$ of colloidal Fe). The large-colloid Fe presented at the beginning of anoxia was 0.39 ± 0.01 mg/g_{DW-sed} and then decreased during anoxic period to reach 0.15 ± 0.12 mg/g_{DW-sed} on day 45.

Once the flasks were opened (day 46), both Fe(II) and truly dissolved Fe disappeared immediately (Figs. 49b and 50). Fe remained only in colloidal form, especially in the small colloidal fraction ($62-85\%$ of total water-mobilizable Fe). During the reoxygenation of the suspension, the total amount of water-mobilization Fe remained unchanged from day 45 to day 56 (1.1 ± 0.1 mg/g_{DW-sed}), but then raised up to 1.7 ± 0.4 mg/g_{DW-sed} on day 63. Fe was no more detected in fraction below 300 kDa.

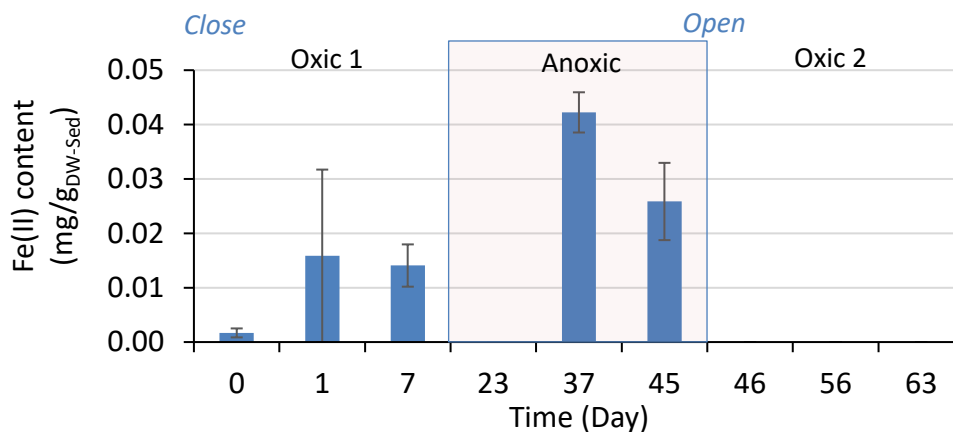


Figure 50. Evolution of Fe²⁺ in fraction below 10 kDa along the incubation.

III.3.2.3.3.2.2. Aluminum

Throughout the whole incubation, water-mobilizable aluminum (Al) were released from sediment to solution in two main fractions: large and small colloids (Fig. 49c). Al was never quantified in the truly



dissolved fraction, and intermediate colloidal fraction could not be evaluated considering standard deviation.

During the first oxic condition, the quantities of water-mobilizable Al were low, from 0.08 ± 0.02 mg/g_{DW-sed} to 0.11 ± 0.01 mg/g_{DW-sed} and were composed by approximately 66 ± 30 % of large-colloidal Al and 34 ± 20 % of small-colloidal Al. After being purged with nitrogen gas, water-mobilizable Al decreased its quantities, mainly by a 2.6-time lower in large colloidal fraction from 0.066 ± 0.009 mg/g_{DW-sed} to 0.025 ± 0.004 mg/g_{DW-sed} between day 7 and day 23, and by a 3.6-time lower in small-colloidal fraction from 0.045 ± 0.008 mg/g_{DW-sed} to 0.013 ± 0.004 mg/g_{DW-sed} between day 23 and day 37.

However, at the end of anoxic condition (day 45), water-mobilizable Al increased importantly to reach 0.26 ± 0.06 mg/g_{DW-sed} mainly by a 6.6-time higher in large-colloidal Al (representing 80 ± 20 % of total water-mobilizable Al) and a 2.5-time higher in small-colloidal Al (representing 13 ± 3 % of total water-mobilizable Al).

During the second oxic condition, the contribution of small-colloidal Al to total water-mobilizable Al increased. Right after batch opening (day 46), quantity of water-mobilizable Al decreased to 0.20 ± 0.02 mg/g_{DW-sed}, but small-colloidal Al raised by 2.2-fold and attributed a proportion of 35 ± 3 %. In the following days of second oxic period, the amount of small-colloidal Al remained relatively stable. Meanwhile, large-colloidal Al decreased significantly to be at 0.042 ± 0.004 mg/g_{DW-sed} (day 56) and then increased to reach 0.11 ± 0.05 mg/g_{DW-sed} (day 63).

III.3.2.3.3.2.3. Manganese

Content of water-mobilizable manganese (Mn) was very low throughout all experiment and increased gradually to reach the maximum 0.096 ± 0.016 mg/g_{DW-sed} during anoxic condition (day 45) (Fig. 49d). Considering the standard deviation and under detection limit results, Mn concentrations presented in other fractions were not quantifiable.

Truly dissolved Mn was dominated throughout the whole incubation and attributed 61 – 99 % of total water-mobilizable Mn contents, particularly in anoxic condition.

During the second oxic condition, the value of water-mobilizable Mn gradually decreased to be at 0.027 ± 0.007 mg/g_{DW-sed} on day 63. Right after batch opening, there was an increase in quantity of small-colloidal Mn to 0.020 ± 0.003 mg/g_{DW-sed} (day 46) but then this Mn fraction became unquantified during the rest of second oxic period.

III.3.2.3.3.2.4. Calcium

The content of calcium (Ca) varied significantly between 0.68 ± 0.05 mg/g_{DW-sed} and 1.8 ± 0.4 mg/g_{DW-sed} along the incubation (Fig. 49e). The initial amount of Ca (at 0.70 ± 0.08 mg/g_{DW-sed}) corresponded to Ca concentration present in synthetic solution. A flash release of Ca under large colloidal form was noted during the first oxic period on day 1 (at 0.366 ± 0.188 mg/g_{DW-sed}) and then disappeared on day 7.

Throughout the incubation, either in oxic or anoxic periods, truly dissolved Ca was the dominant fraction of Ca with proportion varying between 50 ± 20 % and 80 ± 30 %, except on day 1.

Once anoxia developed, Ca concentration became significantly higher with a maximum content of 1.8 ± 0.4 mg/g_{DW-sed} on day 45 and noted by a significant increase, of 2.6-fold, in colloidal Ca (from 0.35 ± 0.09 mg/g_{DW-sed} on day 37 to 0.9 ± 0.3 mg/g_{DW-sed} on day 45) that represented about 50 ± 30 % of total water-mobilizable Ca. During the second oxic period, the level of Ca declined back to initial range of 0.7 ± 0.1 mg/g_{DW-sed} on day 63.

III.3.2.3.3.2.5. Magnesium

The majority of magnesium (Mg) was present in fraction below 10 kDa throughout the experiment with proportion of 81 – 100 % of total Mg contents in fraction below 1 μ m (Fig. 49f).

During the first oxic period, Mg concentration was stable and corresponded to initial concentration present in the synthetic solution. When closing the flasks, truly dissolved Mg levels (fraction below 10 kDa) increased gradually from 0.12 ± 0.01 mg/g_{DW-sed} (day 7) to 0.30 ± 0.02 mg/g_{DW-sed} (day 45) and then slowly declined during the opening back to 0.13 ± 0.02 mg/g_{DW-sed} on day 63.

II.3.2.3.3.3. Geochemical modelling by Visual Minteq

According to chemical equilibrium simulation in the absence of organic matters, the minerals FCO₃-apatite and vivianite can precipitate between day 37 and day 45 of anoxic incubation considering ionic concentration in fraction below 10 kDa according to saturation index (SI). The SI of vivianite and FCO₃-apatite were oversaturated at 1.36 and 7.43, respectively, on day 37 then were found at 0.5 (near equilibrium) and 6.1 on day 45, respectively. The simulation of redox transition from anoxic to oxic condition on day 45, without taking into account the role of dissolved organic matter, revealed the formation of hematite in fraction lower than 10 kDa and formation of hematite, hydroxyapatite and FCO₃-apatite in fraction lower than 0.2 μ m.

III.3.2.4. Discussion

III.3.2.4.1. Biogeochemical redox dynamic along sediment incubation

At the beginning of incubation, sediment solutions were not immediately purged with N₂ and contained dissolved oxygen corresponding thus to oxic condition. Redox potential remained high and decreased slowly despite of batch closure because low amount of sediment was used (Fig. 46a). The followed N₂ purge on day 15 allowed to accelerate the O₂ depletion, thus favored the development of sub-oxic condition and followed by anoxia started from day 23. The consumption of oxygen was caused by respiration of benthic organisms, oxidation of organic matter that lead to the release of CO₂, and inorganic nutrients (ammonia and phosphate). Without O₂ supply, the degradation of organic matter continued via the development of anoxia and anaerobic by stepwise. Generally, the oxidation of OM by anaerobic respiration organisms use a sequence of electron acceptors: nitrate, Mn and Fe oxy(hydroxy)des and then sulfates in order of decreasing energy demand. During sediment incubation, the successive reduction of electron acceptors led to the decrease of nitrate concentration (denitrification) (Fig. 47) followed by the increase of Fe(II) and Mn concentrations (Figs. 5b and 5d). Sulfate concentration began to decrease at day 37 but significant amount remained in solution (7.2 ± 0.7 mg/L) (Fig. 46b), showing that the sulfate reduction was not complete or even not operated. Ammoniums increased during anoxia was due to reduction of nitrate and during the second oxic condition was due to aerobic respiration (ammonification). Along the reduction, the pH increased until the end of anoxic condition, due to the consumption of H⁺ upon nitrate and Fe, Mn reduction. This rise of pH was concomitant with the blocking of CO₂ production during OM mineralization; it resulted in

elevation of alkalinity (Fig. 46b). The opening of the batches allowed rapid supply with oxygen leading to the increase of redox potential and loss of alkalinity upon degassing of CO₂ and drop of pH.

III.3.2.4.2. Sedimentary P released during sequential oxic-anoxic-oxic phases

In previous studies, it is well established that ‘dissolved’ P (phosphorus measured by the molybdenum blue method in the fraction inferior to 0.45 or 0.2 μm) release is maximal in anoxic condition and that one of the dominant mechanisms is the reductive dissolution of iron oxide coupled to microbial oxidation of organic matter (Litchman and Nguyen, 2008; Salas et al., 2010) and competition of P and OM for sorption sites (Sato and Comerford, 2005). Considering total water-mobilizable P, we confirmed that reducing condition promotes the strong release of P (40 % of total sedimentary P) comparing to oxidizing condition where P released corresponded only to 1 % of total sedimentary P. However, P was released mainly under colloidal fraction that represented about 90 % of P_{WM} (Fig. 47). During the first phase of anoxia (Eh= 58 mV on day 37), the majority of colloidal P was recovered in the fraction between 300 KDa and 0.45 μm (small and intermediate colloids). While anoxic condition was fortified, the P_{WM} concentration did not evolve in total content, but involved in a shift between colloidal size classes, from intermediate to large colloid. The size evolution of colloidal P lead to the dominant association of P to large colloidal fraction (0.45-1 μm) which is generally not considered when assessing usual “dissolved P” concentration. Truly dissolved P remained low and, above all, instable. Instead of increase during anoxia, in contrary to what was expected during anoxia, the truly dissolved P fraction showed a decrease in prolonged incubation. When condition became oxic again, the truly dissolved P disappeared completely and approximately a half of large colloidal P dropped (Fig. 48). However, a significant amount of P remained in colloidal fraction, mainly inferior to 0.2 μm during the second oxic phase.

The traditional measurement of “dissolved” P using molybdenum blue method (SRP) is widely applied for 0.45-μm filtrates and often defined as orthophosphates despite increasing evidence that this method also quantifies a part of soluble unreactive P (SUP) according to the presence of colloid size ranges from as low as a few nanometers. Numerous studies had pointed out a varying degree of colloidal P to be hidden within SRP measurement (Haygarth et al., 1997; Shand et al., 2000; Filella et al., 2006; Zang et al., 2013; Gu et al., 2018). With the present results, we strongly support that operationally defined “dissolved” fraction is mainly colloid whereas truly dissolved P represents at maximum 10 % of water-mobilizable P. Moreover, colloidal P in fraction higher than 0.45 μm can represent up to 60 % of total P_{WM} at the end of anoxic period, highlighting that coarse colloids are thus a bearing-P phase of major importance. In water, the speciation of P is closely related to its bioavailability. In general, orthophosphates are immediately available, whereas the significance of colloidal P bioavailability is not well elucidated. Among a few researches focuses on the bioavailability of colloidal P, nano-colloids sized below 100 nm could be considered as bioavailable P. For example, colloidal P sized below 50 nm was shown to be as efficient as a solution of 5 μM phosphate in supporting algal growth (Van Moorlegem et al., 2013). However, colloidal P is mostly not immediately available for algae but is likely to be labile in a week (Baken et al., 2014). In lake, a monitoring of nano-colloidal P (sized 1-10 nm) and chlorophyll by Saeed et al. (2018) did provide an evidence for growth response of phytoplankton uptake via an elevation of chlorophyll level in adjacent to the presence of nano-colloidal P in lake hypolimnion.

According to these observations, we raised thus two questions: (1) Which mechanisms are involved in the production of colloidal P during anoxic condition? and (2) Why are P_{WM} higher in second oxic phase than first oxic phase and what are subsequent consequences on P mobility?

III.3.2.4.3. How anoxia induces mobilization of colloidal phosphorus?

III.3.2.4.3.1. Release of dissolved and colloidal P

The production/mobilization of colloids is generally caused by complex processes and has been revealed to be associated to changes in solution ionic strength, redox condition, pH and solution chemistry that influence surface charge of colloids as well as interparticle interaction (VandeVoort et al., 2013; Yan et al., 2016). It has been well demonstrated that the release of colloid from soil or sediment is strongly attributed to the reductive dissolution of cementing Fe oxides (Henderson et al., 2012; Yan et al., 2016, Ryan and Gschwend, 1990) or can be generated subsequently by reprecipitation of Fe and Mn once conditions became favorable (Zänker et al., 2006; Wolthoorn et al., 2004; Gunnars et al., 2002). Once the colloids are mobilized and dispersed in solution, the association of colloids with organic compounds can impact the stability of dispersed colloids via increase interparticle steric/electrostatic repulsion and modify the aging/crystallinity of minerals (Henneberry et al., 2012; Colombo et al., 2015; Yan et al., 2016; Liao et al., 2017; Li et al., 2019).

Therefore, in our case, the colloids produced during anoxic condition mostly consisted of iron, organic carbon and calcium and their releases were concomitant with increase in pH as well as OC and Fe^{2+} content increase in solution. This supports the fact that the release of colloid could be largely associated to the dissolution of Fe-oxide cementing agents or amorphous Fe coating that resulted in the fragmentation of sediment and lead to release of pre-existing P-containing colloids trapped in sediment matrix. In addition, the increase in solution pH can play a role in promoting colloid release to suspension upon fortified electrostatic repulsion between colloids or between colloids and particles via increasing negative surface charges of colloids and sediment surface. Nevertheless, during anoxic condition, in addition to iron release, a strong release of organic matter was observed and strongly related to colloid dynamic. The natural colloids commonly have heterogenous composition of both organic and mineral species (Gottselig et al., 2017a; Nguyen et al., 2020). The association of colloids with negatively charged organic compounds increased interparticle steric/electrostatic repulsion and therefore, play a similar role as increasing pH in enhancing the release of colloids from sediment matrix (Yan et al., 2016).

On the other hand, the dissolution of iron mineral could also cause a pulse release of truly dissolved P into the aqueous phase, as shown by the strong correlation between P and Fe^{2+} in fraction below 10 kDa ($R^2 = 0.96$). The mean P/Fe molar ratio released in truly dissolved fraction was of 0.5 indicated that phosphorus and iron were previously coprecipitated in sediment (Gunnars et al., 2002). Therefore, during anoxia, the dissolution of P-bearing iron cementing agents should be the main factors that controlled the release of colloidal and truly dissolved P.

III.3.2.4.3.2. Depletion of dissolved and possible formation of secondary phosphate mineral

The concomitant release of truly dissolved P and Fe within the first 14 days of anoxia (day 23 to 37) was followed by a decrease of them in the last 8 days (day 37 to 45) (Fig. 47). This truly dissolved P decrease can be attributed to (i) P incorporation in secondary mineral Fe oxides such as vivianite ($\text{Fe}_3(\text{PO}_4)_2 \cdot 8\text{H}_2\text{O}$) or apatite and/or (ii) re-adsorption of P to organo-mineral surface such as colloid or sediment.

Geochemical modelling calculation using concentrations of major ions, metals, nutrients in the fraction below 10 kDa on day 37 and day 45 illustrated that vivianite and FeCO_3 -apatite were able to precipitate according to saturation index (SI). These two minerals are widely considered as authigenic P-bearing

phase in sediment (März et al., 2018). The formation of vivianite in reducing sediment has been described previously to occur in elevated availability of ferrous and phosphate in pore water and under low production of free sulphide (Rothe et al., 2015;2016). The dissolution of Fe(III) oxy(hydr)oxydes, serving as ferrous source, accompanied with high release of scavenged orthophosphates acted as a precursor phase of vivianite precipitation (Rothe et al., 2016). The vivianite formation has been widely reported, and not limited to soil but also in freshwater system, particularly, they are commonly found during early diagenesis of organic sediment receiving high nutrient loads (Lemos et al., 2007; Taylor et al., 2008; Cosmidis et al., 2014). During first oxic period, the SI toward vivianite indicated undersaturation, due to low Fe and P amounts. When anoxia developed, the SI increased and reached value corresponding to oversaturation on day 37 and then near equilibrium on day 45, reinforcing the hypothesis of vivianite precipitation during anoxia. Concerning apatite, the onset precipitation of such mineral is commonly controlled by kinetic factor and is a slow process that could exceed several months (Trichet et al., 1994). Furthermore, most of Ca was observed in truly dissolved fraction (below 10 kDa). Therefore, the short period of anoxic phase (22 days) in our experimental setting might not induce ideal conditions for apatite formation.

The second hypothesis concerns the possible re-adsorption of dissolved P on organo-mineral colloids. It is well known that the association of Ca^{2+} and Mn^{2+} to carboxylic or phenolic groups of organic matter often affects surface charges of organic/organomineral colloids and can activate adsorption of phosphate onto these cation bonds (Iskrenova-Tchoukova et al., 2010; Thurman, 2012; Audette et al., 2020). The evolution of Ca and Mn contents and distribution during anoxia revealed their concomitant increase with OC in colloidal concentrations, implying the surface bridging of cations (Ca^{2+} and Mg^{2+}) on surface of organic matter that may favor adsorption of truly dissolved P, by surface complexation.

III.3.2.4.3.3. Size evolution of colloidal P

Along anoxic incubation not only a raise in quantity of colloidal P was observed, but also a shift in size class of colloidal P was noted, especially during the last 8 days (day 37 to 45, Fig. 47) when there was no remarkable evolution in quantity. The first factor to be considered during this size transformation of colloids is the significant presence of multivalent cations, such as Fe^{2+} , Ca^{2+} , Mg^{2+} and Mn^{2+} , acting as coagulants that neutralize negative charges of released colloids and destabilize colloids to form agglomerates of larger size. In contrast to the role of Fe in redox dynamic condition, Al was not impacted by anoxic incubation until the last 8 days of anoxia when a high increase of large colloidal Al was observed. This increase of colloidal Al was only observed for large colloidal fraction and could be derived as an indirect impact of iron cement dissolution that promote release of colloidal Al within sediment structure and followed by flocculation.

Our data also showed an important increase of organic carbon in fraction below $0.2 \mu\text{m}$ during anoxic phase, which is associated to anaerobic OM degradation. This presence of organic matter can promote aggregation of the organic matter-iron(II) colloids (Bastviken et al., 2004; Liao et al., 2017) and explain the gradual development of larger size colloidal P during prolonged anoxic incubation. A strong correlation of between P and OC in fraction $0.45 - 1 \mu\text{m}$ ($R^2 = 0.9992$) provides a hint for surface complexing of colloidal P with organic matter to form larger size colloids.

III.3.2.4.4. Behavior of colloidal P during transition phase between anoxic and second oxic conditions

The switching from anoxic to oxic condition had led to the strong decrease of P_{WM} . A half of colloidal P was removed during batch opening (day 45 to day 46). The decrease was effective for truly dissolved P and above all for large colloidal P fraction (0.45-1 μm).

At the end of anoxic phase, the truly dissolved P was $0.027 \pm 0.008 \text{ mg P/g}_{DW-Sed}$ and then dropped to under limit of detection on the first day of opening, in parallel of Fe^{2+} concentration that decreased from $0.11 \pm 0.01 \text{ mg Fe}^{2+}/\text{g}_{DW-Sed}$ to $0.005 \pm 0.001 \text{ mg Fe}^{2+}/\text{g}_{DW-Sed}$. At this transition condition, geochemical calculations revealed the oxidation of Fe(II) into Fe(III) leading to an oversaturation state toward ferric oxide and thus possible precipitation. These newly formed Fe(III) oxides could favor truly dissolved P sorption or coprecipitation (Elzinga and Sparks, 2007) and forming thus colloidal P under the second oxidative stage.

For colloidal fraction, the large colloidal P in oxic condition decrease drastically. This removal could be due to flocculation processes triggered by the oxidation of Fe^{2+} to Fe^{3+} and following iron oxy(hydr)oxide precipitation that can act as coagulant for large colloids. Remaining colloidal fraction also contained high levels of Mn and Mg, however the thermodynamic of solution, tested with Visual Minteq, did not showed the possibility of their precipitation. Even though, their declining concentration in dissolved fraction provided evidence that Mn and Mg were redistributed to solid fractions, hence, they might rather be bound to negatively charged surface of colloids or particulate phase, hence, as Ca, act as bridges for phosphate sorption (Tipping, 2002; Tipping and Heaton, 1983). This flocculation of colloidal P can also explain a shifting from nano-colloids to small/intermediate colloids during the first 10 days of second oxic phase (day 46 to 56).

Notwithstanding, as presented in Figs. 47 and 49a, during batch opening, the decrease of large colloidal P was more likely to be related to the decrease of large colloidal OC rather than due to Fe dynamic because colloidal Fe was not strongly impacted and was stable during oxic condition. Large colloidal P was illustrated in previous section to be formed by the agglomeration of colloids by coagulants or with organic matter. At the end of anoxic phase, a very high C/Fe molar ratio was observed at 11.5 for large colloids, indicating the organic matter embedded completely colloids inside their structure. Right after opening, this C/Fe molar ratio dropped by 30 %, in combination with decline of both colloidal P and OC in fraction below 0.2 μm , this could suggest colloid aggregation/flocculation. As a consequence, this further aggregation/flocculation of colloids according to high level of OM occurred immediately at anoxic-oxic transition to form particulate P and return to be redeposited in sediment transition point (Yan et al., 2016).

Despite a half of P_{WM} released during anoxia was removed at batch opening, about a half content of P_{WM} kept being suspended in solution even when condition became oxic and mainly present in colloidal form. As discussed in previous section, the colloidal P generated during anoxic phase can contain a wide variety of composition, including iron phosphate minerals (eg. vivianite) and organo-mineral P. Vivianite is not easy to be solubilized (Rothe et al., 2016), thus probably contributes significantly to residual colloidal P in oxic phase. Meanwhile the association of negatively charged organic matter on mineral colloids can stabilize dispersed P-colloids due to interparticle steric/electrostatic repulsion and lowering aggregation as well as crystallization of iron minerals (Angelico et al., 2014; Colombo et al., 2015; Yan et al., 2016). Considering co-precipitation of mineral and organic matter during second oxic phase, the molar ratio of C/Fe for all size fractions remained ranging from 1.1 to 9.6, indicating a partially coverage of mineral surface by organic matter (Chen et al., 2014) and could maintain colloids to be dispersed. This finding is of great concern for environmental implication because once being

released from anoxic sediment, these stable colloidal P is highly dynamic and can migrate for longer distance to reach surface water and can be a source of nutrient for aquatic species.

III.3.2.5. Conclusion

Reducing condition facilitated an important mobilization of water-mobilizable P (dissolved and colloidal P) with predominant release of colloidal P (approximately 90 % of water-mobilizable P). The return to oxidative condition of the batches did not induce a return to initial P distribution as observed in the first oxic stage. P_{WM} was only partially immobilized with main impact on truly dissolved P and a half of colloidal P, in particular large colloids. In general, the initial stage of anoxic condition induced P release in formed of truly dissolved phosphorus and small colloidal P as well as the release of cations and organic matter through reductive dissolution of iron minerals and anaerobic organic matter decomposition. Latterly, this complex solution chemistry could lead to a suit of reactions that favor the formation of secondary phosphate mineral, such as vivianite, and re-adsorption of freshly released phosphates to colloids. Furthermore, according to solution chemistry (concentrations of organic matter and cationic coagulants), the shift towards larger size of P-colloids could be induced via coprecipitation and bridging aggregation/flocculation. The presence by a half of colloidal P under second oxic phase might derived from (i) the remaining of stable P-containing colloidal aggregates previously mobilized under anoxic phase and (ii) a minor amount of the newly formed colloids due to coprecipitation of P with iron(III) oxides generated under newly oxic phase. Our findings thus shed a light on the remarkable release of colloidal P during anoxia and that a major part of this colloidal P remain dispersed in solution even under following oxic condition. The release and stability of these colloidal P from sediment under changing redox condition contributes importantly to improve knowledge of P mobility at sediment-water interface in particularly and for freshwater ecosystem in general.

Acknowledgements:

This work was supported by the France's Nouvelle-Aquitaine Regional Council; the EDF Electric utility company; and the "Dam and Water Quality" Chair of Excellence, University of Limoges Partnership Foundation.

III.3.3. Limitation of freeze drying pretreatment on quantification of colloid suspension

III.3.3.1. Study context

The freeze-drying is the process of water removal through ice sublimation from frozen materials under vacuum (Adams, 2007). Unlike other preservation techniques such as air-drying and oven-drying, freeze-drying is considered as less disruptive method that minimize the alteration or damage of original structure of examined sample by limiting shrinkage due to surface tension caused by water evaporation (Hoffmann et al., 2004; Nègre et al., 2004; Perrott, 1977). Freeze-drying is commonly used to preserve soils and sediment for long-term conservation serving the investigations of phosphorus sorption, organic matters turnover and trace metals speciation (Islam et al., 1997; Rapin et al., 1986; Bordas and Bourg, 1998; Xu et al., 2012; Rolffhus et al., 2015; Kim et al., 2016; Xu et al., 2019; Chiaia-Hernández et al., 2020). Furthermore, several studies applied freeze-drying to quantify dry mass of colloids or to preserve colloidal samples for chemical analysis. For example, Missong et al., (2016) used freeze-drying to weight the dry mass of water-dispersible colloids released from soil and prepared for ^{31}P -NMR analysis. Meanwhile Yan et al., (2016) freeze-dried colloidal pellets separated by successive centrifugations (corresponding cut-off sizes are 1 μm and 0.1 μm) to measure colloidal concentration extracted from soil.

Despite a wide assumption that freeze-drying does not deteriorate samples (Kodamatani et al., 2017), several studies have pointed out the influence of sample pretreatment by freeze-drying on P sorption and fractionation in sediment, disrupt organic matter and modify metal speciation (Zhang et al., 2001; Hjorth, 2004; Hung et al., 2012). Futhermore, in this thesis, freeze-drying of sediment caused significant decrease in colloidal mass (due to precipitation of Fe and Al acting as cementing agents for agglomeration of colloids and of colloid to particles) and changes in chemical composition of colloids (enrichment in P, Ca and OC) (see section III.1.2.3.2). These findings strongly emphasize the significant impacts of sediment preservation by freeze-drying on colloid' elemental composition and colloid stability. Since no bibliographic information highlights the influence of freeze-drying on colloidal fraction, this complementary part of this thesis devotes to providing some remarks on this subject. For this, the quantification of colloids was done with freeze-drying pretreatment for samples collected during incubation of sediment under anoxic condition (see Part II.3.2).

III.3.3.2. Materials and methods

A 30-mL aliquot of water-mobilizable fraction (0 – 1 μm) separated by successive filtrations (at 2.7 μm and 1 μm), was transferred to a polypropylene 60-mL tube and frozen at $-20\text{ }^\circ\text{C}$ for 24 h. The frozen suspensions were freeze-dried for 3 days until completed removal of water was achieved. It should be noted that before starting freeze-dry, all containers were covered with parafilm and poked several holes by a needle to avoid the loss of material by vacuum. The dry weight of water-mobilizable fraction (M_{WM}) was quantified with a Sartorius balance providing a read-out of 0.00001 g.

The concentration of water-mobilizable fraction (C_{WM}) was then reported in milligrams of water-mobilizable dry weight per gram of sediment dry weight ($\text{mg/g}_{\text{DW-Sed}}$). Because water-mobilizable fraction comprised of both dissolved species and colloidal particles, concentration of colloidal particles (CC_i) was then calculated by the subtraction of C_{WM} by total dissolved salt concentration (TDS) (Eq. 17). The concentration of phosphate was measured by molybdenum blue method according to Murphy and Riley, (1962). The TDS was determined as the sum of all inorganic substances present in fraction below 10 kDa ($\text{Fe}^{2+}/\text{Fe}^{3+}$, Al^{3+} , P-PO_4^{3-} , Ca^{2+} , Mn^{2+} , Mg^{2+} , Na^+ , NH_4^+ , K^+ , F^- , Cl^- , NO_2^- , NO_3^- , SO_4^{2-} , HCO_3^-) and reported in $\text{mg/g}_{\text{DW-Sed}}$. The anionic and cationic concentrations of Na^+ , NH_4^+ , K^+ , F^- , Cl^- , NO_2^- , NO_3^- , SO_4^{2-} were determined by ionic chromatography (Agilent). The concentration of HCO_3^- was

measured by acid titration until pH reach 4.3. The concentrations of Fe, Al, Ca, Mn, Mg in fraction below 10 kDa were quantified with MP-AES without acid digestion. All analysis were done on fraction below 10 kDa. The TDS, in this case, can be underestimated due to other unanalyzed elements which, in turn, can lead to overestimation of CC_1 . The overestimation of TDS in fraction below 10 kDa, which can be caused by fragmentation of colloids with ultrafiltration, was excluded due to the similar observation in ionic concentration between fraction below 0.2 μm and 10 kDa.

Equation 17. Estimation of colloidal concentration (CC_1) by subtraction of concentration of water-mobilizable fraction (C_{WM}) to total dissolved salts (TDS). C_{WM} was determined after freeze-drying water-mobilizable fraction.

$$CC_1 (mg/g_{DW-seed}) = C_{WM} (mg/g_{DW-seed}) - TDS (mg/g_{DW-seed})$$

The estimated colloidal concentration CC_1 was then compared to partial colloidal concentration (CC_2) determined as the sum of all analyzed elemental composition in colloidal fraction 10 kDa – 1 μm (ΣCC_i), regarding to P, OC, Fe, Al, Ca, Mn, Mg contents (Eq. 18). This determination of CC_2 is another way to estimate colloidal concentration but can underestimate actual colloidal concentration due to presence of other unanalyzed elements. The colloidal elemental concentrations (CC_i) of P, Fe, Al, Ca, Mn, Mg were determined as differences between total concentrations in fraction below 1 μm and dissolved concentrations in fraction below 10 kDa. The total concentration of P in fraction below 1 μm was measured after persulfate digestion according to US EPA 365.1 method (1993) and quantified by molybdenum blue method according to Murphy and Riley, (1962). The concentrations of Fe, Al, Ca, Mn, Mg in fraction below 1 μm were quantified with MP-AES with acid digestion. Colloidal concentration of OC was measured by TOC-analyzer (Shimadzu) and accounted for fraction 0.2 – 1 μm because of contamination in fraction 10 kDa – 0.2 μm from ultrafiltration materials.

Equation 18. Estimation of colloidal concentration (CC_2) as the sum of colloidal concentrations (ΣCC_i) of analyzed elements “i” varying among P, OC, Fe, Al, Ca, Mn, Mg) in fraction 10 kDa – 1 μm .

$$CC_2 = \Sigma CC_i = CC_P + CC_{OC} + CC_{Fe} + \dots$$

All these chemical analysis were done on fresh sample of water-mobilizable fraction and measurement methods are detailed in Part II.

III.3.3.3. Results and discussion

As shown in Figure 51, throughout the incubation, concentration of colloids ranged up to 9.3 ± 1.4 $\text{mg/g}_{DW-seed}$ and were only found at the end of anoxic 1 (days 37 and 45), and during oxic 2 (days 46 – 63). The other days, no colloids were quantified. This result of colloid concentration quantified after freeze-drying of water-mobilizable fraction demonstrated that colloids were released only in certain sampling points. Furthermore, during phase Oxic 1, the levels of C_{WM} were relatively lower than TDS, particularly on day 7 where C_{WM} was 27 ± 8 % smaller than TDS. In fact, colloids can be found at a level of approximately 5 $\text{mg/g}_{DW-seed}$ in water (see Part III.1.2), therefore the zero observation of colloids during this first period of incubation seems to be a bias, of analytical technique or quantification method itself.

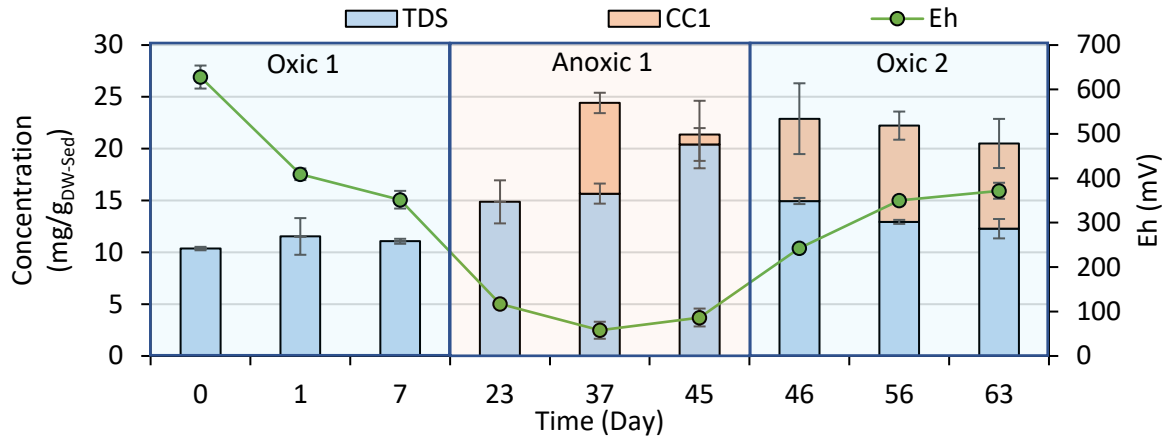


Figure 51. The concentrations of total dissolved salts (TDS) and calculated colloidal concentration in freeze-dried fraction sample ($< 1 \mu\text{m}$). Data obtained from the incubation of fresh sediment under redox oscillation (see section II.2.3). Method of colloid quantification was freeze-drying of fraction below $1 \mu\text{m}$.

In comparison with CC_2 (Fig. 52), the sum of colloidal elemental concentrations (P, OC, Fe, Al, Ca, Mn, Mg) in fraction $10 \text{ kDa} - 1 \mu\text{m}$ appeared significantly different than CC_1 for all sampling days. During phase Oxidic-1, CC_2 ranged from 0.66 ± 0.13 to $1.04 \pm 0.14 \text{ mg/g}_{\text{DW-Sed}}$ and revealed that colloids were present from the very first moment of the incubation, which is contrast to zero release observed with CC_1 . During phases Anoxic-1 and Oxidic-2, the CC_2 ranged from 2.12 ± 0.31 to $3.75 \pm 0.36 \text{ mg/g}_{\text{DW-Sed}}$ and were 2.9 – 4.4 times lower than CC_1 , except on day 45. However, to some extents, this variability observed between CC_1 and CC_2 , particularly to higher CC_2 values from day 0 to day 23, can provide evidence for the loss of materials in colloidal fraction upon freeze-drying treatment of water-mobilizable fraction, and that the smaller CC_2 from day 37 to day 63 (except day 45) could be due to unanalyzed elements.

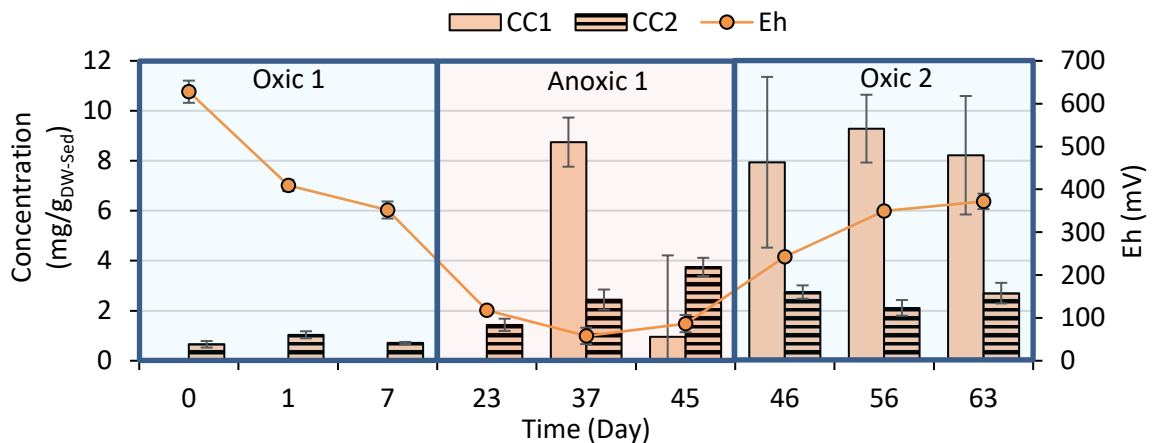


Figure 52. The concentration of colloidal fractions ($10 \text{ kDa} - 1 \mu\text{m}$) estimated by sum of analyzed elements (P, OC*, Fe, Al, Ca, Mn, Mg) in fresh water-mobilizable fraction (below $1 \mu\text{m}$) without freeze-drying. Data obtained from the incubation of fresh sediment under redox oscillation (see section II.2.3). *Colloidal concentration of OC was accounted for fraction $0.2 - 1 \mu\text{m}$ due to contamination from ultrafiltration material for fraction $10 \text{ kDa} - 0.2 \mu\text{m}$.

By comparison the results of CC_1 and CC_2 , a significant mass of colloids could be lost during freeze-drying (from 8-100 %). The freeze-drying removes water by sublimation of ice, however, if concentration of material are low, the interparticle forces between colloids are not sufficient to retain colloids from flying off with the flow of ice under vacuum (Brydon et al., 1963). Though, a hint for the breakdown of interparticle bonds between colloids during freeze-drying might be seen by the powdery and fluffy structure of colloids (Fig. 53b) compared to what is obtained by oven evaporation (at 30°C, Fig. 53a). However, this phenomena has not been stated elsewhere nor subjected to recent researches, therefore, the proposition of colloid moving with ice sublimation cannot be considered as a reliable hypothesis.

Another hypothesis relied on the impact of drying on hydrophobicity of dispersed colloids initiated by Klitzke and Lang, (2007), could suggest that the loss of colloids with ice might also be induced by the increase in hydrophilicity of colloids that enhance hydrogen bonding of colloids towards water molecules which results in removal of both ice crystal and adhesion colloids. However, this effect of freeze-drying on surface hydrophobicity of colloids cannot be deduced in this study and needs further investigation.

A third hypothesis could be due to the fragmentation of colloids under very high centrifugation forces (6000g) during ultrafiltration that can release nanocolloids sized lower than 10 kDa and pass through the ultrafiltration unit membrane. The impact of centrifugation at high speed was shown to have impacts on increasing both organic and inorganic species in dissolved fraction (see Part III.1.2, elemental content of fraction below 0.2 μm by protocol e, Fig. 25b). The high centrifugation force perhaps disrupted the organo-mineral colloids that generally have lower stability and adhesion forces. The release of nanocolloids after ultrafiltration at 10 kDa could contribute to overestimate TDS level by increasing the contents of Fe, Al, Ca, Mn, Mg in fraction below 10 kDa determined by MP-AES. This overestimation of TDS would then lead to underestimation of CC_1 .

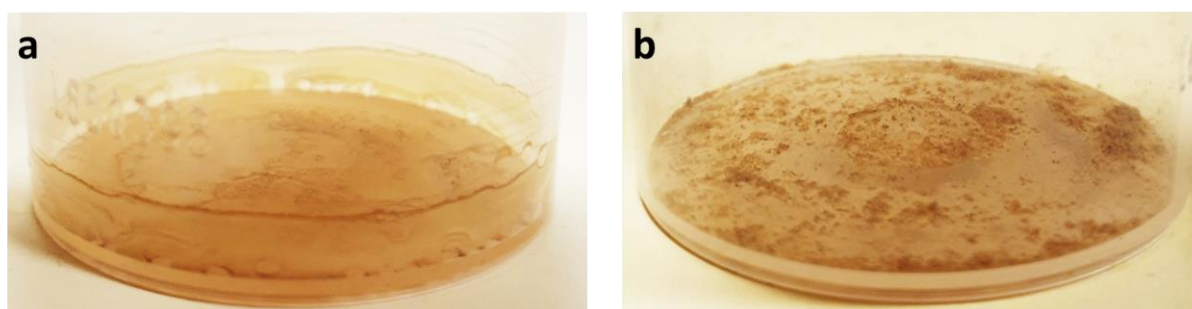


Figure 53. Effect of water evaporation at 30°C (a) and freeze-drying (b) on structure of water-mobilizable fraction (including colloids and dissolved species).

Based on these preliminary experimental results, it can be deduced that the application of freeze-drying to pretreat water-mobilizable fraction for afterward quantification of colloidal concentration is not recommended, particularly for sedimentary colloids in regard to loss of colloidal material under ice sublimation and vacuum. This problem has not been indicated in literature that freeze-dried colloidal material and thus requires further examination to identify the real impacts of freeze-drying on sedimentary colloidal. For this, a proposition is to examine the differences in colloidal concentration and colloid composition obtained from oven-dried and freeze-dried colloidal sample. In case the loss of colloids caused by low density and interparticle forces, the increase of colloidal concentration could be achieved by CFF separation at high concentration factor.

III.3.3.4. Conclusion

In general, the use of freeze-drying as a pre-treatment for colloid quantification showed drawbacks on the recovery quantity of colloids. This lower colloid recovery could be a result of either freeze-drying process (vacuum of low-density particles, change in colloid hydrophobicity) or the impact of centrifugation-based ultrafiltration process (induce release of nanocolloids due to fragmentation of larger size colloids). Further examination could be interesting to elucidate which parameter affect the use of freeze-drying on colloid quantification, for example, characterization of colloid surface properties and checking the impact of ultrafiltration unit on size of colloids. Though, according to obtained results, it is recommended not using freeze-drying protocol to obtain the dry mass of colloids. Other quantification protocols could be employed, such as drying at 30°C or turbidity (Yan et al., 2017b).

III.3.4. Conclusion

Concerning the mobility and behavior of P in association with colloids under redox dynamic condition, the main messages are:

- Between 67 % and 100 % of released P during oxic/anoxic/oxic cycles was in colloidal form, mainly in 300 kDa-0.45 μm fraction.
- P release was promoted in anoxia:
 - o About 40 % of total sedimentary P can be released under water-mobilizable form (below 1 μm) during anoxic condition.
 - o The release of colloidal P could be due to reductive dissolution of iron cement.
 - o Truly dissolved P was unstable under prolonged anoxia, probably by secondary mineral formation.
- Oxic condition induced very low production of colloidal P:
 - o Major part of anoxia-released colloidal P remained in oxic solution.
 - o About 20 % of total sedimentary P remained in suspension under colloidal form (sized 300 kDa-0.45 μm) when condition got oxic again.
- Flocculation/agglomeration of colloidal P during extended anoxia to form large colloidal size and during extended oxic condition to form small/intermediate colloidal size, probably due to OM surface complexation and release of coagulants (Fe^{2+} , Ca^{2+} , Mg^{2+} and Mn^{2+}).

Concerning the quantification of colloids, the use of freeze-drying as a pretreatment to obtain dry colloidal mass is not recommended due to possible mass loss under vacuum.

Part IV : General discussion and conclusion

Previous study of Champsanglard dam reservoir suggested that sediments can release P not only under dissolved inorganic phosphorus (DIP) but also under colloidal form (Rapin, 2018). From this supposition and from growing evidence on colloidal-bound P transport in various matrices (soil, water, vadose sediment, groundwater), an investigation on the presence of colloidal P in the sediment as well as sedimentary colloids mobility in reservoir sediments was of great interest.

In this context, this PhD work aimed to evaluate the role of sediments accumulated in dam reservoir (Champsanglard, Creuse River, France) to release P and to assess the contribution of colloids in the mobility and bioavailability of P.

Experimental part of this work assembled the results concerning the following tasks:

- Characterization of Champsanglard sediments (presented for each Part III.1, III.2 and III.3).
- Assessment of the role of the methods selected for colloid extraction, separation and for sediment storage on the quantification of water-mobilizable sedimentary colloids (fraction 0.2 – 1 μm) and P (Part III. 1).
- Evaluation of the potential of Champsanglard sediments to release colloids (fraction 0 – 1 μm) and P :
 - o under sediment resuspension (Part III.2).
 - o under changing redox condition (Part III.3).

The synthesis and main outcomes of this dissertation is aimed to provide a new prospect of the internal P load from sediment to water column in reservoir context, considering the colloidal fraction.

IV.1. How sediment storage mode and colloid extraction/separation protocol influence on the quantity and quality of colloids recovered from sediment matrix?

Natural colloids are heterogenous in size and composition (organic, mineral, organo-mineral). In sediments, colloids could be present in interstitial space or be attached to organic and mineral particles or in association with other colloids (Kretzschmar et al., 1999). Subsequently, the quantification and characterization of sedimentary mobilizable colloids require an appropriate method for colloid extraction from raw materials as well as suitable method for colloid separation from truly dissolved and particulate fractions. Moreover, because the extraction of colloids is done under laboratory condition, thus, an appropriate method to store sediment dedicated to the colloid extraction after field sampling is also necessary.

On these subjects, the first stage of this research work devoted on an evaluation of various methods for colloids extraction (agitation, sonication), colloids separation (filtration, centrifugation and their combination) and sediment storage prior to colloid recovery (wet sediment, drying at 20°C, drying at 40°C and freeze drying). It was conducted with Champsanglard sediment sampled in the lacustrine part of the reservoir. At this stage, we also provided a preliminary evaluation on the importance of P present in colloidal form compared to truly dissolved P.

The results (presented in part III.1) demonstrated that each examined method provided a different result comparing to each other with a factor up to 40, either in terms of mass or quality (chemical composition, size distribution) of recovered colloids. According to an evaluation of the quantity and chemical properties of the recovered colloids between the examined methods, an identification of proper approach to isolate colloids from sediment was proposed.



The results of the evaluation of colloids extraction from the sediment by various methods indicated that sonication (at 240 J/mL) provided more powerful energy and generated more colloids than the less energetic agitation. The change in colloidal size distribution, shape toward more globular and chemical composition towards more organic was demonstrated. The colloids released under the ultrasonic field may contain not only labile colloids present in porewater, but also the colloids generated upon disruption of the sediment structure and colloidal agglomeration. The alkaline extraction is also not recommended because a higher pH can release additional colloids by the dissolution of organic binding agent in aggregates or between colloids and sedimentary particles. Furthermore, when dealing with the evaluation of sedimentary P mobility, this method leads to overestimation because of P desorption due to competition for sorption sites with hydroxide ions.

Regarding separation of colloids following extraction, one of the interesting outcomes is that a filtration at 1 μm is not sufficient because of rapid filter clogging and thus underestimation in the mass of recovered colloids. In contrast, the application of the sole centrifugation (*i.e.*, successive centrifugations, in replacement of 1 μm filtration) can easily lead to inaccuracies in the cut-off size due to heterogeneity in particle density, and eventually overestimation of the colloid quantity. In this case of heterogenous sample, the filtration at 1 μm is necessary and important to ensure correct cut-off size. However, it is important to perform a preliminary pre-separation to avoid filter clogging by removal of large particles with either filtration (*e.g.*, 2.7 μm) or centrifugation (*e.g.*, at 272 g and during 6 min for a particle density of 2.42).

Concerning the modes of sediment storage and compared to fresh wet sediment, large colloids extracted from dried sediments showed higher concentrations of organic carbon (1.2 to 1.5-fold) and P (1.5 to 2.9-fold), and particularly significant increase in Ca (2.6-fold) concentration after freeze-drying. Therefore, attention should be paid to how the sediment is stored prior to colloid extraction. This finding also reveals the impact of single drying and rewetting on mobilization of sedimentary colloids by a decline from 12 to 75 % in mass depending on drying mode.

In conclusion, the correct approach to isolate sedimentary colloids is necessary to be identify according to sample characteristics. For the case of Champsanglard sediments, the proper approach is (i) to extract colloids from fresh wet sediment using low mechanical energy such as agitation and (ii) to separate colloids from suspension (containing particles, colloids and dissolved species) by filtration with pre-separation at higher cut-off size using filtration (*e.g.*, 2.7 μm) or centrifugation (*e.g.*, at 272 g and during 6 min for a particle density of 2.42). A proposal guideline allowing feasible and correct selection of colloid extraction protocol from sediment is presented in Fig. 54.

In addition to the evaluation of proper colloid recovery methods, this chapter provides, on the other aspect, a confirmation on the important presence of P in the sediment in colloidal forms. It concerns not only large fraction 0.2-1 μm but also the fraction operationally defined as dissolved (below 0.2 μm). The amount of sedimentary P bound to colloids was significantly higher, 4 to 34-fold depending on the recovery method, than truly dissolved P and attributed a proportion of up to 5.8 % of total sedimentary P, justifying further evaluation in reservoir context.

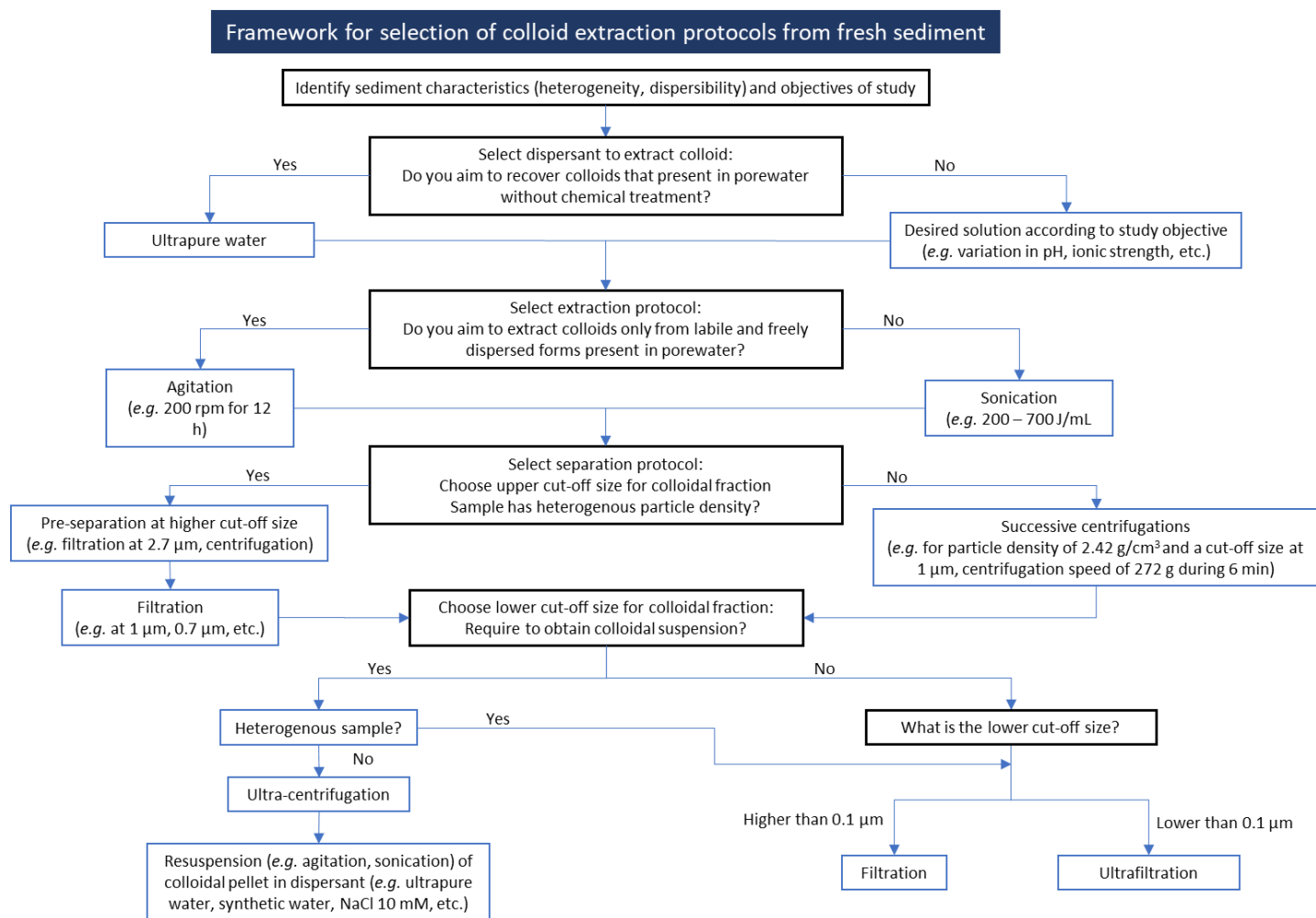


Figure 54. Framework for selecting a method for of colloid extraction from a sediment matrix.

Research into validating the most appropriate method to recover colloids from sediment is still far from complete. Further examination should include testing different solid-liquid mass ratios, the duration of the extraction and the power of extraction (agitation and sonication). It is also important to consider the sediment characteristics (e.g., compare the quantity and quality of colloids recovered from sediment that is poor in P and OM, or richer in clay minerals, or sediment originated from calcareous watershed). In addition, there is no validated method for accurate quantification of dry colloidal mass, thus, it is important to develop this quantification method. If such evaluations could be performed, it would be possible to develop a standard normalized procedure for isolating colloids from sediment or other matrices. This standard for colloid recovery procedure could support feasible cross-studies comparison.

IV.2. What is the potential of reservoir sediment to release colloids and colloidal P?

IV.2.1. In-situ variability in water-mobilizable fractions of colloids and colloidal P from reservoir surface sediments

The accumulation of sediments in a dam reservoir behaves differently than in a natural lake due to the intermediate hydrodynamic characteristics between the river and the lake. The spatial distribution of the sediment in reservoirs is complex, unevenly and dependent on deposit location and hydrodynamic

energy (Abraham et al., 1999). The preferential accumulation of fine sediment usually occurs in low-energy zones, such as deeper zones and shoreline areas (Rose et al., 1993; Kirk and Bradley, 1995).

The need to investigate the spatial variability of the potential of sediment to release colloids and P in Champsanglard reservoir is justified by important spatial heterogeneity in (i) chemical composition of accumulated sediment and (ii) sedimentary P stock and speciation as revealed by sequential extraction by Rapin et al., (2020). In addition, the Champsanglard dam induces a fluctuation of water-level up to few meters in the reservoir, and thus a part of sediment, located in banks and tails of dam reservoir, could be impacted by drying during low water flow. In this study, we demonstrated that sediment drying has a significant impact on the physicochemical characteristics of recovered colloids (Part III.1.2), therefore the potential of the sediments impacted by drying could be different compared to the permanently submerged sediments.

Despite previous evidence of the intrinsic presence of water mobilizable colloids and P in the sediment accumulated in lacustrine part of the reservoir (Nguyen et al., 2020), their occurrence in sediments deposited along and across the reservoir remained questionable. Therefore, in order to assess the spatial distribution of water mobilizable colloids and P at the reservoir scale, an *in-situ* investigation had taken into account the: (i) longitudinal variability according to channel hydrodynamic and morphology and (ii) lateral variability according to changes in local hydraulic pattern and topography (Part III.2). The results of this part provide notable information about the spatial heterogeneous potential of sediment to release water-mobilizable colloids and P.

For all studied sites, results showed that the size of colloids was polydisperse and was not significantly impacted by different deposition sites. The variability in the content of water-mobilizable colloids from bottom sediments was strongly correlated to sediment granulometry. Indeed, higher amount of water mobilizable colloids was found for fine-grained sediments. This indicated that the distribution of sedimentary colloids was dependent on deposition of fine-grained particles, the process mainly driven by flow dynamic and channel morphology (Fig. 55). The potential of the sediment to release colloids and P was higher for bottom sediments accumulated in the lacustrine part of the reservoir and increased towards the dam, in comparison to bottom sediments accumulated in the riverine zone. The quantity of colloids suitable for mobilization in riverine bottom sediments was attributed to about 0.35 ± 0.02 % of the sediment mass whereas for lacustrine bottom sediments this amount was averagely at 1.5 ± 0.04 % of the sediment mass.

Chemical composition of the recovered colloids reflected the geological context of the watershed (mainly granitic). However, it did not strongly inherit the chemical properties of in-situ sediment and was rather influenced by in-situ biogeochemical dynamics, such as removal of organic colloids with more turbulent upstream flow and Fe recycling upon periodical development of anoxia in the bottom of lacustrine area. Colloids found in riverine bottom sediments were richer in P, Fe and Ca than colloids from lacustrine bottom sediments (Fig. 55).

In lacustrine bottom sediments, the water-mobilizable P (P_{WM}) represented an average of 4.4 % of total sedimentary P and a major part of this P_{WM} (91 %) was in colloidal form (Fig. 55). Meanwhile, in riverine bottom sediments, the P_{WM} were attributed to 3.7 % of total sedimentary P, averagely, and contained lower proportion of colloidal P (80 % of P_{WM}) (Fig. 55). Whatever the localization of sediment, this result has pointed out that sedimentary released colloids are richer in P than sediment themselves and thus represent a phosphorus hot spot inside sediment. These lower quantities of P_{WM} and proportion of colloidal P in riverine bottom sediment compared to lacustrine one was mainly due to the decline of

large colloidal P. This decline could be explained by increased organic matter oxidation in more oxygenated environment involving the degradation of colloids.

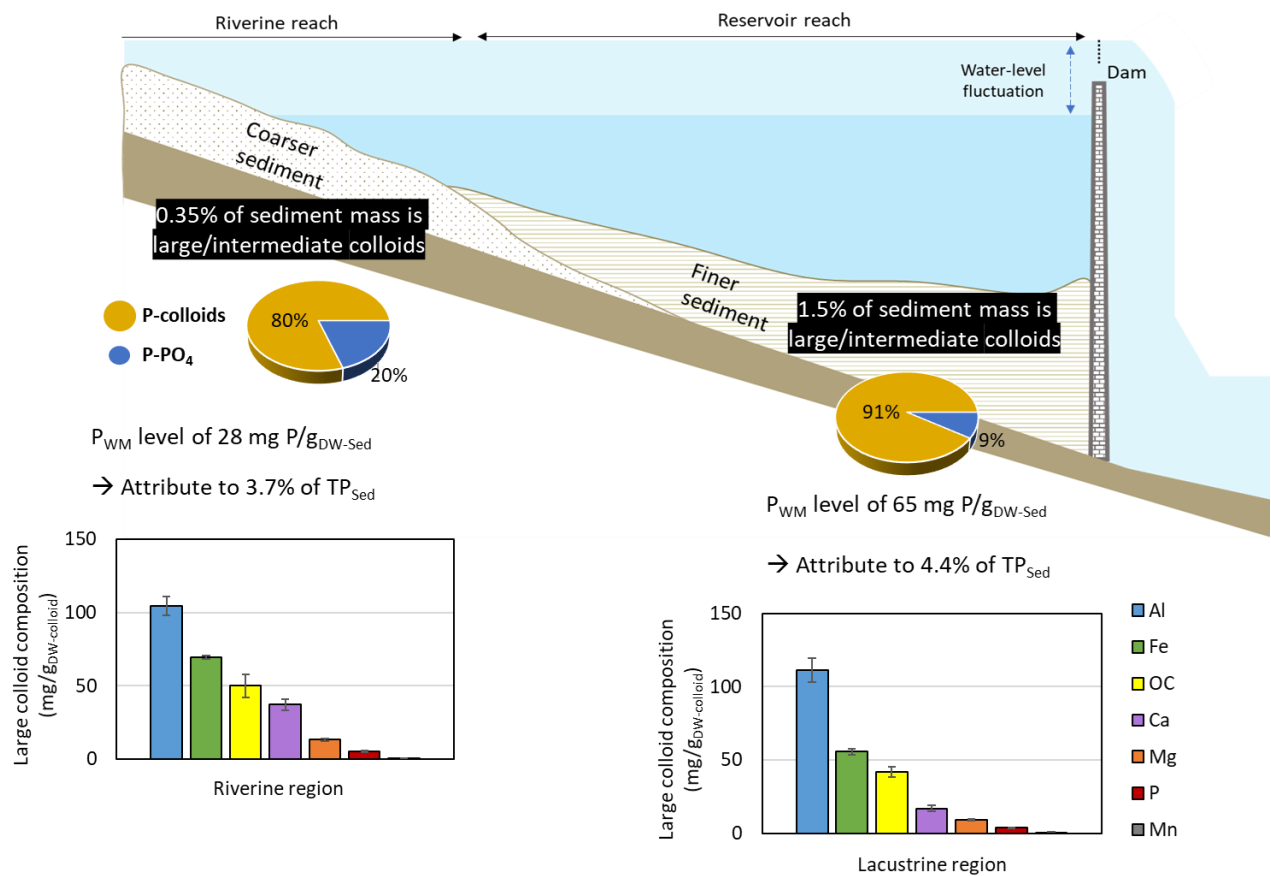


Figure 55. Variability in mass (mg/g_{DW-sediment}) and chemical composition of large colloids (mg/g_{DW-colloid}), and partitioning of water-mobilizable P between riverine and lacustrine regions of Champsanglard reservoir.

The Champsanglard reservoir featured by two inlets of tributary, one located in the tail of the reservoir (point 7) and another located in the lacustrine zone (point 3) that is coupled with meandering bend (namely confluent meander bend). The entering of two tributaries showed a significant impact on the allocation of water-mobilizable colloids to the downstream of confluence (Fig. 56). The more turbulent conditions at the mixing boundary of two flows prevent the finest and low-density particles from settling and even resuspend deposited material. At the same time, the tributaries carry an additional load of suspended materials either from tributary flow or from the bank erosion that contributes to downstream deposition. In our system, higher quantity of water mobilizable colloids was detected on site 2, the site in the downstream of the tributary in the confluent meander bend (Fig. 56), with a significant elevation in colloid quantity by 30 % to reach a maximum quantity of colloids at 2.3 % of sediment mass. This redistribution of colloids with turbulent flow was effective mainly for organic colloids in which higher organic concentration was found in downstream deposition of tributaries (Fig. 56). Therefore, higher organic concentration in recovered colloids was found in the sediment deposited downstream of confluent meander bend (site 2). The impact of this tributary on the quantity of P_{WM} in downstream sediment (site 2) and on partitioning between colloidal and dissolved forms were not significant (Fig. 56). However, a slight lower in percentage of P_{WM} to total sediment P was noticed in the downstream of both tributaries, for instances, from 5.2 ± 0.1 % at confluent meander bend dropped to 4.5 ± 0.2 % in deposited downstream sediment (site 2) and from 4.4 ± 0.3 % at tail confluence dropped to 3.5 ± 0.2 % in downstream sediment (site 6).

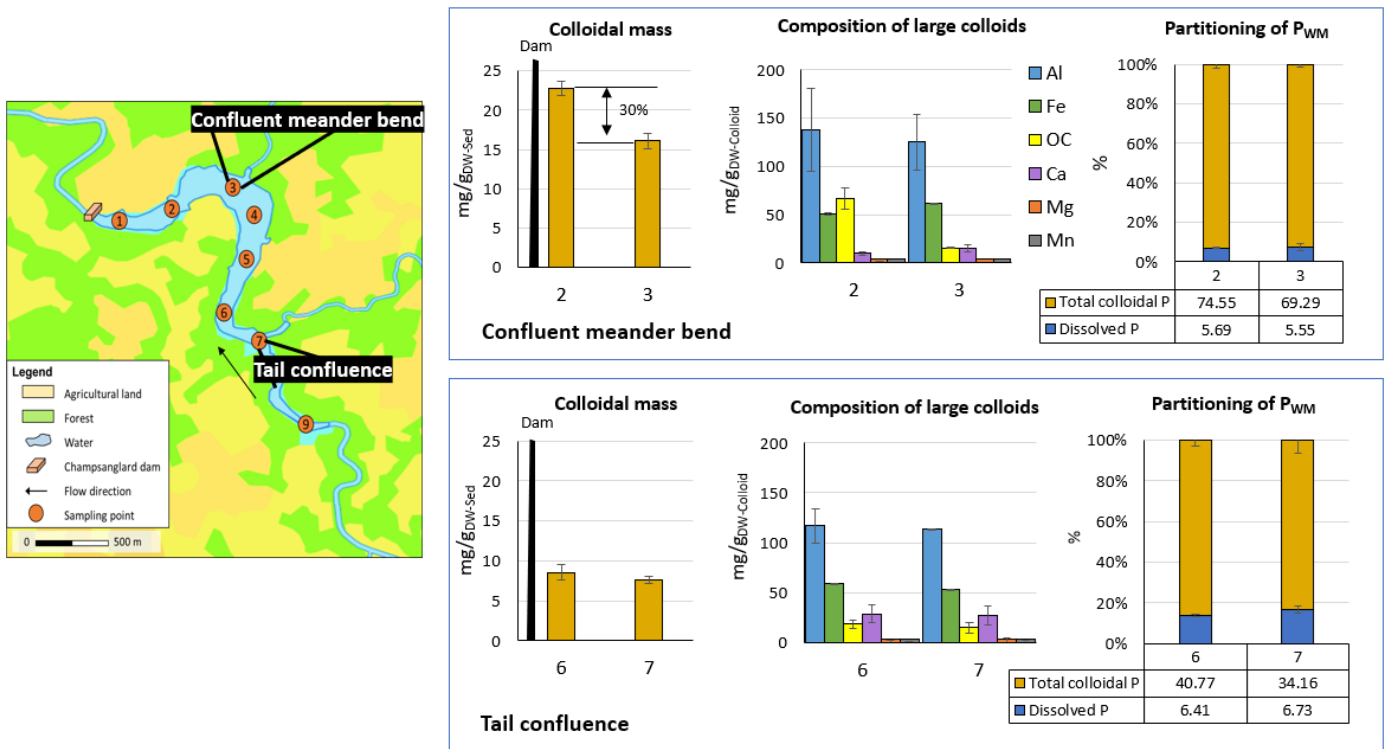


Figure 56. Variabilities in mass (mg/g_{DW-sediment}) and chemical composition of large colloids (mg/g_{DW-colloid}), and partitioning of water-mobilizable P under downstream influence of tributaries.

Together with lacustrine zone, the shoreline of riverine part of reservoir was also characterized by lower energy flow and sediments located in this area also contained higher reserve of colloids than the sediments located in higher energy riverbed. However, unlike the strong influence of channel morphology and hydrodynamic on colloid mobility in lacustrine zone, the bank sediments were more affected by the variations in the water table level. The fluctuations in water level lead to the alternating desiccation (at low-flow) and rewetting (at high-flow) of sediments deposited in the bank of the channel. The regular alternation between drying and rewetting of sediment showed strong impact on water-mobilizable colloids and P levels (Fig. 57). Quantity of water-mobilizable colloids in bank sediments were attributed from 0.65 % to 1.7 % of sediment mass and were higher than observed for bottom sediments with a factor from 1.7 to 6. The higher amount of colloids in sediments towards the land was highly linked to duration of air exposure and frequency of drying/rewetting. Bank sediments exhibited also differences in chemical composition of their colloids in comparison with bottom sediments. The concentrations of P, Ca and Mg in colloids were lower for bank sediments than in colloids from associated bottom sediments. Among bank sediments, the concentrations of P, OC, Fe, Al in large colloids showed a tendency to decrease with increasing bank surface altitude.

The quantity of P_{WM} across the river transect was not related to the amount of water-mobilizable colloids. P_{WM} level was higher in bank than in bottom sediments, with the highest P_{WM} found in sediments located at the shoreline and experienced rapid drying and rewetting. Among bank sediments, the higher bank surface altitude and the lower frequency and duration of rewetting were observed together with the lower level of large colloidal P but higher levels of dissolved and small/nano colloidal P (below 0.2 μm). As shown in Fig. 57, the P_{WM} in sediment that was regularly submerged (site 8A) contained 20 % of dissolved P and 80 % of colloidal P. Whereas, the P_{WM} in sediments that are regularly desiccated (at

higher bank surface altitude) contain generally higher proportion of dissolved P (50 % for sites 8B - 8C and 80 % for site 9B) and lower proportion of colloidal P (50 % for site 8B - 8C and 20 % for site 9B). In a scenario of global climate change, the fluctuation of water level could be reinforced and cause higher loss in sedimentary dissolved P and subsequently, higher P availability in associated water body of this areas.

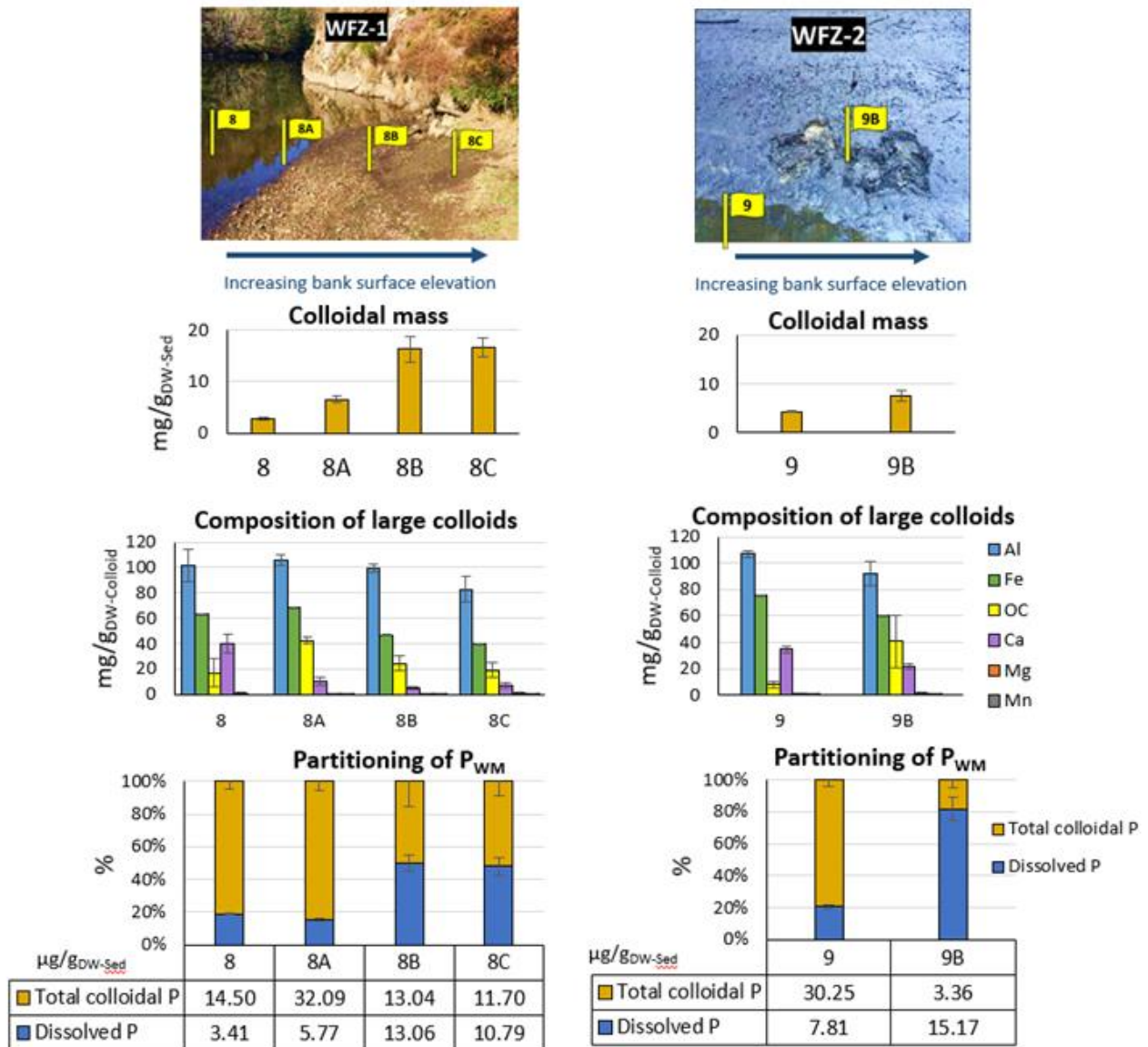


Figure 57. Variabilities in mass (mg/g_{DW-sediment}) and chemical composition (mg/g_{DW-colloid}) of large colloids and partitioning of water-mobilizable P across two transects of water-level fluctuation zones (WFZ-1 and WFZ-2).

IV.2.2. Potential of lacustrine sediment to mobilize colloidal P upon anoxic condition

According to the field investigation in spatial variability of sedimentary P-colloid along Champsanglard reservoir, the sediments accumulated in lacustrine region contained higher level of water-mobilizable P, especially in large/intermediate colloidal form, than in riverine region. Lacustrine region is often characterized by deeper (about 12 m) and more stagnant water that can favor the development of anoxic condition in bottom sediment with stratified water layer. The finding of Rapin et al., (2019) concerning the presence of temporal anoxic condition in the reservoir water in the lacustrine part of the Champsanglard and their hypothesis regarding the formation of colloids under the oxidation of

previously reduced sedimentary iron, the sense to investigate the fate and behavior of colloidal P under redox changing conditions was reinforced.

Therefore, in order to assess the colloidal phosphorus mobility at the water/sediment interface, a laboratory experimentation was performed by incubating sediment submitted to changing redox condition, and a particular focus was made on colloidal fraction.

First major result of this experimentation is that a strong amount of phosphorus, corresponding to $0.8 \text{ mg P/g}_{\text{DW-Sed}}$ was released in solution during oxic/anoxic/oxic incubation, represented about $40 \pm 5 \%$ of total sedimentary P. This points out a non-permanent retention of P in this sediment. The release of P_{WM} was mainly operated under anoxia. Indeed, during the first oxic stage, it represented only $1.0 \pm 0.2 \%$ of total P in sediment, highlighting that permanent oxic condition restricts the mobilization of sedimentary P in colloidal and dissolved forms compared to anoxia. This important P generation and release under anoxia could be linked to complex reactions that encompassing redox dynamic of Fe, organic matter evolution and presence of multivalent cations. In fact, Fe oxy(hydr)oxides are a host phase of P and can act as cementing agents, binding organo-mineral colloids together or with sediment. Reductive dissolution of iron minerals could be one of the key mechanisms involved in the release of both dissolved and colloidal P. Under oxic condition, such redox-sensible species (Fe) do not transform, and low amount of sedimentary P reloaded the water. Moreover, the change in solution pH and mobilization of organic compounds in anoxia were likely to impact on surface interaction, by increasing negative surface charges of colloids and particles and enhancing electrostatic repulsion between colloid-colloid and between colloid-particle. As iron, organic matter acts also as binding agent in aggregates or between colloids and sedimentary particles and its release can thus promote colloids mobilization.

The second major result is that the released P_{WM} was mostly present in colloidal fraction (from 67 % to 97 % of P_{WM}) and that a transformation in size class of colloidal P occurred during anoxia from small/intermediate size (300 kDa – $0.45 \mu\text{m}$) in the first 14 days, then, to large size ($0.45 - 1 \mu\text{m}$) by the end of anoxia stage (22 days). Surprisingly, the release of truly dissolved P, instead of continued to increase over time with extended anoxia, was unstable throughout the incubation and a major part (78 % of maximum released dissolved P at $0.08 \pm 0.04 \text{ mg P/g}_{\text{DW-Sed}}$) was depleted from solution in the meantime of colloidal size shifting. The monitoring of truly dissolved fraction and colloidal composition over time indicates that various parameters and processes could contribute to these phenomena. Increase in pH during anoxia led to the released of organic matter that on one hand stabilized the dispersed colloid and keeping them suspended, and on another hand, promote aggregation of the organic matter-iron(II) colloids and contribute to formation of large colloidal P via surface complexation. These two effects of organic compounds could be overlap and induce complex colloidal system. Furthermore, a precipitation of commonly found authigenic iron phosphate minerals, the vivianite, was effectively able to occur according to thermodynamic and could explain for depletion of truly dissolved P during anoxia. The role of multivalent cations such as Fe^{2+} , Ca^{2+} , Mg^{2+} and Mn^{2+} present in solution could impact on re-adsorption of dissolved P on organo-mineral surface via surface bridging or act as coagulants that neutralize negative charges of released colloids and destabilize colloids to form agglomerates of larger size.

The third major result is that a return to oxic condition after anoxic stage, which did not allow a return to initial stage with very low P mobilization from sediment. In this condition, a large amount of P_{WM} was still present, at $0.45 \pm 0.08 \text{ mg P/g}_{\text{DW-Sed}}$ ($22 \pm 4 \%$ of P_{Sed}) in sediment solution and could be able for a liberation from interstitial water to overlying water once sediment gets disturbed, especially in nano-colloidal form (10 – 300 kDa) at first then mainly in small/intermediate colloidal form (300 kDa

–0.45 μm). This is a main result for reservoir management. Sediment oxygenation permits the formation of small/intermediate colloidal P englobing approximately 80 % of P_{WM} and 15 % of total sedimentary P. At this stage, organic matter seemed to be a major factor controlling the dynamic of P. A high organic content in solution can constraint flocculation process, stabilize small/intermediate colloidal P and limit the redeposition of colloids into sediment.

This study highlights the enormous release of sedimentary P to reservoir solution in form of colloids once anoxia developed at the bottom of reservoir. The more important remark is the stable suspension of these colloidal P even in oxic water once being liberated. Therefore, in the context of large dam reservoir where temporal anoxic condition occurs, the risk of bottom sediment to reload P to water column is high and durable since the form of mobilized P is labile, dynamic but stable.

IV.3. The releasing risk of water-mobilizable P from reservoir sediment to water column

According to the results concerning the evaluation of the potential release of water-mobilizable P from reservoir sediments upon resuspension (Part III. 2) and concerning the notable release of water-mobilizable P under anoxia (Part III. 3), it is relevant to highlight the risky zones and conditions responsible for P release from sediments to reservoir water.

Bottom sediments accumulated in lacustrine part of the reservoir exhibited higher amount of water-mobilizable P than bottom sediments occurring in riverine area. The power of sediment mechanical perturbation played an important role of the quantity of mobilizable large P-colloids (0.2 - 1 μm). For example, the release of large/intermediate P-colloids from the lacustrine bottom sediment accumulated in site 2 and under oxic condition was $6.5 \pm 2.2 \mu\text{g P/g}_{\text{DW-Sed}}$ ($0.32 \pm 0.11 \%$ of P_{Sed}) under gentle perturbed condition (manual batched agitation during first oxic stage of redox experiment) and was 12-fold lower than under the more vigorous perturbed condition (agitation at 200 rpm, 24 h) at $70.7 \pm 3.1 \mu\text{g P/g}_{\text{DW-Sed}}$ ($3.9 \pm 0.2 \%$ of P_{Sed}) (Table 19). The release of small/nano colloidal P under oxic condition was low for both gentle and more vigorous agitation, at $11.1 \pm 0.7 \mu\text{g P/g}_{\text{DW-Sed}}$ respectively ($0.54 \pm 0.04 \%$ of P_{Sed}) and $3.9 \pm 0.2 \mu\text{g P/g}_{\text{DW-Sed}}$ ($0.21 \pm 0.01 \%$ of P_{Sed}), respectively. This observation indicates that the mobilization of large P-colloids from sediment to water column can occur at low amount and without significant changes in physical and chemical properties of solution and was fortified when sediment experienced more turbulent condition, like resuspension.

Under anoxic condition, the amount of sedimentary P released in large colloidal form increased up to 75-fold to reach $0.49 \pm 0.09 \text{ mg/g}_{\text{DW-Sed}}$ and attributed to $23.9 \pm 4.6 \%$ of P_{Sed} (Table 25). In addition, an important release of sedimentary P was also observed in small/nano colloidal fraction, at $0.30 \pm 0.01 \text{ mg/g}_{\text{DW-Sed}}$ ($14.7 \pm 0.6 \%$ of P_{Sed}). Thus, it is possible that during summertime, the development of anoxia in hypolimnion of reservoir upon thermal stratification lead to an important release of sedimentary P to water column under colloidal form (especially the large colloids) without sediment resuspension.

As for the riverine section of the reservoir, the surface sediments accumulated in this part are more oxygenated compared to lacustrine sediments, and the bank sediments are additionally affected by fluctuations in the water-level. This bank sediments frequently subjected to drying and rewetting, have a high potential to release large P-colloids (site 2, Table 25) and comparable to the bottom sediments upon resuspension. The highest release of the small/nano P-colloids were obtained also for bank sediments, at site 8A and site 8C can release comparable amounts at $11.1 \pm 1.6 \text{ mg/g}_{\text{DW-Sed}}$ ($1.6 \pm 0.3 \%$ of P_{Sed}) and $11.7 \pm 2.1 \text{ mg/g}_{\text{DW-Sed}}$ ($1.3 \pm 0.3 \%$ of P_{Sed}) respectively (Table 25). It should also be noted that bank sediments subjected to water-level fluctuations release up to 4.5-fold more dissolved P than

bottom sediments upon resuspension (Part III. 2). Consequently, special attention should be paid to the sediment deposited in water-level fluctuation zone, as they can release bioavailable P.

Table 25. Comparison in water-mobilizable P, small/nano and large colloidal P release from sediment under various conditions (mechanical resuspension and changing redox condition) between riverine and lacustrine areas and between bank and bottom deposition. Releasing condition of resuspension refers to agitation of sediment under laboratory condition (orbital agitation at 200 rpm, results showed in Part III.2). Releasing condition under oxic phase refers to gentle agitation under the first oxic phase of redox changing experiment (results showed in Part III.3.2). Releasing condition under anoxic phase refers to gentle agitation under the anoxic phase of redox changing experiment (results showed in Part III.3.2).

Note: NA: not available, ND: not determined, < LOQ: inferior to limit of quantification

Zone of reservoir		Riverine						Lacustrine					
Sediment sampling site		Bank 8C		Bank 8A		Bottom 8		Bottom 2					
Releasing condition		Resuspension		Resuspension		Resuspension		Resuspension		Oxic		Anoxic	
		Mean	SD	Mean	SD	Mean	SD	Mean	SD	Mean	SD	Mean	SD
Water-mobilizable P	µg/g sed	23.0	3.0	38.0	3.0	17.9	0.8	80.0	4.0	19.0	3.0	800.0	100.0
	% TP sed	2.4%	0.3%	5.6%	0.3%	2.5%	0.4%	4.5%	0.2%	0.9%	0.1%	40.00%	5.0%
Small/nano colloidal P	µg/g sed	11.7	2.0	11.0	2.0	0.5	0.1	3.9	0.1	11.1	0.7	300	20.0
	% TP sed	1.3%	0.2%	1.6%	0.2%	0.1%	0.0%	0.2%	0.0%	0.5%	0.0%	14.7%	0.6%
Large/intermediate colloidal P	µg/g sed	< LOQ	< LOQ	21.0	1.5	14.0	0.8	71	4	6.5	2.1	500.0	100.0
	% TP sed	NA	NA	3.1%	0.3%	2.0%	0.4%	3.9%	0.2%	0.3%	0.1%	24.0%	5.0%
	mg/g colloid	NA	NA	3.30	0.40	5.30	0.40	3.10	0.20	ND	ND	ND	ND

Apart from evaluating the potential of reservoir sediments to release water-mobilizable P, this work also highlights the release of other elements like OC, Fe, Al and Ca in form colloidal and dissolved form (Table 26). In oxic condition, the highest potential to release large colloidal OC, Fe and Al were obtained for bank sediments deposited at the shoreline, frequently submitted to drying and rewetting (site 8A) and lacustrine bottom sediments with resuspension (site 2, Table 25), as for P. Under anoxic condition, for site 2, the level of P in large colloids is far higher than what were observed in all other tested conditions, and far higher than the levels of OC, Fe, Al and Ca. Further investigations should be carried out to identify the involved processes.

Table 26. Comparison of the content of large colloidal OC, Fe, Al and Ca released from sediments under various conditions (mechanical resuspension and changing redox condition) between riverine and lacustrine regions and between bank and bottom deposition. Releasing condition of resuspension refers to sediment agitation under laboratory condition (results showed in Part III.2). Releasing condition under oxic phase refers to gentle agitation under the first oxic phase of redox changing experiment (results showed in Part III.3.2). Releasing condition under anoxic phase refers to gentle agitation under the anoxic phase of redox changing experiment (results showed in Part III.3.2).

Note: NA: not available, ND: not determined.

Zone of reservoir		Riverine						Lacustrine					
Sediment sampling site		Bank (site 8C)		Bank (site 8A)		Bottom (site 8)		Bottom (site 2)					
Releasing condition		Resuspension		Resuspension		Resuspension		Resuspension		Oxic		Anoxic	
		Mean	SD	Mean	SD	Mean	SD	Mean	SD	Mean	SD	Mean	SD
Large colloidal OC	mg/g sed	0.30	0.05	0.29	0.01	0.04	0.02	1.6	0.3	0.11	0.03	0.62	0.12
	% OC sed	0.24	0.04	0.42	0.01	0.14	0.08	1.6	0.3	0.10	0.03	0.6	0.2
	mg/g colloid	20	6	43	4	20	20	70	20	ND	ND	ND	ND
Large colloidal Fe	mg/g sed	0.66	0.03	0.44	0.03	0.18	0.02	1.16	0.08	0.11	0.02	0.2	0.2
	% Fe sed	1.3%	0.08	1.2	0.1	0.46	0.05	1.4	0.1	0.13	0.02	0.2	0.2
	mg/g colloid	40	5	69	3	64	2	51	4	ND	ND	ND	ND
Large colloidal Al	mg/g sed	1.36	0.06	0.69	0.05	0.27	0.01	3	2	0.07	0.01	0.22	0.05
	% Al sed	2.6	0.3	1.6%	0.2	0.66	0.02	2.1	0.7	0.04	0.01	0.14	0.03
	mg/g colloid	90	10	106	5	110	20	140	50	ND	ND	ND	ND
Large colloidal Ca	mg/g sed	0.12	0.03	0.06	0.01	0.11	0.01	0.22	0.05	0.0019	0.0033	0.3	0.3
	% Ca sed	1.6	0.4	1.2	0.3	3.0	0.6	2.7	0.7	0.02	0.04	4	4
	mg/g colloid	8	3	10.	4	40	8	10	3	ND	ND	ND	ND

Prospects to broaden this study:

This thesis pointed out the main role of colloidal fraction in internal P loads in Champsanglard reservoir. It also highlights the spatial variability of sedimentary colloids and associated P along reservoir, considering tributary influence and specific behaviour of bank sediments. In order to fulfil the understanding about the processes involved in mobility of colloidal P from sediment to water column, in the future it could be interesting to examine the following subjects:

- Single drying and rewetting (air-dry mode, part III.1.2) of lacustrine sediment was shown to induce higher release of small and nano P-colloids compared to wet sediment. Also, the *in-situ* bank sediments deposited in riverine area, and affected by several DRW cycles, showed higher release of large and small/nano colloidal P than permanently submerged sediments (part III.2). Therefore, it is important to test the impact of different frequency and duration of drying and rewetting cycles on the release of water-mobilizable P of reservoir sediments. Especially in the context of sediments excavation related to dam management and in the context of climatic changes that influence hydrological patterns. This could evaluate the risk sediment drying and rewetting in the release of P (both small/nano and large colloids) during sediment drying and resuspension.
- Temporal thermal stratification can induce repeated anoxic and oxic phases at the bottom sediment. therefore, the evaluation of colloidal P dynamic under oscillating redox conditions is necessary to better evaluate the risk of internal colloidal P loads.
- Since colloidal fraction is dynamic and continuously undergoes mobilization and removal in aquatic environment, the monitoring of colloids and associated P under changing redox condition should be

carried out in less discrete sampling time, for example, sampling can be taken each day. Another proposition is to work with higher volume of sample for each batch to allow more types of analysis, such as DRX analysis for mineral phases, SEM-EDS observation for size and morphology of colloids, FTIR spectroscopy for identify functional groups of OM.

The spatiotemporal variability in colloids and associated P should be examined and compared between various dam reservoirs to better identify the key factors controlling their dynamics in reservoir context.

IV.4. Environmental aspects and impacts/practices

This thesis highlights the spatial distribution of sedimentary colloids susceptible to be released in dam reservoir upon sediment resuspension and under changing redox condition. A considerable amount of colloidal P in addition to truly dissolved P can be liberated from sediments to reservoir water, especially when the sediment was impacted by the water-level fluctuation and/or subjected to anoxia. The release of highly bioavailable forms of P from sediment could contribute to phytoplankton growth and maintaining eutrophication in reservoir. Therefore, the management of the dam reservoir should consider the physico-chemical conditions that can involve in higher P release from sediments: anoxia and drying/rewetting. For these purposes, management strategies of dam reservoir should take into account the following:

- Limit the development of anoxic condition in lacustrine zone of the reservoir. This management strategy has been already recommended as a prevention against eutrophication and methanization. Several techniques have been implemented such as bubble diffusion (Dijk and Vuuren, 2012; Lima Neto, 2019) and hypolimnetic aeration (Singleton and Little, 2006). Though the aeration of hypolimnion replenishes dissolved oxygen, this operation should be carefully considered because it can cause resuspension of sediment and thus induce important P load to water column (as highlighted in table 19).
- Control the drying/rewetting frequency of bank sediment: Reservoir water level should be managed to avoid important water-level fluctuation that responsible for emergence and drying of bank sediments, for example, by limit residence time or rapidly replenish water after reservoir emptying. Another proposition could be to remove bank sediments that are rich in OM and P in case of long-term emergence.

In addition, the release of water-mobilizable P from sediments to water could induce different environmental impacts depending on season. For example, in case of summer thermal stratification, anoxia-induced release of water-mobilizable P can favor bloom of phytoplankton. Furthermore, even when conditions get oxic again, the P release from sediment could still represent a P load, able to sustain eutrophication. In case of cold season, primary production is limited, the resuspension of water-mobilizable P from sediment could migrate with downstream flow and impact the downstream dam reservoir or contribute to P transport towards the ocean. The dissolved and small colloidal P (both considered as bioavailable) generated in the bank sediments upon drying, can be flushed and transported downstream during higher water level and thereby maintain phytoplankton bloom in lacustrine part of the reservoir.

Bibliographic references

- Abraham, J., Allen, P.M., Dunbar, J.A., Dworkin, S.I., 1999. Sediment type distribution in reservoirs: sediment source versus morphometry. *Environmental Geology* 38, 101–110. <https://doi.org/10.1007/s002540050406>
- Adair, J.H., Suvaci, E., Sindel, J., 2001. Surface and Colloid Chemistry, in: Buschow, K.H.J., Cahn, R.W., Flemings, M.C., Ilchner, B., Kramer, E.J., Mahajan, S., Veysière, P. (Eds.), *Encyclopedia of Materials: Science and Technology*. Elsevier, Oxford, pp. 1–10. <https://doi.org/10.1016/B0-08-043152-6/01622-3>
- Adams, G., 2007. The Principles of Freeze-Drying, in: Day, J.G., Stacey, G.N. (Eds.), *Cryopreservation and Freeze-Drying Protocols, Methods in Molecular Biology™*. Humana Press, Totowa, NJ, pp. 15–38. https://doi.org/10.1007/978-1-59745-362-2_2
- Ahearn, D.S., Dahlgren, R.A., 2005. Sediment and nutrient dynamics following a low-head dam removal at Murphy Creek, California. *Limnology and Oceanography* 50, 1752–1762. <https://doi.org/10.4319/lo.2005.50.6.1752>
- Al-Essa, K., Khalili, F., 2018. Adsorption of Humic Acid onto Jordanian Kaolinite Clay: Effects of Humic Acid Concentration, pH, and Temperature. *Science Journal of Chemistry* 6, 1. <https://doi.org/10.11648/j.sjc.20180601.11>
- Alewell, C., Ringeval, B., Ballabio, C., Robinson, D.A., Panagos, P., Borrelli, P., 2020. Global phosphorus shortage will be aggravated by soil erosion. *Nature Communications* 11, 4546. <https://doi.org/10.1038/s41467-020-18326-7>
- Aller, R.C., 2014. 8.11 - Sedimentary Diagenesis, Depositional Environments, and Benthic Fluxes, in: Holland, H.D., Turekian, K.K. (Eds.), *Treatise on Geochemistry (Second Edition)*. Elsevier, Oxford, pp. 293–334. <https://doi.org/10.1016/B978-0-08-095975-7.00611-2>
- Alvarez, R., Evans, L.A., Milham, P.J., Wilson, M.A., 2004. Effects of humic material on the precipitation of calcium phosphate. *Geoderma* 118, 245–260. [https://doi.org/10.1016/S0016-7061\(03\)00207-6](https://doi.org/10.1016/S0016-7061(03)00207-6)
- Amelung, W., & Zech, W., 1999. Minimisation of organic matter disruption during particle-size fractionation of grassland epipedons. *Geoderma*, 92(1-2), 73-85.
- Amirtharajah, A., Raveendran, P., 1993. Detachment of colloids from sediments and sand grains, in: Tadros, Th.F., Gregory, J. (Eds.), *Colloids in the Aquatic Environment*. Elsevier, Oxford, pp. 211–227. <https://doi.org/10.1016/B978-1-85861-038-2.50018-8>
- Anderson, D.M., Glibert, P.M., Burkholder, J.M., 2002. Harmful algal blooms and eutrophication: Nutrient sources, composition, and consequences. *Estuaries* 25, 704–726. <https://doi.org/10.1007/BF02804901>
- Andersson, G., Granéli, W., Stenson, J., 1988. The influence of animals on phosphorus cycling in lake ecosystems. *Hydrobiologia* 170, 267–284. <https://doi.org/10.1007/BF00024909>
- Andrade, V.S., Wiegand, C., Pannard, A., Gagneten, A.M., Pédrot, M., Bouhnik-Le Coz, M., Piscart, C., 2020. How can interspecific interactions in freshwater benthic macroinvertebrates modify trace element availability from sediment? *Chemosphere* 245, 125594. <https://doi.org/10.1016/j.chemosphere.2019.125594>
- Angelico, R., Ceglie, A., He, J.-Z., Liu, Y.-R., Palumbo, G., Colombo, C., 2014. Particle size, charge and colloidal stability of humic acids coprecipitated with Ferrihydrite. *Chemosphere* 99, 239–247. <https://doi.org/10.1016/j.chemosphere.2013.10.092>
- Anschutz, P., Chaillou, G., Lecroart, P., 2007. Phosphorus diagenesis in sediment of the Thau Lagoon. *Estuarine, Coastal and Shelf Science, Biogeochemical and contaminant cycling in sediments from a human-impacted coastal lagoon* 72, 447–456. <https://doi.org/10.1016/j.ecss.2006.11.012>

- Arai, Y., Sparks, D.L., 2007. Phosphate Reaction Dynamics in Soils and Soil Components: A Multiscale Approach. *Advances in Agronomy* 94, 135–179. [https://doi.org/10.1016/S0065-2113\(06\)94003-6](https://doi.org/10.1016/S0065-2113(06)94003-6)
- Arnold, R.G., DiChristina, T.J., Hoffmann, M.R., 1988. Reductive dissolution of Fe(III) oxides by *Pseudomonas* sp. 200. *Biotechnol. Bioeng.* 32, 1081–1096. <https://doi.org/10.1002/bit.260320902>
- Audette, Y., Smith, D.S., Parsons, C.T., Chen, W., Rezanezhad, F., Van Cappellen, P., 2020. Phosphorus binding to soil organic matter via ternary complexes with calcium. *Chemosphere* 260, 127624. <https://doi.org/10.1016/j.chemosphere.2020.127624>
- Azam, H.M., Alam, S.T., Hasan, M., Yameogo, D.D.S., Kannan, A.D., Rahman, A., Kwon, M.J., 2019. Phosphorous in the environment: characteristics with distribution and effects, removal mechanisms, treatment technologies, and factors affecting recovery as minerals in natural and engineered systems. *Environmental Science and Pollution Research* 26, 20183–20207. <https://doi.org/10.1007/s11356-019-04732-y>
- Bacchin, P., Espinasse, B., Bessiere, Y., Fletcher, D.F., Aimar, P., 2006. Numerical simulation of colloidal dispersion filtration: description of critical flux and comparison with experimental results. *Desalination, International Congress on Membranes and Membrane Processes* 192, 74–81. <https://doi.org/10.1016/j.desal.2005.05.028>
- Bajpai, P., 2018. Chapter 19 - Colloid and Surface Chemistry, in: Bajpai, P. (Ed.), *Biermann's Handbook of Pulp and Paper* (Third Edition). Elsevier, pp. 381–400. <https://doi.org/10.1016/B978-0-12-814238-7.00019-2>
- Baken, S., Moens, C., van der Grift, B., Smolders, E., 2016a. Phosphate binding by natural iron-rich colloids in streams. *Water Res.* 98, 326–333. <https://doi.org/10.1016/j.watres.2016.04.032>
- Baken, S., Nawara, S., Van Moorleggem, C., Smolders, E., 2014. Iron colloids reduce the bioavailability of phosphorus to the green alga *Raphidocelis subcapitata*. *Water Research* 59, 198–206. <https://doi.org/10.1016/j.watres.2014.04.010>
- Baken, S., Regelink, I.C., Comans, R.N.J., Smolders, E., Koopmans, G.F., 2016b. Iron-rich colloids as carriers of phosphorus in streams: A field-flow fractionation study. *Water Research* 99, 83–90. <https://doi.org/10.1016/j.watres.2016.04.060>
- Baker, D.B., Johnson, L.T., Confesor, R.B., Crumrine, J.P., Guo, T., Manning, N.F., 2019. Needed: Early-term adjustments for Lake Erie phosphorus target loads to address western basin cyanobacterial blooms. *Journal of Great Lakes Research* 45, 203–211. <https://doi.org/10.1016/j.jglr.2019.01.011>
- Baldwin, D.S., Mitchell, A.M., 2000. The effects of drying and re-flooding on the sediment and soil nutrient dynamics of lowland river–floodplain systems: a synthesis. *Regulated Rivers: Research & Management* 16, 457–467. [https://doi.org/10.1002/1099-1646\(200009/10\)16:5<457::AID-RRR597>3.0.CO;2-B](https://doi.org/10.1002/1099-1646(200009/10)16:5<457::AID-RRR597>3.0.CO;2-B)
- Balesdent, J., Petraud, J.P., & Feller, C., 1991. Some effects of ultrasonic vibrations on size-distribution of soil organic matter. *Science du Sol (France)*.
- Baoligao, B., Xu, F., Chen, X., Wang, X., Chen, W., 2016. Acute impacts of reservoir sediment flushing on fishes in the Yellow River. *Journal of Hydro-environment Research* 13, 26–35. <https://doi.org/10.1016/j.jher.2015.11.003>
- Bartlett, R., James, B., 1980. Studying Dried, Stored Soil Samples — Some Pitfalls. *Soil Science Society of America Journal* 44, 721–724. <https://doi.org/10.2136/sssaj1980.03615995004400040011x>
- Bastviken, D., Persson, L., Odham, G., Tranvik, L., 2004. Degradation of dissolved organic matter in oxic and anoxic lake water. *Limnology and Oceanography* 49, 109–116. <https://doi.org/10.4319/lo.2004.49.1.0109>

- Beauchemin, S., Hesterberg, D., Chou, J., Beauchemin, M., Simard, R.R., Sayers, D.E., 2003. Speciation of phosphorus in phosphorus-enriched agricultural soils using X-ray absorption near-edge structure spectroscopy and chemical fractionation. *Journal of Environmental Quality* 32, 1809–1819.
- Bergendahl, J., & Grasso, D. (1998). Colloid generation during batch leaching tests: Mechanics of disaggregation. *Colloids and Surfaces A: Physicochemical and Engineering Aspects*, 135(1-3), 193-205.
- Berhe, A. A., & Kleber, M., 2013. Erosion, deposition, and the persistence of soil organic matter: mechanistic considerations and problems with terminology. *Earth Surface Processes and Landforms*, 38(8), 908-912.
- Berkowitz, B., Dror, I., Yaron, B., 2008. *Contaminant Geochemistry: Interactions and Transport in the Subsurface Environment*. Springer Science & Business Media.
- Berthold, M., Wulff, R., Reiff, V., Karsten, U., Nausch, G., Schumann, R., 2019. Magnitude and influence of atmospheric phosphorus deposition on the southern Baltic Sea coast over 23 years: implications for coastal waters. *Environmental Sciences Europe* 31, 27. <https://doi.org/10.1186/s12302-019-0208-y>
- Bessiere, Y., Fletcher, D.F., Bacchin, P., 2008. Numerical simulation of colloid dead-end filtration: Effect of membrane characteristics and operating conditions on matter accumulation. *Journal of Membrane Science* 313, 52–59. <https://doi.org/10.1016/j.memsci.2007.12.064>
- Best, J.L., & Rhoads, B.L., 2008. Sediment transport, bed morphology and the sedimentology of river channel confluences. *River confluences, tributaries and the fluvial network*, 45-72.
- Beutel, M.W., 2006. Inhibition of ammonia release from anoxic profundal sediments in lakes using hypolimnetic oxygenation. *Ecological Engineering, The Growth of Ecological Engineering: The Fifth Annual Conference of the American Ecological Engineering Society* 28, 271–279. <https://doi.org/10.1016/j.ecoleng.2006.05.009>
- Biermann, C.J., 1996. 21 - Colloid and Surface Chemistry, in: Biermann, C.J. (Ed.), *Handbook of Pulp and Papermaking (Second Edition)*. Academic Press, San Diego, pp. 421–437. <https://doi.org/10.1016/B978-012097362-0/50025-X>
- Björkman, K.M., Karl, D.M., 2003. Bioavailability of dissolved organic phosphorus in the euphotic zone at Station ALOHA, North Pacific Subtropical Gyre. *Limnology and Oceanography* 48, 1049–1057. <https://doi.org/10.4319/lo.2003.48.3.1049>
- Blackwell, M.S.A., Brookes, P.C., de la Fuente-Martinez, N., Murray, P.J., Snars, K.E., Williams, J.K., Haygarth, P.M., 2009. Effects of soil drying and rate of re-wetting on concentrations and forms of phosphorus in leachate. *Biology and Fertility of Soils* 45, 635–643. <https://doi.org/10.1007/s00374-009-0375-x>
- Bocaniov, S.A., Ullmann, C., Rinke, K., Lamb, K.G., Boehrer, B., 2014. Internal waves and mixing in a stratified reservoir: Insights from three-dimensional modeling. *Limnologica* 49, 52–67. <https://doi.org/10.1016/j.limno.2014.08.004>
- Bol, R., Julich, D., Brödlin, D., Siemens, J., Kaiser, K., Dippold, M.A., Spielvogel, S., Zilla, T., Mewes, D., von Blanckenburg, F., Puhmann, H., Holzmann, S., Weiler, M., Amelung, W., Lang, F., Kuzyakov, Y., Feger, K.-H., Gottselig, N., Klumpp, E., Missong, A., Winkelmann, C., Uhlig, D., Sohrt, J., von Wilpert, K., Wu, B., Hagedorn, F., 2016. Dissolved and colloidal phosphorus fluxes in forest ecosystems—an almost blind spot in ecosystem research. *Journal of Plant Nutrition and Soil Science* 179, 425–438. <https://doi.org/10.1002/jpln.201600079>
- Bollyn, J., Castelein, L., Smolders, E., 2019. Fate and bioavailability of phosphorus loaded to iron oxyhydroxide nanoparticles added to weathered soils. *Plant Soil* 438, 297–311. <https://doi.org/10.1007/s11104-019-04008-x>

- Bomans, E., Fransen, K., Gobin, A., Mertens, J., Michiels, P., Vandendriessche, H., Vogels, N., 2005. Addressing phosphorus related problems in farm practice. *Eur. Comm., DG Environ., Brussels*.
- Borch, T., Kretzschmar, R., Kappler, A., Cappellen, P.V., Ginder-Vogel, M., Voegelin, A., Campbell, K., 2010. Biogeochemical Redox Processes and their Impact on Contaminant Dynamics. *Environ. Sci. Technol.* 44, 15–23. <https://doi.org/10.1021/es9026248>
- Bordas, F., Bourg, A.C.M., 1998. A Critical Evaluation of Sample Pretreatment for Storage of Contaminated Sediments to be Investigated for the Potential Mobility of their Heavy Metal Load. *Water, Air, & Soil Pollution* 103, 137–149. <https://doi.org/10.1023/A:1004952608950>
- Boström, B., Persson, G., Broberg, B., 1988. Bioavailability of different phosphorus forms in freshwater systems. *Hydrobiologia* 170, 133–155. <https://doi.org/10.1007/BF00024902>
- Boussu, K., Belpaire, A., Volodin, A., Van Haesendonck, C., Van der Meeren, P., Vandecasteele, C., Van der Bruggen, B., 2007. Influence of membrane and colloid characteristics on fouling of nanofiltration membranes. *Journal of Membrane Science* 289, 220–230. <https://doi.org/10.1016/j.memsci.2006.12.001>
- Bowen, W.R., Jenner, F., 1995. Theoretical descriptions of membrane filtration of colloids and fine particles: An assessment and review. *Advances in Colloid and Interface Science* 56, 141–200. [https://doi.org/10.1016/0001-8686\(94\)00232-2](https://doi.org/10.1016/0001-8686(94)00232-2)
- Bradford, S.A., Yates, S.R., Bettahar, M., & Simunek, J., 2002. Physical factors affecting the transport and fate of colloids in saturated porous media. *Water resources research*, 38(12), 63-1.
- Brant, J.A., Childress, A.E., 2004. Colloidal adhesion to hydrophilic membrane surfaces. *Journal of Membrane Science* 241, 235–248. <https://doi.org/10.1016/j.memsci.2004.04.036>
- Bretier, M., Dabrin, A., Bessueille-Barbier, F., Coquery, M., 2019. The impact of dam flushing event on dissolved trace elements concentrations: Coupling integrative passive sampling and discrete monitoring. *Science of the Total Environment* 656, 433–446. <https://doi.org/10.1016/j.scitotenv.2018.11.303>
- Brownawell, B.J., 1986. The role of colloidal organic matter in the marine geochemistry of PCB's (Thesis). Massachusetts Institute of Technology and Woods Hole Oceanographic Institution. <https://doi.org/10.1575/1912/3932>
- Brydon, J.E., Rice, H.M., Soott, G.C., 1963. Note on the recovery of clays from suspension by freeze-drying. *Can. J. Soil. Sci.* 43, 404–405. <https://doi.org/10.4141/cjss63-050>
- Buermann, Y., Du Preez, H.H., Steyn, G.J., Harmse, J.T., Deacon, A., 1995. Suspended silt concentrations in the lower Olifants River (Mpumalanga) and the impact of silt releases from the Phalaborwa Barrage on water quality and fish survival. *Koedoe* 38, 11–34.
- Buettner, S.W., Kramer, M.G., Chadwick, O.A., Thompson, A., 2014. Mobilization of colloidal carbon during iron reduction in basaltic soils. *Geoderma* 221–222, 139–145. <https://doi.org/10.1016/j.geoderma.2014.01.012>
- Buffle, J., De Vitre, R.R., Perret, D., Leppard, G.G., 1989. Physico-chemical characteristics of a colloidal iron phosphate species formed at the oxic-anoxic interface of a eutrophic lake. *Geochimica et Cosmochimica Acta* 53, 399–408. [https://doi.org/10.1016/0016-7037\(89\)90391-8](https://doi.org/10.1016/0016-7037(89)90391-8)
- Buffle, J., Leppard, G.G., 1995. Characterization of Aquatic Colloids and Macromolecules. 1. Structure and Behavior of Colloidal Material - Environmental Science & Technology (ACS Publications) [WWW Document]. URL <https://pubs.acs.org/doi/abs/10.1021/es00009a004> (accessed 1.11.19).
- Calero, J., Ontiveros-Ortega, A., Aranda, V., Plaza, I., 2017. Humic acid adsorption and its role in colloidal-scale aggregation determined with the zeta potential, surface free energy and the

- extended-DLVO theory. *European Journal of Soil Science* 68, 491–503. <https://doi.org/10.1111/ejss.12431>
- Cavalcante, H., Araújo, F., Noyma, N.P., Becker, V., 2018. Phosphorus fractionation in sediments of tropical semiarid reservoirs. *Science of The Total Environment* 619–620, 1022–1029. <https://doi.org/10.1016/j.scitotenv.2017.11.204>
- Cavaliere, E., Homann, P., 2012. Elwha River Sediments: Phosphorus Characterization and Dynamics Under Diverse Environmental Conditions. *nwsc* 86, 95–107. <https://doi.org/10.3955/046.086.0202>
- Cervi, E.C., Hudson, M., Rentschler, A., & Burton Jr, G.A., 2019. Metal Toxicity During Short-Term Sediment Resuspension and Redeposition in a Tropical Reservoir. *Environmental toxicology and chemistry*, 38(7), 1476–1485.
- Chadwick, S.P., Babiarz, C.L., Hurley, J.P., Armstrong, D.E., 2006. Influences of iron, manganese, and dissolved organic carbon on the hypolimnetic cycling of amended mercury. *Science of The Total Environment, Selected papers from the 7th International Conference on Mercury as a Global Pollutant, Ljubljana, Slovenia June 27 - July 2, 2004* 368, 177–188. <https://doi.org/10.1016/j.scitotenv.2005.09.039>
- Chaffin, J.D., Kane, D.D., 2010. Burrowing Mayfly (Ephemeroptera: Ephemeridae: Hexagenia spp.) Bioturbation and Bioirrigation: A Source of Internal Phosphorus Loading in Lake Erie. *jglr* 36, 57–63. <https://doi.org/10.1016/j.jglr.2009.09.003>
- Channarayappa, C., Biradar, D.P., 2018. *Soil Basics, Management and Rhizosphere Engineering for Sustainable Agriculture*. CRC Press.
- Chao, B.F., Wu, Y.H., Li, Y.S., 2008. Impact of artificial reservoir water impoundment on global sea level. *Science* 320, 212–214. <https://doi.org/10.1126/science.1154580>
- Châtellier, X., Grybos, M., Abdelmoula, M., Kemner, K.M., Leppard, G.G., Mustin, C., West, M.M., Paktunc, D., 2013. Immobilization of P by oxidation of Fe(II) ions leading to nanoparticle formation and aggregation. *Applied Geochemistry* 35, 325–339. <https://doi.org/10.1016/j.apgeochem.2013.04.019>
- Chatterjee, A., Mandal, M.K., Chaurasia, N., 2019. Chapter 17 - Microbial services in agro-environmental management, in: Singh, J.S. (Ed.), *New and Future Developments in Microbial Biotechnology and Bioengineering*. Elsevier, pp. 259–272. <https://doi.org/10.1016/B978-0-12-818258-1.00017-0>
- Chattopadhyay, S., Chattopadhyay, D., 2003. Colloidal properties of sediments, in: Middleton, G.V., Church, M.J., Coniglio, M., Hardie, L.A., Longstaffe, F.J. (Eds.), *Encyclopedia of Sediments and Sedimentary Rocks*. Springer Netherlands, Dordrecht, pp. 157–159. https://doi.org/10.1007/978-1-4020-3609-5_51
- Chen, A., Arai, Y., 2020. Current uncertainties in assessing the colloidal phosphorus loss from soil, in: *Advances in Agronomy*. Academic Press. <https://doi.org/10.1016/bs.agron.2020.05.002>
- Chen, B., Beckett, R., Tri, N., 2001. Pollutant-colloid association by field-flow fractionation. In *Encyclopedia of Chromatography* (pp. 629–632). Marcel Dekker.
- Chen, C., Dynes, J.J., Wang, J., Sparks, D.L., 2014. Properties of Fe-Organic Matter Associations via Coprecipitation versus Adsorption. *Environ. Sci. Technol.* 48, 13751–13759. <https://doi.org/10.1021/es503669u>
- Chen, M., Ding, S., Wu, Y., Fan, X., Jin, Z., Tsang, D.C.W., Wang, Y., Zhang, C., 2019. Phosphorus mobilization in lake sediments: Experimental evidence of strong control by iron and negligible influences of manganese redox reactions. *Environmental Pollution* 246, 472–481. <https://doi.org/10.1016/j.envpol.2018.12.031>

- Chen, M., Xu, N., Cao, X., Zhou, K., Chen, Z., Wang, Y., Liu, C., 2015. Facilitated transport of anatase titanium dioxides nanoparticles in the presence of phosphate in saturated sands. *Journal of Colloid and Interface Science* 451, 134–143. <https://doi.org/10.1016/j.jcis.2015.04.010>
- Chen, V., Fane, A.G., Madaeni, S., Wenten, I.G., 1997. Particle deposition during membrane filtration of colloids: transition between concentration polarization and cake formation. *Journal of Membrane Science* 125, 109–122. [https://doi.org/10.1016/S0376-7388\(96\)00187-1](https://doi.org/10.1016/S0376-7388(96)00187-1)
- Cheng, T., Saiers, J.E., 2015. Effects of dissolved organic matter on the co-transport of mineral colloids and sorptive contaminants. *Journal of Contaminant Hydrology* 177–178, 148–157. <https://doi.org/10.1016/j.jconhyd.2015.04.005>
- Chhabra, R., Basavaraj, M.G. (Eds.), 2019. Chapter 13 - Colloidal Dispersions, in: Coulson and Richardson's Chemical Engineering (Sixth Edition). Butterworth-Heinemann, pp. 693–737. <https://doi.org/10.1016/B978-0-08-101098-3.00014-7>
- Chiaia-Hernández, A.C., Scheringer, M., Müller, A., Stieger, G., Wächter, D., Keller, A., Pintado-Herrera, M.G., Lara-Martin, P.A., Bucheli, T.D., Hollender, J., 2020. Target and suspect screening analysis reveals persistent emerging organic contaminants in soils and sediments. *Science of The Total Environment* 740, 140181. <https://doi.org/10.1016/j.scitotenv.2020.140181>
- Chirinos, L.R., Urrutia, R., Fagel, N., Bertrand, S., Gamboa, N., Araneda, A., Zaror, C., 2005. CHEMICAL PROFILES IN LAKE SEDIMENTS IN LAGUNA CHICA DE SAN PEDRO (BIO-BIO REGION, CHILE). *Journal of the Chilean Chemical Society* 50, 697–710. <https://doi.org/10.4067/S0717-97072005000400010>
- Chislock, M.F., Doster, E., Zitomer, R.A., Wilson, A.E., 2013. Eutrophication: causes, consequences, and controls in aquatic ecosystems. *Nature Education Knowledge* 4, 10.
- Chittleborough, D. J., Hotchin, D. M., & Beckett, R., 1992. Sedimentation field-flow fractionation: A new technique for the fractionation of soil colloids. *Soil Science*, 153(5), 341-348.
- Chotpantararat, S., Kiatvarankul, N., 2018. Facilitated transport of cadmium with montmorillonite KSF colloids under different pH conditions in water-saturated sand columns: Experiment and transport modeling. *Water Research* 146, 216–231. <https://doi.org/10.1016/j.watres.2018.09.010>
- Chu, F.-F., Shen, X.-F., Lam, P.K.S., Zeng, R.J., 2015. Polyphosphate during the Regreening of *Chlorella vulgaris* under Nitrogen Deficiency. *Int J Mol Sci* 16, 23355–23368. <https://doi.org/10.3390/ijms161023355>
- Chung, S.W., Ko, I.H., Kim, Y.K., 2008. Effect of reservoir flushing on downstream river water quality. *Journal of Environmental Management* 86, 139–147. <https://doi.org/10.1016/j.jenvman.2006.11.031>
- Cieśla, M., Bartoszek, L., Gruca-Rokosz, R., 2020. Characteristics and origin of suspended matter in a small reservoir in Poland. *Ecohydrology & Hydrobiology* 20, 73–82. <https://doi.org/10.1016/j.ecohyd.2019.05.003>
- Coker, E.H., Hotchkiss, R.H., Johnson, D.A., 2009. Conversion of a Missouri River Dam and Reservoir to a Sustainable System: Sediment Management1. *JAWRA Journal of the American Water Resources Association* 45, 815–827. <https://doi.org/10.1111/j.1752-1688.2009.00324.x>
- Cole, J.J., Prairie, Y.T., Caraco, N.F., McDowell, W.H., Tranvik, L.J., Striegl, R.G., Duarte, C.M., Kortelainen, P., Downing, J.A., Middelburg, J.J., Melack, J., 2007. Plumbing the Global Carbon Cycle: Integrating Inland Waters into the Terrestrial Carbon Budget. *Ecosystems* 10, 172–185. <https://doi.org/10.1007/s10021-006-9013-8>
- Colombo, C., Palumbo, G., Sellitto, V.M., Cho, H.G., Amalfitano, C., Adamo, P., 2015. Stability of coprecipitated natural humic acid and ferrous iron under oxidative conditions. *Journal of Geochemical Exploration* 151, 50–56. <https://doi.org/10.1016/j.gexplo.2015.01.003>

- Conley, D.J., Paerl, H.W., Howarth, R.W., Boesch, D.F., Seitzinger, S.P., Havens, K.E., Lancelot, C., Likens, G.E., 2009. Ecology. Controlling eutrophication: nitrogen and phosphorus. *Science* 323, 1014–1015. <https://doi.org/10.1126/science.1167755>
- Constantine, J.A., Dunne, T., Ahmed, J., Legleiter, C., & Lazarus, E.D., 2014. Sediment supply as a driver of river meandering and floodplain evolution in the Amazon Basin. *Nature Geoscience*, 7(12), 899-903.
- Cordell, D., White, S., 2011. Peak Phosphorus: Clarifying the Key Issues of a Vigorous Debate about Long-Term Phosphorus Security. *Sustainability* 3, 2027–2049. <https://doi.org/10.3390/su3102027>
- Correll, D.L., 1998. The role of phosphorus in the eutrophication of receiving waters: A review. *Journal of Environmental Quality* 27, 261–266. <https://doi.org/10.2134/jeq1998.00472425002700020004x>
- Cosmidis, J., Benzerara, K., Morin, G., Busigny, V., Lebeau, O., Jézéquel, D., Noël, V., Dublet, G., Othmane, G., 2014. Biomineralization of iron-phosphates in the water column of Lake Pavin (Massif Central, France). *Geochimica et Cosmochimica Acta* 126, 78–96. <https://doi.org/10.1016/j.gca.2013.10.037>
- Corzo, A., Jiménez-Arias, J.L., Torres, E., García-Robledo, E., Lara, M., & Papaspyrou, S., 2018. Biogeochemical changes at the sediment–water interface during redox transitions in an acidic reservoir: exchange of protons, acidity and electron donors and acceptors. *Biogeochemistry*, 139(3), 241-260.
- Csiki, S.J., Rhoads, B.L., 2014. Influence of four run-of-river dams on channel morphology and sediment characteristics in Illinois, USA. *Geomorphology* 206, 215–229. <https://doi.org/10.1016/j.geomorph.2013.10.009>
- Curran, J.C., Waters, K.A., Cannatelli, K.M., 2015. Real time measurements of sediment transport and bed morphology during channel altering flow and sediment transport events. *Geomorphology, Laboratory Experiments in Geomorphology 46th Annual Binghamton Geomorphology Symposium 18-20 September 2015* 244, 169–179. <https://doi.org/10.1016/j.geomorph.2015.03.009>
- Cuss, C.W., Donner, M.W., Grant-Weaver, I., Noernberg, T., Pelletier, R., Sinnatamby, R.N., Shotyk, W., 2018. Measuring the distribution of trace elements amongst dissolved colloidal species as a fingerprint for the contribution of tributaries to large boreal rivers. *Science of The Total Environment* 642, 1242–1251. <https://doi.org/10.1016/j.scitotenv.2018.06.099>
- Dadi, T., Rinke, K., Friese, K., 2020. Trajectories of Sediment-Water Interactions in Reservoirs as a Result of Temperature and Oxygen Conditions. *Water* 12, 1065. <https://doi.org/10.3390/w12041065>
- Dagesse, D., 2011. Effect of freeze-drying on soil aggregate stability. *Soil Science Society of America Journal* 75, 2111–2121.
- Dai, M., Buesseler, K. O., Ripple, P., Andrews, J., Belastock, R. A., Gustafsson, Ö., & Moran, S. B., 1998. Evaluation of two cross-flow ultrafiltration membranes for isolating marine organic colloids. *Marine Chemistry*, 62(1-2), 117-136.
- Danen-Louwerse, H.J., Lijklema, L., Coenraats, M., 1995. Coprecipitation of phosphate with calcium carbonate in Lake Veluwe. *Water Research* 29, 1781–1785. [https://doi.org/10.1016/0043-1354\(94\)00301-M](https://doi.org/10.1016/0043-1354(94)00301-M)
- Darke, A.K., Walbridge, M.R., 2000. Al and Fe Biogeochemistry in a floodplain forest: Implications for P retention. *Biogeochemistry* 51, 1–32. <https://doi.org/10.1023/A:1006302600347>
- Das, B.M., Sobhan, K., 2013. *Principles of Geotechnical Engineering*. Cengage Learning.

- de Jonge, L.W., Moldrup, P., Rubaæk, G.H., Schelde, K., Djurhuus, J., 2004. Particle leaching and particle-facilitated transport of phosphorus at field scale. *Vadose Zone Journal* 3, 462–470. <https://doi.org/10.2113/3.2.462>
- de Mesquita Filho, M.V., Torrent, J., 1993. Phosphate sorption as related to mineralogy of a hydrosequence of soils from the Cerrado region (Brazil). *Geoderma* 58, 107–123. [https://doi.org/10.1016/0016-7061\(93\)90088-3](https://doi.org/10.1016/0016-7061(93)90088-3)
- De Paolis, F., Kukkonen, J., 1997. Binding of organic pollutants to humic and fulvic acids: Influence of pH and the structure of humic material. *Chemosphere* 34, 1693–1704. [https://doi.org/10.1016/S0045-6535\(97\)00026-X](https://doi.org/10.1016/S0045-6535(97)00026-X)
- de Vicente, I., Andersen, F.Ø., Hansen, H.C.B., Cruz-Pizarro, L., Jensen, H.S., 2010. Water level fluctuations may decrease phosphate adsorption capacity of the sediment in oligotrophic high mountain lakes. *Hydrobiologia* 651, 253–264. <https://doi.org/10.1007/s10750-010-0304-x>
- Decina, S.M., Templer, P.H., Hutyra, L.R., 2018. Atmospheric Inputs of Nitrogen, Carbon, and Phosphorus across an Urban Area: Unaccounted Fluxes and Canopy Influences. *Earth's Future* 6, 134–148. <https://doi.org/10.1002/2017EF000653>
- Degueldre, C., Baeyens, B., Goerlich, W., Riga, J., Verbist, J., Stadelmann, P., 1989. Colloids in water from a subsurface fracture in granitic rock, Grimsel Test Site, Switzerland. *Geochimica et Cosmochimica Acta* 53, 603–610. [https://doi.org/10.1016/0016-7037\(89\)90003-3](https://doi.org/10.1016/0016-7037(89)90003-3)
- Degueldre, C., Pfeiffer, H.-R., Alexander, W., Wernli, B., Bruetsch, R., 1996. Colloid properties in granitic groundwater systems. I: Sampling and characterisation. *Applied Geochemistry* 11, 677–695. [https://doi.org/10.1016/S0883-2927\(96\)00036-4](https://doi.org/10.1016/S0883-2927(96)00036-4)
- Degueldre, C., Triay, I., Kim, J. I., Vilks, P., Laaksoharju, M., & Miekeley, N. (2000). Groundwater colloid properties: a global approach. *Applied Geochemistry*, 15(7), 1043-1051. [https://doi.org/10.1016/S0883-2927\(99\)00102-X](https://doi.org/10.1016/S0883-2927(99)00102-X)
- Denef, K., Six, J., Bossuyt, H., Frey, S.D., Elliott, E.T., Merckx, R., Paustian, K., 2001. Influence of dry–wet cycles on the interrelationship between aggregate, particulate organic matter, and microbial community dynamics. *Soil Biology and Biochemistry* 33, 1599–1611. [https://doi.org/10.1016/S0038-0717\(01\)00076-1](https://doi.org/10.1016/S0038-0717(01)00076-1)
- Derjaguin, B., & Landau, L., 1941. The theory of stability of highly charged lyophobic sols and coalescence of highly charged particles in electrolyte solutions. *Acta Physicochim. URSS*, 14(633-52), 58.
- Derkachov, G., Jakubczyk, D., Kolwas, K., Piekarski, K., Shopa, Y., Woźniak, M., 2020. Dynamic light scattering investigation of single levitated micrometre-sized droplets containing spherical nanoparticles. *Measurement* 158, 107681. <https://doi.org/10.1016/j.measurement.2020.107681>
- Despriée, J., Gageonnet, R., Voinchet, P., Bahain, J.J., Falguères, C., Duvalard, J., Varache, F., 2004. Pleistocene fluvial systems of the Creuse river (Middle Loire Basin - Centre Region, France) [Les systèmes fluviaux pléistocènes de la Creuse (Bassin moyen de la Loire, Région Centre, France)]. *Quaternaire* 15, 77–86. <https://doi.org/10.3406/quate.2004.1756>
- Dhont, J.K.G. (Ed.), 1996. Chapter 7 - Sedimentation, in: *Studies in Interface Science, An Introduction to Dynamics of Colloids*. Elsevier, pp. 443–493. [https://doi.org/10.1016/S1383-7303\(96\)80009-3](https://doi.org/10.1016/S1383-7303(96)80009-3)
- Dickerson, K.D., Medley, K.A., Havel, J.E., 2010. Spatial variation in zooplankton community structure is related to hydrologic flow units in the Missouri river, USA. *River Research and Applications* 26, 605–618. <https://doi.org/10.1002/rra.1268>
- Dijk, M.V., Vuuren, S.V., 2012. Destratification induced by bubble plumes as a means to reduce evaporation from open impoundments. <https://doi.org/10.4314/WSA.V35I2.76731>

- Dekker, L.W., Doerr, S.H., Oostindie, K., Ziogas, A.K., & Ritsema, C.J., 2001. Water repellency and critical soil water content in a dune sand. *Soil Science Society of America Journal*, 65(6), 1667-1674.
- Doucet, F.J., Lead, J.R., Santschi, P.H., 2007. Colloid-Trace Element Interactions in Aquatic Systems, in: *Environmental Colloids and Particles*. John Wiley & Sons, Ltd, pp. 95-157. <https://doi.org/10.1002/9780470024539.ch3>
- Duiker, S.W., Rhoton, F.E., Torrent, J., Smeck, N.E., Lal, R., 2003. Iron (hydr)oxide crystallinity effects on soil aggregation. *Soil Science Society of America Journal* 67, 606-611.
- Dukhin, A.S., Goetz, P.J., 2017. Chapter 2 - Fundamentals of Interface and Colloid Science, in: Dukhin, A.S., Goetz, P.J. (Eds.), *Characterization of Liquids, Dispersions, Emulsions, and Porous Materials Using Ultrasound (Third Edition)*. Elsevier, pp. 19-83. <https://doi.org/10.1016/B978-0-444-63908-0.00002-8>
- Dupas, R., Tittel, J., Jordan, P., Musolff, A., Rode, M., 2018. Non-domestic phosphorus release in rivers during low-flow: Mechanisms and implications for sources identification. *Journal of Hydrology* 560, 141-149. <https://doi.org/10.1016/j.jhydrol.2018.03.023>
- East, A.E., Logan, J.B., Mastin, M.C., Ritchie, A.C., Bountry, J.A., Magirl, C.S., Sankey, J.B., 2018. Geomorphic Evolution of a Gravel-Bed River Under Sediment-Starved Versus Sediment-Rich Conditions: River Response to the World's Largest Dam Removal. *Journal of Geophysical Research: Earth Surface* 123, 3338-3369. <https://doi.org/10.1029/2018JF004703>
- Edwards, A.C., Withers, P.J.A., 2007. Linking phosphorus sources to impacts in different types of water body. *Soil Use and Management* 23, 133-143. <https://doi.org/10.1111/j.1475-2743.2007.00110.x>
- Effler, S.W., Matthews, D.A., 2004. Sediment resuspension and drawdown in a water supply reservoir. *J Am Water Resources Assoc* 40, 251-264. <https://doi.org/10.1111/j.1752-1688.2004.tb01023.x>
- Ekholm, P., & Krogerus, K., 2003. Determining algal-available phosphorus of differing origin: routine phosphorus analyses versus algal assays. *Hydrobiologia*, 492(1-3), 29-42.
- Ellison, M.E., & Brett, M.T., 2006. Particulate phosphorus bioavailability as a function of stream flow and land cover. *Water research*, 40(6), 1258-1268.
- Elzinga, E.J., Sparks, D.L., 2007. Phosphate adsorption onto hematite: An in situ ATR-FTIR investigation of the effects of pH and loading level on the mode of phosphate surface complexation. *Journal of Colloid and Interface Science* 308, 53-70. <https://doi.org/10.1016/j.jcis.2006.12.061>
- Emer, C., Venticinque, E.M., Fonseca, C.R., 2013. Effects of dam-induced landscape fragmentation on amazonian ant-plant mutualistic networks. *Conserv. Biol.* 27, 763-773. <https://doi.org/10.1111/cobi.12045>
- Ermolin, M.S., Fedotov, P.S., 2016. Separation and characterization of environmental nano- and submicron particles. *Reviews in Analytical Chemistry* 35, 185-199. <https://doi.org/10.1515/revac-2016-0006>
- European Environment Agency (2018). Retrieved from <https://www.eea.europa.eu/data-and-maps/indicators/nutrients-in-freshwater/nutrients-in-freshwater-assessment-published-9>
- FAO (2004) Utilisation des phosphates naturels pour une agriculture durable. Retrieved from <http://www.fao.org/3/y5053f/y5053f00.htm#Contents%20Chapter%20II>
- Fan, W., Chen, M., Yang, S., Wu, L., 2015. Centrifugation-assisted Assembly of Colloidal Silica into Crack-Free and Transferrable Films with Tunable Crystalline Structures. *Scientific Reports* 5, 12100. <https://doi.org/10.1038/srep12100>

- Feng, X., Simpson, A.J., Simpson, M.J., 2005. Chemical and mineralogical controls on humic acid sorption to clay mineral surfaces. *Organic Geochemistry* 36, 1553–1566. <https://doi.org/10.1016/j.orggeochem.2005.06.008>
- Ferreira, J.G., Andersen, J.H., Borja, A., Bricker, S.B., Camp, J., Cardoso da Silva, M., Garcés, E., Heiskanen, A.-S., Humborg, C., Ignatiades, L., Lancelot, C., Menesguen, A., Tett, P., Hoepffner, N., Claussen, U., 2011. Overview of eutrophication indicators to assess environmental status within the European Marine Strategy Framework Directive. *Estuarine, Coastal and Shelf Science* 93, 117–131. <https://doi.org/10.1016/j.ecss.2011.03.014>
- Filella, M., Deville, C., Chanudet, V., Vignati, D., 2006. Variability of the colloidal molybdate reactive phosphorous concentrations in freshwaters. *Water Research* 40, 3185–3192. <https://doi.org/10.1016/j.watres.2006.07.010>
- Filippelli, G.M., 2008. The Global Phosphorus Cycle: Past, Present, and Future. *Elements* 4, 89–95. <https://doi.org/10.2113/GSELEMENTS.4.2.89>
- Filstrup, C.T., Lind, O.T., 2010. Sediment transport mechanisms influencing spatiotemporal resuspension patterns in a shallow, polymictic reservoir. *Lake and Reservoir Management* 26, 85–94. <https://doi.org/10.1080/07438141.2010.490771>
- Fink, J.R., Inda, A.V., Bavaresco, J., Barrón, V., Torrent, J., Bayer, C., 2016. Adsorption and desorption of phosphorus in subtropical soils as affected by management system and mineralogy. *Soil and Tillage Research* 155, 62–68. <https://doi.org/10.1016/j.still.2015.07.017>
- Fonseca, R.M.F., Barriga, F.J.A.S., Conceição, P.I.S.T., 2010. Clay minerals in sediments of Portuguese reservoirs and their significance as weathering products from over-eroded soils: a comparative study of the Maranhão, Monte Novo and Divor Reservoirs (South Portugal). *Int J Earth Sci (Geol Rundsch)* 99, 1899–1916. <https://doi.org/10.1007/s00531-009-0488-3>
- Forber, K.J., Ockenden, M.C., Wearing, C., Hollaway, M.J., Falloon, P.D., Kahana, R., Villamizar, M.L., Zhou, J.G., Withers, P.J.A., Beven, K.J., Collins, A.L., Evans, R., Hiscock, K.M., Macleod, C.J.A., Haygarth, P.M., 2017. Determining the Effect of Drying Time on Phosphorus Solubilization from Three Agricultural Soils under Climate Change Scenarios. *Journal of Environment Quality* 46, 1131. <https://doi.org/10.2134/jeq2017.04.0144>
- Friedl, G., Wüest, A., 2002. Disrupting biogeochemical cycles - Consequences of damming. *Aquat. sci.* 64, 55–65. <https://doi.org/10.1007/s00027-002-8054-0>
- Froelich, P.N., Klinkhammer, G.P., Bender, M.L., Luedtke, N.A., Heath, G.R., Cullen, D., Dauphin, P., Hammond, D., Hartman, B., Maynard, V., 1979. Early oxidation of organic matter in pelagic sediments of the eastern equatorial Atlantic: suboxic diagenesis. *Geochimica et Cosmochimica Acta* 43, 1075–1090. [https://doi.org/10.1016/0016-7037\(79\)90095-4](https://doi.org/10.1016/0016-7037(79)90095-4)
- Gaillardet, J., Viers, J., Dupré, B., 2003. 5.09 - Trace Elements in River Waters, in: Holland, H.D., Turekian, K.K. (Eds.), *Treatise on Geochemistry*. Pergamon, Oxford, pp. 225–272. <https://doi.org/10.1016/B0-08-043751-6/05165-3>
- Galizia Tundisi, J., 2018. Reservoirs: New challenges for ecosystem studies and environmental management. *Water Security* 4–5, 1–7. <https://doi.org/10.1016/j.wasec.2018.09.001>
- Gálvez, J.A., & Niell, F.X., 1992. Sediment resuspension in a monomictic eutrophic reservoir. *Hydrobiologia*, 235(1), 133-141.
- Gaoa, L., 2012. Phosphorus Release from the Sediments in Rongcheng Swan Lake under Different pH Conditions. *Procedia Environmental Sciences*, 18th Biennial ISEM Conference on Ecological Modelling for Global Change and Coupled Human and Natural System 13, 2077–2084. <https://doi.org/10.1016/j.proenv.2012.01.197>
- Gautreau, E., Volatier, L., Nogaro, G., Gouze, E., Mermillod-Blondin, F., 2020. The influence of bioturbation and water column oxygenation on nutrient recycling in reservoir sediments. *Hydrobiologia* 847, 1027–1040. <https://doi.org/10.1007/s10750-019-04166-0>

- Gavrilescu, M., 2014. Chapter 17 - Colloid-Mediated Transport and the Fate of Contaminants in Soils, in: Fanun, M. (Ed.), *The Role of Colloidal Systems in Environmental Protection*. Elsevier, Amsterdam, pp. 397–451. <https://doi.org/10.1016/B978-0-444-63283-8.00017-X>
- Gerke, J., 2010. Humic (organic matter)-Al(Fe)-phosphate complexes: An underestimated phosphate form in soils and source of plant-available phosphate. *Soil Science* 175, 417–425. <https://doi.org/10.1097/SS.0b013e3181f1b4dd>
- Ghosh, K., Schnitzer, M., 1980. Macromolecular structures of humic substances. *Soil Science* 129, 266–276.
- Gimbert, L. J., Haygarth, P. M., Beckett, R., & Worsfold, P. J., 2005. Comparison of Centrifugation and Filtration Techniques for the Size Fractionation of Colloidal Material in Soil Suspensions Using Sedimentation Field-Flow Fractionation. *Environmental Science & Technology*, 39(6), 1731–1735. <https://doi.org/10.1021/es049230u>
- Gimbert, L. J., Haygarth, P. M., Beckett, R., & Worsfold, P. J., 2006. The Influence of Sample Preparation on Observed Particle Size Distributions for Contrasting Soil Suspensions using Flow Field-Flow Fractionation. *Environmental Chemistry*, 3(3), 184. <https://doi.org/10.1071/EN06029>
- Gislason, S.R., Wolff-Boenisch, D., Stefansson, A., Oelkers, E.H., Gunnlaugsson, E., Sigurdardottir, H., Sigfusson, B., Broecker, W.S., Matter, J.M., Stute, M., Axelsson, G., Fridriksson, T., 2010. Mineral sequestration of carbon dioxide in basalt: A pre-injection overview of the CarbFix project. *International Journal of Greenhouse Gas Control* 4, 537–545. <https://doi.org/10.1016/j.ijggc.2009.11.013>
- Glenn, C.R., Prévôt, L., Lucas, J. (Eds.), 2000. Chapter: Variations in the global phosphorus cycle, in: *Marine Authigenesis: From Global to Microbial*. SEPM (Society for Sedimentary Geology). <https://doi.org/10.2110/pec.00.66>
- Glibert, P.M., 2017. Eutrophication, harmful algae and biodiversity — Challenging paradigms in a world of complex nutrient changes. *Marine Pollution Bulletin, Special Issue: Hong Kong Conference 2016* 124, 591–606. <https://doi.org/10.1016/j.marpolbul.2017.04.027>
- Glindemann, D., Edwards, M., Schrems, O., 2004. Phosphine and methylphosphine production by simulated lightning—a study for the volatile phosphorus cycle and cloud formation in the earth atmosphere. *Atmospheric Environment* 38, 6867–6874. <https://doi.org/10.1016/j.atmosenv.2004.09.002>
- Golterman, H.L., 2001. Phosphate release from anoxic sediments or 'What did Mortimer really write?'. *Hydrobiologia* 450, 99–106. <https://doi.org/10.1023/A:1017559903404>
- Gottselig, N., Bol, R., Nischwitz, V., Vereecken, H., Amelung, W., Klumpp, E., 2014. Distribution of Phosphorus-Containing Fine Colloids and Nanoparticles in Stream Water of a Forest Catchment. *Vadose Zone Journal* 13, 0. <https://doi.org/10.2136/vzj2014.01.0005>
- Gottselig, N., Amelung, W., Kirchner, J.W., Bol, R., Eugster, W., Granger, S.J., Hernández-Crespo, C., Herrmann, F., Keizer, J.J., Korkiakoski, M., Laudon, H., Lehner, I., Löfgren, S., Lohila, A., Macleod, C.J.A., Mölder, M., Müller, C., Nasta, P., Nischwitz, V., Paul-Limoges, E., Pierret, M.C., Pilegaard, K., Romano, N., Sebastià, M.T., Stähli, M., Voltz, M., Vereecken, H., Siemens, J., Klumpp, E., 2017a. Elemental Composition of Natural Nanoparticles and Fine Colloids in European Forest Stream Waters and Their Role as Phosphorus Carriers: Colloids in European forest streams. *Global Biogeochemical Cycles* 31, 1592–1607. <https://doi.org/10.1002/2017GB005657>
- Gottselig, N., Nischwitz, V., Meyn, T., Amelung, W., Bol, R., Halle, C., Vereecken, H., Siemens, J., Klumpp, E., 2017b. Phosphorus Binding to Nanoparticles and Colloids in Forest Stream Waters. *Vadose Zone Journal* 16, vzj2016.07.0064. <https://doi.org/10.2136/vzj2016.07.0064>

- Grolimund, D., Elimelech, M., Borkovec, M., Barmettler, K., Kretzschmar, R., & Sticher, H., 1998. Transport of in situ mobilized colloidal particles in packed soil columns. *Environmental Science & Technology*, 32(22), 3562-3569.
- Grover, J.P., Scott, J.T., Roelke, D.L., Brooks, B.W., 2020. Dynamics of nitrogen-fixing cyanobacteria with heterocysts: a stoichiometric model. *Mar. Freshwater Res.* 71, 644–658. <https://doi.org/10.1071/MF18361>
- Grybos, M., Michot, L.J., Skiba, M., Billard, P., & Mustin, C., 2010. Dissolution of anisotropic colloidal mineral particles: evidence for basal surface reactivity of nontronite. *Journal of colloid and interface science*, 343(2), 433-438.
- Grybos, M., Billard, P., Desobry-Banon, S., Michot, L.J., Lenain, J.F., & Mustin, C., 2011. Bio-dissolution of colloidal-size clay minerals entrapped in microporous silica gels. *Journal of Colloid and Interface Science*, 362(2), 317-324.
- Gs, T., Marti, O., Yunya, Y., Tammy, M., Darren, H., Lorence, O., 2017. Managing urban runoff in residential neighborhoods: Nitrogen and phosphorus in lawn irrigation driven runoff. *PLoS One* 12, e0179151–e0179151. <https://doi.org/10.1371/journal.pone.0179151>
- Gu, S., 2017. Release of dissolved and colloidal phosphorus from riparian wetlands: a field and laboratory assessment of the mechanisms and controlling factors (These de doctorat). Rennes 1.
- Gu, S., Gruau, G., Malique, F., Dupas, R., Petitjean, P., Gascuel-Oudou, C., 2018. Drying/rewetting cycles stimulate release of colloidal-bound phosphorus in riparian soils. *Geoderma* 321, 32–41. <https://doi.org/10.1016/j.geoderma.2018.01.015>
- Gualtieri, C., Filizola, N., de Oliveira, M., Santos, A.M., & Ianniruberto, M., 2018. A field study of the confluence between Negro and Solimões Rivers. Part 1: Hydrodynamics and sediment transport. *Comptes Rendus Geoscience*, 350(1-2), 31-42.
- Gudasz, C., Bastviken, D., Steger, K., Premke, K., Sobek, S., Tranvik, L.J., 2010. Temperature-controlled organic carbon mineralization in lake sediments. *Nature* 466, 478–481.
- Gunnars, A., Blomqvist, S., Johansson, P., Andersson, C., 2002. Formation of Fe (III) oxyhydroxide colloids in freshwater and brackish seawater, with incorporation of phosphate and calcium. *Geochimica et Cosmochimica Acta* 66, 745–758.
- Guo, M., Li, X., Song, C., Liu, G., Zhou, Y., 2020. Photo-induced phosphate release during sediment resuspension in shallow lakes: A potential positive feedback mechanism of eutrophication. *Environmental Pollution* 258, 113679. <https://doi.org/10.1016/j.envpol.2019.113679>
- Guo, X., Zhu, X., Yang, Z., Ma, J., Xiao, S., Ji, D., Liu, D., 2020. Impacts of cascade reservoirs on the longitudinal variability of fine sediment characteristics: A case study of the Lancang and Nu Rivers. *Journal of Hydrology* 581, 124343. <https://doi.org/10.1016/j.jhydrol.2019.124343>
- Guzman, G., Alcantara, E., Barron, V., Torrent, J., 1994. Phytoavailability of phosphate adsorbed on ferrihydrite, hematite, and goethite. *Plant and Soil (Netherlands)*.
- Habets, F., Molénat, J., Carluer, N., Douez, O., Leenhardt, D., 2018. The cumulative impacts of small reservoirs on hydrology: A review. *Science of The Total Environment* 643, 850–867. <https://doi.org/10.1016/j.scitotenv.2018.06.188>
- Hahn, J., Opp, C., Evgrafova, A., Groll, M., Zitzer, N., & Laufenberg, G., 2018. Impacts of dam draining on the mobility of heavy metals and arsenic in water and basin bottom sediments of three studied dams in Germany. *Science of the Total Environment*, 640, 1072-1081.
- Hamad-Schifferli, K., 2014. Chapter 2 - Stability of Dispersions and Interactions in Nanostructured Fluids, in: Berti, D., Palazzo, G. (Eds.), *Colloidal Foundations of Nanoscience*. Elsevier, Amsterdam, pp. 33–46. <https://doi.org/10.1016/B978-0-444-59541-6.00002-3>

- Hasselov, M., Buessler, K., Pike, S., & Dai, M., 2007. Application of cross-flow ultrafiltration for the determination of colloidal abundances in suboxic ferrous-rich ground waters. *Science of The Total Environment*, 372(2–3), 636–644. <https://doi.org/10.1016/j.scitotenv.2006.10.001>
- Hart, B.T., Douglas, G.B., Beckett, R., Van Put, A., Van Grieken, R.E., 1993. Characterization of colloidal and particulate matter transported by the Magela Creek system, northern Australia. *Hydrological Processes* 7, 105–118.
- Hartland, A., Lead, J. R., Slaveykova, V., O'Carroll, D., & Valsami-Jones, E. (2013). The environmental significance of natural nanoparticles. *Nature education knowledge*, 4(8), 7.
- Hayes, N.M., Deemer, B.R., Corman, J.R., Razavi, N.R., Strock, K.E., 2017. Key differences between lakes and reservoirs modify climate signals: A case for a new conceptual model. <https://doi.org/10.1002/lo2.10036>
- Haygarth, P.M., Warwick, M.S., House, W.A., 1997. Size distribution of colloidal molybdate reactive phosphorus in river waters and soil solution. *Water Research* 31, 439–448. [https://doi.org/10.1016/S0043-1354\(96\)00270-9](https://doi.org/10.1016/S0043-1354(96)00270-9)
- He, X., Zheng, Z., Li, T., He, S., Zhang, X., Wang, Y., Huang, H., Yu, H., Liu, T., Lin, C., 2019. Transport of colloidal phosphorus in runoff and sediment on sloping farmland in the purple soil area of south-western China. *Environmental Science and Pollution Research* 26, 24088–24098. <https://doi.org/10.1007/s11356-019-05735-5>
- He, Xiaoling, Zheng, Z., Li, T., He, S., Zhang, X., Wang, Y., Huang, H., Yu, H., Liu, T., Lin, C., 2019. Transport of colloidal phosphorus in runoff and sediment on sloping farmland in the purple soil area of south-western China. *Environ Sci Pollut Res* 26, 24088–24098. <https://doi.org/10.1007/s11356-019-05735-5>
- He, Z.L., Yang, X., Yuan, K.N., Zhu, Z.X., 1994. Desorption and plant-availability of phosphate sorbed by some important minerals. *Plant Soil* 162, 89–97. <https://doi.org/10.1007/BF01416093>
- Heathwaite, A. L., Dils, R. M., 2000. Characterising phosphorus loss in surface and subsurface hydrological pathways. *Sci. Total Environ.* 251–252, 523–538. [https://doi.org/10.1016/s0048-9697\(00\)00393-4](https://doi.org/10.1016/s0048-9697(00)00393-4)
- Heathwaite, L., Haygarth, P., Matthews, R., Preedy, N., Butler, P., 2005. Evaluating colloidal phosphorus delivery to surface waters from diffuse agricultural sources. *J. Environ. Qual.* 34, 287–298.
- Heberling, F., Bosbach, D., Eckhardt, J.-D., Fischer, U., Glowacky, J., Haist, M., Kramar, U., Loos, S., Müller, H.S., Neumann, T., Pust, C., Schäfer, T., Stelling, J., Ukrainczyk, M., Vinograd, V., Vučak, M., Winkler, B., 2014. Reactivity of the calcite–water-interface, from molecular scale processes to geochemical engineering. *Applied Geochemistry* 45, 158–190. <https://doi.org/10.1016/j.apgeochem.2014.03.006>
- Henderson, R., Kabengi, N., Mantripragada, N., Cabrera, M., Hassan, S., Thompson, A., 2012. Anoxia-Induced Release of Colloid- and Nanoparticle-Bound Phosphorus in Grassland Soils. *Environ. Sci. Technol.* 46, 11727–11734. <https://doi.org/10.1021/es302395r>
- Henneberry, Y.K., Kraus, T.E.C., Nico, P.S., Horwath, W.R., 2012. Structural stability of coprecipitated natural organic matter and ferric iron under reducing conditions. *Organic Geochemistry* 48, 81–89. <https://doi.org/10.1016/j.orggeochem.2012.04.005>
- Hens, M., Merckx, R., 2002. The role of colloidal particles in the speciation and analysis of “dissolved” phosphorus. *Water Research* 36, 1483–1492. [https://doi.org/10.1016/S0043-1354\(01\)00349-9](https://doi.org/10.1016/S0043-1354(01)00349-9)
- Hinsinger, P., 2001. Bioavailability of soil inorganic P in the rhizosphere as affected by root-induced chemical changes: a review. *Plant and Soil* 237, 173–195. <https://doi.org/10.1023/A:1013351617532>

- Hjorth, T., 2004. Effects of freeze-drying on partitioning patterns of major elements and trace metals in lake sediments. *Analytica Chimica Acta* 526, 95–102. <https://doi.org/10.1016/j.aca.2004.08.007>
- Ho, C.-C., 2013. Colloidal State and Its Development, in: Tadros, T. (Ed.), *Encyclopedia of Colloid and Interface Science*. Springer, Berlin, Heidelberg, pp. 85–116. https://doi.org/10.1007/978-3-642-20665-8_9
- Hoeninghaus, D.J., 2018. Dams and River Fragmentation, in: Dellasala, D.A., Goldstein, M.I. (Eds.), *Encyclopedia of the Anthropocene*. Elsevier, Oxford, pp. 241–248. <https://doi.org/10.1016/B978-0-12-809665-9.09826-8>
- Hoffmann, C., Alonso, E.E., Romero, E., 2004. Fabric Changes of a Pellet-Based Bentonite Buffer Material and Their Effects on Mechanical Behaviour, in: Stephanson, O. (Ed.), *Elsevier Geo-Engineering Book Series, Coupled Thermo-Hydro-Mechanical-Chemical Processes in Geo-Systems*. Elsevier, pp. 341–346. [https://doi.org/10.1016/S1571-9960\(04\)80064-8](https://doi.org/10.1016/S1571-9960(04)80064-8)
- Horppila, J., Nurminen, L., 2003. Effects of submerged macrophytes on sediment resuspension and internal phosphorus loading in Lake Hiidenvesi (southern Finland). *Water Research* 37, 4468–4474. [https://doi.org/10.1016/S0043-1354\(03\)00405-6](https://doi.org/10.1016/S0043-1354(03)00405-6)
- House, W.A., Donaldson, L., 1986. Adsorption and coprecipitation of phosphate on calcite. *Journal of Colloid and Interface Science* 112, 309–324. [https://doi.org/10.1016/0021-9797\(86\)90101-3](https://doi.org/10.1016/0021-9797(86)90101-3)
- Hu, J. D., Zevi, Y., Kou, X. M., Xiao, J., Wang, X. J., Jin, Y., 2010. Effect of dissolved organic matter on the stability of magnetite nanoparticles under different pH and ionic strength conditions. *Science of The Total Environment* 408, 3477–3489. <https://doi.org/10.1016/j.scitotenv.2010.03.033>
- Hung, W. N., Lin, T. F., Chiu, C. H., Chiou, C. T., 2012. On the use of a freeze-dried versus an air-dried soil humic acid as a surrogate of soil organic matter for contaminant sorption. *Environmental Pollution* 160, 125–129. <https://doi.org/10.1016/j.envpol.2011.08.054>
- Hupfer, M., Gächter, R., Giovanoli, R., 1995. Transformation of phosphorus species in settling seston and during early sediment diagenesis. *Aquatic Science* 57, 305–324. <https://doi.org/10.1007/BF00878395>
- Hupfer, M., Gloess, S., Grossart, H.-P., 2007. Polyphosphate-accumulating microorganisms in aquatic sediments. *Aquatic Microbial Ecology* 47, 299–311. <https://doi.org/10.3354/ame047299>
- Iritani, E., Katagiri, N., Yamashita, Y., 2017. Effect of membrane morphology on rising properties of filtration resistance in microfiltration of dilute colloids. *AIChE Journal* 63, 3511–3522. <https://doi.org/10.1002/aic.15719>
- Iskrenova-Tchoukova, E., Kalinichev, A.G., Kirkpatrick, R.J., 2010. Metal Cation Complexation with Natural Organic Matter in Aqueous Solutions: Molecular Dynamics Simulations and Potentials of Mean Force. *Langmuir* 26, 15909–15919. <https://doi.org/10.1021/la102535n>
- Islam, K.R., Weil, R.R., Mulchi, C.L., Glenn, S.D., 1997. Freeze-dried soil extraction method for the measurement of microbial biomass C. *Biol Fertil Soils* 24, 205–210. <https://doi.org/10.1007/s003740050232>
- Islam, Md.A., Morton, D.W., Johnson, B.B., Pramanik, B.K., Mainali, B., Angove, M.J., 2018. Metal ion and contaminant sorption onto aluminium oxide-based materials: A review and future research. *Journal of Environmental Chemical Engineering* 6, 6853–6869. <https://doi.org/10.1016/j.jece.2018.10.045>
- ISO, 1994. ISO 9963-1:1994 - Water quality - Determination of alkalinity - Part 1: Determination of total and composite alkalinity.
- Jan, J., Borovec, J., Kopáček, J., Hejzlar, J., 2013. What do results of common sequential fractionation and single-step extractions tell us about P binding with Fe and Al compounds in non-calcareous sediments? *Water Research* 47, 547–557. <https://doi.org/10.1016/j.watres.2012.10.053>

- Jarvie, H.P., Mortimer, R.J.G., Palmer-Felgate, E.J., Quinton, K.St., Harman, S.A., Carbo, P., 2008. Measurement of soluble reactive phosphorus concentration profiles and fluxes in river-bed sediments using DET gel probes. *Journal of Hydrology, Characterization and apportionment of nutrient and sediment sources in catchments* 350, 261–273. <https://doi.org/10.1016/j.jhydrol.2007.10.041>
- Jeppesen, E., Søndergaard, M., Jensen, J.P., Havens, K.E., Anneville, O., Carvalho, L., Coveney, M.F., Deneke, R., Dokulil, M.T., Foy, B., Gerdeaux, D., Hampton, S.E., Hilt, S., Kangur, K., Köhler, J., Lammens, E.H.H.R., Lauridsen, T.L., Manca, M., Miracle, M.R., Moss, B., Nöges, P., Persson, G., Phillips, G., Portielje, R., Romo, S., Schelske, C.L., Straile, D., Tatrai, I., Willén, E., Winder, M., 2005. Lake responses to reduced nutrient loading - An analysis of contemporary long-term data from 35 case studies. *Freshwater Biology* 50, 1747–1771.
- Jiang, C. L., Séquaris, J. M., Vereecken, H., Klumpp, E., 2012. Effects of inorganic and organic anions on the stability of illite and quartz soil colloids in Na-, Ca- and mixed Na–Ca systems. *Colloids and Surfaces A: Physicochemical and Engineering Aspects* 415, 134–141. <https://doi.org/10.1016/j.colsurfa.2012.10.007>
- Jiang, X., Bol, R., Nischwitz, V., Siebers, N., Willbold, S., Vereecken, H., Amelung, W., Klumpp, E., 2015. Phosphorus Containing Water Dispersible Nanoparticles in Arable Soil. *Journal of Environmental Quality* 44, 1772–1781. <https://doi.org/10.2134/jeq2015.02.0085>
- Jin, X., Rong, N., Zhang, W., Meng, X., Shan, B., 2019. Bioavailability of organic phosphorus in an eutrophic lake: Insights from an in-situ experiment. *Ecological Indicators* 107, 105622. <https://doi.org/10.1016/j.ecolind.2019.105622>
- Jin, X., Wang, S., Pang, Y., Chang Wu, F., 2006. Phosphorus fractions and the effect of pH on the phosphorus release of the sediments from different trophic areas in Taihu Lake, China. *Environmental Pollution* 139, 288–295. <https://doi.org/10.1016/j.envpol.2005.05.010>
- Jørgensen, S.E., Löffler, H., Rast, W., Straškraba, M. (Eds.), 2005. Chapter 6 - Management of Reservoirs, in: *Developments in Water Science*. Elsevier, pp. 315–372. [https://doi.org/10.1016/S0167-5648\(05\)80027-9](https://doi.org/10.1016/S0167-5648(05)80027-9)
- Jossette, G., Leporcq, B., Sanchez, N., Philippon, 1999. Biogeochemical mass-balances (C, N, P, Si) in three large reservoirs of the Seine basin (France). *Biogeochemistry* 47, 119–146. <https://doi.org/10.1007/BF00994919>
- Judy, J.D., Kirby, J.K., Farrell, M., McLaughlin, M.J., Wilkinson, S.N., Bartley, R., Bertsch, P.M., 2018. Colloidal nitrogen is an important and highly-mobile form of nitrogen discharging into the Great Barrier Reef lagoon. *Scientific Reports* 8, 12854. <https://doi.org/10.1038/s41598-018-31115-z>
- Kaebernick, M., Neilan, B. A., Börner, T., & Dittmann, E., 2000. Light and the transcriptional response of the microcystin biosynthesis gene cluster. *Applied and environmental microbiology*, 66(8), 3387-3392.
- Kaiser, M., Berhe, A.A., 2014. How does sonication affect the mineral and organic constituents of soil aggregates? A review. *Journal of Plant Nutrition and Soil Science* 177, 479–495. <https://doi.org/10.1002/jpln.201300339>
- Kaiser, M., Kleber, M., & Berhe, A.A., 2015. How air-drying and rewetting modify soil organic matter characteristics: an assessment to improve data interpretation and inference. *Soil Biology and Biochemistry*, 80, 324-340.
- Kalbitz, K., Schwesig, D., Rethemeyer, J., Matzner, E., 2005. Stabilization of dissolved organic matter by sorption to the mineral soil. *Soil Biology and Biochemistry* 37, 1319–1331. <https://doi.org/10.1016/j.soilbio.2004.11.028>
- Kalinichev, A.G., Kirkpatrick, R.J., 2007. Molecular dynamics simulation of cationic complexation with natural organic matter. *European Journal of Soil Science* 58, 909–917. <https://doi.org/10.1111/j.1365-2389.2007.00929.x>

- Kotai, J., 1972. Instruction of preparations of modified nutrient medium Z8 for algae. Oslo: Norwegian Institute for Water Research. Publication B-11/69.
- Kaplan, D.I., Bertsch, P.M., Adriano, D.C., Miller, W.P., 1993. Soil-borne mobile colloids as influenced by water flow and organic carbon. *Environ. Sci. Technol.* 27, 1193–1200. <https://doi.org/10.1021/es00043a021>
- Keller, A.A., Auset, M., 2007. A review of visualization techniques of biocolloid transport processes at the pore scale under saturated and unsaturated conditions. *Advances in Water Resources, Biological processes in porous media: From the pore scale to the field* 30, 1392–1407. <https://doi.org/10.1016/j.advwatres.2006.05.013>
- Kerr, J.G., Burford, M., Olley, J., Udy, J., 2010. The effects of drying on phosphorus sorption and speciation in subtropical river sediments. *Mar. Freshwater Res.* 61, 928–935. <https://doi.org/10.1071/MF09124>
- Khilar, K.C., Fogler, H.S., 1998. *Migrations of Fines in Porous Media, Theory and Applications of Transport in Porous Media*. Springer Netherlands. <https://doi.org/10.1007/978-94-015-9074-7>
- Kim, L.H., Choi, E., Stenstrom, M.K., 2003. Sediment characteristics, phosphorus types and phosphorus release rates between river and lake sediments. *Chemosphere* 50, 53–61. [https://doi.org/10.1016/S0045-6535\(02\)00310-7](https://doi.org/10.1016/S0045-6535(02)00310-7)
- Kim, M.S., Lee, W.S., Kumar, K.S., Shin, K.H., Robarge, W., Kim, M., Lee, S.R., 2016. Effects of HCl pretreatment, drying, and storage on the stable isotope ratios of soil and sediment samples. *Rapid Communications in Mass Spectrometry* 30, 1567–1575. <https://doi.org/10.1002/rcm.7600>
- Kim, S.B., Yavuz Corapcioglu, M., Kim, D.J., 2003. Effect of dissolved organic matter and bacteria on contaminant transport in riverbank filtration. *Journal of Contaminant Hydrology* 66, 1–23. [https://doi.org/10.1016/S0169-7722\(03\)00025-1](https://doi.org/10.1016/S0169-7722(03)00025-1)
- Kim, S. T., Cho, H. R., Jung, E. C., Cha, W., Baik, M. H., & Lee, S., 2017. Asymmetrical flow field-flow fractionation coupled with a liquid waveguide capillary cell for monitoring natural colloids in groundwater. *Applied Geochemistry*, 87, 102-107.
- Kinsman-Costello, L.E., Hamilton, S.K., O'Brien, J.M., Lennon, J.T., 2016. Phosphorus release from the drying and reflooding of diverse shallow sediments. *Biogeochemistry* 130, 159–176. <https://doi.org/10.1007/s10533-016-0250-4>
- Klitzke, S., Lang, F., 2007. Hydrophobicity of Soil Colloids and Heavy Metal Mobilization. *Journal of Environmental Quality* 36, 1187–1193. <https://doi.org/10.2134/jeq2006.0427>
- Klitzke, S., Lang, F., Kaupenjohann, M., 2008. Increasing pH releases colloidal lead in a highly contaminated forest soil.
- Kloster, N., Brigante, M., Zanini, G., Avena, M., 2013. Aggregation kinetics of humic acids in the presence of calcium ions. *Colloids and Surfaces A: Physicochemical and Engineering Aspects* 427, 76–82. <https://doi.org/10.1016/j.colsurfa.2013.03.030>
- Kodamatani, H., Maeda, C., Balogh, S.J., Nollet, Y.H., Kanzaki, R., Tomiyasu, T., 2017. The influence of sample drying and storage conditions on methylmercury determination in soils and sediments. *Chemosphere* 173, 380–386. <https://doi.org/10.1016/j.chemosphere.2017.01.053>
- Kondolf, G.M., Gao, Y., Annandale, G.W., Morris, G.L., Jiang, E., Zhang, J., Cao, Y., Carling, P., Fu, K., Guo, Q., Hotchkiss, R., Peteuil, C., Sumi, T., Wang, H.-W., Wang, Z., Wei, Z., Wu, B., Wu, C., Yang, C.T., 2014. Sustainable sediment management in reservoirs and regulated rivers: Experiences from five continents. *Earth's Future* 2, 256–280. <https://doi.org/10.1002/2013EF000184>

- Konsoer, K.M., Rhoads, B.L., 2014. Spatial–temporal structure of mixing interface turbulence at two large river confluences. *Environ Fluid Mech* 14, 1043–1070. <https://doi.org/10.1007/s10652-013-9304-5>
- Köster, M., Babenzien, H.-D., Black, H.J., Dahlke, S., Gerbersdorf, S., Meyercordt, J., Meyer-Reil, L.-A., Rieling, T., Stodian, I., Voigt, A., 2000. Significance of aerobic and anaerobic mineralization processes of organic carbon in sediments of a shallow coastal inlet in the southern Baltic Sea, in: Flemming, B.W., Delafontaine, M.T., Liebezeit, G. (Eds.), *Proceedings in Marine Science, Muddy Coast Dynamics and Resource Management*. Elsevier, pp. 185–194. [https://doi.org/10.1016/S1568-2692\(00\)80015-7](https://doi.org/10.1016/S1568-2692(00)80015-7)
- Kowalczywska-Madura, K., Dondajewska, R., Gołdyn, R., Kozak, A., Messyasz, B., 2018. Internal Phosphorus Loading from the Bottom Sediments of a Dimictic Lake During Its Sustainable Restoration. *Water Air Soil Pollut* 229. <https://doi.org/10.1007/s11270-018-3937-4>
- Krachler, R.F., Krachler, R., Stojanovic, A., Wielander, B., Herzig, A., 2009. Effects of pH on aquatic biodegradation processes. *Biogeosciences Discussions* 6, 491–514. <https://doi.org/10.5194/bgd-6-491-2009>
- Kretzschmar, R., Borkovec, M., Grolimund, D., Elimelech, M., 1999. Mobile Subsurface Colloids and Their Role in Contaminant Transport, in: *Advances in Agronomy*. Elsevier, pp. 121–193. [https://doi.org/10.1016/S0065-2113\(08\)60427-7](https://doi.org/10.1016/S0065-2113(08)60427-7)
- Kretzschmar, R., Robarge, W.P., Amoozegar, A., 1995. Influence of Natural Organic Matter on Colloid Transport Through Saprofite. *Water Resources Research* 31, 435–445. <https://doi.org/10.1029/94WR02676>
- Kretzschmar, R., Sticher, H., Hesterberg, D., 1997. Effects of Adsorbed Humic Acid on Surface Charge and Flocculation of Kaolinite. *Soil Science Society of America Journal* 61, 101–108. <https://doi.org/10.2136/sssaj1997.03615995006100010016x>
- Kunz, M.J., Anselmetti, F.S., Wüest, A., Wehrli, B., Vollenweider, A., Thüning, S., Senn, D.B., 2011. Sediment accumulation and carbon, nitrogen, and phosphorus deposition in the large tropical reservoir Lake Kariba (Zambia/Zimbabwe). *Journal of Geophysical Research: Biogeosciences* 116. <https://doi.org/10.1029/2010JG001538>
- Kwak, D.-H., Jeon, Y.-T., Duck Hur, Y., 2018. Phosphorus fractionation and release characteristics of sediment in the Saemangeum Reservoir for seasonal change. *International Journal of Sediment Research* 33, 250–261. <https://doi.org/10.1016/j.ijsrc.2018.04.008>
- Lasaga, A.C., 1981. Rate laws of chemical reactions. *Rev. Mineral.;* (United States) 8.
- Le Moal, M., Gascuel-Oudou, C., Ménesguen, A., Souchon, Y., Étrillard, C., Levain, A., Moatar, F., Pannard, A., Souchu, P., Lefebvre, A., Pinay, G., 2019. Eutrophication: A new wine in an old bottle? *Science of The Total Environment* 651, 1–11. <https://doi.org/10.1016/j.scitotenv.2018.09.139>
- Lead, J.R., Davison, W., Hamilton-Taylor, J., Buffle, J., 1997. Characterizing Colloidal Material in Natural Waters. *Aquatic Geochemistry* 3, 213–232. <https://doi.org/10.1023/A:1009695928585>
- Lee, J.K., 1998. Surface Charge Effects on Particulate Retention by Microporous Membrane Filters in Liquid Filtration. *Environmental Engineering Research* 3, 97–104.
- Lelong, F., Tardy, Y., Grandin, G., Trescases, J.J., Boulange, B., 1976. Chapter 3 - pedogenesis, chemical weathering and processes of formation of some supergene ore deposits, in: Wolf, K.H. (Ed.), *Supergene and Surficial Ore Deposits, Handbook of Strata-Bound and Stratiform Ore Deposits*. Elsevier, Amsterdam, pp. 93–173. <https://doi.org/10.1016/B978-0-444-41403-8.50007-8>
- Lemos, V.P., Costa, M.L. da, Lemos, R.L., Faria, M.S.G. de, 2007. Vivianite and siderite in lateritic iron crust: an example of bioreduction. *Química Nova* 30, 36–40. <https://doi.org/10.1590/S0100-40422007000100008>

- Lepage, H., Launay, M., Le Coz, J., Angot, H., Miège, C., Gairoard, S., Radakovitch, O., Coquery, M., 2020. Impact of dam flushing operations on sediment dynamics and quality in the upper Rhône River, France. *Journal of Environmental Management* 255, 109886. <https://doi.org/10.1016/j.jenvman.2019.109886>
- Leppard, G.G., 1997. Colloidal organic fibrils of acid polysaccharides in surface waters: electron-optical characteristics, activities and chemical estimates of abundance. *Colloids and Surfaces A: Physicochemical and Engineering Aspects, Aquatic Colloid and Surface Chemistry* 120, 1–15. [https://doi.org/10.1016/S0927-7757\(96\)03676-X](https://doi.org/10.1016/S0927-7757(96)03676-X)
- Lewandowski, J., Hupfer, M., 2005. Effect of macrozoobenthos on two-dimensional small-scale heterogeneity of pore water phosphorus concentrations in lake sediments: A laboratory study. *Limnology and Oceanography* 50, 1106–1118. <https://doi.org/10.4319/lo.2005.50.4.1106>
- Li, B., Brett, M.T., 2015. The relationship between operational and bioavailable phosphorus fractions in effluents from advanced nutrient removal systems. *Int. J. Environ. Sci. Technol.* 12, 3317–3328. <https://doi.org/10.1007/s13762-015-0760-y>
- Li, J., Dong, S., Liu, S., Yang, Z., Peng, M., Zhao, C., 2013. Effects of cascading hydropower dams on the composition, biomass and biological integrity of phytoplankton assemblages in the middle Lancang-Mekong River. *Ecological Engineering* 60, 316–324. <https://doi.org/10.1016/j.ecoleng.2013.07.029>
- Li, Q., Xie, L., Jiang, Y., Fortner, J.D., Yu, K., Liao, P., Liu, C., 2019. Formation and stability of NOM-Mn(III) colloids in aquatic environments. *Water Research* 149, 190–201. <https://doi.org/10.1016/j.watres.2018.10.094>
- Liang, X., Jin, Y., Zhao, Y., Wang, Z., Yin, R., Tian, G., 2016. Release and migration of colloidal phosphorus from a typical agricultural field under long-term phosphorus fertilization in southeastern China. *J Soils Sediments* 16, 842–853. <https://doi.org/10.1007/s11368-015-1290-4>
- Liang, X., Liu, J., Chen, Y., Li, H., Ye, Y., Nie, Z., Su, M., Xu, Z., 2010. Effect of pH on the release of soil colloidal phosphorus. *Journal of Soils and Sediments* 10, 1548–1556. <https://doi.org/10.1007/s11368-010-0275-6>
- Liao, P., Li, W., Jiang, Y., Wu, J., Yuan, S., Fortner, J.D., Giammar, D.E., 2017. Formation, Aggregation, and Deposition Dynamics of NOM-Iron Colloids at Anoxic–Oxic Interfaces. *Environ. Sci. Technol.* 51, 12235–12245. <https://doi.org/10.1021/acs.est.7b02356>
- Likens, G.E., Loucks, O.L., 1978. Analysis of five North American lake ecosystems: III. Sources, loading and fate of nitrogen and phosphorus: With 6 tables in the text. *Internationale Vereinigung für theoretische und angewandte Limnologie: Verhandlungen* 20, 568–573.
- Lima Neto, I.E., 2019. Impact of artificial destratification on water availability of reservoirs in the Brazilian semiarid. *Anais da Academia Brasileira de Ciências* 91. <https://doi.org/10.1590/0001-3765201920171022>
- Lindegren, M., Persson, P., 2009. Competitive adsorption between phosphate and carboxylic acids: quantitative effects and molecular mechanisms. *European Journal of Soil Science* 60, 982–993. <https://doi.org/10.1111/j.1365-2389.2009.01171.x>
- Liro, M., 2016. Development of sediment slug upstream from the Czorsztyn Reservoir (southern Poland) and its interaction with river morphology. *Geomorphology* 253, 225–238. <https://doi.org/10.1016/j.geomorph.2015.09.018>
- Liro, M., 2014. Conceptual model for assessing the channel changes upstream from dam reservoir. *Quaestiones Geographicae* 33.
- Litchman, E., Nguyen, B.L.V., 2008. Alkaline phosphatase activity as a function of internal phosphorus concentration in freshwater phytoplankton (1). *J. Phycol.* 44, 1379–1383. <https://doi.org/10.1111/j.1529-8817.2008.00598.x>

- Liu, J., Yang, J., Liang, X., Zhao, Y., Cade-Menun, B.J., Hu, Y., 2014. Molecular Speciation of Phosphorus Present in Readily Dispersible Colloids from Agricultural Soils. *Soil Science Society of America Journal* 78, 47. <https://doi.org/10.2136/sssaj2013.05.0159>
- Liu, Z., Flury, M., Harsh, J.B., Mathison, J.B., Vogs, C., 2013. Colloid mobilization in an undisturbed sediment core under semiarid recharge rates. *Water Resources Research* 49, 4985–4996. <https://doi.org/10.1002/wrcr.20343>
- López, P., López-Tarazón, J.A., Casas-Ruiz, J.P., Pompeo, M., Ordoñez, J., Muñoz, I., 2016. Sediment size distribution and composition in a reservoir affected by severe water level fluctuations. *Science of The Total Environment*, 5th Special Issue SCARCE: River Conservation under Multiple stressors: Integration of ecological status, pollution and hydrological variability 540, 158–167. <https://doi.org/10.1016/j.scitotenv.2015.06.033>
- Lopez, P., Marcé, R., Ordoñez, J., Urrutia, I., Armengol, J., 2009. Sedimentary phosphorus in a cascade of five reservoirs (Lozoya River, Central Spain). *Lake and Reservoir Management* 25, 39–48. <https://doi.org/10.1080/07438140802714353>
- Lucassen, E., Smolders, A.J., Roelofs, J.G., 2002. Potential sensitivity of mires to drought, acidification and mobilisation of heavy metals: the sediment S/(Ca+ Mg) ratio as diagnostic tool. *Environmental pollution* 120, 635–646.
- Luo, P., Morrison, I., Dudkiewicz, A., Tiede, K., Boyes, E., O’Toole, P., Park, S., Boxall, A.B., 2013. Visualization and characterization of engineered nanoparticles in complex environmental and food matrices using atmospheric scanning electron microscopy. *J Microsc* 250, 32–41. <https://doi.org/10.1111/jmi.12014>
- Lyvén, B., Hassellöv, M., Turner, D. R., Haraldsson, C., & Andersson, K., 2003. Competition between iron-and carbon-based colloidal carriers for trace metals in a freshwater assessed using flow field-flow fractionation coupled to ICPMS. *Geochimica et Cosmochimica Acta*, 67(20), 3791-3802. [https://doi.org/10.1016/S0016-7037\(03\)00087-5](https://doi.org/10.1016/S0016-7037(03)00087-5)
- Ma, J., Guo, H., Weng, L., Li, Y., Lei, M., & Chen, Y. (2018). Distinct effect of humic acid on ferrihydrite colloid-facilitated transport of arsenic in saturated media at different pH. *Chemosphere*, 212, 794-801.
- Maavara, T., Parsons, C.T., Ridenour, C., Stojanovic, S., Dürr, H.H., Powley, H.R., Van Cappellen, P., 2015. Global phosphorus retention by river damming. *Proc Natl Acad Sci U S A* 112, 15603–15608. <https://doi.org/10.1073/pnas.1511797112>
- Macintosh, K.A., Mayer, B.K., McDowell, R.W., Powers, S.M., Baker, L.A., Boyer, T.H., Rittmann, B.E., 2018. Managing Diffuse Phosphorus at the Source versus at the Sink. *Environmental Science and Technology* 52, 11995–12009. <https://doi.org/10.1021/acs.est.8b01143>
- Maeck, A., DelSontro, T., McGinnis, D.F., Fischer, H., Flury, S., Schmidt, M., Fietzek, P., Lorke, A., 2013. Sediment Trapping by Dams Creates Methane Emission Hot Spots. *Environ. Sci. Technol.* 47, 8130–8137. <https://doi.org/10.1021/es4003907>
- Mahmood, Q., Khan, A.F., Khan, A., 2014. Chapter 25 - Colloids in the Environmental Protection—Current and Future Trends, in: Fanun, M. (Ed.), *The Role of Colloidal Systems in Environmental Protection*. Elsevier, Amsterdam, pp. 635–677. <https://doi.org/10.1016/B978-0-444-63283-8.00025-9>
- Majdalani, S., Michel, E., Di-Pietro, L., Angulo-Jaramillo, R., 2008. Effects of wetting and drying cycles on in situ soil particle mobilization. *European Journal of Soil Science* 59, 147–155. <https://doi.org/10.1111/j.1365-2389.2007.00964.x>
- Mankasingh, U., Gísladóttir, G., 2019. Early indicators of soil formation in the Icelandic sub-arctic highlands. *Geoderma* 337, 152–163. <https://doi.org/10.1016/j.geoderma.2018.09.002>

- Maria, E., Crançon, P., Le Coustumer, P., Bridoux, M., Lespes, G., 2020. Comparison of preconcentration methods of the colloidal phase of a uranium-containing soil suspension. *Talanta* 208, 120383. <https://doi.org/10.1016/j.talanta.2019.120383>
- Martínez-Mena, M., Almagro, M., García-Franco, N., Vente, J. D., García, E., & Boix-Fayos, C., 2019. Fluvial sedimentary deposits as carbon sinks: organic carbon pools and stabilization mechanisms across a Mediterranean catchment. *Biogeosciences*, 16(5), 1035-1051.
- März, C., Riedinger, N., Sena, C., Kasten, S., 2018. Phosphorus dynamics around the sulphate-methane transition in continental margin sediments: Authigenic apatite and Fe(II) phosphates. *Marine Geology* 404, 84–96. <https://doi.org/10.1016/j.margeo.2018.07.010>
- McCarthy, J.F., McKay, L.D., 2004. Colloid Transport in the Subsurface Past, Present, and Future Challenges. *Vadose Zone Journal* 3, 326–337. <https://doi.org/10.2113/3.2.326>
- McKelvie, I. D., Peat, D. M., & Worsfold, P. J., 1995. Analytical perspective. Techniques for the quantification and speciation of phosphorus in natural waters. In *Analytical Proceedings Including Analytical Communications* 32 (10), 437–445. Royal Society of Chemistry.
- Mekonnen, M.M., Hoekstra, A.Y., 2018. Global Anthropogenic Phosphorus Loads to Freshwater and Associated Grey Water Footprints and Water Pollution Levels: A High-Resolution Global Study. *Water Resources Research* 54, 345–358. <https://doi.org/10.1002/2017WR020448>
- Mentler, A., Mayer, H., Strauß, P., Blum, W.E.H., 2004. Characterisation of soil aggregate stability by ultrasonic dispersion. *Int. Agrophys.* 18, 39–45.
- Meysman, F.J.R., Galaktionov, O.S., Gribsholt, B., Middelburg, J.J., 2006. Bioirrigation in permeable sediments: Advective pore-water transport induced by burrow ventilation. *Limnology and Oceanography* 51, 142–156. <https://doi.org/10.4319/lo.2006.51.1.0142>
- Miao, T., Wang, J., Zeng, Y., Liu, G., Chen, X., 2018. Polysaccharide-Based Controlled Release Systems for Therapeutics Delivery and Tissue Engineering: From Bench to Bedside. *Advanced Science* 5, 1700513. <https://doi.org/10.1002/advs.201700513>
- Miller, J.O., Karathanasis, A.D., 2014. Chapter 1 - Biosolid Colloids as Environmental Contaminant Carriers, in: Fanun, M. (Ed.), *The Role of Colloidal Systems in Environmental Protection*. Elsevier, Amsterdam, pp. 1–18. <https://doi.org/10.1016/B978-0-444-63283-8.00001-6>
- Mills, T.J., Anderson, S.P., Bern, C., Aguirre, A., Derry, L.A., 2017. Colloid Mobilization and Seasonal Variability in a Semiarid Headwater Stream. *Journal of Environment Quality* 46, 88. <https://doi.org/10.2134/jeq2016.07.0268>
- Missong, A., Bol, R., Willbold, S., Siemens, J., Klumpp, E., 2016. Phosphorus forms in forest soil colloids as revealed by liquid-state ³¹P-NMR. *Journal of Plant Nutrition and Soil Science* 179, 159–167. <https://doi.org/10.1002/jpln.201500119>
- Missong, A., Holzmann, S., Bol, R., Nischwitz, V., Puhmann, H., v. Wilpert, K., Siemens, J., Klumpp, E., 2018. Leaching of natural colloids from forest topsoils and their relevance for phosphorus mobility. *Science of The Total Environment* 634, 305–315. <https://doi.org/10.1016/j.scitotenv.2018.03.265>
- Mohanty, S.K., Saiers, J.E., Ryan, J.N., 2015. Colloid Mobilization in a Fractured Soil during Dry–Wet Cycles: Role of Drying Duration and Flow Path Permeability. *Environmental Science & Technology* 49, 9100–9106. <https://doi.org/10.1021/acs.est.5b00889>
- Mohanty, S.K., Saiers, J.E., Ryan, J.N., 2014. Colloid-Facilitated Mobilization of Metals by Freeze–Thaw Cycles. *Environmental Science & Technology* 48, 977–984. <https://doi.org/10.1021/es403698u>
- Montalvo, D., Degryse, F., McLaughlin, M.J., 2015. Natural colloidal P and its contribution to plant P uptake. *Environmental Science and Technology* 49, 3427–3434. <https://doi.org/10.1021/es504643f>

- Morris, G.L., 2020. Classification of Management Alternatives to Combat Reservoir Sedimentation. *Water* 12, 861. <https://doi.org/10.3390/w12030861>
- Morrison, M.A., Benoit, G., 2001. Filtration Artifacts Caused by Overloading Membrane Filters. *Environ. Sci. Technol.* 35, 3774–3779. <https://doi.org/10.1021/es010670k>
- Morse, J.W., Arvidson, R.S., Lüttge, A., 2007. Calcium Carbonate Formation and Dissolution. *Chem. Rev.* 107, 342–381. <https://doi.org/10.1021/cr050358j>
- Moura, D.S., Lima Neto, I.E., Clemente, A., Oliveira, S., Pestana, C.J., Aparecida de Melo, M., Capelo-Neto, J., 2020. Modeling phosphorus exchange between bottom sediment and water in tropical semiarid reservoirs. *Chemosphere* 246. <https://doi.org/10.1016/j.chemosphere.2019.125686>
- Munger, Z.W., Carey, C.C., Gerling, A.B., Hamre, K.D., Doubek, J.P., Klepatzki, S.D., McClure, R.P., Schreiber, M.E., 2016. Effectiveness of hypolimnetic oxygenation for preventing accumulation of Fe and Mn in a drinking water reservoir. *Water Research* 106, 1–14. <https://doi.org/10.1016/j.watres.2016.09.038>
- Munkholm, L.J., Kay, B.D., 2002. Effect of Water Regime on Aggregate-tensile Strength, Rupture Energy, and Friability. *Soil Science Society of America Journal* 66, 702–709. <https://doi.org/10.2136/sssaj2002.7020>
- Murali, R., Murthy, C. N., & Chamyal, L. S., 2012. Characterization of colloids in the late Quaternary sediment sequences of Mahi river basin, Gujarat, India. *Current Science*, 1209-1215.
- Murphy, J. A. M. E. S., & Riley, J. P. (1962). A modified single solution method for the determination of phosphate in natural waters. *Analytica chimica acta*, 27, 31-36.
- Nègre, M., Leone, P., Trichet, J., Défarge, C., Boero, V., Gennari, M., 2004. Characterization of model soil colloids by cryo-scanning electron microscopy. *Geoderma* 121, 1–16. <https://doi.org/10.1016/j.geoderma.2003.09.011>
- Newman, E.I., 2008. *Applied ecology and environmental management*. John Wiley & Sons.
- Nguyen, D.N., Grybos, M., Rabiet, M., Deluchat, V., 2020. How do colloid separation and sediment storage methods affect water-mobilizable colloids and phosphorus? An insight into dam reservoir sediment. *Colloids and Surfaces A: Physicochemical and Engineering Aspects* 606, 125505. <https://doi.org/10.1016/j.colsurfa.2020.125505>
- Niemistö, J., Silvonen, S., Horppila, J., 2019. Effects of hypolimnetic aeration on the quantity and quality of settling material in a eutrophied dimictic lake. *Hydrobiologia*. <https://doi.org/10.1007/s10750-019-04160-6>
- Niirnberg, G.K., 1994. *Phosphorus Release from Anoxic Sediments: What We Know and How We Can Deal with It*, 1st ed. Limnetica, 1-4.
- Noël, V., Kumar, N., Boye, K., Barragan, L., Lezama-Pacheco, J.S., Chu, R., Tolic, N., Brown, G.E., Bargar, J.R., 2020. FeS colloids – formation and mobilization pathways in natural waters. *Environ. Sci.: Nano* 7, 2102–2116. <https://doi.org/10.1039/C9EN01427F>
- Norgbey, E., Li, Y., Ya, Z., Li, R., Nwankwegu, A.S., Takyi-Annan, G.E., Luo, F., Jin, W., Huang, Y., Sarpong, L., 2020. High resolution evidence of iron-phosphorus-sulfur mobility at hypoxic sediment water interface: An insight to phosphorus remobilization using DGT-induced fluxes in sediments model. *Science of The Total Environment* 724, 138204. <https://doi.org/10.1016/j.scitotenv.2020.138204>
- North, R.L., Johansson, J., Vandergucht, D.M., Doig, L.E., Liber, K., Lindenschmidt, K.-E., Baulch, H., Hudson, J.J., 2015. Evidence for internal phosphorus loading in a large prairie reservoir (Lake Diefenbaker, Saskatchewan). *Journal of Great Lakes Research*, Special Issue on Characterization and dynamics of a large multi-purpose prairie reservoir: Lake Diefenbaker, Saskatchewan, Canada 41, 91–99. <https://doi.org/10.1016/j.jglr.2015.07.003>

- Nürnberg, G.K., 2009. Assessing internal phosphorus load – Problems to be solved. *Lake and Reservoir Management* 25, 419–432. <https://doi.org/10.1080/00357520903458848>
- Nürnberg, G.K., Tarvainen, M., Ventelä, A.-M., Sarvala, J., 2012. Internal phosphorus load estimation during biomanipulation in a large polymictic and mesotrophic lake. *Inland Waters* 2, 147–162. <https://doi.org/10.5268/IW-2.3.469>
- Ohshima, H., 2014. Chapter 1 - Interaction of colloidal particles, in: Ohshima, H., Makino, K. (Eds.), *Colloid and Interface Science in Pharmaceutical Research and Development*. Elsevier, Amsterdam, pp. 1–28. <https://doi.org/10.1016/B978-0-444-62614-1.00001-6>
- OIEau, Bulletin national de situation hydrologique du 13 août 2019 [online], 2019, available on « <https://www.eaufrance.fr/publications/bsh/2019-08> » (consulted 17/07/2020)
- Opdyke, N.D., Channell, J.E.T., 1996. 3 - Magnetization Processes and Magnetic Properties of Sediments, in: Opdyke, N.D., Channell, J.E.T. (Eds.), *International Geophysics, Magnetic Stratigraphy*. Academic Press, pp. 26–48. [https://doi.org/10.1016/S0074-6142\(06\)80005-7](https://doi.org/10.1016/S0074-6142(06)80005-7)
- Orihel, D.M., Baulch, H.M., Casson, N.J., North, R.L., Parsons, C.T., Seckar, D.C.M., Venkiteswaran, J.J., 2017. Internal phosphorus loading in Canadian freshwaters: A critical review and data analysis. <http://www.nrcresearchpress.com/doi/abs/10.1139/cjfas-2016-0500>
- Pacina, J., Lendáková, Z., Štojdl, J., Matys Grygar, T., Dolejš, M., 2020. Dynamics of Sediments in Reservoir Inflows: A Case Study of the Skalka and Nechanice Reservoirs, Czech Republic. *ISPRS International Journal of Geo-Information* 9, 258. <https://doi.org/10.3390/ijgi9040258>
- Pakhomova, S.V., Hall, P.O., Kononets, M.Y., Rozanov, A.G., Tengberg, A., & Vershinin, A.V., 2007. Fluxes of iron and manganese across the sediment–water interface under various redox conditions. *Marine Chemistry*, 107(3), 319–331.
- Palanques, A., Guillén, J., Puig, P., Grimalt, J.O., 2020. Effects of flushing flows on the transport of mercury-polluted particulate matter from the Flix Reservoir to the Ebro Estuary. *Journal of Environmental Management* 260, 110028. <https://doi.org/10.1016/j.jenvman.2019.110028>
- Paludan, C., Jensen, H.S., 1995. Sequential extraction of phosphorus in freshwater wetland and lake sediment: Significance of humic acids. *Wetlands* 15, 365–373. <https://doi.org/10.1007/BF03160891>
- Parfitt, R.L., 1989. Phosphate reactions with natural allophane, ferrihydrite and goethite. *Journal of Soil Science* 40, 359–369. <https://doi.org/10.1111/j.1365-2389.1989.tb01280.x>
- Parfitt, R.L., Russell, J.D., Farmer, V.C., 1976. Confirmation of the surface structures of goethite (α -FeOOH) and phosphated goethite by infrared spectroscopy. *J. Chem. Soc., Faraday Trans. 1* 72, 1082–1087. <https://doi.org/10.1039/F19767201082>
- Park, S.-J., Seo, M.-K., 2011. Chapter 1 - Intermolecular Force, in: Park, S.-J., Seo, M.-K. (Eds.), *Interface Science and Technology, Interface Science and Composites*. Elsevier, pp. 1–57. <https://doi.org/10.1016/B978-0-12-375049-5.00001-3>
- Parsons, C.T., Rezanezhad, F., O.; Connell, D.W., Van Cappellen, P., 2017. Sediment phosphorus speciation and mobility under dynamic redox conditions. *Biogeosciences Discussions* 1–36. <https://doi.org/10.5194/bg-2016-533>
- Peiffer, S., Wan, M., 2016. Reductive Dissolution and Reactivity of Ferric (Hydr)oxides: New Insights and Implications for Environmental Redox Processes, in: *Iron Oxides*. John Wiley & Sons, Ltd, pp. 31–52. <https://doi.org/10.1002/9783527691395.ch3>
- Perret, D., Newman, M.E., Nègre, J.-C., Chen, Y., Buffle, J., 1994. Submicron particles in the rhine river-I. Physico-chemical characterization. *Water Research* 28, 91–106. [https://doi.org/10.1016/0043-1354\(94\)90123-6](https://doi.org/10.1016/0043-1354(94)90123-6)

- Perrott, K.W., 1977. Freeze-drying of soil clays. *Geoderma* 17, 219–224. [https://doi.org/10.1016/0016-7061\(77\)90052-0](https://doi.org/10.1016/0016-7061(77)90052-0)
- Pestana, I. A., Azevedo, L. S., Bastos, W. R., & de Souza, C. M. M., 2019. The impact of hydroelectric dams on mercury dynamics in South America: A review. *Chemosphere*, 219, 546-556.
- Peter, D.H., Castella, E., Slaveykova, V.I., 2014. Effects of a reservoir flushing on trace metal partitioning, speciation and benthic invertebrates in the floodplain. *Environ. Sci.: Processes Impacts* 16, 2692–2702. <https://doi.org/10.1039/C4EM00387J>
- Pettersson, K., Boström, B., Jacobsen, O., 1988. Phosphorus in sediments - speciation and analysis. *Hydrobiologia* 48, 91–101. https://doi.org/10.1007/978-94-009-3109-1_7
- Phillips, C.B., Dallmann, J.D., Jerolmack, D.J., & Packman, A.I., 2019. Fine-Particle Deposition, Retention, and Resuspension Within a Sand-Bedded Stream Are Determined by Streambed Morphodynamics. *Water Resources Research*, 55(12), 10303-10318.
- Piccolo, A., 2002. The supramolecular structure of humic substances: A novel understanding of humus chemistry and implications in soil science, in: *Advances in Agronomy*. Academic Press, pp. 57–134. [https://doi.org/10.1016/S0065-2113\(02\)75003-7](https://doi.org/10.1016/S0065-2113(02)75003-7)
- Pokrajac, D., Manes, C., & McEwan, I., 2007. Peculiar mean velocity profiles within a porous bed of an open channel. *Physics of Fluids*, 19(9), 098109.
- Poikane, S., Kelly, M.G., Salas Herrero, F., Pitt, J.-A., Jarvie, H.P., Claussen, U., Leujak, W., Lyche Solheim, A., Teixeira, H., Phillips, G., 2019. Nutrient criteria for surface waters under the European Water Framework Directive: Current state-of-the-art, challenges and future outlook. *Science of The Total Environment* 695, 133888. <https://doi.org/10.1016/j.scitotenv.2019.133888>
- Poirier, S.-C., Whalen, J.K., Michaud, A.R., 2012. Bioavailable Phosphorus in Fine-Sized Sediments Transported from Agricultural Fields.
- Postel, S.L., Daily, G.C., Ehrlich, P.R., 1996. Human Appropriation of Renewable Fresh Water. *Science* 271, 785. <https://doi.org/10.1126/science.271.5250.785>
- Postma, D., Jakobsen, R., 1996. Redox zonation: Equilibrium constraints on the Fe(III)/SO₄-reduction interface. *Geochimica et Cosmochimica Acta* 60, 3169–3175. [https://doi.org/10.1016/0016-7037\(96\)00156-1](https://doi.org/10.1016/0016-7037(96)00156-1)
- Preece, E.P., Moore, B.C., Skinner, M.M., Child, A., Dent, S., 2019. A review of the biological and chemical effects of hypolimnetic oxygenation. *Lake and Reservoir Management* 35, 229–246. <https://doi.org/10.1080/10402381.2019.1580325>
- Quik, J.T.K., Stuart, M.C., Wouterse, M., Peijnenburg, W., Hendriks, A.J., van de Meent, D., 2012. Natural colloids are the dominant factor in the sedimentation of nanoparticles. *Environ. Toxicol. Chem.* 31, 1019–1022. <https://doi.org/10.1002/etc.1783>
- Raine, S.R., So, H.B., 1997. An investigation of the relationships between dispersion, power, and mechanical energy using the end-over-end shaking and ultrasonic methods of aggregate stability assessment. *Soil Res.* 35, 41–54. <https://doi.org/10.1071/s96063>
- Ran, Y., Fu, J. M., Sheng, G.Y., Beckett, R., & Hart, B.T., 2000. Fractionation and composition of colloidal and suspended particulate materials in rivers. *Chemosphere*, 41(1–2), 33–43.
- Ranville, J. F., Chittleborough, D. J., Shanks, F., Morrison, R. J., Harris, T., Doss, F., & Beckett, R., 1999. Development of sedimentation field-flow fractionation-inductively coupled plasma mass-spectrometry for the characterization of environmental colloids. *Analytica chimica acta*, 381(2-3), 315-329.
- Rapin, A., 2018. Mobilité du phosphore sédimentaire en contexte de retenues de barrage hydroélectrique (PhD Thesis). Limoges.

- Rapin, Anne, Grybos, M., Rabiet, M., Mourier, B., Deluchat, V., 2019. Phosphorus mobility in dam reservoir affected by redox oscillations: An experimental study. *Journal of Environmental Sciences* 77, 250–263. <https://doi.org/10.1016/j.jes.2018.07.016>
- Rapin, A., Rabiet, M., Mourier, B., Grybos, M., Deluchat, V., 2020. Sedimentary phosphorus accumulation and distribution in the continuum of three cascade dams (Creuse River, France). *Environ Sci Pollut Res* 27, 6526–6539. <https://doi.org/10.1007/s11356-019-07184-6>
- Rapin, Francois., Tessier, Andre., Campbell, P.G.C., Carignan, Richard., 1986. Potential artifacts in the determination of metal partitioning in sediments by a sequential extraction procedure. *Environ. Sci. Technol.* 20, 836–840. <https://doi.org/10.1021/es00150a014>
- Regelink, I. C., Voegelin, A., Weng, L., Koopmans, G. F., & Comans, R. N., 2014. Characterization of colloidal Fe from soils using field-flow fractionation and Fe K-edge X-ray absorption spectroscopy. *Environmental science & technology*, 48(8), 4307-4316.
- Reitzel, K., Jensen, H.S., Egemose, S., 2013. pH dependent dissolution of sediment aluminum in six Danish lakes treated with aluminum. *Water research* 47, 1409–1420.
- Reynolds, C.S., Davies, P.S., 2001. Sources and bioavailability of phosphorus fractions in freshwaters: a British perspective. *Biol Rev Camb Philos Soc* 76, 27–64.
- Rick, A. R., & Arai, Y. (2011). Role of natural nanoparticles in phosphorus transport processes in ultisols. *Soil Science Society of America Journal*, 75(2), 335-347. <https://doi.org/10.2136/sssaj2010.0124nps>
- Rolfhus, K.R., Hurley, J.P., Bodaly, R.A. (Drew), Perrine, G., 2015. Production and Retention of Methylmercury in Inundated Boreal Forest Soils. *Environ. Sci. Technol.* 49, 3482–3489. <https://doi.org/10.1021/es505398z>
- Rose, K.A., Brenkert, A.L., Schohl, G.A., Onishi, Y., Hayworth, J.S., Holly, F., Perkins, W., Beard, L., Cook, R.B., Waldrop, W., 1993. Multiple Model Analysis of Sediment Transport and Contaminant Distribution in the Clinch River/Watts Bar Reservoir, Tennessee, USA*. *Water Science and Technology* 28, 65–78. <https://doi.org/10.2166/wst.1993.0605>
- Rothe, M., Kleeberg, A., Grüneberg, B., Friese, K., Pérez-Mayo, M., Hupfer, M., 2015. Sedimentary Sulphur:Iron Ratio Indicates Vivianite Occurrence: A Study from Two Contrasting Freshwater Systems. *PLoS One* 10. <https://doi.org/10.1371/journal.pone.0143737>
- Rothe, M., Kleeberg, A., Hupfer, M., 2016. The occurrence, identification and environmental relevance of vivianite in waterlogged soils and aquatic sediments. *Earth-Science Reviews* 158, 51–64. <https://doi.org/10.1016/j.earscirev.2016.04.008>
- Rowley, M.C., Grand, S., Verrecchia, É.P., 2018. Calcium-mediated stabilisation of soil organic carbon. *Biogeochemistry* 137, 27–49. <https://doi.org/10.1007/s10533-017-0410-1>
- Roy, K., Kar, S., Das, R.N., 2015. Chapter 1 - Background of QSAR and Historical Developments, in: Roy, K., Kar, S., Das, R.N. (Eds.), *Understanding the Basics of QSAR for Applications in Pharmaceutical Sciences and Risk Assessment*. Academic Press, Boston, pp. 1–46. <https://doi.org/10.1016/B978-0-12-801505-6.00001-6>
- Roy, S.B., Dzombak, D.A., 1998. Sorption nonequilibrium effects on colloid-enhanced transport of hydrophobic organic compounds in porous media. *Journal of Contaminant Hydrology* 30, 179–200. [https://doi.org/10.1016/S0169-7722\(97\)00040-5](https://doi.org/10.1016/S0169-7722(97)00040-5)
- Różyło, K., Bohacz, J., 2020. Microbial and enzyme analysis of soil after the agricultural utilization of biogas digestate and mineral mining waste. *Int. J. Environ. Sci. Technol.* 17, 1051–1062. <https://doi.org/10.1007/s13762-019-02522-0>
- Ruban, V., López-Sánchez, J. F., Pardo, P., Rauret, G., Muntau, H., & Quevauviller, P., 2001. Harmonized protocol and certified reference material for the determination of extractable

contents of phosphorus in freshwater sediments—a synthesis of recent works. *Fresenius' journal of analytical chemistry*, 370(2-3), 224-228.

- Ruhl, N., DeAngelis, H., Crosby, A.M., Roosenburg, W.M., 2014. Applying a reservoir functional-zone paradigm to littoral bluegills: differences in length and catch frequency? *PeerJ* 2, e528. <https://doi.org/10.7717/peerj.528>
- Ruttenberg, K., 2014. 10.13—The global phosphorus cycle. *Treatise on Geochemistry* 499–558.
- Ruttenberg, K.C., 2019. Phosphorus Cycle☆, in: Cochran, J.K., Bokuniewicz, H.J., Yager, P.L. (Eds.), *Encyclopedia of Ocean Sciences (Third Edition)*. Academic Press, Oxford, pp. 447–460. <https://doi.org/10.1016/B978-0-12-409548-9.10807-3>
- Ruttenberg, K.C., 2003. 8.13 - The Global Phosphorus Cycle, in: Holland, H.D., Turekian, K.K. (Eds.), *Treatise on Geochemistry*. Pergamon, Oxford, pp. 585–643. <https://doi.org/10.1016/B0-08-043751-6/08153-6>
- Ruttenberg, K.C., Berner, R.A., 1993. Authigenic apatite formation and burial in sediments from non-upwelling, continental margin environments. *Geochimica et Cosmochimica Acta* 57, 991–1007. [https://doi.org/10.1016/0016-7037\(93\)90035-U](https://doi.org/10.1016/0016-7037(93)90035-U)
- Ryan, J.N., Gschwend, P.M., 1992. Effect of iron diagenesis on the transport of colloidal clay in an unconfined sand aquifer. *Geochimica et Cosmochimica Acta* 56, 1507–1521. [https://doi.org/10.1016/0016-7037\(92\)90220-D](https://doi.org/10.1016/0016-7037(92)90220-D)
- Saeed, H., Hartland, A., Lehto, N.J., Baalousha, M., Sikder, M., Sandwell, D., ... & Hamilton, D.P., 2018. Regulation of phosphorus bioavailability by iron nanoparticles in a monomictic lake. *Scientific reports*, 8(1), 1-14.
- Salas, E.C., Berelson, W.M., Hammond, D.E., Kampf, A.R., Nealson, K.H., 2010. The impact of bacterial strain on the products of dissimilatory iron reduction. *Geochimica et Cosmochimica Acta* 74, 574–583. <https://doi.org/10.1016/j.gca.2009.10.039>
- Salim, R., Cooksey, B.G., 1981. The effect of centrifugation on the suspended particles of river waters. *Water Research* 15, 835–839. [https://doi.org/10.1016/0043-1354\(81\)90137-8](https://doi.org/10.1016/0043-1354(81)90137-8)
- Salm, S., Allen, D., Nester, E., Anderson, D., 2015. *Nester's Microbiology: A Human Perspective*. McGraw-Hill Higher Education.
- Salvador, D., Churro, C., & Valério, E., 2016. Evaluating the influence of light intensity in *mcyA* gene expression and microcystin production in toxic strains of *Planktothrix agardhii* and *Microcystis aeruginosa*. *Journal of microbiological methods*, 123, 4-12.
- Sato, S., Comerford, N.B., 2005. Influence of soil pH on inorganic phosphorus sorption and desorption in a humid brazilian Ultisol. *Revista Brasileira de Ciência do Solo* 29, 685–694. <https://doi.org/10.1590/S0100-06832005000500004>
- Scheinost, A.C., 2005. METAL OXIDES, in Hillel, D. (Ed.), *Encyclopedia of Soils in the Environment*. Elsevier, Oxford, pp. 428–438. <https://doi.org/10.1016/B0-12-348530-4/00194-6>
- Schindler, D.W., Carpenter, S.R., Chapra, S.C., Hecky, R.E., Orihel, D.M., 2016. Reducing Phosphorus to Curb Lake Eutrophication is a Success. *Environ. Sci. Technol.* 50, 8923–8929. <https://doi.org/10.1021/acs.est.6b02204>
- Schomakers, J., Zehetner, F., Mentler, A., Ottner, F., Mayer, H., 2015. Study of soil aggregate breakdown dynamics under low dispersive ultrasonic energies with sedimentation and X-ray attenuation. *Int Agrophys* 29, 501–508. <https://doi.org/10.1515/intag-2015-0057>
- Schönbrunner, I.M., Preiner, S., Hein, T., 2012. Impact of drying and re-flooding of sediment on phosphorus dynamics of river-floodplain systems. *Science of The Total Environment* 432, 329–337. <https://doi.org/10.1016/j.scitotenv.2012.06.025>

- Schröder, J.J., Smit, A.L., Cordell, D., Rosemarin, A., 2011. Improved phosphorus use efficiency in agriculture: a key requirement for its sustainable use. *Chemosphere* 84, 822–831. <https://doi.org/10.1016/j.chemosphere.2011.01.065>
- Seaman, J.C., Bertsch, P. M., & Strom, R.N., 1997. Characterization of colloids mobilized from southeastern coastal plain sediments. *Environmental science & technology*, 31(10), 2782–2790.
- Sen, T.K., Mahajan, S.P., Khilar, K.C., 2002. Colloid-Associated contaminant transport in porous media: 1. Experimental studies. *AIChE Journal* 48, 2366–2374. <https://doi.org/10.1002/aic.690481026>
- Sen, T. K., & Khilar, K. C., 2006. Review on subsurface colloids and colloid-associated contaminant transport in saturated porous media. *Advances in colloid and interface science*, 119(2-3), 71–96. <https://doi.org/10.1016/j.cis.2005.09.001>
- Senn, A.C., Kaegi, R., Hug, S.J., Hering, J.G., Mangold, S., Voegelin, A., 2015. Composition and structure of Fe(III)-precipitates formed by Fe(II) oxidation in water at near-neutral pH: Interdependent effects of phosphate, silicate and Ca. *Geochimica et Cosmochimica Acta* 162, 220–246. <https://doi.org/10.1016/j.gca.2015.04.032>
- Sepehrnia, N., Fishkis, O., Huwe, B., Bachmann, J.A., 2018. Natural colloid mobilization and leaching in wettable and water repellent soil under saturated condition. <https://doi.org/10.1515/johh-2017-0058>
- Séguaris, J.M., Klumpp, E., Vereecken, H., 2013. Colloidal properties and potential release of water-dispersible colloids in an agricultural soil depth profile. *Geoderma* 193–194, 94–101. <https://doi.org/10.1016/j.geoderma.2012.10.014>
- Shah, R.A., Achyuthan, H., Puthan-Veetil, R.-S., Derwaish, U., Rafiq, M., 2019. Sediment distribution pattern and environmental implications of physico-chemical characteristics of the Akkulam-Veli Lake, South India. *Appl Water Sci* 9, 188. <https://doi.org/10.1007/s13201-019-1054-1>
- Shand, C.A., Smith, S., Edwards, A.C., Fraser, A.R., 2000. Distribution of phosphorus in particulate, colloidal and molecular-sized fractions of soil solution. *Water Research* 34, 1278–1284.
- Shang, J., Flury, M., Chen, G., Zhuang, J., 2008. Impact of flow rate, water content, and capillary forces on in situ colloid mobilization during infiltration in unsaturated sediments. *Water Resources Research* 44. <https://doi.org/10.1029/2007WR006516>
- Shard, A.G., Sparnacci, K., Sikora, A., Wright, L., Bartczak, D., Goenaga-Infante, H., Minelli, C., 2018. Measuring the relative concentration of particle populations using differential centrifugal sedimentation. *Anal. Methods* 10, 2647–2657. <https://doi.org/10.1039/C8AY00491A>
- Shaw, D.J., 1992. 8 - Colloid stability, in: Shaw, D.J. (Ed.), *Introduction to Colloid and Surface Chemistry* (Fourth Edition). Butterworth-Heinemann, Oxford, pp. 210–243. <https://doi.org/10.1016/B978-0-08-050910-5.50012-8>
- Shchukin, E.D., Pertsov, A.V., Amelina, E.A., Zelenev, A.S., 2001. General Introduction, in: Shchukin, E.D., Pertsov, A.V., Amelina, E.A., Zelenev, A.S. (Eds.), *Studies in Interface Science, Colloid and Surface Chemistry*. Elsevier, pp. xii–xxvi. [https://doi.org/10.1016/S1383-7303\(01\)80002-8](https://doi.org/10.1016/S1383-7303(01)80002-8)
- Shen, J., Yuan, L., Zhang, J., Li, H., Bai, Z., Chen, X., Zhang, W., Zhang, F., 2011. Phosphorus Dynamics: From Soil to Plant. *Plant Physiol.* 156, 997. <https://doi.org/10.1104/pp.111.175232>
- Sheppard, R.Y., Milliken, R.E., Russell, J.M., Dyar, M.D., Sklute, E.C., Bijaksana, S., Melles, M., 2020. MINERAL AND CHEMICAL CHANGES IN A 100 M LONG SEDIMENT CORE FROM LAKE TOWUTI, INDONESIA AND IMPLICATIONS FOR MAFIC LACUSTRINE SEDIMENTS IN GALE CRATER, MARS. 2.
- Shirazi, S., Lin, C.J., & Chen, D., 2010. Inorganic fouling of pressure-driven membrane processes—A critical review. *Desalination*, 250(1), 236–248.

- Šimek, K., Horňák, K., Jezbera, J., Nedoma, J., Vrba, J., Straškrábová, V., Macek, M., Dolan, J.R., Hahn, M.W., 2006. Maximum growth rates and possible life strategies of different bacterioplankton groups in relation to phosphorus availability in a freshwater reservoir. *Environmental Microbiology* 8, 1613–1624. <https://doi.org/10.1111/j.1462-2920.2006.01053.x>
- Sinaj, S., Mächler, F., Frossard, E., Faisse, C., Oberson, A., Morel, C., 1998. Interference of colloidal particles in the determination of orthophosphate concentrations in soil water extracts. *Communications in Soil Science and Plant Analysis* 29, 1091–1105. <https://doi.org/10.1080/00103629809370011>
- Singleton, V.L., Little, J.C., 2006. Designing Hypolimnetic Aeration and Oxygenation Systems – A Review. *Environ. Sci. Technol.* 40, 7512–7520. <https://doi.org/10.1021/es060069s>
- Sivonen, K., 1990. Effects of light, temperature, nitrate, orthophosphate, and bacteria on growth of and hepatotoxin production by *Oscillatoria agardhii* strains. *Applied and environmental microbiology*, 56(9), 2658-2666.
- Smith, L., Watzin, M.C., Druschel, G., 2011. Relating sediment phosphorus mobility to seasonal and diel redox fluctuations at the sediment–water interface in a eutrophic freshwater lake. *Limnology and Oceanography* 56, 2251–2264. <https://doi.org/10.4319/lo.2011.56.6.2251>
- Smith, V.H., 2003. Eutrophication of freshwater and coastal marine ecosystems a global problem. *Environ Sci & Pollut Res* 10, 126–139. <https://doi.org/10.1065/espr2002.12.142>
- Smith, V.H., Schindler, D.W., 2009. Eutrophication science: where do we go from here? *Trends in Ecology & Evolution* 24, 201–207. <https://doi.org/10.1016/j.tree.2008.11.009>
- Smith, V.H., Tilman, G.D., Nekola, J.C., 1999. Eutrophication: impacts of excess nutrient inputs on freshwater, marine, and terrestrial ecosystems. *Environmental Pollution* 100, 179–196. [https://doi.org/10.1016/S0269-7491\(99\)00091-3](https://doi.org/10.1016/S0269-7491(99)00091-3)
- So, H.B., Cook, G.D., Raine, S.R., 1997. An examination of the end-over-end shaking technique for measuring soil dispersion. *Soil Res.* 35, 31–40. <https://doi.org/10.1071/s96062>
- Søndergaard, M., Jensen, J.P., Jeppesen, E., 2003. Role of sediment and internal loading of phosphorus in shallow lakes. *Hydrobiologia* 506, 135–145. <https://doi.org/10.1023/B:HYDR.0000008611.12704.dd>
- Southam, D.C., Lewis, T.W., McFarlane, A.J., Borrmann, T., Johnston, J.H., 2008. Calcium–phosphorus interactions at a nano-structured silicate surface. *Journal of Colloid and Interface Science* 319, 489–497. <https://doi.org/10.1016/j.jcis.2007.12.012>
- Speth, T.F., Gusses, A.M., & Summers, R.S., 2000. Evaluation of nanofiltration pretreatments for flux loss control. *Desalination*, 130(1), 31-44.
- Steiner, Z., Lazar, B., Reimers, C.E., Erez, J., 2019. Carbonates dissolution and precipitation in hemipelagic sediments overlaid by supersaturated bottom-waters – Gulf of Aqaba, Red Sea. *Geochimica et Cosmochimica Acta* 246, 565–580. <https://doi.org/10.1016/j.gca.2018.12.007>
- Stolpe, B., Guo, L., Shiller, A. M., & Aiken, G. R., 2013. Abundance, size distributions and trace-element binding of organic and iron-rich nanocolloids in Alaskan rivers, as revealed by field-flow fractionation and ICP-MS. *Geochimica et Cosmochimica Acta*, 105, 221-239.
- Stumm, W., 1993. Aquatic colloids as chemical reactants: surface structure and reactivity, in: *Colloids in the Aquatic Environment*. Elsevier, pp. 1–18.
- Stumm, W., Morgan, J.J., 1995. *Aquatic Chemistry: Chemical Equilibria and Rates in Natural Waters*, 3rd Edition [WWW Document]. Wiley.com. URL <https://www.wiley.com/en-us/Aquatic+Chemistry%3A+Chemical+Equilibria+and+Rates+in+Natural+Waters%2C+3rd+Edition-p-9780471511854> (accessed 2.6.19).
- Sun, D., Bi, Q., Li, K., Zhu, J., Zhang, Q., Jin, C., Lu, L., Lin, X., 2018. Effect of Soil Drying Intensity During an Experimental Drying-Rewetting Event on Nutrient Transformation and Microbial

- Community Composition. *Pedosphere* 28, 644–655. [https://doi.org/10.1016/S1002-0160\(17\)60450-8](https://doi.org/10.1016/S1002-0160(17)60450-8)
- Sun, X.J., Qin, B.Q., Zhu, G.W., Zhang, Z.P., Gao, Y.X., 2007. [Release of colloidal N and P from sediment of lake caused by continuing hydrodynamic disturbance]. *Huan Jing Ke Xue* 28, 1223–1229.
- SurrIDGE, B.W.J., Heathwaite, A.L., Baird, A.J., 2007. The Release of Phosphorus to Porewater and Surface Water from River Riparian Sediments. *Journal of Environment Quality* 36, 1534. <https://doi.org/10.2134/jeq2006.0490>
- Suter, Daniel., Banwart, Steven., Stumm, Werner., 1991. Dissolution of hydrous iron(III) oxides by reductive mechanisms. *Langmuir* 7, 809–813. <https://doi.org/10.1021/la00052a033>
- Taguchi, V.J., Olsen, T.A., Natarajan, P., Janke, B.D., Gulliver, J.S., Finlay, J.C., Stefan, H.G., 2020. Internal loading in stormwater ponds as a phosphorus source to downstream waters. *Limnology and Oceanography Letters* n/a. <https://doi.org/10.1002/lol2.10155>
- Tajana P., 2016. Charging Behavior of Clays and Clay Minerals in Aqueous Electrolyte Solutions — Experimental Methods for Measuring the Charge and Interpreting the Results, in: Ahmed Abdelmonem (Ed.), *Clays, Clay Minerals and Ceramic Materials Based on Clay Minerals*. IntechOpen, Rijeka, p. Ch. 3. <https://doi.org/10.5772/62082>
- Tang, C.Y., Chong, T.H., Fane, A.G., 2011. Colloidal interactions and fouling of NF and RO membranes: A review. *Advances in Colloid and Interface Science* 164, 126–143. <https://doi.org/10.1016/j.cis.2010.10.007>
- Tang, Q., Collins, A.L., Wen, A., He, X., Bao, Y., Yan, D., Long, Y., Zhang, Y., 2018. Particle size differentiation explains flow regulation controls on sediment sorting in the water-level fluctuation zone of the Three Gorges Reservoir, China. *Science of The Total Environment* 633, 1114–1125. <https://doi.org/10.1016/j.scitotenv.2018.03.258>
- Tang, X., Wu, M., Li, R., 2018a. Distribution, sedimentation, and bioavailability of particulate phosphorus in the mainstream of the Three Gorges Reservoir. *Water Research* 140, 44–55. <https://doi.org/10.1016/j.watres.2018.04.024>
- Tang, X., Wu, M., Li, R., 2018b. Phosphorus distribution and bioavailability dynamics in the mainstream water and surface sediment of the Three Gorges Reservoir between 2003 and 2010. *Water Research* 145, 321–331. <https://doi.org/10.1016/j.watres.2018.08.041>
- Taylor, K.G., Hudson-Edwards, K.A., Bennett, A.J., Vishnyakov, V., 2008. Early diagenetic vivianite [Fe₃(PO₄)₂ · 8H₂O] in a contaminated freshwater sediment and insights into zinc uptake: A μ -EXAFS, μ -XANES and Raman study. *Applied Geochemistry* 23, 1623–1633. <https://doi.org/10.1016/j.apgeochem.2008.01.009>
- Teja, A.S., Koh, P.Y., 2009. Synthesis, properties, and applications of magnetic iron oxide nanoparticles. *Progress in Crystal Growth and Characterization of Materials* 55, 22–45. <https://doi.org/10.1016/j.pcrysgrow.2008.08.003>
- Teodoru, C., Wehrli, B., 2005. Retention of Sediments and Nutrients in the Iron Gate I Reservoir on the Danube River. *Biogeochemistry* 76, 539–565. <https://doi.org/10.1007/s10533-005-0230-6>
- Thurman, E.M., 2012. *Organic geochemistry of natural waters*. Springer Science & Business Media.
- Thurman, E.M., 1985. *Organic geochemistry of natural waters*. Springer Science & Business Media.
- Tipping, E., 2002. *Cation Binding by Humic Substances* by Edward Tipping [WWW Document]. Cambridge Core. <https://doi.org/10.1017/CBO9780511535598>
- Tipping, E., Berggren, D., Mulder, J., Woof, C., 1995. Modelling the solid–solution distributions of protons, aluminium, base cations and humic substances in acid soils. *European Journal of Soil Science* 46, 77–94. <https://doi.org/10.1111/j.1365-2389.1995.tb01814.x>

- Tipping, E., Heaton, M.J., 1983. The adsorption of aquatic humic substances by two oxides of manganese. *Geochimica et Cosmochimica Acta* 47, 1393–1397. [https://doi.org/10.1016/0016-7037\(83\)90297-1](https://doi.org/10.1016/0016-7037(83)90297-1)
- Toner, J.D., Catling, D.C., 2020. A carbonate-rich lake solution to the phosphate problem of the origin of life. *PNAS* 117, 883–888. <https://doi.org/10.1073/pnas.1916109117>
- Tran, E., Klein Ben-David, O., Teutch, N., Weisbrod, N., 2016. Influence of heteroaggregation processes between intrinsic colloids and carrier colloids on cerium(III) mobility through fractured carbonate rocks. *Water Research* 100, 88–97. <https://doi.org/10.1016/j.watres.2016.04.075>
- Tran, E.L., Teutsch, N., Klein-BenDavid, O., Weisbrod, N., 2018. Uranium and Cesium sorption to bentonite colloids under carbonate-rich environments: Implications for radionuclide transport. *Science of The Total Environment* 643, 260–269. <https://doi.org/10.1016/j.scitotenv.2018.06.162>
- Trichet, J., Krajewski, K.P., Cappellen, P.V., 1994. Biological processes and apatite formation in sedimentary environments. <https://doi.org/10.5169/SEALS-167475>
- Tromp, T.K., Van Cappellen, P., Key, R.M., 1995. A global model for the early diagenesis of organic carbon and organic phosphorus in marine sediments. *Geochimica et Cosmochimica Acta* 59, 1259–1284. [https://doi.org/10.1016/0016-7037\(95\)00042-X](https://doi.org/10.1016/0016-7037(95)00042-X)
- Tsezos, M., Bell, J.P., 1989. Comparison of the biosorption and desorption of hazardous organic pollutants by live and dead biomass. *Water Research* 23, 561–568. [https://doi.org/10.1016/0043-1354\(89\)90022-5](https://doi.org/10.1016/0043-1354(89)90022-5)
- Tulve, N.S., Young, T.C., 1999. Isolation and Characterization of the Natural Colloidal Material From the Fox River. *Lake and Reservoir Management* 15, 231–238. <https://doi.org/10.1080/07438149909354120>
- Turner, B.L., Kay, M.A., Westermann, D.T., 2004. Colloidal phosphorus in surface runoff and water extracts from semiarid soils of the western United States. *J. Environ. Qual.* 33, 1464–1472.
- Ulén, B., & Snäll, S. (2007). Forms and retention of phosphorus in an illite-clay soil profile with a history of fertilisation with pig manure and mineral fertilisers. *Geoderma*, 137(3-4), 455-465.
- Urrutia, O., Erro, J., Guardado, I., Francisco, S.S., Mandado, M., Baigorri, R., Yvin, J.C., Garcia-Mina, J.M., 2014. Physico-chemical characterization of humic-metal-phosphate complexes and their potential application to the manufacture of new types of phosphate-based fertilizers. *Journal of Plant Nutrition and Soil Science* 177, 128–136. <https://doi.org/10.1002/jpln.201200651>
- Usman, A., Kuzyakov, Y., Stahr, K., 2005. Effect of clay minerals on immobilization of heavy metals and microbial activity in a sewage sludge-contaminated soil. *Journal of Soils and Sediments* 5, 245–252. <https://doi.org/10.1065/jss2005.05.141>
- USEPA, 1993. Method 365.1: Determination of phosphorus by semi-automated colorimetry. *Methods for chemical analysis of water and wastes. Revision 2.*
- US EPA, 2004. Method 9045D (SW-846). Soil and waste pH. US Environmental Protection Agency, epa.gov, 9045, 1-5.
- US EPA, 2007. Method 3015A (SW-846). Microwave Assisted Acid Digestion of Aqueous Samples and Extracts. *Revision, 1*, 25.
- Valipour, R., Boegman, L., Bouffard, D., Rao, Y.R., 2017. Sediment resuspension mechanisms and their contributions to high-turbidity events in a large lake. *Limnology and Oceanography* 62, 1045–1065. <https://doi.org/10.1002/lno.10485>
- Van Cappellen, P., Maavara, T., 2016. Rivers in the Anthropocene: Global scale modifications of riverine nutrient fluxes by damming. *Ecology & Hydrobiology, New Challenges and*

- Van Moorleghem, C., De Schutter, N., Smolders, E., Merckx, R., 2013. The bioavailability of colloidal and dissolved organic phosphorus to the alga *Pseudokirchneriella subcapitata* in relation to analytical phosphorus measurements. *Hydrobiologia* 709, 41–53. <https://doi.org/10.1007/s10750-013-1442-8>
- Van Riemsdijk, W.H., Weng, L., Hiemstra, T., 2007. Ion - Colloid - Colloid Interactions, in: Frimmel, F.H., Von Der Kammer, F., Flemming, H.-C. (Eds.), *Colloidal Transport in Porous Media*. Springer, Berlin, Heidelberg, pp. 205–249. https://doi.org/10.1007/978-3-540-71339-5_8
- VandeVoort, A.R., Livi, K.J., Arai, Y., 2013. Reaction conditions control soil colloid facilitated phosphorus release in agricultural Ultisols. *Geoderma* 206, 101–111. <https://doi.org/10.1016/j.geoderma.2013.04.024>
- Varga, G., Gresina, F., Újvári, G., Kovács, J., Szalai, Z., 2019. On the reliability and comparability of laser diffraction grain size measurements of paleosols in loess records. *Sedimentary Geology* 389, 42–53. <https://doi.org/10.1016/j.sedgeo.2019.05.011>
- Varol, M., 2020. Spatio-temporal changes in surface water quality and sediment phosphorus content of a large reservoir in Turkey. *Environmental Pollution* 259, 113860. <https://doi.org/10.1016/j.envpol.2019.113860>
- Vauthier, C., Cabane, B., & Labarre, D., 2008. How to concentrate nanoparticles and avoid aggregation?. *European Journal of Pharmaceutics and Biopharmaceutics*, 69(2), 466-475.
- Verwey, E.J.W., & Overbeek, J.T.G., 1955. Theory of the stability of lyophobic colloids. *Journal of Colloid Science*, 10(2), 224-225.
- Vörösmarty, C.J., Meybeck, M., Fekete, B., Sharma, K., Green, P., Syvitski, J.P.M., 2003. Anthropogenic sediment retention: major global impact from registered river impoundments. *Global and Planetary Change, The supply of flux of sediment along hydrological pathways: Anthropogenic influences at the global scale* 39, 169–190. [https://doi.org/10.1016/S0921-8181\(03\)00023-7](https://doi.org/10.1016/S0921-8181(03)00023-7)
- Vuillemin, A., Friese, A., Wirth, R., Schuessler, J.A., Schleicher, A.M., Kemnitz, H., ... & Kallmeyer, J., 2020. Vivianite formation in ferruginous sediments from Lake Towuti, Indonesia. *Biogeosciences*, 17, 1955-1973.
- Wan, J., Yuan, X., Han, L., Ye, H., Yang, X., 2020. Characteristics and Distribution of Organic Phosphorus Fractions in the Surface Sediments of the Inflow Rivers around Hongze Lake, China. *Int J Environ Res Public Health* 17. <https://doi.org/10.3390/ijerph17020648>
- Wan, J., & Wilson, J.L., 1994. Colloid transport in unsaturated porous media. *Water Resources Research*, 30(4), 857-864.
- Wang, C., Feng, B., Tian, C., Tian, Y., Chen, D., Wu, X., Li, G., Xiao, B., 2018. Quantitative study on the survivability of *Microcystis* colonies in lake sediments. *Journal of Applied Phycology* 30, 495–506. <https://doi.org/10.1007/s10811-017-1246-8>
- Wang, H., Adeleye, A.S., Huang, Y., Li, F., Keller, A.A., 2015. Heteroaggregation of nanoparticles with biocolloids and geocolloids. *Advances in Colloid and Interface Science, Colloid and Polymer Interfaces in Bio-resources and Environments* 226, 24–36. <https://doi.org/10.1016/j.cis.2015.07.002>
- Wang, H.W., Kondolf, M., Tullos, D., Kuo, W.C., 2018. Sediment Management in Taiwan's Reservoirs and Barriers to Implementation. *Water* 10, 1034. <https://doi.org/10.3390/w10081034>
- Wang, W.X., Guo, L., 2000. Bioavailability of colloid-bound Cd, Cr, and Zn to marine plankton. *Marine Ecology Progress Series* 202, 41–49.

- Wang, X., Zhou, J., Wu, Yanhong, Bol, R., Wu, Yong, Sun, H., Bing, H., 2020. Fine sediment particle microscopic characteristics, bioavailable phosphorus and environmental effects in the world largest reservoir. *Environmental Pollution* 114917. <https://doi.org/10.1016/j.envpol.2020.114917>
- Wang, Y., Li, K., Liang, R., Han, S., Li, Y., 2019. Distribution and Release Characteristics of Phosphorus in a Reservoir in Southwest China. *International Journal of Environmental Research and Public Health* 16, 303. <https://doi.org/10.3390/ijerph16030303>
- Wang, Y., Shen, Z., Niu, J., Liu, R., 2009. Adsorption of phosphorus on sediments from the Three-Gorges Reservoir (China) and the relation with sediment compositions. *Journal of Hazardous Materials* 162, 92–98. <https://doi.org/10.1016/j.jhazmat.2008.05.013>
- Weber, J., Chen, Y., Jamroz, E., Miano, T., 2018. Preface: humic substances in the environment. *J Soils Sediments* 18, 2665–2667. <https://doi.org/10.1007/s11368-018-2052-x>
- Weißbecker, C., Buscot, F., & Wubet, T., 2017. Preservation of nucleic acids by freeze-drying for next generation sequencing analyses of soil microbial communities. *Journal of Plant Ecology*, 10(1), 81-90.
- Weisbrod, N., Tran, E., Cohen, M., Zvikelsky, O., Tang, X., 2018. Colloid and colloid-facilitated transport in fractured rocks 20, 2224.
- Welch, E.B., Cooke, G.D., 2005. Internal Phosphorus Loading in Shallow Lakes: Importance and Control. *Lake and Reservoir Management* 21, 209–217. <https://doi.org/10.1080/07438140509354430>
- Wen, S., Wang, H., Wu, T., Yang, J., Jiang, X., Zhong, J., 2020. Vertical profiles of phosphorus fractions in the sediment in a chain of reservoirs in North China: Implications for pollution source, bioavailability, and eutrophication. *Science of The Total Environment* 704, 135318. <https://doi.org/10.1016/j.scitotenv.2019.135318>
- White, A.K., Metcalf, W.W., 2007. Microbial Metabolism of Reduced Phosphorus Compounds. *Annual Review of Microbiology* 61, 379–400. <https://doi.org/10.1146/annurev.micro.61.080706.093357>
- Wikiniyadhane, R., Chotpanarat, S., Ong, S.K., 2015. Effects of kaolinite colloids on Cd²⁺ transport through saturated sand under varying ionic strength conditions: Column experiments and modeling approaches. *Journal of Contaminant Hydrology* 182, 146–156. <https://doi.org/10.1016/j.jconhyd.2015.08.008>
- Wildi, W., Dominik, J., Loizeau, J.L., Thomas, R.L., Favarger, P.-Y., Haller, L., Perroud, A., Peytremann, C., 2004. River, reservoir and lake sediment contamination by heavy metals downstream from urban areas of Switzerland. *Lakes and Reservoirs: Research and Management* 9, 75–87. <https://doi.org/10.1111/j.1440-1770.2004.00236.x>
- Wilkinson, K.J., Lead, J.R., 2007. *Environmental Colloids and Particles: Behaviour, Separation and Characterisation*. John Wiley & Sons.
- Willard, L.L., 1979. *Chemical equilibria in soils*. Chichester, UK: John Wiley & Sons.
- Wilson, M.J., 2004. Weathering of the primary rock-forming minerals: processes, products and rates. *Clay Minerals* 39, 233–266. <https://doi.org/10.1180/0009855043930133>
- Wolthoorn, A., Temminghoff, E.J.M., Weng, L., van Riemsdijk, W.H., 2004. Colloid formation in groundwater: effect of phosphate, manganese, silicate and dissolved organic matter on the dynamic heterogeneous oxidation of ferrous iron. *Applied Geochemistry* 19, 611–622. <https://doi.org/10.1016/j.apgeochem.2003.08.003>
- Worsfold, P., McKelvie, I., Monbet, P., 2016. Determination of phosphorus in natural waters: A historical review. *Analytica Chimica Acta* 918, 8–20. <https://doi.org/10.1016/j.aca.2016.02.047>

- Woszczyk, M., 2016. Precipitation of calcium carbonate in a shallow polymictic coastal lake: Assessing the role of primary production, organic matter degradation and sediment mixing. *Oceanological and Hydrobiological Studies*, 45(1), 86.
- Wu, H., Chen, J., Xu, J., Zeng, G., Sang, L., Liu, Q., Yin, Z., Dai, J., Yin, D., Liang, J., Ye, S., 2019. Effects of dam construction on biodiversity: A review. *Journal of Cleaner Production* 221, 480–489. <https://doi.org/10.1016/j.jclepro.2019.03.001>
- Wu, H., Lin, Y., Wu, J., Zeng, L., Zeng, D., Du, J., 2008. Surface Adsorption of Iron Oxide Minerals for Phenol and Dissolved Organic Matter. *Earth Science Frontiers* 15, 133–141. [https://doi.org/10.1016/S1872-5791\(09\)60013-0](https://doi.org/10.1016/S1872-5791(09)60013-0)
- Wu, Y., Ma, H. L., & Peng, Y. Z., 2018. Effects of storage temperature and time on the contents of different nitrogen forms in fresh soil samples. *Ying yong sheng tai xue bao= The journal of applied ecology*, 29(6), 1999–2006.
- Xie, M., Wang, N., Gaillard, J.-F., Packman, A.I., 2018. Interplay between flow and bioturbation enhances metal efflux from low-permeability sediments. *Journal of Hazardous Materials* 341, 304–312. <https://doi.org/10.1016/j.jhazmat.2017.08.002>
- Xu, D., Ding, S., Li, B., Jia, F., He, X., Zhang, C., 2012. Characterization and optimization of the preparation procedure for solution P-31 NMR analysis of organic phosphorus in sediments. *J Soils Sediments* 12, 909–920. <https://doi.org/10.1007/s11368-012-0510-4>
- Xu, H., Ji, L., Kong, M., Xu, M., Lv, X., 2019. Abundance, chemical composition and lead adsorption properties of sedimentary colloids in a eutrophic shallow lake. *Chemosphere* 218, 534–539. <https://doi.org/10.1016/j.chemosphere.2018.11.147>
- Xu, H., Xu, M., Li, Y., Liu, X., Guo, L., Jiang, H., 2018. Characterization, origin and aggregation behavior of colloids in eutrophic shallow lake. *Water Research* 142, 176–186. <https://doi.org/10.1016/j.watres.2018.05.059>
- Xu, H., Yang, C., Jiang, H., 2016. Aggregation kinetics of inorganic colloids in eutrophic shallow lakes: Influence of cyanobacterial extracellular polymeric substances and electrolyte cations. *Water Research* 106, 344–351. <https://doi.org/10.1016/j.watres.2016.10.023>
- Xu, K., Milliman, J.D., 2009. Seasonal variations of sediment discharge from the Yangtze River before and after impoundment of the Three Gorges Dam. *Geomorphology* 104, 276–283. <https://doi.org/10.1016/j.geomorph.2008.09.004>
- Yan, J., Lazouskaya, V., Jin, Y., 2016. Soil Colloid Release Affected by Dissolved Organic Matter and Redox Conditions. *Vadose Zone Journal* 15, 0. <https://doi.org/10.2136/vzj2015.02.0026>
- Yan, J., Manelski, R., Vasilas, B., Jin, Y., 2018. Mobile Colloidal Organic Carbon: An Underestimated Carbon Pool in Global Carbon Cycles? *Front. Environ. Sci.* 6. <https://doi.org/10.3389/fenvs.2018.00148>
- Yan, J., Meng, X., Jin, Y., 2017. Size-Dependent Turbidimetric Quantification of Suspended Soil Colloids. *Vadose Zone Journal* 16, 0. <https://doi.org/10.2136/vzj2016.10.0098>
- Yang, S.L., Milliman, J.D., Xu, K.H., Deng, B., Zhang, X.Y., Luo, X.X., 2014. Downstream sedimentary and geomorphic impacts of the Three Gorges Dam on the Yangtze River. *Earth-Science Reviews* 138, 469–486. <https://doi.org/10.1016/j.earscirev.2014.07.006>
- Yang, X., Wu, X., Hao, H., He, Z., 2008. Mechanisms and assessment of water eutrophication. *J Zhejiang Univ Sci B* 9, 197–209. <https://doi.org/10.1631/jzus.B0710626>
- Yang, Y., Wen, B., Wang, C., Hou, Y., 2019. Two-dimensional velocity distribution modeling for natural river based on UHF radar surface current. *Journal of Hydrology* 577, 123930. <https://doi.org/10.1016/j.jhydrol.2019.123930>

- Yang, Y., Yang, J., Zhang, X., 2018. A qPCR method to quantify bioavailable phosphorus using indigenous aquatic species. *Environmental Sciences Europe* 30, 32. <https://doi.org/10.1186/s12302-018-0163-z>
- Yuan, S., Tang, H., Xiao, Y., Chen, X., Xia, Y., & Jiang, Z., 2018. Spatial variability of phosphorus adsorption in surface sediment at channel confluences: Field and laboratory experimental evidence. *Journal of Hydro-Environment Research*, 18, 25-36.
- Kaczmarek Z., Kindler J., 1982. *The Operation of Multiple Reservoir Systems. The Operation of Multiple Reservoir Systems.*
- Zaenker, H., Arnold, T., Huettig, G., Bernhard, G., Nitsche, H., 2005. Formation of colloids by the weathering of rock material. Presented at the MIGRATION 2005, 10 international conference on chemistry and migration behaviour of actinides and fission products in the geosphere, France.
- Zang, L., Tian, G.M., Liang, X.Q., He, M.M., Bao, Q.B., Yao, J.H., 2013. Profile Distributions of Dissolved and Colloidal Phosphorus as Affected by Degree of Phosphorus Saturation in Paddy Soil. *Pedosphere* 23, 128–136. [https://doi.org/10.1016/S1002-0160\(12\)60088-5](https://doi.org/10.1016/S1002-0160(12)60088-5)
- Zänker, H., Hennig, C., 2014. Colloid-borne forms of tetravalent actinides: A brief review. *Journal of Contaminant Hydrology* 157, 87–105. <https://doi.org/10.1016/j.jconhyd.2013.11.004>
- Zänker, H., Hüttig, G., Arnold, T., Nitsche, H., 2006. Formation of iron-containing colloids by the weathering of phyllite. *Aquat Geochem* 12, 299–325. <https://doi.org/10.1007/s10498-006-9000-x>
- Zarfl, C., Lucía, A., 2018. The connectivity between soil erosion and sediment entrapment in reservoirs. *Current Opinion in Environmental Science & Health, Sustainable soil management and land restoration* 5, 53–59. <https://doi.org/10.1016/j.coesh.2018.05.001>
- Zarfl, C., Lumsdon, A.E., Berlekamp, J., Tydecks, L., Tockner, K., 2014. A global boom in hydropower dam construction. *Aquatic Sciences* 77, 161–170. <https://doi.org/10.1007/s00027-014-0377-0>
- Zhang, B., Fang, F., Guo, J., Chen, Y., Li, Z., Guo, S., 2012. Phosphorus fractions and phosphate sorption-release characteristics relevant to the soil composition of water-level-fluctuating zone of Three Gorges Reservoir. *Ecological Engineering* 40, 153–159. <https://doi.org/10.1016/j.ecoleng.2011.12.024>
- Zhang, S., Wang, S., Shan, X., 2001. Effect of sample pretreatment upon the metal speciation in sediments by a sequential extraction procedure. *Chemical Speciation & Bioavailability* 13, 69–74. <https://doi.org/10.3184/095422901782775435>
- Zhang, Siliang, Yi, Q., Buyang, S., Cui, H., Zhang, Shiwen, 2020. Enrichment of bioavailable phosphorus in fine particles when sediment resuspension hinders the ecological restoration of shallow eutrophic lakes. *Science of The Total Environment* 710, 135672. <https://doi.org/10.1016/j.scitotenv.2019.135672>
- Zhang, Siliang, Yi, Q., Buyang, S., Cui, H., Zhang, Shiwen, 2019. Enrichment of bioavailable phosphorus in fine particles when sediment resuspension hinders the ecological restoration of shallow eutrophic lakes. *Science of The Total Environment* 135672. <https://doi.org/10.1016/j.scitotenv.2019.135672>
- Zhang, W., Zhu, X., Jin, X., Meng, X., Tang, W., Shan, B., 2017. Evidence for organic phosphorus activation and transformation at the sediment–water interface during plant debris decomposition. *Science of The Total Environment* 583, 458–465. <https://doi.org/10.1016/j.scitotenv.2017.01.103>
- Zhao, L., Shangguan, Y., Yao, N., Sun, Z., Ma, J., Hou, H., 2020. Soil migration of antimony and arsenic facilitated by colloids in lysimeter studies. *Science of The Total Environment* 728, 138874. <https://doi.org/10.1016/j.scitotenv.2020.138874>

- Kirk, Z.C, Bradley N.S., 1995. Long-Term Simulation of Fine-Grained Sediment Transport in Large Reservoir. *Journal of Hydraulic Engineering* 121, 773–781. [https://doi.org/10.1061/\(ASCE\)0733-9429\(1995\)121:11\(773\)](https://doi.org/10.1061/(ASCE)0733-9429(1995)121:11(773))
- Zirkler, D., Lang, F., Kaupenjohann, M., 2012. “Lost in filtration”—The separation of soil colloids from larger particles. *Colloids and Surfaces A: Physicochemical and Engineering Aspects* 399, 35–40. <https://doi.org/10.1016/j.colsurfa.2012.02.021>

Hybrid silica gel as a new tool for testing the bioavailability of colloidal P for phytoplankton uptake.

I. Introduction

Phosphorus is one of the restrictive elements in the primary productivity of terrestrial aquatic environment and is considered as the main contributor in freshwater eutrophication (Cavalcante et al., 2018). Both transfer of P along the land-water continuum as well as the release of P from accumulated sediments may contribute to the increase of P concentration in aquatic systems (river, lakes). It has been commonly known that the orthophosphates are directly available form of P for plankton to uptake (Boström et al., 1988) and that the rate of orthophosphate release from soil/sediment varies depending on P sources (organic, mineral) and operating mechanisms involved (desorption, mineral dissolution, organic matter degradation). However, the supply in orthophosphate in an aquatic system is often accompanied by simultaneous supply in colloidal P (Filella et al., 2006; Gu, 2017). Therefore, better knowledge of the bioavailability of colloidal P is necessary. Especially the evaluation of the bioavailability of sedimentary P-colloids that are easily mobilizable during mechanical disturbance or redox changes (Henderson et al., 2012; Schroeder et al., 2019) because the release of sedimentary colloids may be a critical factor controlling (bioavailable) P load to surface freshwater. It has been shown that nano colloids significantly affect the bioavailability of P and facilitate P transport in the environment (Saeed et al., 2018; Gottseling et al., 2017; Montalvo et al., 2015; Ekholm and Krogerus, 2003) and there is not the link between biologically available P and chemically reactive P (Ekholm and Krogerus, 2003).

The assessment of P bioavailability is often based on the duration of experimentations and/or on the reconstruction of the conditions observed in natural environment. For example, the evaluation of the bioavailability of particulate P for algae is mostly done in long-term laboratory studies in liquid medium (several weeks), meanwhile for colloidal P it consists mainly in short-term experimentations in liquid medium (Baken et al., 2014; Van Moorlegheem et al., 2013). Thus, the obtained results are different according to various studies. For instance, Ellison and Brett, (2006) found that 17-26 % of particulate P (sized between 8 and 180 μm) are bioavailable for algae *Pseudokirchneriella subcapitata* during a fourteen-day experiment, whereas Ekholm and Krogerus, (2003) identified a various degree of P bioavailability: from 3.4 to 89% depending of the P sources (minimum for the lake bottom sediments and soils, then river water and the highest for wastewater and urban water) and depending on the duration of the bioassay. In contrast, the determination of bioavailability of colloidal P is often carried out in a less than 14-day tests however, the bioavailability of colloidal P was mainly tested on synthetic colloidal materials (Baken et al., 2014; Van Moorlegheem et al., 2013). It was shown that synthetic colloids composed of ferrihydrite and organic matter and characterized by a molar Fe/P ratio of 1 and 178 induced a high response of algal growth rate that is comparable with the growth rate at the medium containing 5 $\mu\text{mol/L}$ orthophosphates (Van Moorlegheem et al., 2013). Using similar synthetic colloids but at lower Fe/P ratio of 0.02-0.17 Baken et al., (2014) demonstrated that the phosphate adsorbed on colloids was not available for algae. These few and contrasting results are not sufficient to conclude the contribution of colloidal P to algal uptake and therefore, highlight the need for further investigation.

The colloidal P is generally neglected in the assessment of total bioavailable P. Though, their dominant appearance in various environment (water, soil, sediment) as well as their ability to transport P, they may contribute to important part in algal uptake (Zhang et al., 2019). Colloidal P can be available either through direct uptake of P (Saeed et al., 2018), through P desorption by competition mechanism such as

with hydroxyl in response to increase in pH (Sato and Comerford, 2005) and through colloids dissolution (for example dissolution of Fe-colloids (Reynolds and Davies, 2001; Litchman and Nguyen, 2008, Van Moorleghe et al., 2013). In the study of Saeed et al., (2018), the elevated chlorophyll level was found to be adjacent with the presence of nano-colloidal P in hypolimnion of monomictic lake.

Assessing the bioavailability of colloids for microorganism (bacteria and algae) is not easy task. The culture medium used in the laboratory for the cultivation of microorganisms must provide all the necessary nutrients required for cell growth and maintain the optimal condition to assure their growth. It is also necessary to assure sterilized condition to avoid external contamination. The growth of microorganisms under laboratory conditions is commonly observed in the liquid medium or in Petri dishes. However, the assessment of the bioavailability of colloids using a liquid medium is not promising due of the flocculation of colloids (together with microorganisms) which on the one hand decrease colloids reactivity and on the other hand probably lead to the death of microorganisms. The assessment of the bioavailability of colloids for microorganisms cannot be carried out an agar-based solid medium, due to uncontrolled impurities contained in the solidifying agent. Agar consists of various organic polymers derived from marine algae and the growth of microorganisms on the surface of the gel has often been affected by the impurities contained in gelling agent. Thus, one of the challenges for scientists interested in the complex interactions between microorganisms and colloids in natural environment and to evaluate the bioavailability of colloids for microbial uptake is to propose the effective solutions to contouring methodological problems such as flocculation of colloids in the culture medium, adsorption of colloids to the microorganisms as well as difficulty in controlling growth of microorganisms on agar-based Petri-dishes. Immobilisation of colloids in an inorganic porous material (silica gel) could provide a solution for contouring many operational problems. Sol-gel technique permit to prepare porous, biologically friendly, mechanically and chemically inert, impurity free, inorganic silica gel (Grybos et al., 2011).

The objective of this study was to to develop silica gel doped with natural P-colloids extracted from bottom sediment of Champsanglard dam reservoir and to test this hybrid materials as a new technique for the assessment of colloids bioavailability. In order to evaluate the potential of colloidal P to support algal and cyanobacteria uptake and growth, the two strains: cyanobacteria *Microcystis aeruginosa* and green algae *Chlorella vulgaris* were chosen for the cultivation under controlled condition in laboratory. The tests were conducted in the manner to (i) check a potential toxicity of the hybrid silica gel (HSG) for both microorganisms, to evaluate spontaneous release of P from HSG in used culture medium, and to evaluate the bioavailability of colloids immobilized in HSG for both microorganisms. The biotests were conducted in the culture medium (i) containing dissolved P (inorganic phosphates), (ii) exempt dissolved P, (iii) exempt dissolved P but containing HSG, (iv) containing dissolved P and HSG. One test was conducted abiotically in the culture medium exempt of dissolved P and containing HSG.

II. Biotest for algal uptake of colloidal P

II.1 Preparation of colloidal suspension for embedding in silica gel

Colloids were extracted from the sediment collected at site 4 on May 2018 using successive filtrations (at 2.7 μm and 1 μm , WVR glass fiber) of a 24-h agitated sediment suspension (wet S/L of 1/10). The extracted colloid suspension was concentrated by evaporation in ventilated oven at 40°C at a 2.4 concentration factor to reach P concentrations of $190 \pm 5 \mu\text{g P/L}$ ($10.2 \pm 0.2 \mu\text{g P/g}_{\text{DW-Sed}}$) for large colloidal P and $650 \pm 20 \mu\text{g P/L}$ ($35.4 \pm 1.0 \mu\text{g P/g}_{\text{DW-Sed}}$) for dissolved P. The concentration of large colloidal P was determined as the differences between total P and dissolved P in fraction below than 1

μm . The concentrations of total P and dissolved P was measured using kit HACH LANGE LCK 349 with and without hydrolysis, respectively.

II.2. Hybrid silica gel (HSG)

The concentrated colloidal suspension ($2.4 \text{ mg}_{\text{DW-Colloid}}/\text{g}_{\text{DW-Sed}}$) was embedded within the silica gel, using a sol-gel technique and tetraethylorthosilicate (TEOS 99,99%, ACROS Organics) as precursor. The silica sol was prepared by sonication under acidic condition to complete TEOS hydrolysis. Before colloids incorporation, the pH of silica sol was increased to about 4 using NaOH (0.1 N) to avoid colloids dissolution, and then to about 5 to accelerate self-condensation and sol-gel transition. Hybrid silica sol was distributed in 2 ml sterile microplate (Thermo Fisher) and left 1 h at room temperature for gelation. The capsules of hybrid silica gels were then sterilized at 121°C by 10-min autoclaving in UPW, rinsed twice and stored at 4°C in sterilized UPW until experimentation. This procedure produces finely grained, homogenous hybrid silica gel (Grybos et al., 2010; Grybos et al., 2011).

The concentration of colloidal P in one capsule of HSG is approximately $30 \mu\text{g P/L}$ per unit of HSG.

II.3. Microorganismes, culture medium and incubation

The green algae *Chlorella vulgaris* CCAP 211/11B and cyanobacteria *Microcystis aeruginosa* PMC 728-11 strains were selected for this study for their rapid growth in synthetic culture medium and their presence in natural aquatic environment. Both strains were supplied by the National Museum of Natural History and Culture collection of algae and protozoa and were non-axenic. Prior to the incubations both strains were cultured separately in modified Z8 medium (Kotai, 1972) at 23°C and light intensity of $20 \mu\text{mol.photon.m}^{-2}.\text{s}^{-1}$ for day/night cycle of 15h/9h (SANYO Versatile environmental test chamber). Z8 medium is widely used for cultivation of algae in freshwater and assure rapid growth (Kotai, 1972; Sivonen, 1990; Kaebernick et al., 2000; Salvador et al., 2016). However, to control dissolved P concentration in the culture medium as well as to remove EDTA from Z8 medium (EDTA can chelate metals such as Fe and thus impact P-colloids stability), we elaborate modified Z8 medium (M-Z8), presented in Table 27.

The algal and cyanobacterial growth were tested in four conditions including (Fig. 58):

Test 1: P-rich M-Z8 medium – this test serve as a reference in the comparison with tests 2 and 3,

Test 2: P-free M-Z8 medium – to check of microorganismes are able to use their internal P stock for assuring its growth,

Test 3: P-free M-Z8 medium packed with HSG - to test if the colloidal P embeded in silica gel is bioavailable,

Test 4: P-rich M-Z8 medium packed with HSG to evaluate the toxicity of HSG – the TEOS -based sol-gel procedure for preparing silica gel produce alcohol as a by product which should be evaluated by autoclaving teatment. Since the HSG has never been used for supporting the growth of algae and cyanobacteria, this test aimed to evaluate any adverse effect could be induced by HSG on the growth of two strains.

The last test 5 was conducted abiotically in the M-Z8 medium exempt of dissolved P but complemented by HSG to evaluate spontanous release of P from colloids.

Table 27. Composition of M-Z8 medium

Ions	Salt	Molar concentration (mmol/L)
Na ⁺	NaNO ₃ , Na ₂ CO ₃ , EDTA-Na ₂ , NaOH, Na ₂ WO ₄ .2H ₂ O	5.8640322
Ca ²⁺	Ca(NO ₃) ₂ .4H ₂ O	0.2448444
Mg ²⁺	MgSO ₄ .7H ₂ O	0.0401623
Fe ³⁺	FeCl ₃ .6H ₂ O	0.0102553
W ⁶⁺	Na ₂ WO ₄ .2H ₂ O	0.0000099
Mo ⁶⁺	(NH ₄) ₆ Mo ₇ O ₂₄ .4H ₂ O	0.0000493
Zn ²⁺	ZnSO ₄ .7H ₂ O	0.0000993
Cd ²⁺	Cd(NO ₃) ₂ .4H ₂ O	0.0000492
Co ²⁺	Co(NO ₃) ₂ .6H ₂ O	0.0000497
Cu ²⁺	CuSO ₄ .5H ₂ O	0.0000496
Ni ²⁺	NiSO ₄ (NH ₄) ₂ SO ₄ .6H ₂ O	0.0000491
Cr ³⁺	Cr(NO ₃) ₃ .9H ₂ O	0.0000102
V ⁴⁺	VOSO ₄	0.0000048
K ⁺	K ₂ HPO ₄ , KBr, KI, KAl(SO ₄) ₂ .12H ₂ O	0.0002495
Al ³⁺	KAl(SO ₄) ₂ .12H ₂ O	0.0000996
B ³⁺	H ₃ BO ₃	0.0049887
Mn ²⁺	MnSO ₄ .2H ₂ O	0.0008469
NH ₄ ⁺	(NH ₄) ₆ Mo ₇ O ₂₄ .4H ₂ O, NiSO ₄ (NH ₄) ₂ SO ₄ .6H ₂ O,	0.0001406
NO ₃ ⁻	NaNO ₃ , Cd(NO ₃) ₂ .4H ₂ O, Co(NO ₃) ₂ .6H ₂ O, Cr(NO ₃) ₃ .9H ₂ O	5.9284540
SO ₄ ²⁻	MgSO ₄ .7H ₂ O, ZnSO ₄ .7H ₂ O, CuSO ₄ .5H ₂ O, VOSO ₄ , KAl(SO ₄) ₂ .12H ₂ O, MnSO ₄ .2H ₂ O	0.0415455
PO ₄ ³⁻	K ₂ HPO ₄	0.1762031
CO ₃ ²⁻	Na ₂ CO ₃	0.1981341
Cl ⁻	FeCl ₃ .6H ₂ O, HCl	0.0407658
Br ⁻	KBr	0.0001003
I ⁻	KI	0.0000495

	Test 1	Test 2	Test 3	Test 4	Test 5
Culture medium	M-Z8	M-Z8	M-Z8	M-Z8	M-Z8
Source of P	Culture medium	—	Only Colloids	Culture medium and colloids	Only Colloids
Total concentration of DIP	5.51 mg/L (MA) 5.46 mg/L (CV)	0.053 mg/L (MA) 0.002 mg/L (CV)	0.173 mg/L (MA) 0.122 mg/L (CV)	5.63 mg/L (MA) 5.58 mg/L (CV)	0.120 mg/L (MA) 0.120 mg/L (CV)
Microorganismes	Yes	Yes	Yes	Yes	Non
Test target	Growth of the microorganismes in the dissolved P-deped medium Reference for test 2 and 4	Growth of the microorganismes without dissolved P (« internal P stock ») Reference for test 3	Growth of the microorganismes without dissolved P but in the presnce of HSG « Bioavailability » of colloids	Growth of the microorganismes in the dissolved P-deped medium and in the presence of HSG « Toxicity » of HSG	Evaluation of the spontaneous release of P from HSG

Figure 58. Testing conditions for algal and cyanobacterial growth responding to colloidal P (test 3), in comparison with nutrient-rich medium (test 1) and nutrient-free medium (test 2). MA is annotated for *Microcystis aeruginosa*. CV is annotated for *Chlorella vulgaris*.

The colloids used for bioassay test contained $190 \pm 5 \mu\text{g P/L}$ after being extracted from sediment and concentrated by evaporation. The size of colloids ranged from 60 to 1000 nm, with two main size classes of 60-100 nm ($42 \pm 10 \%$) and 220-450 nm ($31 \pm 18 \%$). The elemental concentrations of Fe, Al, Ca, OC has not been determined yet (due to Covid-19 pandemic restriction).

The inoculants contained 1.62×10^7 and 3.22×10^7 cells/mL for *C. vulgaris* and *M. aeruginosa*, respectively. The inoculant of *C.vulgaris* contained $25 \pm 1 \mu\text{g P/L}$ and of *M. aeruginosa* contained $710 \pm 10 \mu\text{g P/L}$. Even if extracted fraction ($< 1 \mu\text{m}$) contained DIP, after washing of HSG in UPW, DIP presented in HSG was under detection limit ($< 20 \mu\text{g P/L}$). The addition of inoculant marked the start of uptake experiment. A 4-mL of inoculant was added to a 25-mL of M-Z8 medium for each test condition. The cells in inoculant were neither previously washed nor starved. As shown in Fig. 58, The concentrations of phosphates in culture media were about 5.5 mg P/L for tests 1 and 4 (using P-containing M-Z8 medium), and about $150 \mu\text{g P/L}$ for tests 2 and 3 (using P-free M-Z8 medium and HSG).

Both inoculants were characterized for P content and the number of cells before incubation. During the biotest, optical density (OD) at 750 nm and concentration of dissolved phosphate were monitored regularly to follow the growth of microorganismes and P uptake rate (Table 28). At the beginning and at the end of biotest, the cell number was counted in addition to OD 750 nm along with measurement of Chl-a.

All preparation and sampling were performed in antiseptic condition under the laminar flow hood (BH-EN 2004, FASTER). All materials used were made by glass and were sterilized using autoclave at 121°C and at 1 bar of pression during 20 min.

Table 28. Sampling planification and the analysis for each sampling day during biotest for colloidal P bioavailability in two species *Microcystis aeruginosa* and *Chlorella vulgaris*

Sampling (days)	0	2	5	7	9	26
Analysis	OD 750	OD 750	OD 750	OD 750	OD 750	OD 750
	DIP	DIP	DIP	DIP	DIP	DIP
	Cell number					Cell number
						Chl-a
Sampling volume (mL)	2 mL	2 mL	2 mL	2 mL	2 mL	17 mL
Remained volume (mL)	25 mL	23 mL	21 mL	19 mL	17 mL	0 mL

III. Growth evolution of *Chlorella vulgaris* and *Microcystis aeruginosa* in response to colloidal P

Figure 59 presents the growth curves of green algae *C. vulgaris* and cyanobacteria *M. aeruginosa* to different source of P (inorganic orthophosphates versus natural P-bearing colloids) in comparison with P-free condition.

Comparison between tests will bring information concerning:

- 1 versus 2: capacity of microorganism to use internal P stocks.
- 1 versus 4: potential toxicity of HSG
- 2 versus 3: bioavailability of colloidal P

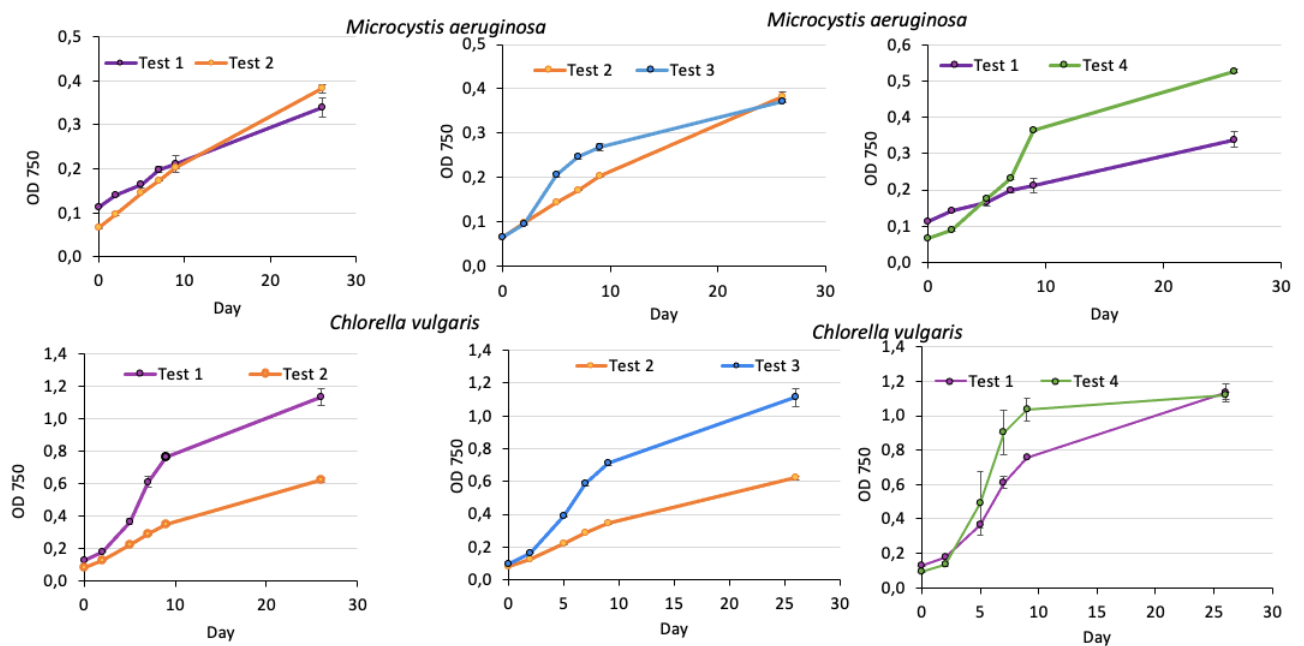


Figure 59. Comparison of green algal growth curve (*Chlorella vulgaris*) and cyanobacteria (*Microcystis aeruginosa*) in different conditions: Test 1: M-Z8 culture medium, Test 2: P-free M-Z8 culture medium, Test 3: P-free M-Z8 containing HSG ; Test 4: M-Z8 culture medium containing HSG.

The growth rate of *C. vulgaris* was comparable between culture mediums using orthophosphate and HSG, with value of 0.21 (Table 29). These growth rates of *C. vulgaris* was significantly higher than in P-free culture medium (growth rate of 0.14, Table 29). It should be noted that P-free culture medium contained a small concentration of orthophosphate originated from inoculant of *C. vulgaris* (2 µg P/L) despite no orthophosphate was added. The continuing growth of *C. vulgaris* under low phosphate concentration in P-free condition could be both due to the consumption of solution phosphate and the use of intracellular P stock. The *C. vulgaris* is one of microorganism species accumulate polyphosphate granules inside the cells that serves as phosphate supply under stress condition (Chu et al., 2015). This polyphosphate reserve within the cell of *C. vulgaris* support their growth but in far lower rates than in phosphate ample conditions.

For *M. aeruginosa*, they have shorter adaption time to the culture medium containing HSG (2 days, test 3, Fig. 1) and higher growth rate (growth rate of 0.19, Table 29) than in orthophosphate culture medium (5 days, test 1, Fig. 59 and growth rate of 0.06, Table 29). This could be due to the bioavailability of other elements in colloids that helped to reduce the lag time of *M. aeruginosa* growth. Comparing with growth evolution of *M. aeruginosa* observed in P-free culture, there was no significant growth enhancement upon present of either orthophosphate or HSG. This suggests the *M. aeruginosa* store P in quantities which may maintain their growth when P are deficient or that the need for P are very low and the remaining P remaining in initial inoculant covered their needs or low quality/health of inoculated cells.

For both species, the increase in OD₇₅₀ between day 9 and day 26 were not significant and implying the stop multiplication of cells. Therefore, a stationary phase can be considered to start from day 9 to day 26. Moreover, the growth of *C. vulgaris* (OD₇₅₀ up to 0.8 and growth rate reach 0.21 on day 9) is more announced than *M. aeruginosa* (OD₇₅₀ up to 0.3 and growth rate reach 0.19 on day 9). This indicated that *C. vulgaris* was in healthier state than *M. aeruginosa* used in this biotest, therefore, from here, the main interpretation will be made according to growth reponse of *C. vulgaris*.

Comparing between orthophosphate and HSG (test 2 versus test 3), *C. vulgaris* performed not only similar growth rate but also similar in growing phases. There was no difference in lag phase between these two conditions, indicating the quick adaptation of green alga to P bound to natural colloids at the same degree of response to free phosphates. This observation is noticeably novel and highly supportive to the bioavailability of colloidal P in HSG. A remark is that the medium culture were not axenic and we supposed that there was the presence of bacteria (Fig. 60), but this could not be verified because of COVID-19 restriction and suspended laboratory work. If the bacteria were present together with *C. vulgaris* the release of P from colloids could be assured by bacterial metabolic activity. At this stage of work we can say that the increase in green color of culture medium throughout the inoculation confirmed a powerful growth of *C. vulgaris* despite presence of bacteria. However, we are not able to state that *C. vulgaris* to uptake P directly from colloids. Furthermore, the co-existence of bacteria can support algal uptake of P because some bacterial species release enzymes, for example enzyme 5'-nucleotidase, sequester carbon-nitrogen complex served for metabolism activity, these enzyme can hydrolyze phosphate from other phosphorus compounds (Björkman and Karl, 2003). The release of phosphates from bacterial hydrolysis could therefore be available for algal uptake. In general, the growth of *C. vulgaris* in response to P-bearing colloids provides evidence that natural colloidal P are bioavailable for green alga, directly or indirectly, as much as orthophosphate does.

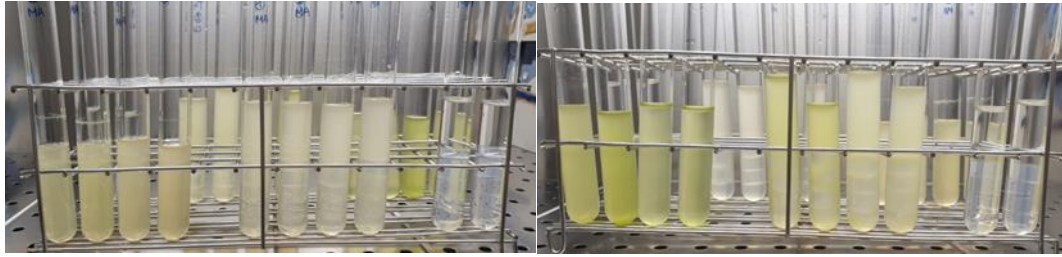


Figure 60. Photography of *M. aeruginosa* (left) and *C. vulgaris* (right) in different test mediums on day 9.

By comparison of the tests 1 (M-Z8 culture medium) and 4 (M-Z8 culture medium and HSG) we constate a higher cell growth in the presence of HSG and for both organisms tested. It suggests that colloids embedded in silica gel facilitate microorganism' growth. It could be related to the presence of P and other elements such as Fe, Ca...

Table 29. Growth rate of *C. vulgaris* and *M. aeruginosa* in different test mediums.

Species	Tested condition	Growth rate	Exponential phase (day)
MA	Test 1	0.105	2-9
	Test 2	0.061	2-7
	Test 3	0.193	2-7
CV	Test 1	0.144	2-9
	Test 2	0.213	2-9
	Test 3	0.213	2-9

IV. Algal uptake rate of phosphorus

As shown in Fig. 58, the initial DIP contained in Test 1 culture medium was used up on day 5 in the case of *C. vulgaris* and day 25 in the case of *M. aeruginosa*. This indicated that the uptake rate of inorganic phosphates by *C. vulgaris* was more rapid than *M. aeruginosa*. The initial concentrations of DIP in solution of Test 2 and Test 3, which were coming from inoculant, was consumed completely after the first 2 days. After 9 days of incubation, all tested culture medium showed the release of DIP back to solution, except Test 1 for *M. aeruginosa*. However, the higher releases of DIP were observed for *C. vulgaris* cultures, especially in Test 1. The release of DIP in solution between day 9 and day 26, in accordance to stationary stage of both algal species observed in this time (Fig. 61), demonstrated that there was probably P release from algal death and cell lysis.

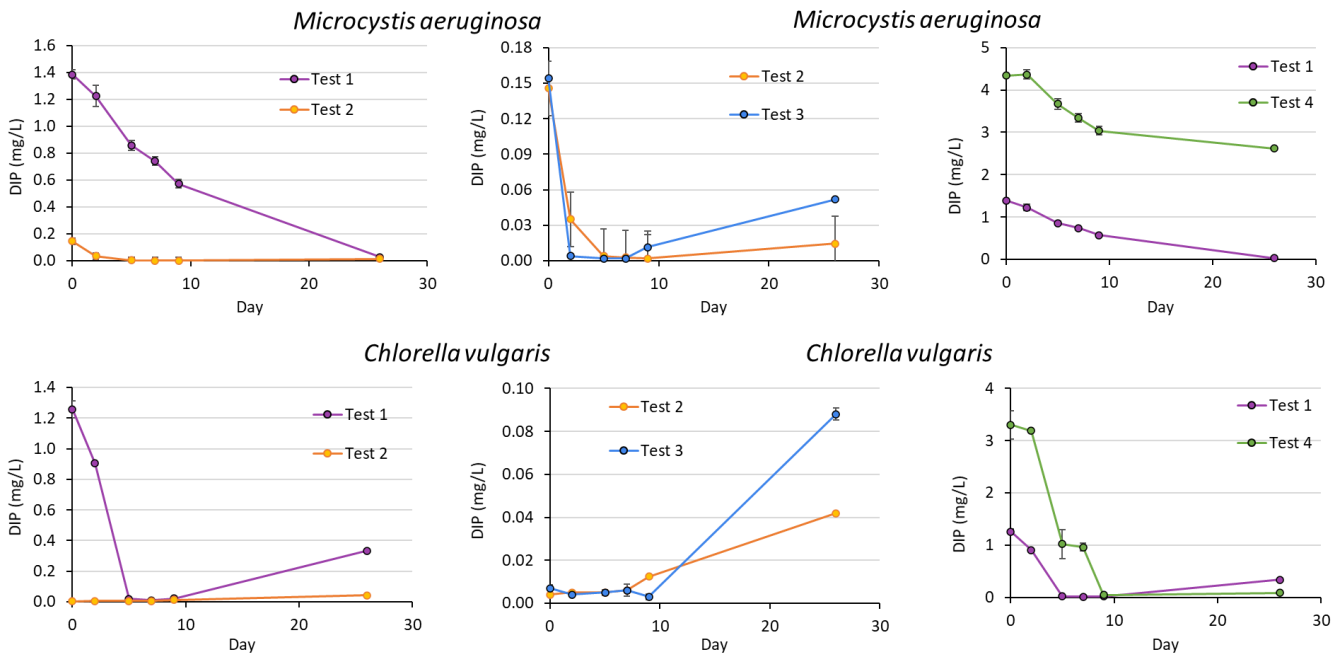


Figure 61. Comparison of residual dissolved inorganic phosphate (DIP) in culture medium of (A) *Chlorella vulgaris* and (B) *Microcystis aeruginosa* in different growing conditions: Test 1: M-Z8 culture medium, Test 2: P-free M-Z8 culture medium, Test 3: P-free M-Z8 containing HSG.

V. Conclusion and perspective

From this preliminary bioassay experimentation, the positive growth response of the two species were not clearly pointed out because all tests were conducted on non-axenic culture medium. The growth results indicated the response of both species and maybe co-developing bacteria. However, the results provide an initial evaluation of bioavailability of colloidal P to a community of green algae and bacteria that was at the same degree with inorganic phosphates. The bioavailability of colloidal P was not observed significantly on community of cyanobacteria and bacteria.

The additional experimentation on axenic cultures were not able to be done due to Covid-19. For further accurate evaluation, the bioassay test should be carried out with pure and healthy algal cells and more frequent monitoring of growth to better define growing phase. Moreover, cells should be washed and starved to remove internal nutrient stock as well as remaining phosphate in culture medium before testing.

Thus, the using of HSG can provide an original way to simulate colloids-microorganism interactions in nutrient controlled environment and to study colloids bioavailability. Moreover, HSG is impurity free and tune able inorganic materials and can be used to screen microbial strains able to use nutrient present in colloids to sustain their growth.

Résumé

Le relargage de phosphore sédimentaire constitue une source interne de nutriments dans les eaux conduisant à l'eutrophisation des milieux aquatiques, en particulier des retenues. Les connaissances actuelles concernant le relargage du P sédimentaire ne tiennent pas compte de la fraction colloïdale, qui est pourtant considérée comme une importante phase porteuse de P, très mobile et potentiellement biodisponible. Cette thèse souligne le rôle majeur des colloïdes sédimentaires vis-à-vis de leur teneur en phosphore ainsi que leur fort potentiel à être mobilisé dans l'eau. Il a été démontré que les colloïdes sont une composante intrinsèque essentielle des sédiments au sein du barrage de Champsanglard (Creuse, France) et qu'ils peuvent être remobilisés à hauteur de 2.3 % de la masse totale du sédiment lors de la resuspension de ce dernier. Le phosphore colloïdal représentait jusqu'à 6 % du phosphore sédimentaire total et 80 % du phosphore total mobilisable. L'étude des différents protocoles d'extraction, de séparation et de conservation des sédiments a permis de proposer une méthodologie opérationnelle permettant la sélection du protocole le plus approprié. Il est ainsi recommandé de réaliser les extractions de colloïdes sur sédiment humides, par une méthode douce (agitation) et de réaliser la séparation des colloïdes extraits par filtration avec une étape de pré-séparation. Les centrifugations successives sont déconseillées car elles conduisent à une estimation biaisée de la quantité et de la qualité des colloïdes extraits. Au travers de l'étude de la retenue de Champsanglard, il a été mis en évidence une forte hétérogénéité de la répartition spatiale de la quantité et de la qualité des colloïdes sédimentaires et du P associé. La granulométrie des sédiments, l'hydrodynamique des écoulements, la présence d'affluents et le marnage apparaissent comme des facteurs clés. La plus importante quantité de colloïdes mobilisables et en particulier les colloïdes de plus grande taille (0.2 – 1 µm) concerne les sédiments lacustres des zones profondes, en amont de la confluence avec les tributaires. Les sédiments de berge régulièrement impactés par le marnage de l'eau relarguent du phosphore sous une forme biodisponible (forme dissoute et nano/petits colloïdes). En condition anoxique, les sédiments ont la capacité de libérer du phosphore colloïdal, dans des proportions largement supérieures au phosphore dissous. Jusqu'à 40 % du phosphore sédimentaire total a ainsi été remobilisé sous forme colloïdale. Lorsque les conditions redeviennent oxiques, une majeure partie du phosphore mobilisé persiste en solution et notamment sous la forme de colloïdes de tailles petites et intermédiaires (300 kDa - 0.45 µm). En conditions d'oxydo-réduction variables, les processus biogéochimiques impliquant le fer et la matière organique seraient les paramètres clés contrôlant la mobilité du P colloïdale. Ce travail met en évidence la nécessité de considérer la contribution des colloïdes pour l'évaluation de la mobilité et de la biodisponibilité du P, en particulier en contexte de retenue de barrage.

Mots-clés : Retenue de barrage, sédiment, colloïde, phosphore, mobilité, biodisponibilité, variabilité spatiale, marnage, anoxie, cycle séchage/humidification, oxydo-réduction, fer, matière organique

Abstract

The mobilization of phosphorus (P) from sediment is a persistent internal nutrient source sustaining eutrophication, especially in reservoir. Current knowledge about sedimentary P release does not consider colloidal form, although it is well-known for its efficiency as P-carrier, its high mobility and potentially bioavailability. This thesis provides new constraints to place sedimentary colloids and sedimentary colloidal P into light concerning their important stock and release potential in the reservoir. Colloids are shown to be an intrinsic component of reservoir sediment, and their recovery under sediment resuspension indicated the contribution of water mobilizable colloids up to 2.3 % of the sediment mass in Champsanglard dam reservoir (Creuse, France). The amount of P associated with colloids was up to 6 % of total sedimentary P and 80 % of water-mobilizable P. After the application of different protocols for colloid extraction, separation and for sediment storage, a framework for selecting appropriated method for colloid recovering from a sediment is proposed. The recommendation for colloid recovery is to work with wet sediment, avoid using high-power extraction protocol (i.e. sonication), using filtration with pre-separation step instead of successive centrifugation to avoid under or overestimation in quantity and quality of recovered colloids. The quantity and quality of sedimentary colloids and associated P varied spatially in the reservoir according to sediment size grain distribution and the influence of flow hydrodynamics, the presence of tributaries and fluctuations in the water-level. The highest content of water mobilizable colloids and especially large colloids (0.2 - 1 µm) were found in lacustrine bottom sediments, downstream of the tributary confluence. Bank sediments impacted by water-level fluctuations released P in bioavailable forms (dissolved P and small/nano P-colloids). Under anoxic condition, the potential of sediment to mobilize colloidal P was significantly higher than truly dissolved P and represented up to 40 % of total sedimentary P. When condition became oxic subsequently, major portion of released P remained in suspension under small/intermediate size (300 kDa - 0.45 µm). In redox changing conditions, the closely linked biogeochemical cycles of iron and organic matter could be the key parameters involved in mobility of colloidal P. This thesis highlights the need to consider colloids and their contribution in the P mobility at the boundary of sediment-water and associated bioavailability to aquatic plankton, particularly in dam reservoir context.

Keywords : Dam reservoir, sediment, colloid, phosphorus, mobility, bioavailability, spatial variability, water-level fluctuation, anoxia, drying/rewetting, redox, iron, organic matter.

